

MINIMALISTIC PROBES FOR PROTEIN FOLDING AND STRUCTURE STUDIES

**Lee Colyer Speight**

A DISSERTATION

in

Chemistry

Presented to the Faculties of the University of Pennsylvania

in

Partial Fulfillment of the Requirements for the

Degree of Doctor of Philosophy

2014

Supervisor of Dissertation

---

E. James Petersson

Assistant Professor of Chemistry

Graduate Group Chairperson

---

Gary A. Molander, Hirschman-Makineni Professor of Chemistry

Dissertation Committee

Barry S. Cooperman, Professor of Chemistry

Carol Deutsch, Professor of Physiology

William P. Dailey, Associate Professor of Chemistry

David M. Chenoweth, Assistant Professor of Chemistry

## *Dedication*

This dissertation is dedicated to all those whose work I have referenced in preparing this document and those mentioned in the acknowledgements (implicitly and explicitly). My sentiments can be best summarized in a quote made famous by Sir Isaac Newton: “If I have seen further it is by standing on the shoulders of giants.”

## ACKNOWLEDGMENT

This body of work would not have been possible without the support and wisdom of many individuals that I have been fortunate enough to interact with in the past several years. I would like to thank my advisor, Professor E. James Petersson for providing me with the opportunity to hone my synthetic skills and learn many intricacies of molecular biology, specifically recombinant protein expression, while consistently maintaining a rigorous challenging environment. I also owe special thanks to the members of my dissertation committee, Professors Cooperman, Chenoweth, Dailey, and Deutsch, for their careful analysis of my work, many helpful suggestions, and support.

I have also been blessed to be the presence of many talented and insightful peers, both within the Petersson laboratory and the University of Pennsylvania's Department of Chemistry at large. While these individuals are almost too numerous to list, each and every member of the Petersson laboratory has either directly or indirectly shaped the way I view academic research and its role in influencing our ever-changing world. I would like to specifically thank my fellow lab members Rebecca Wissner and Anand Muthusamy for countless fruitful discussions, their critical examinations of my work, and, most importantly, their friendship. I am also tremendously in debt to the Smith and Saven laboratories for many useful conversations about my syntheses and protein expressions respectively.

The technical staff of University of Pennsylvania's Department of Chemistry is impressive and their assistance has been invaluable to my work. I would like to thank Dr. Rakesh Koli of the MS facility, Drs. George Furst and Jun Gu of the NMR facilities, Dr. Simon Berritt of the UPenn/Merck High Throughput Experimentation Laboratory, and

Dr. Chris Lanci of the Biological Chemistry Resource Center (BCRC) for all their time and assistance throughout the years. Dr. Chris Lanci, aside from his role in the BCRC, has been a great friend, providing me with advice not only about graduate school and chemistry, but life in general as well.

Part of being a member of a young laboratory has meant learning and setting up new techniques and technologies for future generations of researchers in my group. If I have been successful in this, it has been through the help of Professor Petersson and the numerous experienced scientists that he has allowed me to work under during my time in his laboratory. I would like to specifically thank Professor Matthew Hartmann (Virginia Commonwealth University), Professor Ya-Ming Hou and Dr. Howard Gamper Jr. (Thomas Jefferson University), and Professor Ryan Mehl for all their guidance and support. Additionally, I have had the pleasure of collaborating intensely with Professor Carol Deutsch of the Physiology Department at the University's Medical School. I am grateful for all of the discussions that we have had about the ribosome, my research and career interests, as well as the opportunity to work on a project that was initially far from the focus of my graduate work, but directly in line with my personal curiosities.

Finally, as the work described here required intense dedication and quite a few ~~days weeks months~~ years of long hours, I am quite thankful to those who have been there for me as friends and family. I want to say thank you to Bob Philips, Dallas Powell, Dalton Pownell, Nick and Lisa Blanco, and Dan Ronnenberg for including me in your weekly game night; it has been a fantastic escape. Also, I would like to thank Sean Sheppard for his patience in listening to me babble about science and sustainability and helping me to channel those interests into concrete career goals. Finally, I would like to

thank my family, specifically my mother Susan Colyer, for their support and doing their best to pretend to follow my rants about chemical synthesis and protein dynamics.

## ABSTRACT

### MINIMALISTIC PROBES FOR PROTEIN FOLDING AND STRUCTURE STUDIES

Lee Colyer Speight

Professor E. James Petersson

Site-specific incorporation of fluorescent probes into proteins enhances the ability of researchers to study protein folding and structural dynamics. Currently, the most common fluorescent probe for proteins is green fluorescent protein (GFP). However, the use of GFP, a 28 kDa protein, requires its covalent attachment to a protein of interest. Additionally, this attachment is restricted to either the N- or C-terminus of the protein, drastically limiting the scope of experiments possible. Alternative technologies for the addition of novel fluorescence properties to proteins exist, however they are also limited by the probe size or its method of attachment. Since many proteins of interest are less than or equal to the size of these fluorescent auxiliaries, it is likely that the covalent fusion of the fluorescent apparatus will significantly perturb the native fold or function of the molecule of interest. As such, the development of minimalistic probes for protein functional studies is of great interest to the biochemical community. Acridon-2-ylalanine (Acd) is a minimalistic fluorescent unnatural amino acid (fUAA) that possess a long lifetime ( $\tau = 16$  ns), resistance to photobleaching, a near unity quantum yield ( $\Phi = 0.95$ ), and visible wavelength emissions. While there existed literature precedent for the synthesis of Acd, these methods required harsh conditions and reagents that precluded a high-yielding, scalable synthesis of the fUAA. To this end, we have devised an efficient, scalable 5-step synthesis utilizing Tyr that yields Acd in 87 % overall yield. Recently, we have shown that Acd can be incorporated into proteins *in vivo* and can be a valuable

probe of protein-peptide interactions and protein conformational change due to its blue-wavelength excitation, unique solvatochromic properties, and ability to participate in energy transfer with endogenous amino acids (Trp and Tyr), exogenous fluorophores (methoxycoumarin), and the lanthanide ion  $\text{Eu}^{3+}$ . Furthermore, as the need for minimalistic probes is not limited to fluorescence applications, we have collaborated with the Deutsch laboratory to develop methods for the synthesis of unnatural amino acids capable of probing the interaction between the ribosomal exit tunnel and nascent peptides.

## TABLE OF CONTENTS

ACKNOWLEDGMENT.....	iii
ABSTRACT.....	vi
LIST OF TABLES.....	xi
LIST OF FIGURES.....	xii
LIST OF SCHEMES.....	xv
LIST OF ABBREVIATIONS.....	xvi
CHAPTER 1: THE NEED FOR MINIMALISTIC PROBES FOR PROTEIN STRUCTURE AND FUNCTION STUDIES.....	1
BACKGROUND.....	2
FLUORESCENCE AS A MINIMALLY PERTURBING METHOD FOR MONITORING PROTEIN DYNAMICS.....	4
FLUORESCENT PROTEINS.....	9
PROTEIN BASED CHEMICAL-TAGGING SYSTEMS.....	11
SMALL MOLECULE FLUORESCENCE PROBES.....	13
TRYPTOPHAN ISOSTERES AS MINIMALISTIC FLUORESCENCE PROBES.....	18
SITE-SPECIFIC INCORPORATION OF UNNATURAL AMINO ACIDS.....	21
ORTHOGONAL AMINOACYL-tRNA SYNTHETASES.....	26
SITE-SPECIFIC INCORPORATION OF NOVEL FLUORESCENT AMINO ACIDS.....	30
SITE-SPECIFIC INCORPORATION OF A FLUORESCENCE QUENCHING PROBE.....	41
TOWARDS MORE MINIMALISTIC PROBES FOR FLUORESCENCE AND FUNCTIONAL STUDIES .....	42
CHAPTER 2: ACRIDON-2-YLALANINE: SYNTHESIS, <i>IN VIVO</i> INCORPORATION, AND BIOPHYSICAL STUDIES.....	44

BACKGROUND: ACD PRIOR STUDIES AND PHOTOPHYSICS .....	45
SYNTHESIS OF ACD .....	54
O-aaRS/tRNA PAIR IDENTIFICATION .....	63
<i>IN VIVO</i> INCORPORATION & ALTERNATIVE ACD SYNTHESSES .....	67
BIOPHYSICAL STUDIES: FRET/LRET/PET .....	71
ACD AS AN ENVIRONMENTAL PROBE .....	75
ACD AS A FRET PROBE .....	79
ACD AS A LANTHANIDE LUMINESCENCE SENSITIZER .....	83
ACD AS A PET PROBE .....	85
CONCLUSIONS AND FUTURE WORK .....	90
EXPERIMENTAL METHODS .....	91
General Information .....	91
Synthesis of Acd (1) <i>via</i> p-NO <sub>2</sub> F Route .....	94
Synthesis of Acd (1) <i>via</i> L-Tyrosine Route .....	96
Synthesis of Acd (1) <i>via</i> LiOH saponification and PPA deprotection/cyclization .....	99
Screening of Cross-Coupling Conditions .....	101
Peptide Synthesis and Purification .....	103
Absorption and Fluorescence Spectroscopy of Fluorophore Pairs .....	109
Acd Steady-State Stern-Volmer Experiments .....	114
Acd Fluorescence Lifetime Stern-Volmer Experiments .....	117
Förster Distance Calculations .....	120
Synthetase Sequences .....	123
Cloning of Calmodulin Expression Constructs .....	125
Wild-Type Calmodulin Protein Expression .....	126
Acd Mutant Calmodulin Protein Expression .....	127
Cloning of TIM Expression Constructs .....	129
Wild-Type TIM Expression .....	131
Acd Mutant TIM Expression .....	132
Cloning of $\alpha$ -Synuclein Expression Constructs .....	133
Wild-Type $\alpha$ -Synuclein Expression .....	135
Acd Mutant $\alpha$ -Synuclein Expression .....	136
Trypsin Digest Analysis of Acd Mutants .....	136
Calmodulin Circular Dichroism Measurements .....	138
Calmodulin Peptide Binding Measurements from Steady-State Fluorescence .....	139
Calmodulin Binding Data Fitting .....	140
TIM Unfolding Measurements from Steady-State Fluorescence .....	141
TIM Unfolding from Fluorescence Lifetimes .....	141
 CHAPTER 3: NASCENT PEPTIDES AND THE RIBOSOMAL EXIT TUNNEL .....	 148
BACKGROUND AND PRIOR STUDIES .....	149

ARREST PEPTIDES AS REGULATORY MECHANISMS .....	150
'RESCUE' PEPTIDES PROVIDING ANTIBIOTIC RESISTANCE TO MACROLIDE AND KETOLIDE ANTIBIOTICS.....	153
TOWARDS AN UNDERSTANDING OF THE PHYSIOLOGY AND FUNCTION OF THE RIBOSOMAL EXIT TUNNEL .....	157
AMINOACYLATION AND <i>IN VITRO</i> SENSE REPROGRAMING STRATEGIES.....	162
EXPERIMENTAL METHODS .....	170
General Information.....	170
Synthesis of Tetraalkylammonium Maleimides.....	171
Synthesis of (2R,2'R)-3,3'-disulfanediybis(2-((tert-butoxycarbonyl)amino)propanoic acid) .....	171
Synthesis of bis(3,5-dinitrobenzyl) 3,3'-disulfanediy(2R,2'R)-bis(2-((tert-butoxycarbonyl)amino)propanoate).....	172
General Method for the Syntheses of Succinimide Functionalized Cys-DBEs .....	174
Synthesis of Cys-AMS.....	176
REFERENCES .....	177

## LIST OF TABLES

<b>Table 2.1:</b> CaM Protein Expression .....	73
<b>Table 2.2:</b> TIM Protein Expression .....	73
<b>Table 2.3:</b> $\alpha$ -Synuclein Protein Expression .....	73
<b>Table 2.4:</b> FRET in CaM/Mcm-pOCNC Complexes .....	81
<b>Table 2.5:</b> Acid HPLC Analysis Gradient .....	99
<b>Table 2.6:</b> Calculated and Observed Peptide and Protein Masses .....	107
<b>Table 2.7:</b> Solvent Gradients Used for Peptide Purification and Analysis .....	108
<b>Table 2.9:</b> Exponential Fits to Lifetime TIM Urea Denaturation Data .....	147
<b>Table 3.1:</b> Purification of <b>4</b> .....	174
<b>Table 3.2:</b> Purification of <b>5</b> .....	175
<b>Table 3.3:</b> Purification of <b>6</b> .....	175
<b>Table 3.4:</b> Purification of <b>7</b> .....	175
<b>Table 3.5:</b> MS Analyses of Cys-Succinimide-DBEs .....	176

## LIST OF FIGURES

<b>Figure 1.1:</b> Chromophore Size .....	4
<b>Figure 1.2:</b> Common Protein Fluorescence Experiments .....	8
<b>Figure 1.3:</b> Monitoring A $\beta$ <sub>1-40</sub> Oligomer Formation with FIAsh .....	16
<b>Figure 1.4:</b> Trp Analogue Fluorescence Emission.....	21
<b>Figure 1.5:</b> ‘Honeycomb’ Model of Ribosomal Permissivity.....	26
<b>Figure 1.6:</b> Schematic Diagram of Amber Suppression Technology Utilizing an O-aaRS/tRNA Pair .....	29
<b>Figure 1.7:</b> Line Diagrams of Ribosomally Permissible flUAAs Discussed in This Section.....	30
<b>Figure 1.8:</b> Tracking FtsZ Depolymerization in Cells Using Hco.....	34
<b>Figure 1.9:</b> Simultaneous Observation of Conformational Change and Conductance in a K <sub>v</sub> Channel .....	38
<b>Figure 2.1:</b> Line Diagrams of Acd, Mcm, and 7-azaTrp.....	46
<b>Figure 2.2:</b> Steady-State Stern-Volmer Experiments with Acd and Thioacetamide .....	47
<b>Figure 2.3:</b> Dynamic Stern-Volmer Quenching of Acd.....	48
<b>Figure 2.4:</b> HP35 Model System for Thioamide Quenching of Acd .....	50
<b>Figure 2.5:</b> Acd Stern-Volmer Interactions with Endogenous Amino Acids .....	52
<b>Figure 2.6:</b> Cu(I) and Cu(II) proposed mechanisms for Ullman/Goldberg Biaryl Amine Synthesis .....	57
<b>Figure 2.7:</b> Screening Results .....	60
<b>Figure 2.8:</b> Structures of Acd (1), Bzf, and Brb.....	64

<b>Figure 2.9:</b> aaRS Selection and Confirmation of Acd Incorporation.....	65
<b>Figure 2.10:</b> HPLC, LRMS, and MALDI-MS Analysis of Amino Acids and Protein Expression.....	68
<b>Figure 2.11:</b> Relative Npf to Acd Incorporation .....	70
<b>Figure 2.12:</b> SDS PAGE Gel Analysis of Mutant Protein Expression .....	72
<b>Figure 2.13:</b> Temperature-Dependent Circular Dichroism Spectroscopy of WT CaM and Acd Mutants.....	74
<b>Figure 2.14:</b> CaM Labeling Sites .....	75
<b>Figure 2.15:</b> Native PAGE Gel Analysis of CaM Peptide Binding .....	76
<b>Figure 2.16:</b> Fluorescence Spectra of CaM Mutants with Bound Peptides .....	77
<b>Figure 2.17:</b> Monitoring CaM Binding By Changes in Acd Environment.....	78
<b>Figure 2.18:</b> Fluorescence Spectra of CaM Mutants with Bound Peptides .....	80
<b>Figure 2.19:</b> Fluorescence Spectra of CaM Mutants with Bound Peptides .....	82
<b>Figure 2.20:</b> Monitoring Eu <sup>3+</sup> Binding to CaM by LRET.....	84
<b>Figure 2.21:</b> TIM Annotated Crystal Structure.....	86
<b>Figure 2.22:</b> Fluorescence Spectra of TIM Denaturation in Urea.....	88
<b>Figure 2.23:</b> Monitoring TIM Unfolding By Changes in Average Fluorescence Lifetimes .....	89
<b>Figure 2.24:</b> Representative Structures of p-OCNC Peptides Used in This Work .....	109
<b>Figure 2.25:</b> Absorption and Fluorescence Spectra of Trp .....	110
<b>Figure 2.26:</b> Absorption and Fluorescence Spectra of Mcm, Acd, and Fam.....	111

<b>Figure 2.27:</b> Absorption and Fluorescence Spectra of BODIPY Fl, R6G, and NBD in 100 mM phosphate buffer, pH 7.0.....	113
<b>Figure 2.28:</b> Steady-State Stern-Volmer Titrations of Acd with Amino Acids.....	116
<b>Figure 2.29:</b> Lifetime Stern-Volmer experiments.....	119
<b>Figure 2.30:</b> Distance Dependence of Acd FRET Interactions.....	122
<b>Figure 2.31:</b> Sequences of Candidate Synthetases.....	124
<b>Figure 2.32:</b> CaM Mutagenesis.....	126
<b>Figure 2.33:</b> TIM Mutagenesis.....	131
<b>Figure 2.34:</b> $\alpha$ -Synuclein Mutagenesis .....	134
<b>Figure 2.35:</b> MALDI MS of Trypsinized Proteins.....	137
<b>Figure 2.36:</b> Lifetime TIM-F <sub>74</sub> $\delta$ Urea Denaturation Experiments .....	142
<b>Figure 2.37:</b> Lifetime TIM-Y <sub>101</sub> $\delta$ Urea Denaturation Experiments .....	144
<b>Figure 2.38:</b> Lifetime Acd Urea Experiments.....	146
<b>Figure 3.1:</b> Models of Modes of Action for Macrolide Antibiotics.....	157
<b>Figure 3.2:</b> Conditions Tested for the Thia-Michael Reaction Between NEM and a Protected Cys .....	163
<b>Figure 3.3:</b> Retrosynthetic Analysis of Succinimide Functionalized Cys-DBEs.....	166

## LIST OF SCHEMES

<b>Scheme 2.1:</b> Synthesis of Acd ( <b>1</b> ) Starting from p-NO <sub>2</sub> -F With Modifications Described in This Work .....	56
<b>Scheme 2.2:</b> Synthesis of Acd Starting from Tyr Using H <sub>2</sub> SO <sub>4</sub> as the Final Reagent .....	63
<b>Scheme 2.3:</b> PPA-mediated route to Acd ( <b>1</b> ) .....	69
<b>Scheme 2.4:</b> Action of YigC on Hydroxybenzoate and Proposed YigC decomposition of <b>12</b> to Npf ( <b>11</b> ).....	71
<b>Scheme 3.1:</b> Synthetic Route to Succinimide Derivatized Cys DBEs .....	168
<b>Scheme 3.2:</b> Synthesis of the Cys aaRS Inhibitor: Cys-AMS.....	169

## LIST OF ABBREVIATIONS

aaRS – Aminoacyl tRNA Synthetase

aa-tRNA – Aminoacyl tRNA

Acid – Acridon-2-ylalanine

Ala – Alanine

ANAP – 3-(6-Acetylnaphthalen-2-ylamino)-2-Aminopropanoic Acid

Arg – Arginine

Asn – Asparagine

Asp – Aspartic Acid

CaM – Calmodulin

Cys – Cysteine

EF-Tu – Elongation Factor Temperature Unstable

flUAA – Fluorescent Unnatural Amino Acid

FP – Fluorescent Protein

FRAP – Fluorescence Recovery After Photobleaching

FRET - Förster Resonance Energy Transfer

GFP – Green Fluorescent Protein

Gln – Glutamine

Glu – Glutamic Acid

Gly – Glycine

Hco – 7-Hydroxycoumarin

His – Histidine

HPLC – High Performance Liquid Chromatography

Ile – Isoleucine

Leu – Leucine

Lys – Lysine

MALDI – Matrix Assisted Laser Desorption/Ionization

Met – Methionine

Nap – 3-(2-Naphthyl)Alanine

NMR – Nuclear Magnetic Resonance

o-aaRS/tRNA – Orthogonal Aminoacyl tRNA Synthetase/tRNA Pair

pCNF – *p*-Cyanophenylalanine

PET – Photo-Induced Electron Transfer

Phe – Phenylalanine

pNO<sub>2</sub>-F – *p*-Nitrophenylalanine

Pro – Proline

Ser – Serine

Thr – Threonine

TIM – Triose Phosphate Isomerase

Trp – Tryptophan

Tyr – Tyrosine

UAA – Unnatural Amino Acid

Val – Valine

VCF – Voltage-Clamp Fluorimetry

**CHAPTER 1: THE NEED FOR MINIMALISTIC PROBES FOR PROTEIN  
STRUCTURE AND FUNCTION STUDIES**

Adapted in part with permission from Speight, L.C.; Samata, M.; Petersson, E. J.;  
Minimalist Approaches to Protein Labelling: Getting the Most Fluorescent Bang for Your  
Steric Buck. *Australian Journal of Chemistry*. DOI: 10.1071/CH13554;  
<http://www.publish.csiro.au/?paper=CH13554> (To be published in print on 19 May  
2014).

## **BACKGROUND**

As postulated by C. B. Anfinsen, the classical thermodynamic hypothesis of protein folding states that “the three-dimensional structure of a native protein in its normal physiological milieu ... is the one in which the Gibbs free energy of the whole system is lowest; that is, that the native conformation is determined by the totality of inter-atomic interactions and hence by the amino acid sequence, in a given environment<sup>1</sup>.” Multitudes of literature reports have corroborated this hypothesis since its inception in 1973 leading to it commonly being referred to as “Anfinsen’s Hypothesis<sup>2</sup>.” Thus, as the environment of a protein dictates how its monomeric components interact, studies of these interactions and the overall protein structural architecture should mimic the native state of the protein as closely as can be reasonably achieved. Advances in protein imaging technologies, chiefly x-ray crystallography and nuclear magnetic resonance (NMR) spectroscopy, have enabled protein scientists worldwide to decipher, model, and publish the atomic resolution structures of over 98,000 proteins and protein complexes as of February 2014<sup>3</sup>. While these technologies have unquestionably aided the investigations of all biological researchers, many intricacies of the folding pathways, enzymatic activities, and overall structural dynamics of proteins remain elusive. As with any technique, both x-ray crystallography and NMR spectroscopy have limitations and impose constraints on the analytes to ensure successful imaging at useful resolutions. Such constraints inherent to these methods include the use of nonnative conditions such as salts, pH, solvent, and concentration, all of which can possibly affect the inter-atomic interactions of a protein under analysis<sup>4</sup>. For example, intrinsic to protein structure elucidation by X-ray crystallography is the caveat that the protein being studied must pack orderly into a

crystal lattice, which itself is a significant perturbation of the protein's solution-phase dynamics.

While there have been recent reports of crystallographic and NMR techniques being applied to proteins *in vivo* where the protein is in its native environment, these analyses are still respectively limited by a protein's ability to crystallize or be isotopically labeled at close to millimolar concentrations<sup>5</sup>. Furthermore, the data retrieved from such experiments is also respectively limited to fixed states in a crystal lattice and the microsecond timescale just as the analogous *in vitro* experiments<sup>6</sup>. Efforts towards providing better image and temporal resolution of these analyses are ongoing; however they are still relatively new technologies<sup>7</sup>. Fluorescence spectroscopic analysis of proteins, on the other hand, is not limited by these same constraints and is a generally well understood method for analyzing both monomeric and polymeric biological compounds. Experiments with intrinsically fluorescent or fluorescently labeled proteins are routinely done at micromolar concentrations or lower and the data can be acquired in time intervals as low as fractions of nanoseconds. This enables the facile and accurate observation of changes in fluorescence of either purified analytes or dilute components of complex mixtures. In fact, fluorescence based imaging of proteins has been done *in vivo* since the 1990s and detailed *in vitro* work dates to the 1970s<sup>8</sup>. While fluorescence experiments have the tremendous benefit of being able to be conducted readily in the native context of a protein, the technology does have its own limitations. The use of intrinsic fluorescent probes, such as the amino acids tryptophan (Trp) and tyrosine (Tyr), is complicated by to the abundance of these residues and other moieties in cells that are excited by similar wavelengths of light. Additionally, the accuracy of the measurements

is often constrained by the chemistry necessary to install a fluorescent probe, the size of the probe, or the location of the probe's installation on the protein. Development of fluorescent modifications for proteins has yielded a broad suite of probes and methods that are as structurally and spectroscopically diverse as the applications for which they were designed.

### FLUORESCENCE AS A MINIMALLY PERTURBING METHOD FOR MONITORING PROTEIN DYNAMICS

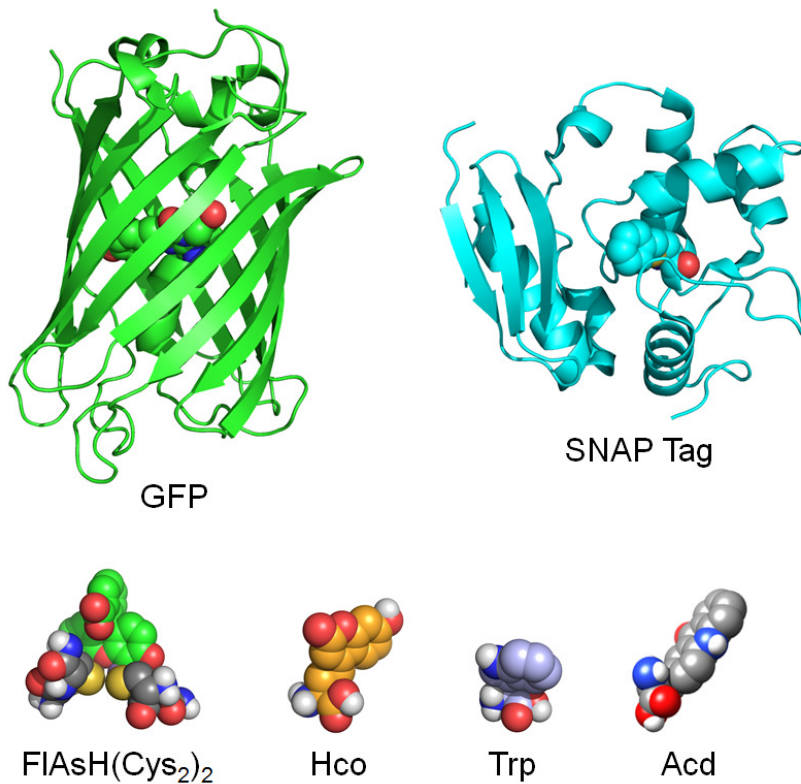


**Figure 1.1:** Chromophore Size. Space-filling renderings of several chromophores, based on either crystal structures or *ab initio* calculations. The green fluorescent protein (GFP) was rendered from PDB ID 1GFL<sup>9</sup>. The benzylated SNAP tag protein was rendered from PDB ID 3L00 (S. Schmitt, B. Mollwitz, F. Pojer, M.

Bannwarth, M. Schiltz, K. Johnsson, unpublished results). The geometry of tetracysteine-bound FIAsh was optimized at the HF/6-31G level, all others were optimized at the AM1 level.

Numerous aspects of protein dynamics, such as folding, conformational changes, binding to other proteins or molecules, and proteolysis, can be examined with fluorescently labeled proteins. Protein folding and conformational changes can be monitored by observation of changes in the fluorescence of a probe relative to a defined starting state. For example, solvatochromic fluorescent probes change their relative fluorescence intensity through a change in the molar absorptivity of the fluorophore( $\epsilon$ ), absorption maxima( $\lambda_{\text{abs}}$ ), emission maxima ( $\lambda_{\text{em}}$ ), or quantum yield ( $\Phi$ ) in response to changes in their local environment. This has been used to monitor the movement of a protein domain or amino acid residue between environments of differing hydrophobicity such as the movement of a probe from the nonpolar interior of a protein to the exterior where it is exposed to bulk polar solvent, typically water. The binding of other molecules to a fluorescently labeled protein of interest can also be observed by solvatochromic effects but more commonly the change in fluorescence due to a change in intramolecular distances between two probes is used. Proteolysis and biomolecular disassociations benefit from being monitored by such a fluorescence technique as the possibility to conduct fluorescence experiments under extremely dilute conditions allows for a robust change in fluorescence due to rapid diffusion of fluorophores.

Two types of energy transfer experiments are commonly used to ascertain the change in distance between two fluorescent probes: Förster resonance energy transfer (FRET) and photoinduced electron transfer (PET) (**Figure 1.2**). FRET experiments rely on the interaction between two probes whose spectral properties are matched such that one

probe, the 'donor' has an appreciable fluorescence emission that overlaps with the absorption spectrum of the other probe, the 'acceptor.' Two facets of this process are important to consider. First, FRET is not the result of a trivial emission-reabsorption process, but rather the result of the coupling of the electronic transition dipoles of the donor and acceptor species that enables the transfer of energy from one to the other. As such, it is not necessary for the acceptor chromophore to have emission properties of its own; these types of acceptor probes are referred to as quenchers because their effects are observed by a decrease in donor emission rather than an appearance of novel longer wavelength emissions. All FRET interactions have a quantitative  $1/(R^6)$  distance dependence that allows for straight-forward time-dependent structural information to be derived (where R is the intermolecular distance between the donor and acceptor). PET experiments solely rely on the quenching of donor fluorescence. However the distance dependence of PET, roughly  $e^{-R}$ , often is too dependent on the pathway between the fluorophore and quencher to interpret accurately. The mechanism of PET quenching can be either through a static or dynamic electron transfer. These two mechanisms differ with regard to whether or not the excited state of the donor is populated, yet the outcome is the same; a decrease in the probability that the fluorophore will emit light. Static PET quenchers form a ground-state complex with the fluorophore that prevents the transition to the excited state by an absorption of a photon while dynamic PET quenchers undergo a coupled reduction or oxidation reaction with the excited state of the fluorophore that causes the fluorophore to return to the ground state by a non-emissive pathway. PET quenchers of utility for biophysical applications are capable of being restored to their original oxidation state under the conditions of the experiment so that the process can

occur repeatedly. On this note, as PET is a redox process, the redox active amino acids Met, His, Lys, Trp, Tyr, and Cys can be valuable PET probes when matched with the appropriate fluorophore. Additionally, some research groups have seen modulation of a fluorophore's fluorescence due to the N-terminal amine of proteins and peptides<sup>10</sup>.

In addition to solvatochromism, it is prudent to consider PET quenching by endogenous biological components of a system, such as the amino acids Trp and Tyr, as another type of environmental effect. Mutagenesis of these residues to avoid these interactions would likely be perturbing to the system and can be avoided by the use of careful controls if a chosen fluorescent probe interacts with these endogenous moieties. Such considerations must be made when any fluorophore is used in a new system, as the native environment of a protein can be quite different from the conditions in which fluorophores are typically characterized (i.e. in pure solvent). However it is within these unique environments that the dynamics of fluorophores can report in ways that other techniques cannot. For example, Lakowicz and others observed that the x-ray structures of proteins reveal that they are tightly packed with a density far too great to allow for the free diffusion of small molecules such as molecular oxygen<sup>11</sup>. However, the fluorescence of Trp residues buried within a variety of proteins' hydrophobic cores is quenched by oxygen, albeit at a significantly decreased extent when compared to that of surface exposed residues. These observations imply that protein structural vibrations must occur on the nanosecond timescale in order for oxygen diffusion to occur and subsequent Trp fluorescence quenching to be observed. While these findings do provide useful information, they also highlight the need for careful probe selection and diligent design of control experiments.

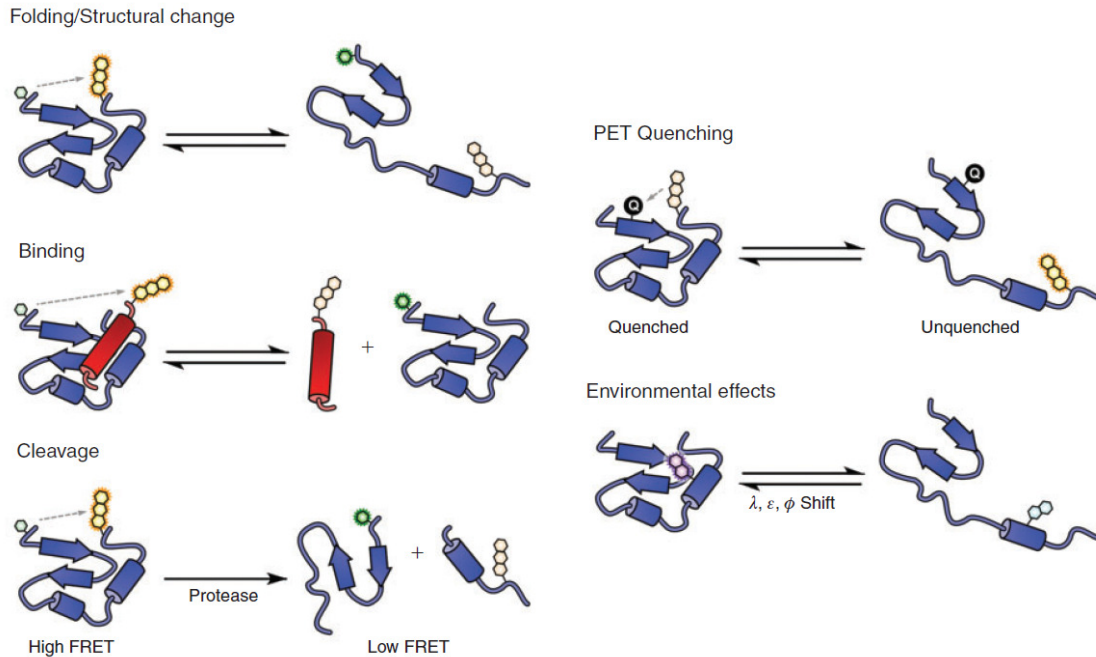


**Figure 1.2:** Common Protein Fluorescence Experiments. Protein conformational changes, protein-protein interactions, and proteolytic cleavage can be monitored by changes in the intra- or intermolecular distance between two FRET (Förster resonance energy transfer) probes. Similar experiments can be conducted with a fluorophore/PET quencher or a single, environmentally sensitive dye.

Technology for the installation of fluorescence moieties to proteins is an area of intense research. The fluorescent probe toolbox available to biophysical researchers is ever expanding and includes probes whose size varies from a single atom substitution made by chemical synthesis to 28 kDa proteins with an internal fluorophore that forms upon protein folding. Methodology for the attachment of these probes varies from co-translational incorporation *via* genetic fusion of a fluorescent protein to a protein of interest, ribosomal incorporation of a fluorescent amino acid, or post-translational modification, which can either be chemoenzymatic or rely on bioorthogonal chemical reactions. Of most interest to protein folding biophysicists are highly site-specific

methods which do not require extensive synthetic chemical post-translation modification. However, owing to their robust nucleophilicity, lysine (Lys) and cysteine (Cys) residues have been used for the installation of fluorophores possessing the appropriate reactive partners. Unfortunately, since the respective amine and thiol groups of these residues are frequently found in other biomolecules, these methods are largely restricted to *in vitro* applications and single Lys or Cys mutants. To overcome these limitations, several unique bioorthogonal reactive handles, such as azides and alkynes, have been site-specifically installed into proteins for subsequent labeling with appropriately functionalized fluorophores. The chemistry involved and/or the scaffolds necessary for their incorporation of these reactive handles are significantly more likely to perturb the native fold or function of a protein rather than a single amino acid substitution<sup>12</sup>. Co-translational incorporation allows one to place fluorophores on the interior of a protein, whereas post-translational attachment is either limited to surface residues or requires that the protein be capable of unfolding and then refolding after modification. Therefore the pursuit of such minimalistic fluorescent probes amenable to site-specific ribosomal installation is the most prudent endeavor for those wishing to image proteins as close to their native state as possible.

## **FLUORESCENT PROTEINS**

First isolated from the jellyfish *Aequorea victoria* in 1962, green fluorescent protein (GFP) has substantively changed biochemical research by allowing straightforward genetic reporting of *in vivo* gene expression and, *via* fusion to a protein of interest,

cellular protein localization and trafficking (**Figure 1.1**)<sup>13</sup>. GFP has subsequently been optimized for enhancing folding (eGFP) as well as derivatized to yield several colored variants<sup>14</sup>. While the utility of these 28 kDa  $\beta$ -barrel proteins may initially seem limited to passive applications such as using fluorescence to determine the cellular fate of a protein target, the multi-colored library of fluorescent proteins (FPs) has been used for a variety of complex applications, the most exciting of which rely on FRET<sup>15</sup>. Using carefully selected FP pairs with significant spectral overlap, FRET probes have been designed for examining diverse biochemical processes such as protease activity, protein-protein interactions, and metal ion homeostasis both *in vitro* and *in vivo*<sup>14, 15</sup>. Typically, these studies are designed such that one colored FP (the donor) is appended to one terminus of a linker, which has been designed as the ‘reporter’ sequence, and the other colored FP (the acceptor) is attached to the other terminus. As this is readily done on the DNA level and cloned into a protein expression vector, studies can easily be done *in vivo*, or *in vitro* following purification of the fusion protein product.

One such example of this methodology being used for an *in vivo* experiment was conducted by the laboratories of G. A. Rutter and M. Merckx. Previously, the Merckx group had developed a genetically encoded FRET-based sensor for the *in vivo* detection of Cu(I) ions by combining copper-binding domains from proteins involved in human copper homeostasis Atox1 and ATP7B and fusing this reporter sequence to two FPs<sup>16</sup>. Mutation of the copper-binding domains to the zinc-binding domains found in ZntA, a zinc transporter protein, and fine tuning of linker lengths allowed for pico- and femtomolar detection of Zn(II) in a subsequent report<sup>17</sup>. However, the emission ratio change upon Zn(II) binding was minimal (a decrease of 15%). By changing the FPs from

eCFP and eYFP to Cerulean FP and Citrine FP and adding mutations to the FPs to promote contacts between the donor and acceptor, the combined groups of Merkx and Rutter were able to enhance the dynamic range from their sensor to a 2.4-fold decrease in emission ratios<sup>18</sup>. These optimizations show that FPs can be used to in FRET-based assays *in vivo*, however, spectral optimizations aside, it is important to account for the large size of the FPs and how this effects their interactions in the system; it is possible that the FP-fusion disrupts the native functions of the protein of interest.

## **PROTEIN BASED CHEMICAL-TAGGING SYSTEMS**

While research into GFP and its colored derivatives has allowed for the development of variants suitable for most spectral applications, others have developed alternative strategies where the fluorophore can be enzymatically attached post-translationally. A product of the Promega Corporation, the HaloTag is a mutated bacterial haloalkane dehalogenase that, when attached to a protein of interest *via* genetic fusion, creates a covalent ester linkage between the protein and a synthetic ligand<sup>19</sup>. As the fluorescent moiety, or any desired ‘cargo,’ is part of the unreactive portion of the synthetic ligand, these probes can be changed by varying the ligand while keeping the same fusion protein, saving a significant amount of time if a particular fluorophore is shown to be suboptimal for an application. This methodology, frequently referred to as ‘protein based chemical-tagging’ has proven to be fairly general and has been used for an array of applications: labeling proteins with fluorescent probes and quantum dots, as well as providing a platform to protein purification. Other protein based chemical-tagging systems that have

been developed include SNAP-tag (based on the human DNA repair protein *O*<sup>6</sup>-alkylguanine-DNA alkyltransferase (hAGT) (**Figure 1.1**))<sup>20</sup>, CLIP-tag (a derivative of SNAP-tag that recognizes *O*<sup>6</sup>-benzylcytosine derivatives)<sup>21</sup>, and TMP-tag (*E. coli* dihydrofolate reductase (eDHFR) that recognizes trimethoprim(TMP)-based tags)<sup>22</sup>. These strategies do not reduce the steric cost of fluorescent labeling with FPs, as the fusion of one of the tagging domains typically adds ~30kDa to the protein of interest. However, they do offer unique applications such as fluorogenic tagging reactions.

V. W. Cornish's laboratory, which developed the TMP-tag methodology, recently reported the use of dual functionalized TMP ligands that enabled fluorogenic labeling of proteins in living cells<sup>23</sup>. Consistent with the TMP moiety's previous role as a therapeutic, synthetic ligands containing TMP have been shown to have high water solubility and cell permeability. These parameters, combined with the high affinity of eDHFR for TMP-ligands ( $K_D \sim 1$  nM), make the TMP chemical tag methodology well suited for high resolution live cell imaging. However, the need to wash out excess probe or labeling reagent is always an issue with chemical based fluorescent labeling. To circumvent this issue, Cornish and coworkers redesigned the TMP ligands to contain both a fluorophore and a quencher. The quencher was specifically anchored on the 'leaving group' portion of ligand such that upon reaction with a Cys residue in a mutant eDHFR, the TMP-fluorophore conjugate would be covalently attached to the fusion protein of interest and the quencher would diffuse away, dramatically increasing the signal from the fluorophore upon excitation. Using the ATTO520 and BHQ1 as the respective fluorophore and quencher in their fluorogenic TMP-tag, the experimenters were able to specifically label the nuclear protein histone 2B with significantly higher resolution and

precision than with previous generation TMP-tags. Additionally, the Cornish group was able to label three distinct cytosolic proteins (TOMM20,  $\alpha$ -actinin, and MLC) in two different cell lines (HEK 293T and MEF) showing that there is no intrinsic localization of the TMP-ligands. Furthermore, the modular design of these ligands allows for future refinement and/or selection of fluorophores and quenchers to meet experimental needs.

### **SMALL MOLECULE FLUORESCENCE PROBES**

Despite the fact that protein based chemical-tagging strategies allow experimenters to readily change fluorophores and utilize fluorogenic labels, there is still a significant steric cost; the required protein fusions are several hundred amino acids in size, rendering them as sterically perturbing as FP based systems. Well aware of this, R. Tsien, whose work with GFP brought its use to the forefront of biochemistry, developed a drastically more minimalistic protein tag. Requiring no more than the specific six amino acid sequence CCPGCC, Tsien and coworkers identified a bisarsenical fluorescein derivative (FLAsH) that binds this tetracysteine motif with high affinity and negligible toxicity when administered with a 10-fold excess of a small vicinal diol such as 1,2-ethanedithiol (**Figure 1.1**)<sup>24</sup>. The probe had the added, and unexpected, benefit of achieving a 5000-fold increase in fluorescence upon binding of the CCPGCC motif, making this system both fluorogenic and tremendously less sterically perturbing than FP or protein based chemical-tag methods. It is also important to note that several research groups have corroborated these claims<sup>25</sup>. Subsequent refinement by the Tsien lab led to the

development of other bisarsenical probes that responds to the CCPGCC motif including the popular ReAsH, based on the resorufin fluorophore<sup>26</sup>.

Aside from simply using the FAsH or ReAsH probes to label proteins *in vivo* and *in vitro*, several groups have devised clever methods of using the turn-on fluorescence properties of these probes as a diagnostic of protein dynamics. The Schepartz laboratory used both FAsH and ReAsH in conjunction with bipartite Cys-Cys motifs to study intramolecular domain interactions as well as intermolecular protein-protein dimerization interactions<sup>27</sup>. It was hypothesized that the space created by the PG section of the CCPGCC motif could be replaced with the space between two protein domains or polypeptide strands; thus binding of the bisarsenical probes would be an indicator of the proximity between two Cys-Cys sequences. With proof-of-principle experiments for successful intramolecular (with aPP and Zip4) and intermolecular (GCN4 and Jun) FAsH/ReAsH binding, the group further showed that they were able to detect defects in protein structure both *in vitro* and *in vivo*. By inducing mutations in GCN4 and Jun that are known to destabilize helix formation and protein dimerization, the Shepartz group found that FAsH and ReAsH fluorescence intensity was greatly decreased in response to these mutants *in vivo*. These experiments highlight the ability of these probes to selectively bind to the tetracysteine motif and thus diagnose disruptions in the orientation of the four cysteine residues and polypeptide structure in complex environments.

The Schepartz report on the use of FAsH and ReAsH to study intramolecular and intermolecular protein dynamics concludes with the assertion that their methodology would be well suited to study the misfolding and aggregation of proteins involved in

protein aggregation pathologies such as Alzheimer's disease and Parkinson's disease. Just a few years later, J. Kelly and coworkers were successful in using the methodology to monitor the formation of early stage oligomers of A $\beta$ <sub>1-40</sub>, which are unresponsive to typical aggregation dyes that detect only later stage fibrils such as thioflavin T (**Figure 1.3**)<sup>28</sup>. By installing Cys-Cys motifs at the N-terminus of A $\beta$ <sub>1-40</sub> monomers synthesized using Fmoc-based solid phase peptide synthesis, the group was able to monitor the formation of early stage oligomers within minutes of beginning aggregation experiments. Thioflavin T, for comparison, takes 12 hours before there is a significant increase in fluorescence indicating fibril formation. Interestingly, the group was also able to observe thioflavin T to FAsH FRET at early stages during the experiments, corroborating others reports that thioflavin T weakly binds to oligomers. Combined with traditional thioflavin T assays, the Kelly lab was able to use their split-FAsH methodology to study the aggregation of A $\beta$ <sub>1-40</sub> *in vitro* in more detail than had previously been done. Their experiments led them to the conclusion that A $\beta$ <sub>1-40</sub> aggregation is not a nucleated polymerization, but rather a nucleated conformational change, a finding which highlights the advantage of the small size and minimal perturbation of the FAsH methodology to study protein dynamics.

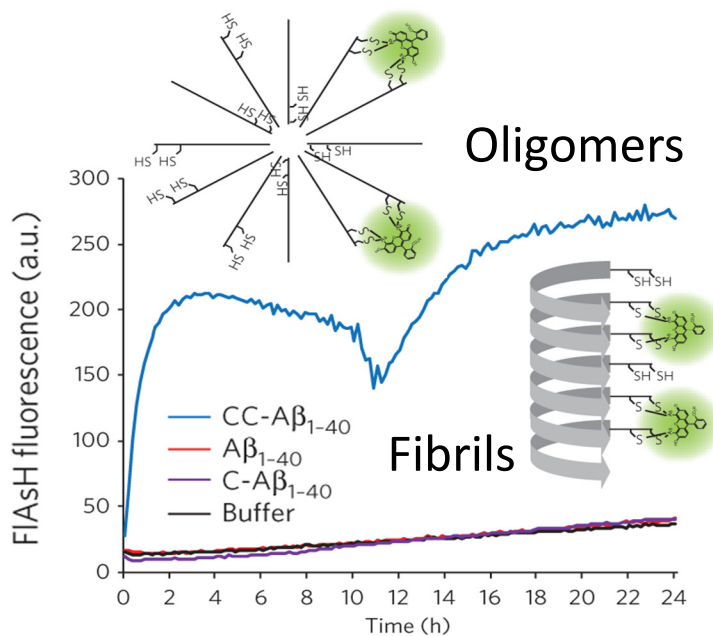


**Figure 1.3:** Monitoring  $A\beta_{1-40}$  Oligomer Formation with FIAsh. FIAsh can bind to both oligomers and fibrils, unlike thioflavin T (ThT), which only binds fibrils. FIAsh fluorescence from the Cys2 mutants of  $A\beta_{1-40}$  monomers indicates the assembly of oligomers before fibrillization. Adapted figure reproduced from Lee *et al.* with permission from Nature Publishing Group<sup>28</sup>.

While the FIAsh methodology allows for the installation of a fluorophore into proteins dependent only on a short peptide tag, it is still an imperfect solution to the problems of FP and chemical-based protein fusion protocols for the fluorescent labeling of proteins. Aside from the cellular toxicity of FIAsh and the related dyes due to their arsenic moieties, the requirement of complex washout procedures, and low specificity owing to reactivity with monothiols and Cys rich proteins pose significant limitations for biophysical investigators<sup>26, 29</sup>. Thus A. Ting and coworkers sought to combine the utility of small peptide tagging protocols with the absolute specificity of genetic FP fusions. The group's first success in this area came with their discovery of the permissivity of the *E. coli* biotinylation enzyme BirA<sup>30</sup>. BirA, previously known to react precisely with a Lys

residue in a 15 residue ‘acceptor protein’ (AP) sequence, has been shown to have only one substrate in *E. coli* and none in mammalian cells<sup>31</sup>. Ting’s group found that wild-type BirA is capable of using an analog of biotin in which the urea functionality has been replaced with a ketone, allowing for a reaction with a fluorescent probe bearing a hydrazide handle. This resulted in a two step procedure for the labeling of proteins in mammalian cell lysate or on the surface of live cells: First, BirA, ATP, and the ketone biotin analog are added to the cell lysate or cell growth medium, allowing for the specific attachment of the biotin analog to the lysine with the AP sequence. Following washout of the ketone compound for *in vivo* applications, the fluorescent hydrazide-containing probe is added and allowed to react with the ketone moiety. This method, while specific, is limited to cell lysate and cell surface applications due to the possibility of hydrazide cross-reactivity with the ketone and aldehyde containing compounds typically found in the cytosol.

Subsequent work within the Ting laboratory with other enzymatic tagging methods suffered from similar limitations. Specifically in their use of a transglutaminase based system, intracellular labeling proved elusive due to several off target labeling events and calcium concentrations that were suboptimal for activity<sup>32</sup>. However, through structure-based evolution of the *E. coli* lipoic acid ligase, Ting’s group was able to create an enzymatic one-step fluorophore ligation method applicable to intracellular tagging of proteins inside live cells<sup>33</sup>. Coined ‘PRIME’ (PRobe Incorporation Mediated by Enzymes), the method involves the mutant lipoic acid ligase, or fluorophore ligase, specifically appending a carboxylic acid derivative of 7-hydroxycoumarin onto a lysine residue within a 13 residue recognition sequence<sup>34</sup>. The experimenters were able to show

robust labeling of proteins in the nucleus and cytosol in various mammalian cell lines that proceeded faster and with significantly less background fluorescence and cytotoxicity than the analogous labeling with FIAsh. However, the system still required the expression of the fluorophore ligase in the cells in which proteins are to be labeled. At high plasmid loading, this led to some background, nonspecific labeling. These limitations aside, Ting and coworkers have used both the BirA and PRIME methodologies to study protein-protein interactions inside living cells<sup>35</sup>.

### **TRYPTOPHAN ISOSTERES AS MINIMALISTIC FLUORESCENCE PROBES**

Although the endogenous amino acids Tyr and Trp are both fluorescent, with Trp typically dominating the emissions spectra of proteins, it is difficult to selectively excite either fluorophore in proteins containing a single Tyr or Trp residue and impossible in proteins containing multiple Tyr or Trp. Despite these limitations, Trp fluorescence has been used to probe the structure, folding, and interactions of proteins due to its low abundance (1%) relative to other residues<sup>36</sup>. Thus, the ideal minimalistic fluorescent probe would be an isosteric analog of Trp with superior spectral properties. Such an endeavor is possible, since it was shown that as early as 1956 that the bacterial translation machinery could use the Trp analogs 7-azaTrp and 2-azaTrp<sup>37</sup> (Note: subsequent publications have yet to reproduce the incorporation of 2-azaTrp)<sup>38</sup>. Additionally, several indole derivatives have been shown to be superior to the parent molecule in the context of biological fluorescence studies; these features include red-shifted absorbance and

fluorescence maxima, enhanced Stoke's shifts, greater environmental sensitivity, and longer fluorescence life-times (**Figure 1.4**)<sup>38-42</sup>.

The most commonly used Trp analogs for biophysical studies are 7-azaTrp and 5-hydroxyTrp. These analogs have been shown to be well suited to use for site-specific genetic incorporation through the use of *E. coli* Trp auxotrophic strains by several research groups, with the first incorporation of 5-hydroxyTrp by A. G. Szabo in 1992 and proof of its minimal perturbing status by J. B. Alexander Ross *et al* in the same year<sup>43</sup>. In 2002, H. Hu and coworkers installed both 7-azaTrp and 5-hydroxyTrp into the sole Trp position of protein G from *Streptococcus* (residue 43) and compared the resulting spectra to those of the wild-type protein<sup>44</sup>. As with the free amino acids, protein G mutants containing 7-azaTrp and 5-hydroxyTrp showed a red-shifted absorbance profile and a significant shoulder in the absorbance at 310 nm, respectively. These spectral enhancements are due to the changes in the separation of the <sup>1</sup>L<sub>a</sub> and <sup>1</sup>L<sub>b</sub> electron transition bands due to the altered electronics of the indole rings. Absorption at longer wavelengths allows the fluorophores to be selectively excited in the presence of endogenous Trp residues. However Hu and colleagues found that the analogs had drastically different environmental sensitivities; the 5-hydroxyTrp mutant was shown to be less sensitive to solvent exposure than Trp (which modestly increases in fluorescence intensity upon shielding the residue from solvent), while the 7-azaTrp mutant's fluorescence increased significantly and blue-shifted slightly upon moving the residue away from solvent. In another example, Broos and coworkers studied the Lys motif (LysM), which is a peptidoglycan binding domain found in both prokaryotes and eukaryotes, and its ligand interactions using these Trp analogs<sup>45</sup>. While it proved to be a

valuable probe these in contexts, the intense sensitivity of 7-azaTrp to polar solvents often results in dramatic quenching of the fluorophore, which can make it too dim to be useful.

N. Budisa has significantly contributed to the exploration of the photophysical properties and *in vivo* incorporation of Trp derivatives, specifically those containing additional endo- and exocyclic nitrogen atoms<sup>38-41</sup>. The intense quenching of 7-azaTrp is due to the ability of both endocyclic nitrogen atoms to participate in hydrogen bonding with separate water molecules. These interactions prevent tautomerization of the azaindole to a more fluorescent isomer and thus diminish the utility of the fluorophore<sup>41</sup>. In efforts to circumvent this problem, Budisa's group has studied the regioisomers 4, 5, and 6-azaTrp. While 6-azaTrp is red-shifted by an additional 30 nm in its absorbance profile, its use has been shown to be problematic in the literature, with some claiming to have trouble reproducing its ribosomal incorporation<sup>40, 46</sup>. 4 and 5-azaTrp were shown to tautomerize only at high pH values (>10), making them resilient to environmental effects in the context of biological applications. Furthermore, Budisa's group showed that 4 and 5-azaindole were capable of being used as substrates by the Trp synthetase (TrpS) in *E. coli*, allowing for *in situ* stereospecific synthesis of the corresponding amino acids from the parent fluorophore<sup>40</sup>. After incorporating both of these Trp analogs, in addition to 7-azaTrp, into human anxA5, Budisa's group compared the changes of each mutant fluorescent protein in response to changes in environment. As in other experiments, the 7-azaTrp mutant was weakly fluorescent when folded, and almost completely quenched upon denaturation and exposure of the residue to bulk solvent. Conversely, the fluorescence spectra of the 4 and 5-azaTrp mutants were largely unchanged in the same

experiment. Furthermore, the 4-azaTrp mutant proved to be the superior probe due to its broad absorbance band at 310 nm, a Stokes shift of 130 nm, and a higher quantum yield. Budisa's work with indole and Trp analogs has also included *N*-methylated derivatives of the aforementioned compounds, those with exocyclic amine substituents, and the application of Trp analogs to the creation of optimized FPs<sup>38, 39, 41</sup>.

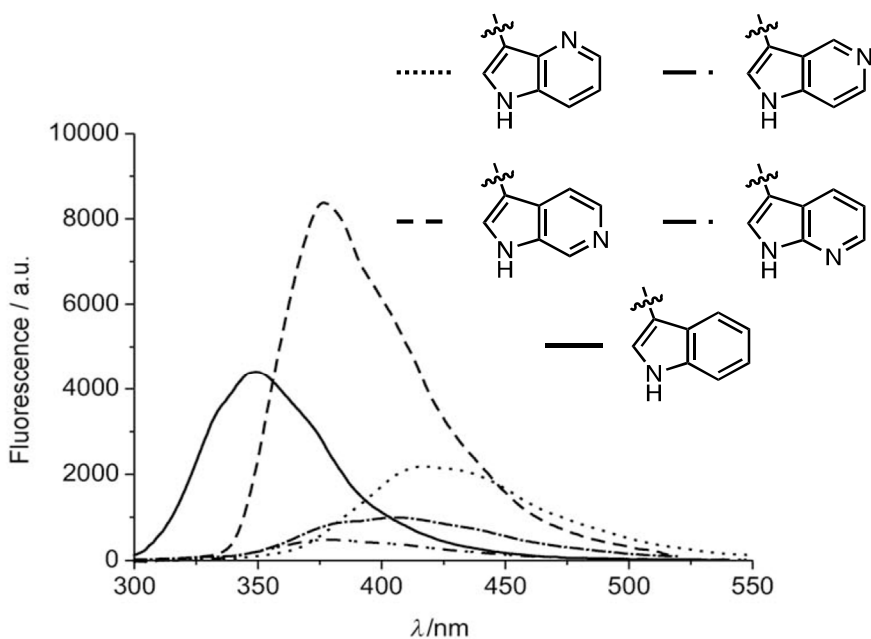


**Figure 1.4:** Trp Analogue Fluorescence Emission. Fluorescence spectra of 4-AzaTrp, 5-AzaTrp, 6-AzaTrp, and 7-AzaTrp are all red-shifted relative to the Trp spectrum with 4-AzaTrp having the greatest bathochromic shift. Adapted figure reproduced from Merkel *et al.* with permission from Wiley-VCH<sup>41</sup>.

## SITE-SPECIFIC INCORPORATION OF UNNATURAL AMINO ACIDS

Site-specific incorporation of exogenous fluorescent unnatural amino acids (fUAAs) into proteins is the best option for the most accurate fluorescent measurements of protein dynamics. Fortunately for protein biophysicists, the ribosome, nature's polypeptide

synthesizer, has been shown to tolerate noncanonical mRNAs, tRNAs, and a suite of amino acids with diverse structures and functions. Several *in vitro* and *in vivo* methods for the site-specific incorporation of unnatural amino acids (UAAs) have been published in the last 25 years (with amber suppression and 4-base codon technologies being the most popular). However, all current methods are limited by the intrinsic size restraints of the ribosomal A, P, and E sites, nascent peptide exit tunnel, as well as the steric constraints of the trafficking protein/GTPase EF-Tu<sup>47-49</sup>.

Fundamental studies that would later provide the basis for genetic code expansion were first conducted by S. Benzer and colleagues in the early 1960s, when a detailed understanding of the macromolecular components of translation was still lacking<sup>50</sup>. Following treatment of Cys-tRNA with the ‘cysteine activating enzyme’ in the presence of ATP, Benzer took the resulting Cys aminoacyl tRNA (aa-tRNA) and removed the thiol group *via* reduction with Raney-Ni. The resulting desulfurized aa-tRNA was then effectively alanine (Ala) tRNA. When this misacylated tRNA was used in a crude translation experiment, Ala was incorporated instead of Cys. These results revealed that ‘activating enzymes,’ later known as aminoacyl tRNA synthetases (aaRSs), know what amino acid to put onto what tRNA, however the macromolecular complex responsible for decoding mRNA only sees the codon on the tRNA, not what amino acid is esterified to its 3’ end. Such findings made it theoretically possible to expand the genetic code by intentional misacylation of tRNA molecules. Shortly over a decade later, S. Hecht’s laboratory was able to chemically aminoacylate a symmetrical phosphorylated adenosine derivative and subsequently enzymatically ligate it on to a truncated tRNA to yield a functional misacylated tRNA<sup>51</sup>. As all tRNAs terminate in the same three nucleotides,

cytidine-cytidine-adenosine, this methodology was shown to be a general method for 'sense-reprogramming' of the genetic code, that is, hijacking a normal coding codon by use of a misacylated corresponding tRNA.

While 'sense-reprogramming' can yield site-specific mutants of proteins containing unnatural amino acids, this methodology requires the use of either auxotrophic cells lines or cell-free systems lacking the natural tRNA for the codon to ensure complete incorporation of the novel amino acid. P. G. Schultz was able to solve this problem and effectively add a 21<sup>st</sup> amino acid to the genetic code by the development of amber suppression technology<sup>52</sup>. The 'UAG' codon, commonly referred to as the amber codon, is the least used codon and had previously been shown to be efficiently suppressed by known suppressor tRNAs for the incorporation of endogenous, but rare, amino acids such as selenocysteine (Note: in the context of this document, suppression refers to the reprogramming of a 'stop' signal in translation into a coding codon). Thus, using a modified version of Hecht's protocol for the production of semisynthetic tRNAs, Schultz and coworkers devised a method for the semisynthesis of full length misacylated tRNAs bearing the anticodon CUA. This new route, in which a dinucleotide, phosphodeoxycytidine-phosphoadenosine (pdCpA), is aminoacylated and then ligated onto a truncated tRNA missing the terminal C and A, dramatically improved the atom economy of Hecht's method as all aminoacylated nucleotides are substrates for the chemoenzymatic ligation reaction (in Hecht's method both 'ends' of the symmetrical phosphorylated adenosine derivative could be aminoacylated, but only one would be transferred in the ligation)<sup>53</sup>. These misacylated amber suppressor tRNAs are then used in conjunction with mRNAs bearing the amber codon at the site of interest in an *in vitro*

translation reaction. A caveat of this methodology is that the UAG codon normally codes for a 'stop,' or termination, in translation and as such the suppressor tRNA competes with release factor 1 (RF 1). Thus, yields are diminished relative to the production of the corresponding wild-type protein due to any premature hydrolysis of the misacylated amber suppressor tRNA and production of truncated protein (where RF 1 outcompetes the suppressor tRNA and terminates translation). Despite these limitations, this technology has proven to be incredibly enabling and a variety of groups have used it to incorporate novel amino acids into proteins in both *in vitro* reactions and by large cells (*via* micro-injection of the misacylated amber suppressor tRNA). Such endeavors opened the door for the incorporation of any amino acid that could be tolerated by the rest of the cellular translation system.

M. Sisido and coworkers have conducted several studies aimed at mapping the size and geometric permissivity of the endogenous translation machinery in both prokaryotes and eukaryotes. In 1999, Sisido's group unveiled the "honeycomb model" describing the regions where benzene groups could be attached to the  $\beta$ -carbon of an amino acid while still allowing for efficient translation (**Figure 1.5**)<sup>54</sup>. This model was the result of testing the *in vitro* incorporation efficiencies of 19 aromatic UAAs in both *E. coli* and rabbit reticulocyte lysate and comparing them to Tyr incorporation. It expanded upon a previous model from the group in which they studied the geometric restraints of 12 aromatic puramycin derivatives<sup>47</sup>. Their findings showed that polyaromatic UAAs are generally well tolerated in both systems (the rabbit reticulocyte system showed marginally more size permissivity) with only two tested positions found not to be tolerated. Sisido's group used this information to guide their site-specific incorporation of several fluorescent

UAAs into streptavidin; L-2-anthrylalanine (antAla) and three coumarin derivatives of homoalanine, glutamic acid (Glu), and aspartic acid (Asp)<sup>55</sup>. The incorporation of these probes into streptavidin allowed the detection of biotin binding at nM concentrations by changes in FRET between an endogenous Trp residue and the flUAA, highlighting the utility of site-specific genetic incorporation of these probes. Several years later, Sisido's group was able to incorporate flUAAs containing 7 different derivatives of the BODIPY fluorophore and, utilizing a 4 base codon methodology, incorporate two different flUAAs into the calcium binding protein calmodulin (CaM) concurrently<sup>56</sup>. This dual incorporation allowed the group to monitor peptide binding by calcium saturated CaM using FRET from one BODIPY UAA to the other, without the concern for background fluorescence from endogenous Tyr or Trp. Sisido's continued work with flUAAs has includes L-2-acridonylalanine (Acd), a blue-wavelength fluorescent amino acid with a long fluorescence lifetime and resilience to photobleaching (**Figure 1.1**)<sup>57</sup>. A general limitation of UAA incorporation using semi-synthetic tRNAs is that the aa-tRNAs are labor intensive to fabricate and prone to hydrolysis. These factors constrain applications to *in vitro* work or micro-injections into large cells. Sisido has since published work utilizing a double alanine EF-Tu mutant (E215A and D216A in *E. coli*) capable of tighter binding to Acd and other polyaromatic UAAs to decrease hydrolysis rates, but this still requires the semi-synthesis of the UAA-tRNA prior to each application.

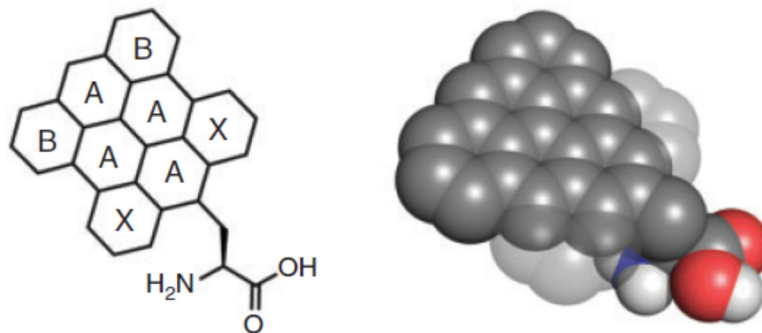


**Figure 1.5:** ‘Honeycomb’ Model of Ribosomal Permissivity. This model, based on Sisido’s work,<sup>54</sup> shows where benzene rings can be attached to the  $\beta$ -carbon of an amino acid for successful ribosomal incorporation. A denotes well-tolerated positions, B denotes moderately tolerated positions, and X denotes forbidden positions.

## ORTHOGONAL AMINOACYL-tRNA SYNTHETASES

Acknowledging the limitations of the use of semi-synthetic misacylated amber suppressor tRNAs for the production of large quantities of site-specific unnatural amino acid mutants of proteins, R. Furter pioneered the use of an orthogonal aaRS/amber suppressor tRNA pair (o-aaRS/tRNA pair) *in vivo* system (**Figure 1.6**)<sup>58</sup>. Using an *E. coli* strain resistant to the incorporation of phenylalanine (Phe) derivatives in conjunction with a permissive yeast Phe aaRS/amber suppressor tRNA pair, Furter was able to site-specifically incorporate *p*-fluorophenylalanine into proteins *in vivo*. The choice of this exogenous aminoacylation system for use in the analog resistant *E. coli* strain was crucial to Furter’s success; the yeast enzyme and tRNA are orthogonal to the *E. coli*’s aminoacylation machinery, that is, there is no cross reaction between the macromolecules from either organism. Explicitly, orthogonality in this context means that no *E. coli* aaRS is capable

of aminoacylating the yeast tRNA and the yeast Phe aaRS is incapable of aminoacylating any *E. coli* tRNA. This orthogonality allowed for the *in vivo* aminoacylation of the yeast amber suppressor tRNA exclusively by the permissive yeast Phe aaRS while the fidelity of the *E. coli* aaRSs and tRNAs remained robust. Aside from greatly reducing the synthetic burden of site-specifically incorporating an unnatural amino acid into a protein, Furter's orthogonal aaRS/amber suppressor tRNA method allowed for production of mutant proteins at yields as high as two-thirds that of the analogous wild-type protein.

In 2001, Schultz was able to tremendously expand upon Furter's use of the o-aaRS/tRNA pair technology by devising protocols to evolve novel o-aaRS/tRNA pairs *in vivo*<sup>59</sup>. After some initial difficulty in crafting an o-aaRS/tRNA pair deriving from a human or yeast source for use in *E. coli*, Schultz's group began examining the factors that could lead to complete orthogonality<sup>60</sup>. In addition to the parameters for orthogonality identified by Furter, Schultz and coworkers stressed the importance of picking an o-aaRS/tRNA pair that has a small dependence of tRNA recognition by the aaRS in the anticodon loop. Such a characteristic was seen as essential for effective amber suppression so that when the anticodon is mutated to CUA, the affinity for the tRNA by the aaRS is maintained. The tyrosyl aaRS/tRNA pair from the archaea *Methanococcus jannaschii* had previously been shown to be orthogonal to the *E. coli* translation machinery in addition to a minimal recognition of the anticodon by the aaRS, and as such was selected for optimization by the Schultz group<sup>61</sup>. To ensure complete orthogonality, the group mutated 11 nucleotides of the tRNA randomly (in addition to mutating the anticodon to CUA) and the resulting o-tRNA was subjected to negative selection in *E. coli*. This negative selection involved inserting a UAG codon in the middle of the coding sequence of the toxic protein barnase,

and then transforming the resulting plasmids, along with a plasmid containing the mutant o-tRNA, into *E. coli*. If the *E. coli* cultures survived, then the candidate o-tRNA was mutated in such a way that its orthogonality was maintained and thus it was not aminoacylated by an endogenous *E. coli* aaRS, preventing production of full-length barnase.

A similar strategy was used to create the mutant o-aaRS enzyme. Based on the crystal structure of a homologous tyrosyl aaRS from *Bacillus stearothermophilus*, the Schultz group identified five residues in the active site that were within close proximity of the hydroxyl group of Tyr. These residues were initially all mutated to Ala and then the resulting DNA construct was subjected to random mutagenesis at these sites. The group combined this library of mutant o-aaRS enzymes with the o-tRNA they had crafted, and used this pair in several rounds of positive selection. Unlike the negative selection used for the generation of the o-tRNA, this procedure involved inserting a TAG codon into the DNA sequence (corresponding to a UAG mRNA codon) of chloroamphenicol acetyltransferase (CAT) and growing *E. coli* cultures in the presence of chloroamphenicol and an unnatural amino acid. *E. coli* cultures that survived exposure to chloroamphenicol were hypothesized to insert either the UAA or an endogenous amino acid in response to the UAG codon to produce full-length CAT. As the probability of either scenario was equal, the surviving *E. coli* strains and their mutant o-aaRS/tRNA pairs were then subjected to the same negative selection used for the generation of the o-tRNA. Just as in the process for generating the o-tRNA, surviving *E. coli* cultures maintained orthogonality and did not produce the full-length toxic protein barnase. The Schultz group, among others, has continued to use this *in vivo* evolution method, or similar

strategies, to develop a broad suite of o-aaRS/tRNA pairs capable of utilizing a diverse catalog of unnatural amino acids bearing novel functional groups or possessing unique properties<sup>62</sup>. Furthermore, several refinements of the o-tRNA sequence have been published that lead to better recognition by components of the *E. coli* translation machinery such as elongation factor thermo unstable (EF-Tu)<sup>63</sup>.

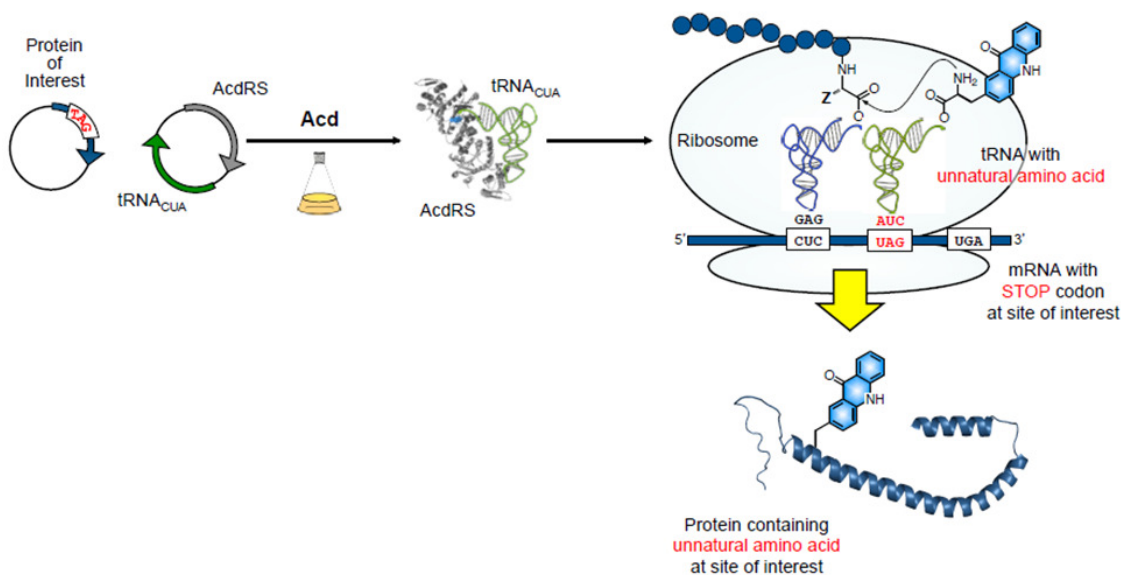


**Figure 1.6:** Schematic Diagram of Amber Suppression Technology Utilizing an O-aaRS/tRNA Pair.

Since the technology for the development of o-aaRS/tRNA pairs relies on selecting against only endogenous components, it would be theoretically possible for an o-aaRS/tRNA pair to have activity for other unnatural amino acids for which it was not evolved. R. Mehl, a former member of the Schultz laboratory, has pioneered the screening of o-aaRS/tRNA pairs for their permissivity<sup>64</sup>. Noting that it is labor intensive to craft an o-aaRS/tRNA pair *de novo* for each new unnatural amino acid that one may desire to utilize as well as the fact that many useful functional groups are essentially isosteric (for example the cyano, ethynyl, and azide moieties), Mehl's group began

screening previously evolved o-aaRS/tRNA pairs for their ability to use unnatural amino acids structurally similar to the one for which they were evolved. Gratifyingly, this approach has been tremendously successful and the Mehl group has been able to incorporate many structurally similar unnatural amino acids using only a few mutant o-aaRS/tRNA pairs. While modest mutants may eventually prove useful or necessary to improve the affinity of the pair for a given unnatural amino acid, this requires much less time and finesse than *de novo* generation of o-aaRS/tRNA pairs.

### SITE-SPECIFIC INCORPORATION OF NOVEL FLUORESCENT AMINO ACIDS

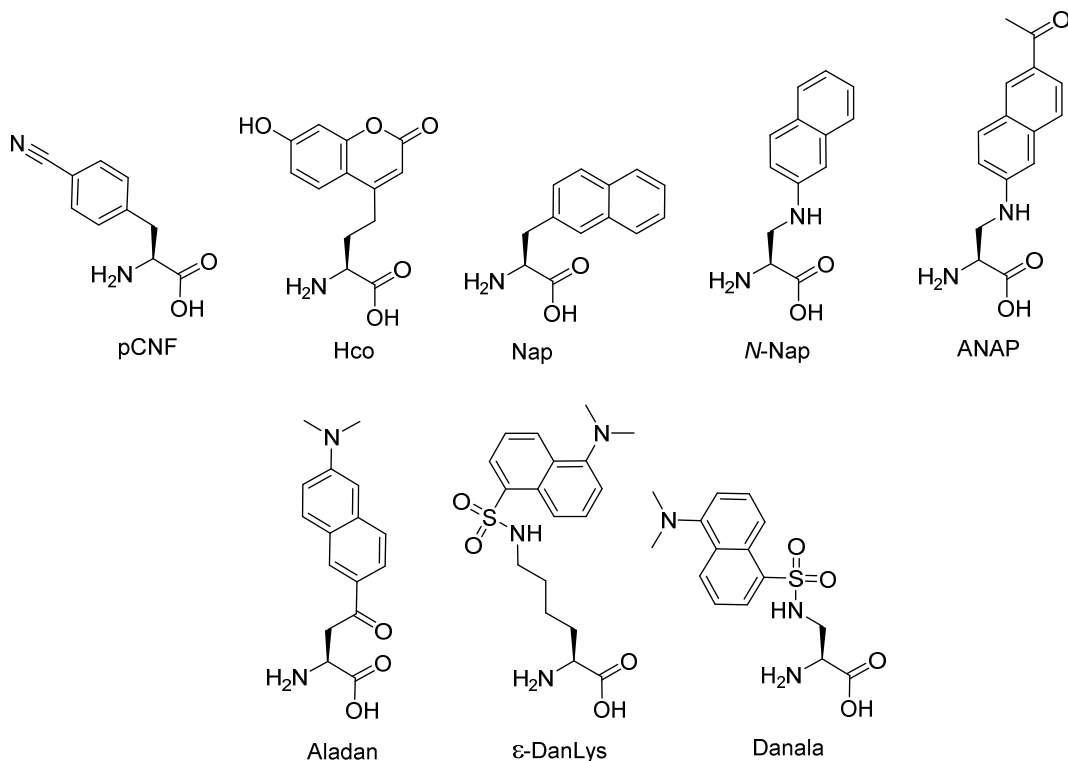


**Figure 1.7:** Line Diagrams of Ribosomally Permissible fUAAs Discussed in This Section.

While an o-aaRS/tRNA pair was first developed to incorporate *p*-cyanophenylalanine (pCNF) site-specifically into proteins as an IR probe, the molecule had previously been

used in synthetic peptides as a FRET donor to Trp<sup>65</sup>. With this in mind, R. Mehl and S. Brewer evolved a new o-aaRS/tRNA pair capable of utilizing both pCNF and the structurally similar flUAA 4-ethynylphenylalanine (pENF) which is also a FRET partner with Trp<sup>66</sup>. pCNF fluorescence has been shown to be extremely sensitive to its surrounding environment. Since the nitrile moiety is capable of hydrogen bonding with bulk water as well as other polar functionalities, D. Raleigh and I. Carrico advise that interpretation of fluorescence measurements in which pCNF changes environment to be done in conjunction with IR measurements<sup>67</sup>. Furthermore, it was found by these investigators that pCNF is also quenched by Tyr and His, albeit at shorter distances than Trp, making donor only controls crucial for interpreting pCNF FRET data<sup>10</sup>. However, with these proper controls, pCNF can be used effectively to measure distances in proteins with an appropriate FRET partner. Other work in the Petersson laboratory, both with synthetic peptides and semi-synthetic proteins, has shown that pCNF is capable of being quenched by backbone thioamides in the context of CaM and the Parkinson's disease protein  $\alpha$ -synuclein<sup>68</sup>.

7-hydroxycoumarin is a small well known fluorophore possessing a high quantum yield, a large Stoke's shift, and, due to the phenol moiety's pKa of roughly 7.8, a pronounced sensitivity to environmental conditions. While the use of this fluorophore had previously been limited to semi-synthetic applications, P. G. Schultz and coworkers were able to evolve an o-aaRS/tRNA pair capable of selectively using an amino acid with the 7-hydroxycoumarin moiety in the amino acid side-chain (Hco)<sup>69</sup>. The initial studies reported in conjunction with the identification of the o-aaRS/tRNA highlighted the environmental sensitivity of the fluorophore; urea chemical denaturation of myoglobin

containing a buried Hco residue showed a positive correlation between the fraction of protein unfolded and an increase in Hco fluorescence, in line with the solvatochromic properties of the fluorophore. The Schultz group continued to exploit the environmental sensitivity of Hco in another study where they incorporated Hco into an antibody and monitored binding of its antigen *via* changes in Hco fluorescence<sup>70</sup>. They noted that it would not have been possible to attach a fluorophore site-specifically using the common method of labeling Cys residues with a fluorophore-maleimide conjugate as several disulfide bonds are required for proper folding of the antibody. Another use of Hco's environmental sensitivity that more explicitly relies on the dynamics of the fluorophore's phenol and its acid/base activity was reported by L. Wang and colleagues<sup>71</sup>. Using the published o-aaRS/tRNA for Hco, the group site-specifically incorporated Hco into the homodimeric substrate protein signal transducer and activator of transcription 3 (STAT3) in order to study the dynamics of phosphorylation of a specific Tyr residue. When properly folded, STAT3 forms a SH2 domain where Trp564 of one monomer is proximal to Tyr705 of the other. Moreover, Trp564 is distal to the Tyr705 residue on the same monomer unit. Thus, by mutating Trp564 to Hco, L. Wang envisioned that the fluorophore's emissions would change in response to the presence or absence of a negatively charged phosphate group on Tyr705 on the other subunit. Their results showed a 13-fold increase in Hco fluorescence upon phosphorylation of Tyr705. This fluorescence increase was shown to be reversible upon addition of the dephosphorylase CIP, highlighting the ability of this technique to truly monitor phosphorylation dynamics of a specific amino acid residue. Furthermore, the experimenters point out that Trp564

and the SH2 domain are well conserved in other STAT proteins, making this a general technique for studying phosphorylation of these substrate STAT proteins.

E. Chapman, in collaboration with P. G. Schultz, has used Hco to monitor the *in vivo* localization of specific proteins in *E. coli*. Two extensively studied *E. coli* proteins, the chaperonin GroEL and the bacterial tubulin homolog FtsZ, have previously proven elusive to accurate visualization in fluorescence localization studies, as fusion to FPs renders these proteins nonfunctional<sup>72</sup>. Attempting to resolve the controversy<sup>73</sup> over whether heat shock induces a change in GroEL cellular localization in conjunction with upregulation, the experimenters installed Hco at position 129 of GroEL and monitored fluorescence recovery after photobleaching (FRAP) with irradiation of a specific portion of single cells<sup>74</sup>. Under all tested stress and heat shock conditions, it was shown that GroEL distribution remained diffuse as there were no significant changes in FRAP relative to cells treated under normal conditions. Additionally, the Hco mutant GroEL was shown to be functional by both ATPase activity in a malachite green assay and its ability to refold and restore enzymatic activity to malate dehydrogenase. Chapman and Schultz's study of FtsZ, done with the aid of the groups of C. Jacobs-Wagner and A. Løbner-Olesen revealed that site-specific Hco incorporation allowed the monitoring of cytoskeletal assembly in living *E. coli* cells with fluorescence microscopy<sup>75</sup>. Mutating Ala10 to Hco with amber suppression technology yielded a FtsZ mutant that was shown to be functional by GTPase activity and subsequent induced polymerization. This functionality allowed the experimenters to knock out endogenous FtsZ and prepare *E. coli* cells containing exclusively Hco10 labeled FtsZ to monitor the polymerization dynamics of the protein. As FP fusion mutants of FtsZ were nonfunctional, previous

experiments had required the co-expression of wild-type FtsZ and thus meant lower resolution in fluorescence images as not all FtsZ molecules were fluorescent.

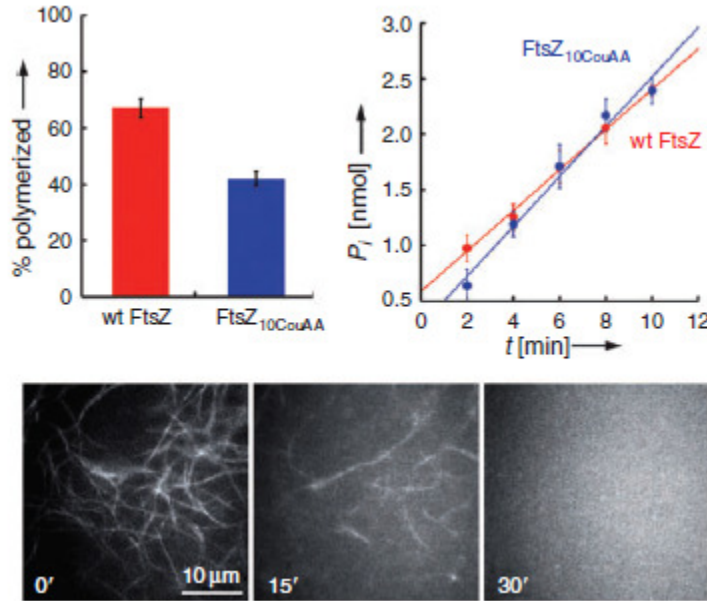


**Figure 1.8:** Tracking FtsZ Depolymerization in Cells Using Hco. FtsZ<sub>10CouAA</sub> (Hco = CouAA) shows a small (~20 %) decrease in polymerization ability (top left) while maintaining GTPase activity close to wild type wt (top right). A time-course depolymerization of FtsZ<sub>10CouAA</sub> at 0, 15, and 30 min following addition of GTP (bottom three panels). Adapted figure reproduced from Charbon *et al.* with permission from Wiley-VCH<sup>75</sup>.

7-hydroxycoumarin's 464 nm emission is well suited to FRET interactions with other exogenous fluorophores such as the BODIPY dyes, making it a useful probe for quantitative binding measurements in biophysical assays. S. Shan's research group used the Hco o-aaRS/tRNA system *in vitro* to generate ribosome-nascent chain complexes (RNCs) where the nascent peptide chain contained a Hco residue<sup>76</sup>. The experimenters noted that they chose to use the o-aaRS/tRNA method as opposed to chemically acylated semi-synthetic tRNA to reduce the amount of Hco used since the enzymatic method gives

higher yields with less material by regenerating hydrolyzed aa-tRNA. As the ribosome has been shown to nonspecifically bind hydrophobic compounds, such as polyaromatic fluorophores like Hco, Shan and coworkers had to keep free Hco concentrations at 50  $\mu\text{M}$  or lower to yield RNCs with Hco only in the backbone of the nascent chain. With these fluorescent RNCs in hand, Shan's group then mutated a nonconserved residue in the signal recognition particle (SRP) to Cys and labeled it with BODIPY-maleimide to create a FRET acceptor to test the functionality of the RNCs. Upon addition of BODIPY-SRP to a solution of RNCs with Hco in the nascent chain, energy transfer was observed with an efficiency of 0.8 at saturating concentrations of labeled SRP. This FRET assay was shown to be specific by a lack of energy transfer in BODIPY-SRP titrations with Hco-RNCs containing a nascent chain engineered to not to be a substrate for SRP. Shan further demonstrated the functionality of the Hco-RNCs by using the calculated FRET efficiency and equilibrium titrations to calculate a  $K_d$  value that agreed with others reported previously for similar complexes. These experiments demonstrate the utility of genetically encoded amino acids to prepare site-specifically labeled complex biomolecules.

The second UAA reported to be site-specifically incorporated *in vivo* in *E. coli* by the Schultz lab was the weakly fluorescent L-3-(2-naphthyl)alanine (Nap)<sup>77</sup>. They also engineered an o-aaRS/tRNA pair derived from an *E. coli* LeuRS for incorporation of Nap in *Saccharomyces cerevisiae*. As the fluorescence properties of this UAA are not particularly useful, this report was more significant for the role of Nap in the development of o-aaRS/tRNA pairs containing large side-chains such as Hco and 3-(6-acetylnaphthalen-2-ylamino)-2-aminopropanoic acid (ANAP). When initial evolution

experiments aimed at creating a o-aaRS/tRNA pair for ANAP failed, Schultz's group attempted to use the pair evolved for Nap as a starting point and engineer specificity for the 6-acetyl group<sup>78</sup>. This strategy proved to be far more successful than their earlier trials and yielded an o-aaRS/tRNA pair for ANAP incorporation in *S. cerevisiae*. Like Hco, ANAP is extremely environmentally sensitive. To probe the utility of monitoring changes in ANAP fluorescence in response to changes in local environment the Schultz group incorporated ANAP into a glutamine-binding protein (QBP) from *E. coli*. This protein contains two globular domains which symmetrically surround a Gln binding site. By mutating a residue within this binding site, Asp160, it was envisioned that the movements of the two globular domains in response to Gln binding could be monitored by changes in ANAP fluorescence. Their experiments showed a large shift in  $\lambda_{em}^{max}$  from 480 nm to 430 nm with fluorescence at 430 nm increasing 5 fold upon addition of Gln. There were no significant changes in fluorescence anisotropy between the Gln bound and free forms of QBP, demonstrating that the change in ANAP fluorescence was due solely to changes in the local environment.

Since the ANAP o-aaRS/tRNA was evolved from an *E. coli* LeuRS, it is orthogonal to all eukaryotic systems, including mammalian cells. In 2013, Schultz and coworkers reported the use of ANAP and its o-aaRS/tRNA in live HEK293 and CHO cells<sup>79</sup>. By designing mutants of several proteins whose cellular localizations were well known, the experimenters demonstrated the ability of site-specifically incorporated ANAP to reliably report on the cellular trafficking of proteins *in vivo*. Additionally, since ANAP is capable of two-photon excitation, the group used this technique to image ANAP containing proteins, rendering this technology applicable to use in situations where light penetration

or phototoxicity from conventional light sources is problematic. A study published concurrently by the group of R. Blunck used the ANAP o-aaRS/tRNA system to site-specifically label K<sub>v</sub> channels in *Xenopus* oocytes<sup>80</sup>. While a fUAA has previously been incorporated site-specifically into an ion channel protein in *Xenopus* oocytes using chemically acylated semi-synthetic tRNA<sup>81</sup>, the Blunck group found that the use of the orthogonal enzymatic system allowed for higher expression levels. The most effective method for simultaneously monitoring the functional and structural dynamics of membrane ion channels is voltage-clamp fluorometry (VCF). Traditionally VCF is limited to the use with labeled Cys-mutant proteins, which are viable only when labeled at surface-accessible residues. This method is accurate because it gives fluorescence data in direct response to changes in voltages applied to cell membranes. However its resolution is limited by the sensitivity of the fluorophore, its proximity to the site of voltage-dependent movement, and perturbations to channel structure due to probe installation. Therefore, Blunck's group used the ANAP o-aaRS/tRNA system to genetically incorporate ANAP at positions most crucial for monitoring the protein's dynamics and not limited by solvent accessibility: V234 (S1 helix; proximal to lower S4 helix), A359 (upper S4 helix), and H486 (lower S6 helix, near C-terminus). By installing ANAP at these positions, the experimenters were able to collect data on the entire gating event beginning with "pre-gating" closed state transitions and up to complete pore opening. Specifically, the group found that the early closed state transitions were only observed in the N-terminal region of the S4 helix and, despite identical voltage dependence, the N-terminal and C-terminal portions of S4 change conformation discontinuously. Additionally, the group found three transitions in the voltage sensor

movements, in line with a hypothesized kinetic model generated from electrophysiological measurements by Schoppa and Sigworth<sup>82</sup>. Blunck's work showed that the use of genetically incorporated flUAAs allow VCF measurements with higher temporal and structural resolution than those made with post-translationally labeled Cys mutants.

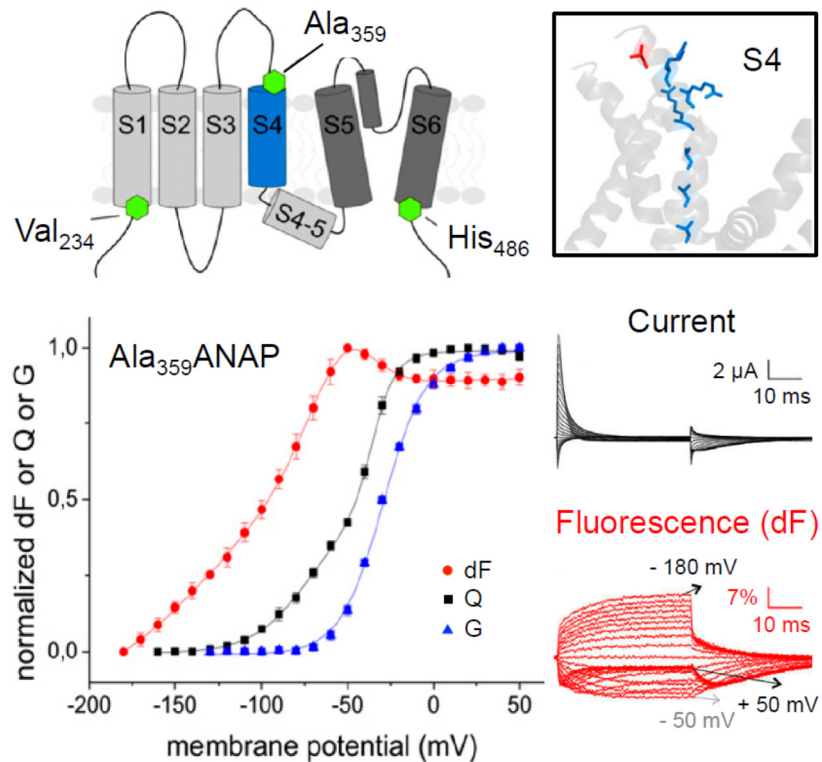


**Figure 1.9:** Simultaneous Observation of Conformational Change and Conductance in a  $K_v$  Channel. Top left: cartoon of transmembrane segments S1-S6 of  $K_v1.2/2.1$  chimera protein. Top right:  $K_v1.2/2.1$  S4 domain, residue  $Ala_{359}$  (location of ANAP installation) is marked in red and Arg residues are shown in blue. Bottom left: fluorescence (dF, red), gating charge (Q, black), and conductance (G, blue) as a function of membrane potential in the  $Ala_{359}ANAP$  mutant. Gating currents and ANAP fluorescence responses after pulses from -90 mV to potentials between -180 and 50 mV. Adapted figure reproduced from Kalstrup *et al.* with permission © (2013) from the National Academy of Sciences<sup>80</sup>.

In similar experiments, the labs of L. Y. Jan and S. Boxer showed that a fluorophore similar to ANAP, Aladan, was tolerated in the translation machinery of *Xenopus* oocytes and were able to create Kir2.1 and *Shaker* potassium channels containing Aladan at various sites<sup>83</sup>. Other work in the lab, with Aladan installed into the IgG-binding domain GB1 *via* solid phase peptide synthesis, replicated the work of A. R. Chamberlin and showed that the fluorescence maxima of the fluorophore is shifted in the context of a protein. By comparing the fluorescence spectra of Aladan at both buried and solvent accessible sites, and ensuring that the orientation of the fluorophore did not change by anisotropy experiments, the experimenters were able to show that changes in Aladan fluorescence can accurately be used to reflect changes in its local environment.

Specifically they found that the more exposed Aladan was to bulk solvent (water) the greater the degree of a bathochromic shift and decrease in fluorescence intensity.

The dansyl fluorophore has been site-specifically incorporated into proteins utilizing a variety of methods and on a variety of amino acid scaffolds. It was first shown to be ribosomally permissible by the lab of A. R. Chamberlin in 1996 when it was site-specifically incorporated into  $\beta$ -galactosidase as  $\epsilon$ -dansyllysine ( $\epsilon$ -danLys) using semi-synthetic tRNA methods<sup>84</sup>.  $\epsilon$ -DanLys was shown to be directly excited at 280 and 295 nm, along with endogenous Trp residues, and selectively excited at the lower energy absorption band of 340 nm. Excitation at 340 nm revealed a fluorescence emission maximum at roughly 500 nm, which is shifted from the spectrum of the fluorophore in water, but in good agreement with spectra of proteins labeled posttranslationally with dansyl chloride.

In 2006, P. G. Schultz and coworkers were able to develop an o-aaRS/tRNA pair, derived from the *E. coli* LeuRS for use in *S. cerevisiae*, capable of utilizing 3-(5-(dimethylamino)naphthalene-1-sulfonamide)propanoic acid (danAla), a fUAA containing the dansyl fluorophore on a unique scaffold<sup>85</sup>. In line with previous reports, Schultz's group found that when danAla was installed at a buried location (Trp33) within the well folded protein human superoxide dismutase (hSOD) the fluorescence increased in intensity and its maxima was blue-shifted. When the protein was chemically denatured with guanidinium hydrochloride, the fluorescence of danAla at buried locations decreased in fluorescence intensity and its blue-shift was relieved. This was shown to be a useful measure of changes in the environment around position 30 in hSOD as the same experiments with the solvent exposed residue 16 (natively Gln) showed no change in response to chemical denaturation.

Like the o-aaRS/tRNA pair for ANAP, the *E. coli* origin of the danAla pair allows its use in a broad suite of eukaryotic systems. L. Wang and coworkers used the technology to incorporate danAla at two sites in the voltage-sensitive domain (VSD) of *Ciona intestinalis* voltage-sensitive phosphatase (CiVSD)<sup>86</sup>. Since there have been reports of CiVSP having different movement speeds in response to the same gating charge between mammalian cells and *Xenopus* oocytes, L. Wang's group conducted their experiments in the neuronal stem cell HCN-A94. Using the rat *Shaker* potassium channel as a model, they created an *in silico* model of CiVSD and picked residues Phe234 and Gln208 as sites to mutate to danAla as these sites are on opposite ends of helix S4 and thus could report on its voltage-dependent movement. As Phe234 is on the intracellular face of the protein and exposed to bulk cytosol, it had proven difficult to label with post-translational

techniques and thus was a prime candidate for study with a genetically incorporated fUAA. The group's results showed that the Phe234danAla mutant showed an increase in fluorescence, indicating a movement of the fluorophore into a less polar environment, while the Gln208danAla mutant showed the opposite. These findings, including the first fluorescence measurement for a label at position 234, showed that the ends of S4 move in opposite directions in response to membrane depolarization. Furthermore, the fact that a slightly more positive membrane voltage was required to depolarize the Gln208danAla mutant relative to wild-type, suggests that the more hydrophobic fluorophore was buried in the hydrophobic lipid membrane, requiring a greater driving force to move. This result, while speculative, is entirely in line with the observed decrease in fluorescence intensity (movement from a hydrophobic to a hydrophilic environment) upon membrane depolarization in this mutant. L. Wang has continued to expand the use of the o-aaRS/tRNA pair in complex systems, including a report of its use in *Caenorhabditis elegans*<sup>87</sup>.

## **SITE-SPECIFIC INCORPORATION OF A FLUORESCENCE QUENCHING PROBE**

The site-specific genetic incorporation of fluorescence probes is not limited to just fluorophores themselves. First used by M. Sisido as early as 1998, *p*-nitrophenylalanine (pNO<sub>2</sub>-F), a ribosomally permissible UAA, has been shown to efficiently accept electrons from the excited states of pyrenyl,  $\beta$ -anthraniloyl, and indole fluorophores, effectively quenching their fluorescence<sup>88</sup>. However early reports by Sisido used chemically acylated

semi-synthetic tRNA and, like early genetically incorporable fUAAs, suffered from low yields and limited applications. In 2006, P. G. Schultz's group evolved an o-aaRS/tRNA pair for use in *E. coli* capable of using pNO<sub>2</sub>-F<sup>89</sup>. Using a model GCN4 leucine zipper protein that is known to spontaneously assemble into parallel coiled-coil homodimers, the group made both single pNO<sub>2</sub>-F and Trp mutants (GCN4 does not natively contain any Trp residues). By adding stoichiometric amounts of F22pNO<sub>2</sub>-F mutant GCN4 into solutions of various GCN4 Trp mutants, the experimenters were able to calculate distances between Trp residues and pNO<sub>2</sub>-F residues by changes in quenching efficiency. As pNO<sub>2</sub>-F has been shown to quench the fluorescence of both endogenous and exogenous fluorophores and an o-aaRS/tRNA has been developed for its genetic incorporation in *E. coli*, it serves as a compliment to the several genetically encodable fUAAs.

## **TOWARDS MORE MINIMALISTIC PROBES FOR FLUORESCENCE AND FUNCTIONAL STUDIES**

Acknowledging the need for truly minimalist site-specific probes to more accurately study protein structure and dynamics, the Petersson lab strives to provide such tools to the biophysical community. We identified Acd as part of a robust study of the ability of red-shifted fluorophores to transfer energy to thioamides, a single atom substitution of the polypeptide backbone capable of quenching fluorescence through a variety of mechanisms. Acd is a ribosomally permissible fluorescent amino acid that possesses a long lifetime ( $\tau = 16$  ns), resilience to photobleaching, a near unity quantum yield ( $\phi =$

0.95), and visible wavelength emission. While previous literature reports relied on semi-synthetic tRNA methodology and *in vitro* translation reactions to site-specifically install Acd into proteins, we, in conjunction with Professor R. A. Mehl of Oregon State University, have identified a permissive o-aaRS/tRNA pair capable of using Acd as a substrate. Furthermore, we have used this orthogonal enzymatic pair to site-specifically incorporate Acd into three proteins and characterize the dynamics of Acd with respect to changes in its local environment and proximity to both endogenous and exogenous fluorescent amino acids.

In addition to work with Acd and other minimally perturbing fluorescent probes, we have collaborated extensively with the C. J. Deutsch laboratory in the Physiology Department of the Perelman School of Medicine at the University of Pennsylvania to study the traversal of nascent peptides through the ribosomal exit tunnel. Previous studies by the Deutsch group have probed the accessibility of Cys residues on a nascent peptide as a way of determining the contours of the exit tunnel as a function of the primary or second structure of a nascent peptide. The results of these studies have indicated that nascent peptides and/or the tunnel rearrange to accommodate sterically large side-chains. To expand upon this, we have worked with the group to explore the difference in transit time of nascent peptides bearing UAAs with unusually large side-chains. These new methods, which involve the probes being ribosomally incorporated as opposed to post-translationally attached, are aimed at better elucidating effects of large sidechains on the time-course of protein elongation and folding in the exit tunnel. Thus, these methods represent a type of minimalistic chemical probe of protein folding, to complement minimalist fluorescent probes such as Acd and its derivatives.

**CHAPTER 2: ACRIDON-2-YLALANINE: SYNTHESIS, *IN VIVO*  
INCORPORATION, AND BIOPHYSICAL STUDIES**

Adapted in part with permission from Goldberg, J. M.; Speight, L. C.; Fegley, M. W.; Petersson, E. J., Minimalist Probes for Studying Protein Dynamics: Thioamide Quenching of Selectively Excitable Fluorescent Amino Acids. *Journal of the American Chemical Society* **2012**, *134* (14), 6088-6091. Copyright (2012) American Chemical Society and Speight, L. C.; Muthusamy, A. K.; Goldberg, J. M.; Warner, J. B.; Wissner, R. F.; Willi, T. S.; Woodman, B. F.; Mehl, R. A.; Petersson, E. J., Efficient Synthesis and In Vivo Incorporation of Acridon-2-ylalanine, a Fluorescent Amino Acid for Lifetime and Forster Resonance Energy Transfer/Luminescence Resonance Energy Transfer Studies. *Journal of the American Chemical Society* **2013**, *135* (50), 18806-18814. Copyright (2013) American Chemical Society.

## **BACKGROUND: ACD PRIOR STUDIES AND PHOTOPHYSICS**

Acridon-2-ylalanine (Acd), a ribosomally permissible fluorescent unnatural amino acid (fUAA) with numerous robust photophysical characteristics, was chosen as a target unnatural amino acid (UAA) for the identification of an orthogonal aminoacyl tRNA synthetase/tRNA (o-aaRS/tRNA) pair to extend its use to *in vivo* applications. The Mehl group's strategy of screening previously evolved mutant o-aaRS/tRNA pairs for their permissivity was chosen as the group had previously worked with UAAs of similar shapes and sizes such those with a benzophenone side-chain. Acd's side-chain fluorophore, a linear fusion of three six-membered rings, is truly a minimalistic probe with a volume of 222 Å<sup>3</sup> making it only modestly larger than Trp (47 % larger; for comparison, fluorescein is > 200 % larger). While this does infer a nontrivial increase in size when replacing a Trp or Tyr residue with Acd, the steric cost of such a substitution comes with several payoffs in terms of fluorescence properties. Acd is a blue wavelength fluorophore with its most useful  $\lambda_{\text{abs}}$  for excitation at 386 nm,  $\lambda_{\text{em}}$  at 420 – 450 nm, a near unity quantum yield in water ( $\Phi = 0.95$ ), modest molar extinction coefficient ( $\epsilon = 5700 \text{ cm}^{-1}$ ), resistance to photobleaching (< 5 % photobleaching after 3 hours of continuous irradiation), and an unusually long fluorescence lifetime ( $\tau = 16 \text{ ns}$ )<sup>57, 90, 91</sup>.

Initial investigations of Acd in the Petersson laboratory involved pairing it with a minimalistic fluorescence quenching probe studied by the group: the thioamide<sup>91</sup>. Our laboratory had previously disclosed our findings that a single atom substitution of an oxygen atom for sulfur in an amide renders the resulting moiety (a thioamide) capable of quenching the fluorescence of endogenous fluorophores such as Tyr and Trp as well as

exogenous probes such as pCNF<sup>92, 93</sup>. However these experiments were limited by the fact that it is difficult to selectively excite these probes in the context of a protein harboring more than one of these residues or in complex mixtures such as cell lysates. In our efforts to solve this problem, we investigated the ability of thioamides to quench more red shifted fluorescence probes with a particular emphasis on those capable of being installed as amino acid side-chains. Our initial studies focused on 7-azatryptophan (7-azaTrp), 7-methoxycoumarin (Mcm), and Acd (**1**) (**Figure 2.1**). Since both 7-azaTrp and Mcm are excited below 350 nm and thioamides absorb very strongly in this region of the spectrum, it was difficult to quantify the quenching effects in Stern-Volmer experiments. Acd fortunately did not display this issue as it is capable of direct excitation by irradiation at 386 nm which is significantly removed from the absorption spectrum of a thioamide. Additionally, Acd has the added benefit of its high quantum yield in water when compared to the other studied probes ( $\phi_{7\text{azaTrp}} = 0.01$  and  $\phi_{\text{Mcm}} = 0.18$ ). Additionally, it is important to note that the emission spectra of neither Acd nor 7-azaTrp or Mcm overlap with the absorption profile of a thioamide, making the mechanism of this quenching Photo-induced Electron Transfer (PET).

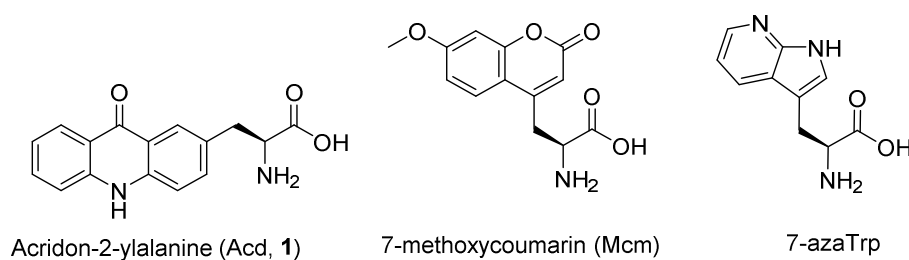


**Figure 2.1:** Line Diagrams of Acd, Mcm, and 7-azaTrp.

Titration of a prototypical thioamide, thioacetamide, into solutions of Acd to create a Stern-Volmer plot revealed that the fluorescence of Acd varied inversely with thioacetamide concentration (**Figure 2.2**). Furthermore, the Stern-Volmer constant,  $K_{SV}$ , increased with temperature suggesting that the observed quenching interaction may result from a dynamic electron transfer event. To further characterize the quenching, time-correlated single photon counting (TCSPC) spectroscopy was used to examine the change in Acd fluorescence lifetimes in the presences of varying concentrations of thioacetamide. These experiments revealed a  $K_{SV}$  that agreed well with the steady-state measurements and all lifetime data could be fit with a single exponential function (**Figure 2.3**).

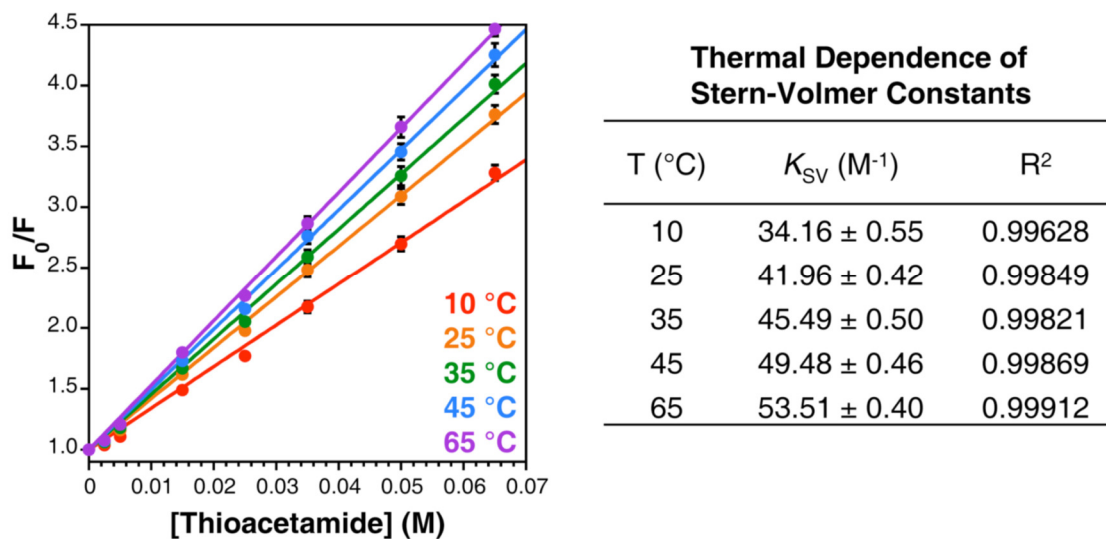


**Figure 2.2:** Steady-State Stern-Volmer Experiments with Acd and Thioacetamide. Left: Stern-Volmer plots of thioacetamide quenching Acd at several temperatures. Error bars are calculated from standard error. Right: Stern-Volmer constants and goodness-of-fit values for each temperature. Reprinted with permission from Goldberg, J. M.; Speight, L. C.; Fegley, M. W.; Petersson, E. J., *Minimalist Probes for Studying*

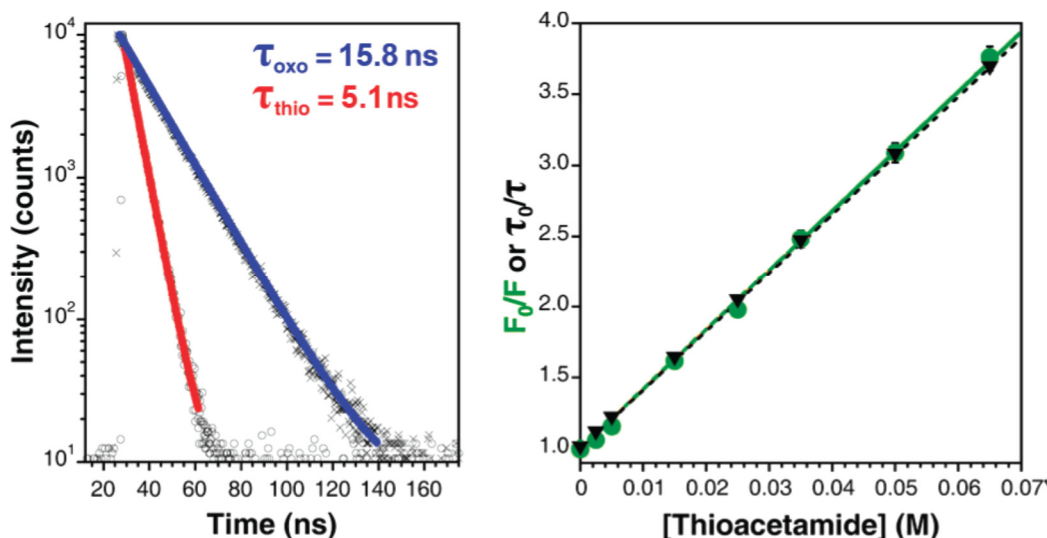


**Figure 2.3:** Dynamic Stern-Volmer Quenching of Acd. Left: Fluorescence lifetime measurements of 2  $\mu$ M Acd in 100 mM phosphate buffer, pH 7.00 at 25  $^{\circ}$ C in the presence of 50 mM acetamide (X, blue fit) or 50 mM thioacetamide (O, red fit). Heavy lines are single exponential fits to the raw data. Right: Stern-Volmer plots of Acd fluorescence intensity (green circles) and lifetime (black triangles) as a function of thioacetamide concentration; error bars represent standard error. Reprinted with permission from Goldberg, J. M.; Speight, L. C.; Fegley, M. W.; Pettersson, E. J., Minimalist Probes for Studying Protein Dynamics: Thioamide Quenching of Selectively Excitable Fluorescent Amino Acids. *Journal of the American Chemical Society* **2012**, *134* (14), 6088-6091. Copyright (2012) American Chemical Society.

To demonstrate the practical utility of the Acd/thioamide fluorescence probe pair we synthesized the well characterized short peptide, the villin headpiece subdomain (or HP35). This polypeptide has been shown by our own laboratory and others to fold into a compact structure where the N- and C-termini are within 20  $\text{\AA}$  of one another. Previously, this construct has been used in our laboratory to examine the F $\ddot{o}$ rster Resonance Energy Transfer (FRET) interaction between *p*-cyanophenylalanine (pCNF) and a thioamide;

however, in these experiments Trp<sub>23</sub> was mutated to Phe to allow for selective excitation of the pCNF fluorophore. As Acd can be directly excited in the presence of Trp, this mutation was not used and HP35 was synthesized with a C-terminal Acd residue and an N-terminal leucine (Leu) harboring a backbone thioamide. Additionally, an oxo-peptide control was also synthesized from the same batch of resin but with the final coupling being done with standard Fmoc-Leu-OH. After confirming that these substitutions did not alter the  $\alpha$ -helical fold of the peptide with circular dichroism (CD) spectroscopy, both steady-state and dynamic fluorescence spectroscopy analyses were performed. In the steady-state 16 % quenching of Acd by the thioamide relative to an oxoamide control was observed at 1 °C. This effect increased with increasing temperature with a plateau of 22 % at 66 °C and a sharp decrease to 15 % at 95 °C (**Figure 2.4**). We justified this by examining the CD spectrum of the construct undergoing a thermal melt. Transforming the data into fraction folded, we observed that as the temperature increased in the 1 – 66 °C range, the folded polypeptide became mildly disordered, thus increasing the probability of Acd contacting the thioamide and its fluorescence being quenched. This quenching effect increased until the polypeptide began to globally unfold and the distance between the probes increased.

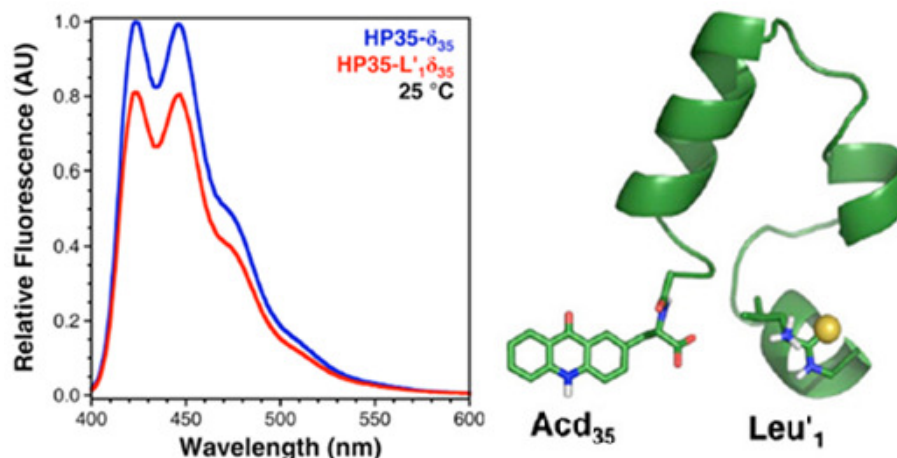


**Figure 2.4:** HP35 Model System for Thioamide Quenching of Acd. Left: Fluorescence intensities of HP35 labeled exclusively with Acd (blue trace) and HP35 labeled with Acd and thioleucine (Leu') at opposite termini (red trace). Right: Ribbon diagram of folded HP35 with Acd and thioleucine represented as line diagrams. Reprinted with permission from Goldberg, J. M.; Speight, L. C.; Fegley, M. W.; Petersson, E. J., Minimalist Probes for Studying Protein Dynamics: Thioamide Quenching of Selectively Excitable Fluorescent Amino Acids. *Journal of the American Chemical Society* **2012**, *134* (14), 6088-6091. Copyright (2012) American Chemical Society.

Interpretation of the dynamic quenching observed in the Acd/thioamide labeled HP35 required more thoughtful deconvolution. Unlike the studies with free Acd, the lifetime data of the Acd/thioamide HP35 could not be fit to a single exponential function. Instead, the dynamic quenching observed could be best fit by a biexponential fit. To understand why this deviated from the data we retrieved by the Stern-Volmer titrations, we subsequently examined the dynamic thioamide quenching of Acd in the context of short proline (Pro) and glycine (Gly) peptides. While oxoamide control peptides could be fit to single exponential functions, none of the dual labeled constructs could. Instead, a biexponential function was also necessary in these cases. The requirement of the biexponential fit in both the HP35 and short peptide examples gives evidence that there is

some quenching that is independent of the Acd/thioamide interaction. This is not an uncommon phenomenon; redox-active amino acids such as tryptophan (Trp), tyrosine (Tyr), histidine (His), methionine (Met), and cysteine (Cys), as well as terminal amines (such as the N-terminus of any polypeptide) have been shown to quench the fluorescence of fluorophores in the context of a protein<sup>10, 91, 94</sup>. The biexponential fit also indicates that there may be two populations of peptide configurations, with greater and lesser degrees of quenching.

As we began to contemplate the incorporation of Acd into large polypeptides and proteins, we sought to thoroughly examine the effect that proteinaceous functional groups could have on the fluorophore. Such environmental effects could be useful in creating dual-labeled proteins and studying changes in folding properties. Further, we deemed it necessary for us to fully understand Acd's dynamics not only for the aforementioned types of experiments, but also to create a background measurement for using Acd as a FRET or PET probe with other exogenous fluorescence probes. After performing Stern-Volmer titrations of Acd with the endogenous amino acids Tyr, Trp, Met, Cys, Met, His, and Gly, it was shown that Acd is quenched significantly by Trp and Tyr (**Figure 2.5**). The lack of spectral overlap between Acd's emissions and Trp and Tyr's absorption spectra combined with the data from both steady-state and dynamic fluorescence measurements indicated that Acd is quenched by these moieties through a PET mechanism. This mechanism has both static (where a nonemissive ground state complex is formed) and dynamic (where an electron is transferred in the excited state) components. These environmental effects reveal that these residues can be used as part of

fluorophore/quencher pairs with Acd and that other uses of Acd, such as FRET, require careful ‘Acd only’ controls to ensure proper measurements.

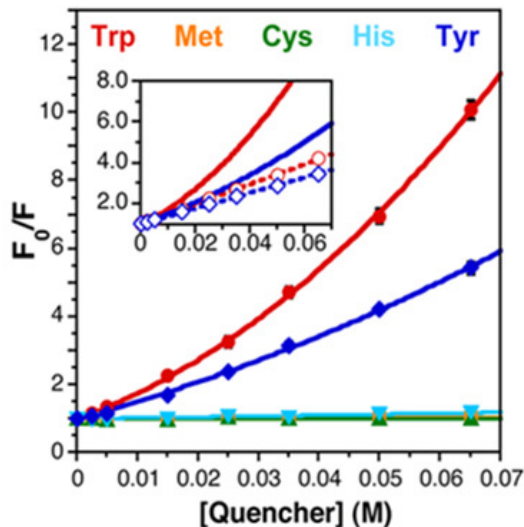


**Figure 2.5:** Acd Stern-Volmer Interactions with Endogenous Amino Acids. Quenching by endogenous amino acids assessed through steady-state fluorescence Stern-Volmer titrations with five amino acids: Trp (filled red circles), Met (orange circles), Cys (green upright triangles), His (pale blue downward triangles), Tyr (filled dark blue diamonds). Tyr methyl ester used for solubility, all other amino acids used as free acids. Inset: Fluorescence lifetime Stern-Volmer titrations with Trp (open red circles) and Tyr (open dark blue diamonds). Steady-state data shown for comparison. Reprinted with permission from Speight, L. C.; Muthusamy, A. K.; Goldberg, J. M.; Warner, J. B.; Wissner, R. F.; Willi, T. S.; Woodman, B. F.; Mehl, R. A.; Petersson, E. J., Efficient Synthesis and In Vivo Incorporation of Acridon-2-ylalanine, a Fluorescent Amino Acid for Lifetime and Förster Resonance Energy Transfer/Luminescence Resonance Energy Transfer Studies. *Journal of the American Chemical Society* **2013**, *135* (50), 18806-18814. Copyright (2013) American Chemical Society.

Due to significant overlap of Trp’s emission spectra within the excitation spectra of Acd, Trp and Acd make a reasonable FRET pair with a Förster radius ( $R_0$ ) of 23 Å. This distance allows robust distance measurements in the 13 – 37 Å range. Trp/Acd FRET

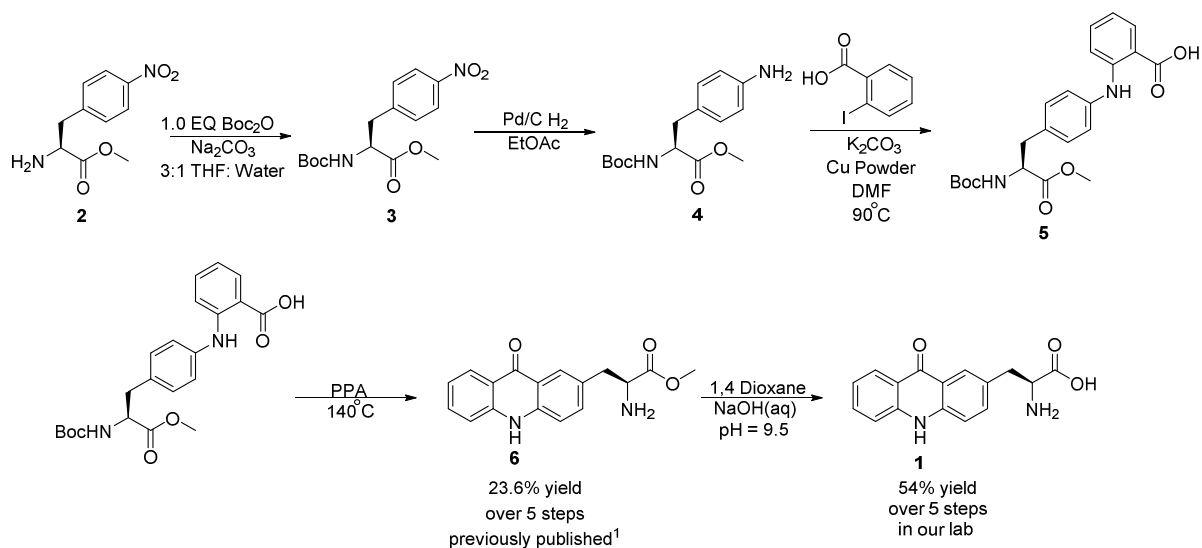
pairs would be very useful because they could be entirely genetically-encoded, eliminating the need for post-translational labeling and purification. However this probe pair is far from ideal as it is difficult to separate the PET quenching effects from a FRET interaction. Additionally, as Acd has a strong absorbance band at 260 nm, one must excite Trp at no less than 290 nm to minimize direct excitation of the acceptor in Trp/Acd FRET experiments. We then examined the utility of other probes for use as a FRET probe with Acd in order to find a pair in which FRET was the only interaction and selective excitation of the donor is possible. With Acd still filling the role of the acceptor in FRET experiments, Mcm is a potent possible donor. The ample spectral overlap of these two fluorescent unnatural amino acids provides a  $R_0$  of 25 Å, making them ideal for distance measurements between 15 – 45 Å. Additionally, Acd can act as the acceptor with several common organic fluorophores such as carboxyfluorescein ( $R_0 = 51$  Å), BODIPY-Fl ( $R_0 = 49$  Å), rhodamine 6G ( $R_0 = 49$  Å), and nitrobenzodioxazole (NBD;  $R_0 = 37$  Å). Only the carboxyfluorescein probe pair was tested in a model peptide system and unfortunately was shown to be non-ideal; the excitation band of carboxyfluorescein extends significantly into the excitation range of Acd. This complication precludes the use of this FRET pair as excitation of Acd at 386 nm leads to substantial direct excitation of carboxyfluorescein. Finally, there is literature precedent for Acd having substantial sensitivity to the polarity of its local environment where  $\Phi$  can change from 0.95 in water to 0.29 in tetrahydrofuran (THF). This sensitivity to local polarity, as well as the other environmental and energy transfer properties of Acd, highlights the probe's versatility as a biophysical tool.

Previously the Sisido group and collaborators have shown that Acd is ribosomally permissible using semi-synthetic tRNA strategies<sup>57</sup>. However, the limitations of this method (aa-tRNA is prone to hydrolysis and semi-synthetic versions are labor intensive to fabricate) inspired us to work with the Mehl group to identify an o-aaRS/tRNA pair capable of selectively using Acd as a substrate. Such a finding would allow us to produce site-specifically Acd labeled proteins on a scale conducive to yielding the milligram quantities of fluorescent protein needed for routine fluorescence experimentation. It is important to note that the generation of an o-aaRS/tRNA pair for Acd does not preclude its use exclusively to *in vivo* applications; however these methods are the most straightforward. Several groups have created *in vitro* translation systems capable of yielding milligram quantities of site-specifically labeled proteins harboring UAAs yet these technologies are generally fairly labor intensive to setup and/or are exclusive to the laboratory in which they were developed<sup>95, 96</sup>. *In vivo* methods on the other hand are much more enabling; if another group desires to take advantage of our methods they would need only a plasmid containing the o-aaRS/tRNA pair and a stock of the UAA to begin their own experiments within days.

## **SYNTHESIS OF ACD**

The first step in the identification of an o-aaRS/tRNA pair and the development of *in vivo* incorporation methods for Acd was to devise an efficient, scalable synthesis of the UAA that could be used to prepare the gram quantities necessary for routine protein expression. These considerations were taken to make the use of Acd as a minimalistic site-specific

fluorescent protein label as general as possible. Previous routes to Acd utilized the UAA *p*-nitrophenylalanine (pNO<sub>2</sub>-F) as the principle starting material<sup>90</sup>. After installation of methyl ester (OMe) and *t*-butyl carbamate (Boc) protecting groups, the resulting compound (**3**) was hydrogenated with palladium on carbon (Pd/C) under a hydrogen atmosphere. While the literature account of this transformation claimed it was high yielding (94 %), our group could not reproduce this efficiency under the described conditions (10% Pd/C in methanol (MeOH) under H<sub>2</sub> for 2 hours). Instead, our group saw the formation of a side-product which could total as much as 15% of the total organic species after filtration of the catalyst. Initially it was assumed that this was an aryl-diazo compound formed by interaction of two product molecules with the Pd catalyst, however careful analysis of the H<sup>1</sup> NMR of this product and the starting material revealed that it was a *N,N'*-diBoc protected species. The formation of this side-product was the result of some of the starting material harboring two Boc-groups on the  $\alpha$ -amine due to the use of an excess of Boc-anhydride in the previous reaction followed by subsequent Pd-mediated transfer of one Boc group to the newly formed amine. Since the *N,N'*-diBoc material exhibited the same mobility on silica gel as the singly N-protected material, these were difficult to separate. Thus, less Boc-anhydride was used in the N-terminal protection, and exclusively singly Boc-protected compound **4** was obtained. Furthermore, as proton transfer would be necessary for this Boc migration to occur, the solvent for the hydrogenation was changed from polar protic MeOH to polar aprotic ethyl acetate (EtOAc). The combined effects of these two changes led to quantitative conversion of the protected aryl nitro amino acid into the protected aryl amine amino acid, a 6 % improvement over the literature precedent (**Scheme 2.1**).



**Scheme 2.1:** Synthesis of Acridone (**1**) Starting from p-NO<sub>2</sub>-F With Modifications Described in This Work.

Following the hydrogenation of the protected aryl nitro amino acid, the next literature step was to couple the resulting amine (**4**) to iodobenzoic acid under copper (Cu) metal catalysis in a transformation known as the Ullman/Goldberg biaryl amine synthesis. Despite the ubiquitous nature of this transformation for the formation of biaryl amines, the mechanism is still poorly understood, especially when Cu powder is employed as the catalyst. Either Cu(I) or Cu(II) mechanisms can be responsible for the observed transformation, and it is possible that using Cu powder allows both mechanisms to be operative in the same pot (**Figure 2.6**). As the relative contributions of the Cu(I) and Cu(II) mechanisms may vary with subtle changes in conditions, it is not surprising that experimentally this transformation was not consistent with respect to the overall yield of the desired biaryl amine (**5**) and/or the levels of side-products formed. Despite these difficulties it was possible to produce gram scale quantities of pure biaryl amine (**5**) for subsequent transformations into the Acridone fluorophore.

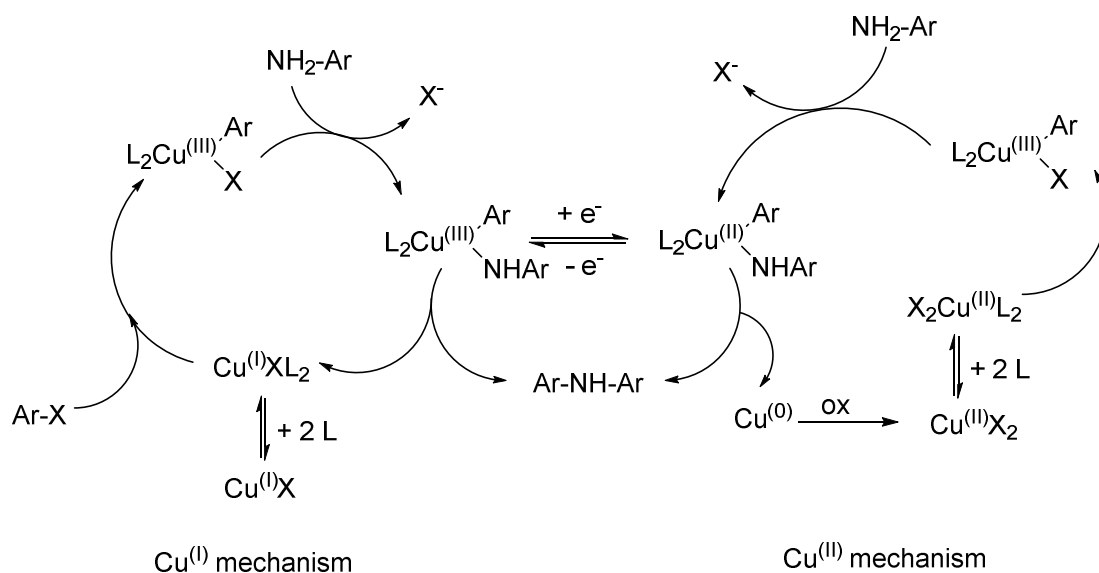


**Figure 2.6:** Cu(I) and Cu(II) proposed mechanisms for Ullman/Goldberg Biaryl Amine Synthesis. X = I, Br, Cl, SCN and L = ligand (typically diamines)

With the protected biaryl amine functionalized amino acid (**4**) in hand, the next step in the literature protocol was to use the strong Lewis acid and mild Brønsted acid polyphosphoric acid (PPA) and heat to catalyze an intramolecular Friedel-Crafts' acylation between the carboxylic acid of the newly coupled aryl ring to the *ortho*-position of the aryl ring closest to the amino acid backbone. This transformation completes the formation of the linear tricyclic heteroaromatic acridone nucleus while liberating the backbone amine from its Boc protecting group due to the acid conditions. As PPA is a strong Lewis acid, but mild Brønsted acid, and no water was deliberately added to the reaction, compound **6** was obtained with the methyl ester intact. As our interest in **Acid** was to use it as substrate for Fmoc based solid-phase peptide synthesis (SPPS) or *in vivo* incorporations, we desired to follow the PPA mediated Friedel-Crafts acylation and Boc deprotection with an immediate treatment with strong nucleophilic hydroxide base to liberate the OMe. These efforts were met with success; we were able to complete our

modified synthesis of the completely deprotected Acd (**1**) in 54 % overall yield. This was a dramatic improvement over the literature protocols for this route which yielded Acd still protected as the OMe in 23.6 % yield (**Scheme 2.1**).

While our laboratory was successful not only in reproducing the literature pNO<sub>2</sub>-F route to Acd but also in improving its yield by over a factor of two, the synthesis was still not ideal. As the principle source of poor yields in the pNO<sub>2</sub>-F route was the Cu powder mediated coupling of **4** to iodobenzoic acid, we focused on this transformation in evaluating new routes to Acd. It was determined that Buchwald-Hartwig Pd-mediated amine cross-couplings could be a viable replacement for the inconsistent Ullman/Goldberg biaryl amine synthesis. The Buchwald-Hartwig amine cross-coupling, in contrast to the Ullman/Goldberg, requires only catalytic amounts of transition metal, more easily manageable solvents than DMF, and has been shown repeatedly in the literature to reliably produce coupled products in high yields<sup>97</sup>. While it would have been possible for us to simply replace the Ullman/Goldberg reaction with the Buchwald-Hartwig and still use the same coupling partners, we envisioned that starting from another more common amino acid would make our new synthetic route more straight-forward, reproducible, and amenable to derivatization.

Examination of the literature for amino acid derivatization revealed that synthesis of *p*-iodophenylalanine was possible in moderate yields. As the iodo functionality is robust in coupling chemistry, it was initially envisioned as an ideal starting place for this new Acd synthesis. However the synthesis of this halogenated Phe derivative requires harsh reagents and conditions, limiting the potential scope of application of our method to

groups equipped to handle such an endeavor and the idea was subsequently abandoned<sup>98</sup>.

While iodo functionalization is known to lead to robust couplings, Buchwald-Hartwig amine couplings are also capable of utilizing triflate (OTf) functionalized coupling partners as electrophiles. Fortunately, there was ample literature precedent for the synthesis of *N*-Boc-Tyr(OTf)-OMe (**9**) and we were able to produce this compound reliably in three steps from Tyr in 96 % overall yield<sup>99</sup>. Furthermore, an acceptable coupling partner was found in the commodity chemical methyl-2-aminobenzoate (commonly known as methyl anthranilate and used as grape flavoring and as a bird repellent).

After identifying these coupling partners, we then took advantage of the collaboration between the University of Pennsylvania's Department of Chemistry and Merck to use the staff and equipment of the High-Throughput Experimentation Laboratory to screen optimal conditions for the Buchwald-Hartwig Pd-mediated amine coupling. The parameters of most interest to us were: solvent, reaction temperature, base, and Pd to ligand ratios. Initial investigations conducted prior to screening revealed that the economical ligand *racemic* 2,2'-bis(diphenylphosphino)-1,1'-binaphthyl (BINAP) was capable of facilitating the desired transformation and as such was kept constant in these initial screens. The other components of the screen kept constant were: 1.2 equivalents of amine and 3.0 equivalents of base relative to **9**, Pd source (palladium(II) diacetate: Pd(OAc)<sub>2</sub>), a reaction time of 4 hours, and heating to 120°C. Results of the screen revealed that the uncommon solvent cyclopentyl methyl ether (CPMe) was marginally better than toluene in serving as the medium for the transformation (**Figure 2.7**). For large scale syntheses, the prohibitive cost of CPMe led us to use toluene instead.

Additionally, the screen indicated that potassium carbonate ( $K_2CO_3$ ) was a better base than any of the analogous cesium ( $Cs_2CO_3$ ), lithium ( $Li_2CO_3$ ), and sodium salts ( $Na_2CO_3$ ). We chose to screen carbonate bases alone as they are known bases for the Buchwald-Hartwig reaction and are economical for large scale syntheses. Furthermore, the screen revealed dramatic decreases in product yield when lowering the Pd loading from 5.2 %. This was surprising to us as there are several reports of Buchwald-Hartwig couplings using much lower catalyst loadings<sup>100</sup>. The results of this screen guided our scale- up optimizations.

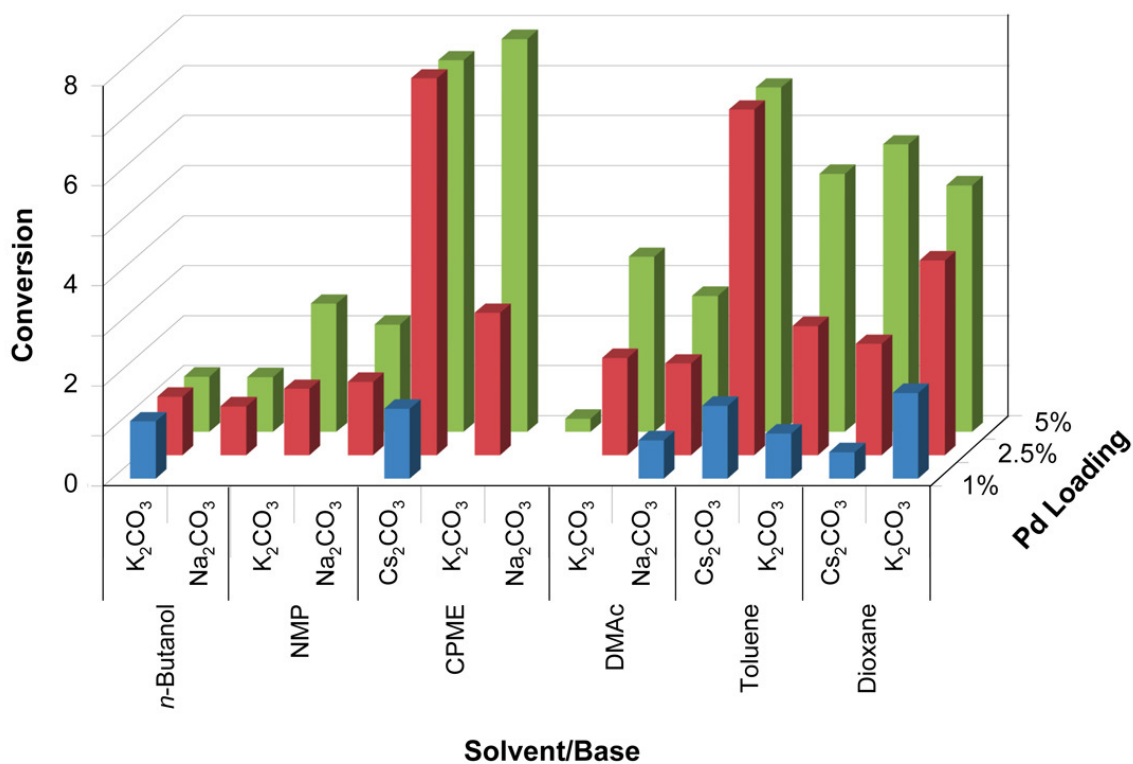


**Figure 2.7:** Screening Results. Coupling of compounds X and Y carried in 96 well plates with varying solvent, base, and Pd(II) acetate compositions. Conversion determined as the ratio of the absorbances at 215 nm of the product peak and a standard peak in HPLC chromatograms. Reprinted with permission from Speight, L. C.; Muthusamy, A. K.; Goldberg, J. M.; Warner, J. B.; Wissner, R. F.; Willi, T. S.; Woodman,

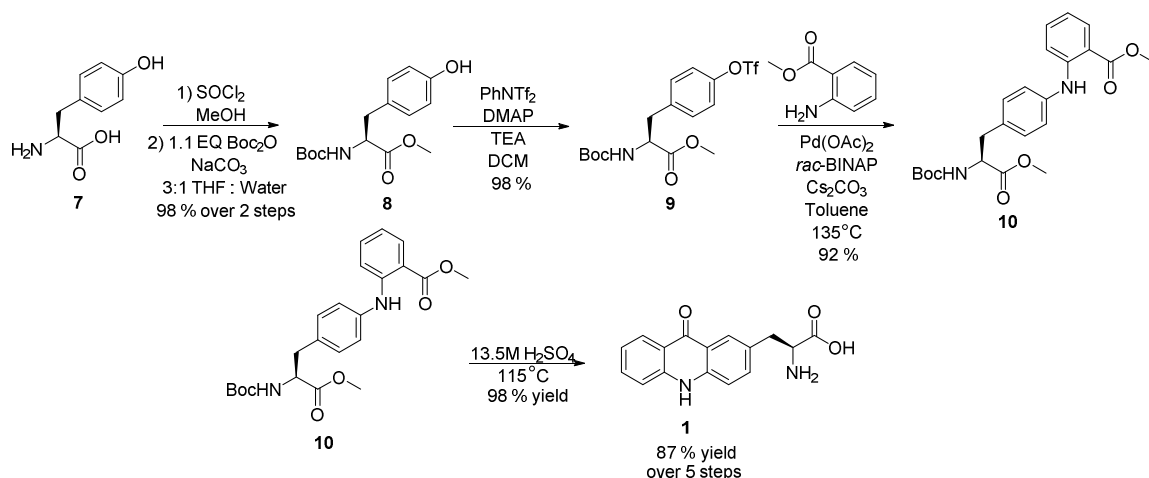
B. F.; Mehl, R. A.; Petersson, E. J., Efficient Synthesis and In Vivo Incorporation of Acridon-2-ylalanine, a Fluorescent Amino Acid for Lifetime and Forster Resonance Energy Transfer/Luminescence Resonance Energy Transfer Studies. *Journal of the American Chemical Society* **2013**, *135* (50), 18806-18814. Copyright (2013) American Chemical Society.

Using the best results from the screen (5.2 % Pd(OAc)<sub>2</sub>, 3.75 % *rac*-BINAP, 3.01 equivalents of K<sub>2</sub>CO<sub>3</sub>, 1.15 equivalents of amine, and 120°C for 4 hours) we were unable to completely drive the reaction to completion at larger scales. Making matters worse, **9** proved to have the same mobility on silica gel as the biaryl amine coupled product (**10**) in all tested solvent mixtures (**Scheme 2.2**). Desiring to move forward with the synthesis to test the full scope of the route, we investigated methods for the selective hydrolysis of the triflate group while keeping the two OMe groups of **10** intact. A method using trialkylammonium hydroxide salts proved to be ineffective or unselective (several days for selective triflate hydrolysis and global hydrolysis of triflate and OMe groups at higher salt loadings)<sup>101</sup>. Interestingly, the same report included a procedure calling for treatment with tetrabutylammonium fluoride (TBAF), which we applied to the mixture of **9** and **10**, resulting in selective triflate hydrolysis while allowing us to recover pure **10** in good yields<sup>101</sup>.

While TBAF treatment of mixtures of **9** and **10** was sufficient to allow us to continue our synthetic route, it was not a permanent fix. Modest increases in the conversion of **9** to **10** were obtained by increasing the reaction temperature to 135°C and prolonging the reaction to 16 hours. These conditions were unsuitable for the use of K<sub>2</sub>CO<sub>3</sub> as this salt decomposed in the presence of the Pd catalyst at high temperature and longer reaction times. Further optimization of the parameters of the reaction to account for this by

changing to  $\text{Cs}_2\text{CO}_3$  as the base, increasing the amine equivalents to 1.32, decreasing the concentration of **9** in toluene, and prolonging the reaction time to 23 hours allowed us to reproducibly convert all of **9** into **10** and recover it after chromatographic purification in greater than 90 % yield at the 250 mg and multi-gram scale.

Continuing our efforts to simplify the synthesis and make it amenable to practice on large scales, we envisioned the use of sulfuric acid ( $\text{H}_2\text{SO}_4$ ) as a replacement for PPA as it is a more common and economical reagent.  $\text{H}_2\text{SO}_4$  has also been shown to catalyze Friedel-Crafts reactions due to its strong Lewis acid character and its strong Brønsted acid character would easily cleave the Boc amine protecting group and both OMe groups (in the presence of water). Gratifyingly, 13.5M  $\text{H}_2\text{SO}_4$  in water at 115°C for 16 hours followed by purification using cation exchange resin produced Acd (**1**) in 98 % yield. HPLC analysis of the product indicated that the compound was greater than 98 % pure, making this final transformation both high yielding and straight-forward to purify. With the high yielding production of the **9**, fully optimized Buchwald-Hartwig amine cross-coupling conditions, and the global deprotection/Friedel-Crafts acylation mediated by  $\text{H}_2\text{SO}_4$ , we established a novel five step synthesis of Acd (**1**) in 87 % yield (**Scheme 2.2**).



**Scheme 2.2:** Synthesis of Acid Starting from Tyr Using H<sub>2</sub>SO<sub>4</sub> as the Final Reagent.

## O-aaRS/tRNA PAIR IDENTIFICATION

In order to identify a mutant o-aaRS/tRNA pair capable of selectively utilizing Acd, we began a collaboration with the Mehl laboratory as it was envisioned that their strategy of screening previously evolved mutant o-aaRS/tRNA pairs would provide useful results faster than evolving an orthogonal pair *de novo*. Furthermore, as Acd is significantly larger than Tyr, using random or rational mutagenesis to carve out a large pocket in the aaRS active site was hypothesized to be a significant endeavor and could result in many inactive mutants due to radical changes to the aaRS overall folding architecture. Thus, the Mehl group first screened their library of mutant o-aaRS/tRNA pairs (all derived from *M. jannaschii* tyrosyl aaRS/tRNA pairs) capable of using three structurally similar amino acids: Nap, *p*-benzoylphenylalanine (Bzf), and 4-(2'-bromoisobutylamido)phenylalanine (Brb) (**Figure 2.8**). As the Mehl laboratory mutant o-aaRS/tRNA pairs were created by negative selection against only endogenous amino acids and were not challenged with

other UAAs, it was possible that one of the mutant o-aaRS/tRNA pairs could accept Acd in preference to the UAA for which it was evolved.

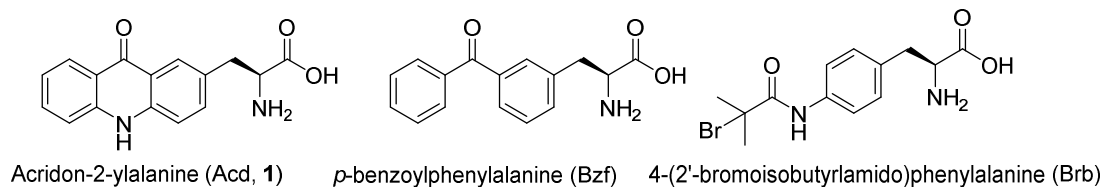


**Figure 2.8:** Structures of Acd (**1**), Bzf, and Brb.

Screening of the mutant o-aaRS/tRNA library was carried out by testing the incorporation of Acd into position 150 of GFP and assessing the GFP fluorescence of suspended cells. As GFP's fluorophore only matures and fluoresces when it is fully translated and folded properly, any GFP fluorescence observed was taken to be the result of the tested mutant o-aaRS/tRNA pair successfully utilizing Acd as a substrate. It is important to note that these mutant o-aaRS/tRNA pairs were already selected against their native amino acid (Tyr in this case), so it was assumed that all observed GFP fluorescence is the result of the mutant o-aaRS/tRNA pair selectively aminoacylating Acd and delivering it to the ribosome in response to the UAG codon. Surprisingly, none of the mutant o-aaRS/tRNA pairs capable of using the structurally similar Nap or Bzf showed any activity towards Acd, even though some mutant Nap o-aaRS/tRNA pairs could use Bzf in addition to Nap. We were able to find two mutant o-aaRS/tRNA pairs capable of using Acd from the Brb library: BrbRS1 and BrbRS3 (**Figure 2.9**). Comparison of these two mutant aaRSs to the Nap aaRS revealed that residue 65 in both aaRSs capable of using Acd was glutamic acid (Glu). By analyzing existing crystal structures of *M. jannaschii* TyrRS mutants, we postulate that this residue makes a stabilizing hydrogen bond with the endocyclic N-H in

the middle ring of the Acd fluorophore. As BrbRS1 showed the best activity, we decided to use it in all subsequent studies and now refer to it as AcdRS<sup>102</sup>.

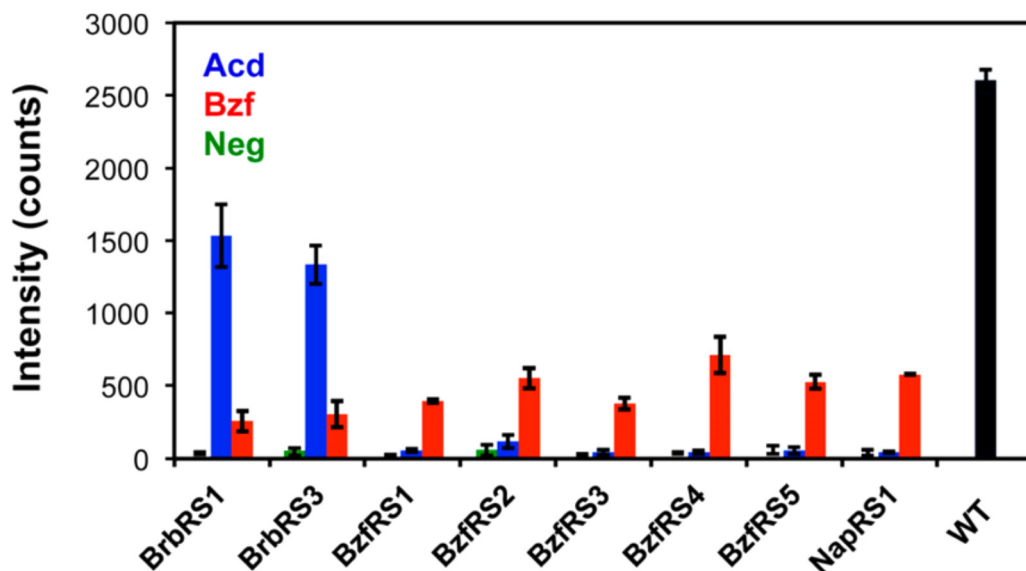


**Figure 2.9:** aaRS Selection and Confirmation of Acd Incorporation. Protein expression levels determined from fluorescence of GFP reporter construct containing a UAG stop codon at position 150. Fluorescence from full-length GFP indicates successful incorporation of a UAA (Acd or Bzf) from a charged tRNA<sub>CUA</sub>. Comparison to expressions containing only proteinogenic amino acids indicates the fidelity of the o-aaRS/tRNA pair (Neg). Fluorescence from WT GFP (black) is shown as a positive control. Reprinted with permission from Speight, L. C.; Muthusamy, A. K.; Goldberg, J. M.; Warner, J. B.; Wissner, R. F.; Willi, T. S.; Woodman, B. F.; Mehl, R. A.; Petersson, E. J., Efficient Synthesis and In Vivo Incorporation of Acridon-2-ylalanine, a Fluorescent Amino Acid for Lifetime and Forster Resonance Energy Transfer/Luminescence Resonance Energy Transfer Studies. *Journal of the American Chemical Society* **2013**, *135* (50), 18806-18814. Copyright (2013) American Chemical Society.

Prior to embarking on rigorous *in vivo* incorporation studies, we explored the mechanism by which the AcdRS is capable of using Acd, but not Tyr. In the wild-type *M. jannaschii* sequence, residue 65 is Leu. Mutagenesis of this residue to Glu not only is necessary for

Acid utilization, but sufficient to remove the ability to use Tyr effectively. Such observations have been independently corroborated with other mutant o-aaRS/tRNA pairs by Tippmann and others<sup>103</sup>. There are an additional three mutations in the AcdRS relative to wild-type; Tyr<sub>32</sub> is mutated to a Gly, Asp<sub>158</sub> to Gly, and Ile<sub>159</sub> to Cys. In all cases an amino acid is mutated to another of smaller size, consistent with the observations of others in terms of opening up the aaRS active site. Despite this precedent for the exclusion of the use of Tyr, we have observed Tyr incorporation even in the presence of Acid. However, this is not a uniform effect as it appears that the position of the UAG codon has a significant effect on Acid over Tyr selectivity as well as the overall yield of Acid containing protein. Many of the Acid proteins expressed in our laboratory contain exclusively Acid at the UAG site while others contain a mixture of both Acid and Tyr. Interestingly, this is seen much more in expressions of  $\alpha$ -synuclein Acid mutants than CaM or triose phosphate isomerase (TIM) Acid mutants. We have only observed significant Tyr incorporation at one site in CaM, none in TIM, and several in  $\alpha$ -synuclein. Others have seen a positional effect with regards to amber suppression in which yields of a mutant protein containing a UAA vary greatly from position to position, even under otherwise identical conditions<sup>96</sup>. While the mechanisms responsible for these positional effects are unclear, current work in both the Mehl and Petersson laboratories is ongoing to make Acid mutant protein expressions more consistent position to position, in addition to creating methods to exclude Tyr entirely.

## ***IN VIVO* INCORPORATION & ALTERNATIVE ACD SYNTHESSES**

While the use of permissive mutant o-aaRS/tRNA pairs is an extremely enabling method of finding a system capable of using a novel UAA, the fact that these macromolecular systems are never challenged against other UAAs became a problem with the use of Acd. The H<sub>2</sub>SO<sub>4</sub> catalyzed Friedel-Crafts intramolecular acylation/global deprotection was shown to produce Acd in high yields and with high purity (> 98 %), however the remaining 2 % of material partially consisted of an aryl decarboxylation side-product, *N*-phenyl-*p*-aminophenylalanine (Npf). Surprisingly, we found Npf to be incorporated into proteins in response to the amber codon in addition to Acd, even when it was present at < 1% of the amino acid stock (analysis by HPLC). As this side-product proved difficult to separate from Acd using silica chromatography and it was hypothesized that its production was likely a result of using the strong Brønsted acid H<sub>2</sub>SO<sub>4</sub>, we adopted a new two-step protocol to avoid its formation. This new procedure utilized lithium hydroxide (LiOH) to saponify both methyl esters followed by treatment with PPA to cyclize the fluorophore and cleave the Boc protecting group. We chose LiOH as previous reports claimed it could be used without racemizing the amino acid's chiral center, but the use of Acd produced in this route in solid phase peptide synthesis (SPPS) showed our material did racemize in this route, but not in the H<sub>2</sub>SO<sub>4</sub> route<sup>104</sup>. We chose PPA because we did not see Npf incorporation using material synthesized with our previous route. Fortunately, application of LiOH saponification and PPA-mediated ring-closing and Boc deprotection yielding Acd of sufficient purity to eliminate Npf incorporation (**Figure 2.10** and **Scheme 2.3**).

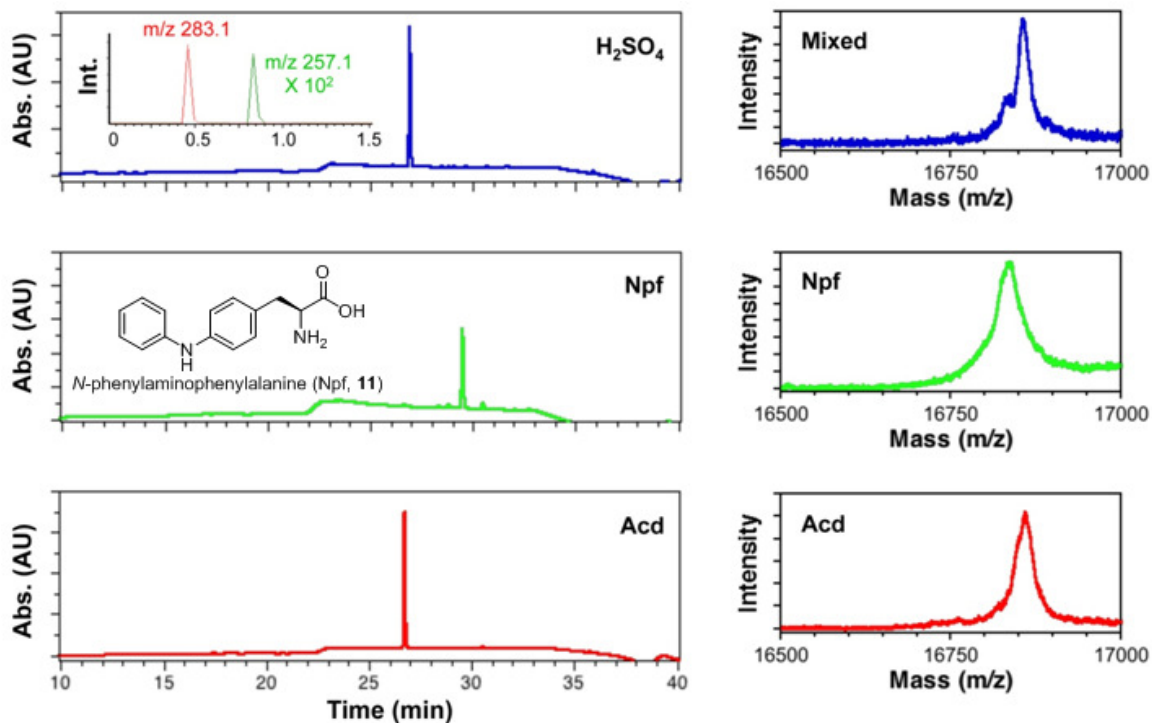
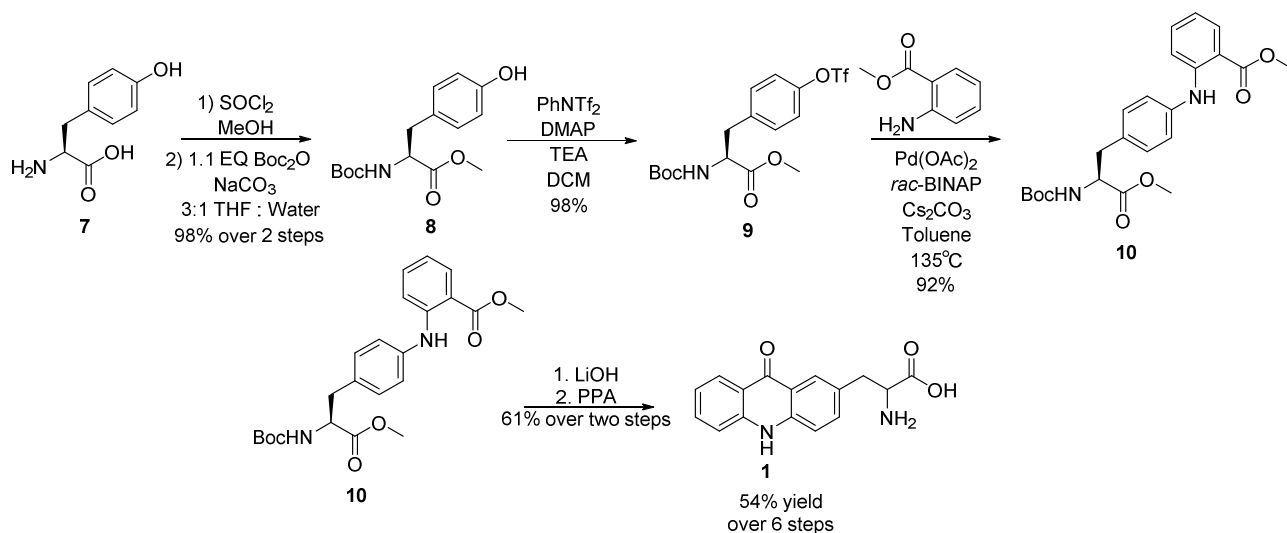


**Figure 2.10:** HPLC, LRMS, and MALDI-MS Analysis of Amino Acids and Protein Expression. Left: HPLC chromatograms of amino acid monomer batches. H<sub>2</sub>SO<sub>4</sub>: Acd batch produced by global deprotection and cyclization in sulfuric acid. Inset shows LRMS selected ion chromatograms for Acd, calculated (M+H)<sup>+</sup> m/z 283.1 and Npf calculated (M+H)<sup>+</sup> m/z 257.1. Weaker Npf ion chromatogram signal scale multiplied by 10<sup>2</sup>. Npf: Authentic Npf sample produced by coupling of aniline to **9**. Acd: Pure Acd batch produced by PPA route. No mass corresponding to Npf was observed in LRMS analysis of this batch. Right: MALDI-MS analysis of full-length CaM-Leu<sub>113</sub>Acd construct expressed using either a ‘Mixed’ Npf/Acd batch from H<sub>2</sub>SO<sub>4</sub> route; authentic Npf, calculated m/z 16833, found 16835; or pure Acd, calculated m/z 16858, found 16859. Reprinted with permission from Speight, L. C.; Muthusamy, A. K.; Goldberg, J. M.; Warner, J. B.; Wissner, R. F.; Willi, T. S.; Woodman, B. F.; Mehl, R. A.; Petersson, E. J., Efficient Synthesis and In Vivo Incorporation of Acridon-2-ylalanine, a Fluorescent Amino Acid for Lifetime and Forster Resonance Energy Transfer/Luminescence Resonance Energy Transfer Studies. *Journal of the American Chemical Society* **2013**, *135* (50), 18806-18814. Copyright (2013) American Chemical Society.



**Scheme 2.3:** PPA-mediated route to Acid (**1**).

Recently we compared direct Npf incorporation to Acid incorporation by examining the fluorescence of a GFP construct harboring an internal amber codon using either of the UAAs and our Acid o-aaRS/tRNA pair. The data indicates that NpF is accepted by the o-aaRS/tRNA pair roughly 1.5 fold better than Acid (**Figure XXX**). While this data alone does not explain the MALDI-MS data that shows a significant amount of Npf incorporation when it only comprises 2 – 5 % of the amino acid stock, we can rationalize this data due to the higher solubility of Npf than Acid as well as the fact that the Acid nucleus is a known DNA intercalator<sup>105</sup>. This intercalating ability of the Acid nucleus could sequester the amino acid in DNA rich sections of the *E. coli* cells and make the effective concentration of Npf available for protein synthesis much higher than that of Acid. Both lower solubility of Acid than Npf and Acid's potential to intercalate into DNA can explain our MALDI-MS data in light of the fact that Npf is only taken 1.5 fold better by our o-aaRS/tRNA pair.

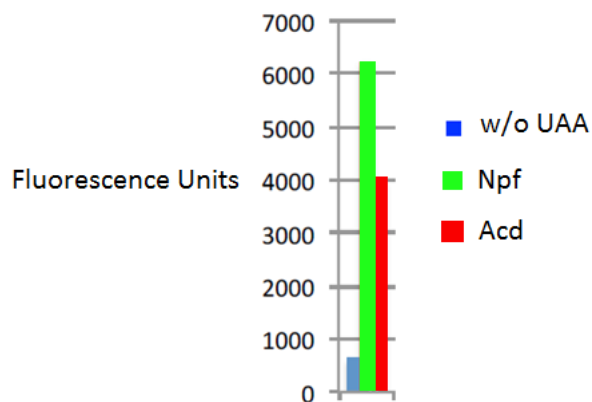
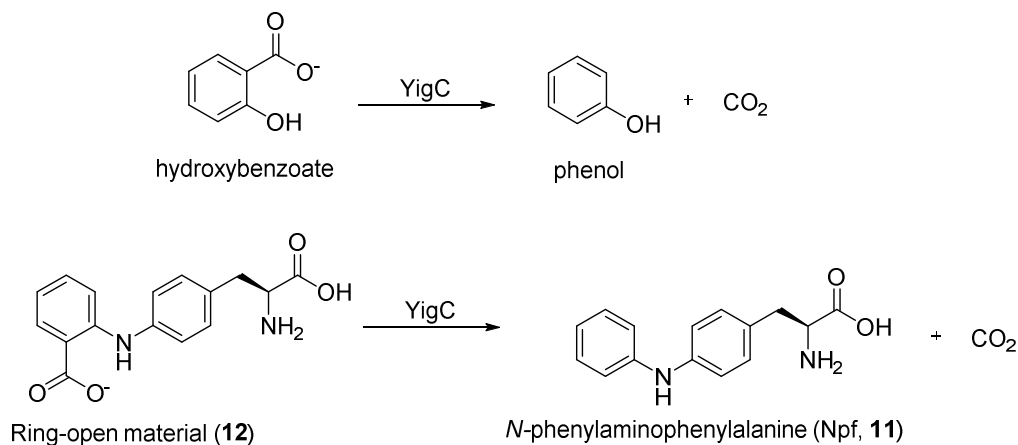


**Figure 2.11:** Relative Npf to Acd Incorporation. Experiment was done using our o-aaRS/tRNA pair, a GFP construct harboring an internal amber codon, and either no UAA, Npf, or Acd. GFP fluorescence of suspended cells was recorded to make the above plot.

Interestingly however, when we tried to use the same cation exchange chromatography we used for the H<sub>2</sub>SO<sub>4</sub> route for this new PPA procedure we saw Npf incorporation without being able to detect it in the Acd stock. Investigation into the composition of the Acd stock revealed a trace amount of deprotected but uncyclized material (**12**). Test expressions with exclusively this compound revealed that its use leads to Npf incorporation in proteins in response to the amber codon. These observations led us to postulate that this material is decarboxylated *in vivo*. As there are not an abundance of enzymes in *E. coli* capable of this transformation, we have identified YigC which is natively responsible for the decarboxylation of hydroxybenzoate as a candidate enzyme (**Scheme 2.4**)<sup>106</sup>. Moreover, YigC is part of the ubiquinone biosynthesis pathway that is known to be up-regulated in *E. coli* when the organism is raised in M9 minimal media, which we routinely use for our expressions of UAA mutant proteins<sup>107</sup>. Fortunately, the isoelectric point (pI) of this uncyclized material (**12**) is 3.3 while Acd's pI is 5.5, enabling

us to separate the materials by selective pH precipitation. We are currently working with the Mehl group to carry out negative selections of our o-aaRS/tRNA pair against Npf acceptance so that we can use the H<sub>2</sub>SO<sub>4</sub> route exclusively as it is higher yielding and produces enantiopure Acd.



**Scheme 2.4:** Action of YigC on Hydroxybenzoate and Proposed YigC decomposition of **12** to Npf (**11**).

## BIOPHYSICAL STUDIES: FRET/LRET/PET

After developing an o-aaRS/tRNA pair and an efficient synthesis, we began to test the utility of Acd incorporation into proteins by expressing Acd mutants of  $\alpha$ -synuclein, TIM, and CaM in *E. coli* (**Figure 2.12**). As noted previously, the yields of these Acd mutant proteins relative to the wild type (WT) varied greatly. The range that we observed differed from 3 % in a TIM mutant to 69 % in a CaM mutant (**Tables 2.1 – 2.3**). Because these are proteins that generally express well, even the 3 % yield enabled us to demonstrate the utility of Acd as a site-specific fluorescent probe in both the CaM and TIM systems.

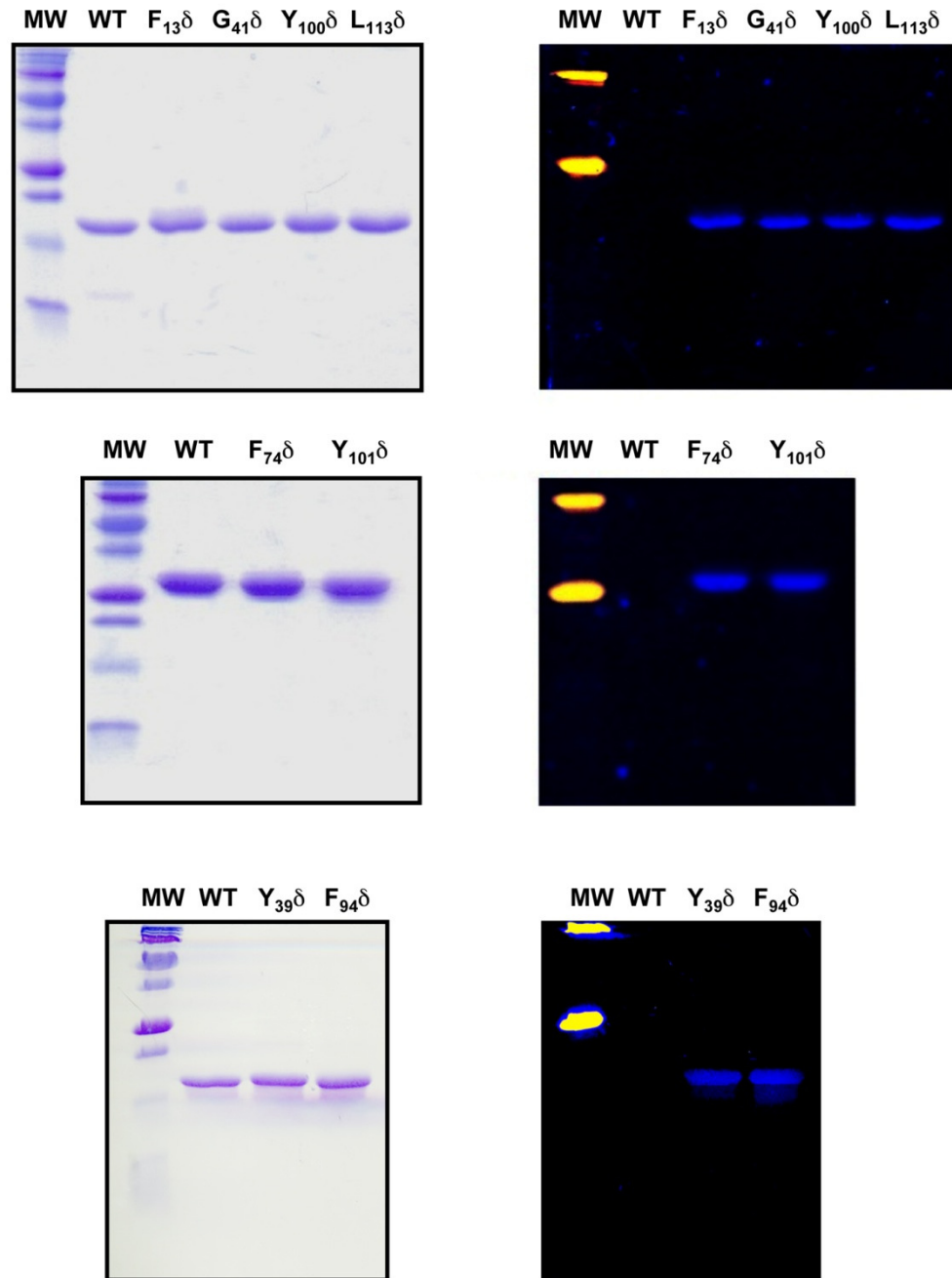


**Figure 2.12:** SDS PAGE Gel Analysis of Mutant Protein Expression. Top: CaM mutants, Middle: TIM mutants, Bottom:  $\alpha$ -synuclein mutants. Coomassie stained gels are shown on the left and fluorescence images on the right. Molecular weight (MW) markers: 7, 10, 17, 25, 40, 50, 75, 100, and 150 kDa. The 25 and 75 kDa markers are fluorescently stained. Reprinted with permission from Speight, L. C.; Muthusamy, A. K.; Goldberg, J. M.; Warner, J. B.; Wissner, R. F.; Willi, T. S.; Woodman, B. F.; Mehl, R. A.; Petersson,

E. J., Efficient Synthesis and In Vivo Incorporation of Acridon-2-ylalanine, a Fluorescent Amino Acid for Lifetime and Forster Resonance Energy Transfer/Luminescence Resonance Energy Transfer Studies. *Journal of the American Chemical Society* **2013**, *135* (50), 18806-18814. Copyright (2013) American Chemical Society.

**Table 2.1:** CaM Protein Expression.

protein	yield (mg/L)	% yield relative to WT
WT	30.0	-
13	16.8	56.0
41	18.1	60.3
100	6.1	20.3
113	20.7	69.0

**Table 2.2:** TIM Protein Expression.

protein	yield (mg/L)	% yield relative to WT
WT	26.4	-
74	4.0	15.2
101	0.8	3.0

**Table 2.3:**  $\alpha$ -Synuclein Protein Expression.

protein	yield (mg/L)	% yield relative to WT
WT	30.0	-
39	2.0	6.7
94	5.0	16.7

We chose CaM as our first model system as this protein has been structurally characterized with a variety of substrates bound, and it has been extensively studied in biophysical experiments. Additionally, we aimed at exploring the perturbations caused by incorporating Acd by placing it at four distinct sites within CaM's sequence, including both surface exposed and buried residues, and replacing both endogenous aromatic and

aliphatic residues (Phe<sub>13</sub>, Gly<sub>41</sub>, Tyr<sub>100</sub>, and Leu<sub>113</sub>). Following expression in *E. coli* and purification by phenyl sepharose chromatography, we ensured that the incorporation of Acd did not significantly disrupt the folding of CaM at any of the four sites. All four Acd mutants, in the absence of Ca<sup>2+</sup>, had melting points within 5 °C of WT CaM as determined by circular dichroism (CD) spectroscopy (**Figure 2.13**). In the presence of Ca<sup>2+</sup> neither WT CaM nor the Acd mutants, could be thermally denatured by heating to 95 °C.

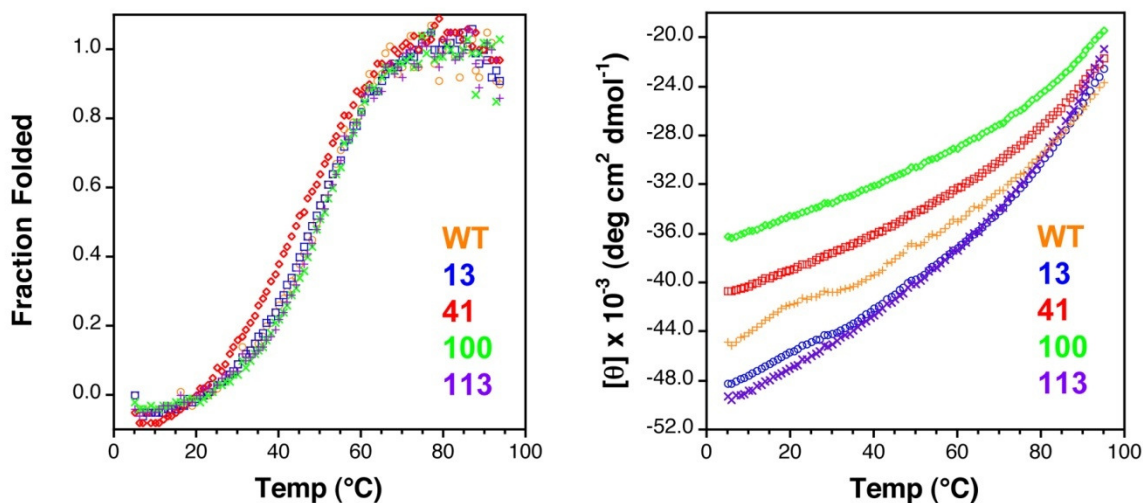


**Figure 2.13:** Temperature-Dependent Circular Dichroism Spectroscopy of WT CaM and Acd Mutants.

Left: Fraction folded as a function of temperature as determined by molar residue ellipticity ( $\theta$ ) at 222 nm measured for 20  $\mu\text{M}$  solutions of each protein in the absence of Ca<sup>2+</sup>. Right: Molar residue ellipticity ( $\theta$ ) at 222 nm measured for 20  $\mu\text{M}$  solutions of each protein in the presence of Ca<sup>2+</sup>. Reprinted with permission from Speight, L. C.; Muthusamy, A. K.; Goldberg, J. M.; Warner, J. B.; Wissner, R. F.; Willi, T. S.; Woodman, B. F.; Mehl, R. A.; Petersson, E. J., Efficient Synthesis and In Vivo Incorporation of Acridon-2-ylalanine, a Fluorescent Amino Acid for Lifetime and Forster Resonance Energy Transfer/Luminescence Resonance Energy Transfer Studies. *Journal of the American Chemical Society* **2013**, *135* (50), 18806-18814. Copyright (2013) American Chemical Society.

## ACD AS AN ENVIRONMENTAL PROBE

As a final test to ensure that Acd incorporation at these sites did not substantially disrupt the normal properties of CaM, we used native PAGE gel analysis to confirm that the Acd mutation did not perturb binding of our target peptide, pOCNC (H<sub>2</sub>N-FRRIARLVGVLREFAFR-CONH<sub>2</sub>). This peptide is derived from an olfactory cyclic nucleotide gated ion channel and its structure in complex with CaM had previously been determined by NMR (**Figure 2.14**)<sup>108</sup>. Its binding affinity to WT CaM has previously been determined to be 3 nM; therefore, we expected that only significant alterations in CaM structure would disrupt binding at 1 – 10 μM<sup>109</sup>. Indeed, all four Acd mutants bound a labeled derivative of pOCNC (**Figure 2.15**).

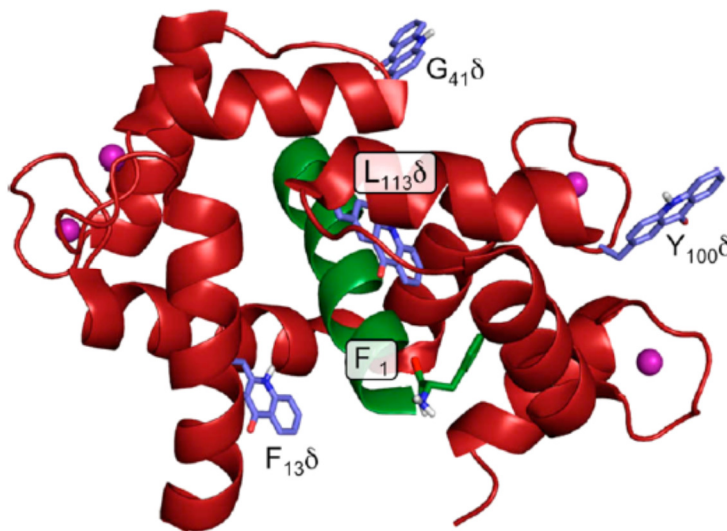


**Figure 2.14:** CaM Labeling Sites. An image showing Acd (blue) at positions 13, 41, 100, and 113 in CaM (red) and highlighting position 1 in the pOCNC peptide (green). Ca<sup>2+</sup> ions are shown as purple spheres. Adapted from PDB 1SYD using PyMol (Schrödinger, LLC; New York, NY) and Spartan (Wavefunction, Inc. Irvine, CA)<sup>108</sup>. Reprinted with permission from Speight, L. C.; Muthusamy, A. K.; Goldberg, J. M.; Warner, J. B.; Wissner, R. F.; Willi, T. S.; Woodman, B. F.; Mehl, R. A.; Petersson, E. J., Efficient

Synthesis and In Vivo Incorporation of Acridon-2-ylalanine, a Fluorescent Amino Acid for Lifetime and Forster Resonance Energy Transfer/Luminescence Resonance Energy Transfer Studies. *Journal of the American Chemical Society* **2013**, *135* (50), 18806-18814. Copyright (2013) American Chemical Society.

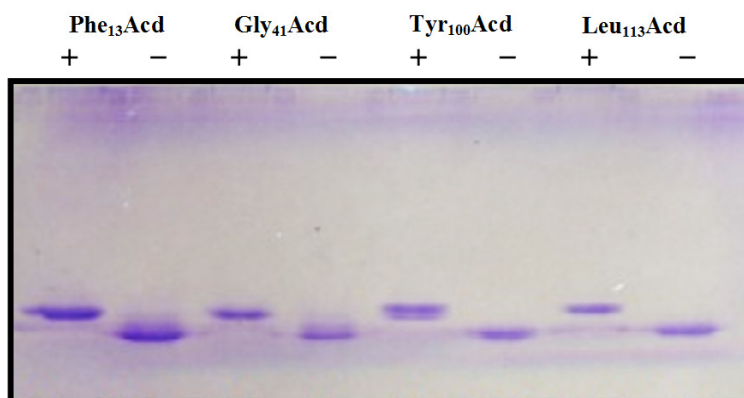


**Figure 2.15:** Native PAGE Gel Analysis of CaM Peptide Binding. PAGE analysis demonstrates upward shift of the CaM protein band upon addition of pOCNC-F', a derivative of pOCNC-F in which Phe has been replaced with a backbone thioamide version of Phe, F'. Reprinted with permission from Speight, L. C.; Muthusamy, A. K.; Goldberg, J. M.; Warner, J. B.; Wissner, R. F.; Willi, T. S.; Woodman, B. F.; Mehl, R. A.; Petersson, E. J., Efficient Synthesis and In Vivo Incorporation of Acridon-2-ylalanine, a Fluorescent Amino Acid for Lifetime and Forster Resonance Energy Transfer/Luminescence Resonance Energy Transfer Studies. *Journal of the American Chemical Society* **2013**, *135* (50), 18806-18814. Copyright (2013) American Chemical Society.

Following these demonstrations of the minimally perturbing nature of Acđ incorporation, we wished to use Acđ to monitor conformational changes associated with the binding of helical peptides to CaM. We then analyzed the fluorescence emission spectra of 10  $\mu$ M CaM with varying concentrations of pOCNC. The fluorescence emission of CaM-Phe<sub>13</sub>Acđ, CaM-Tyr<sub>100</sub>Acđ, and CaM-Leu<sub>113</sub>Acđ were identical in the presence and absence of pOCNC, implying that Acđ does not change environment during the binding of this peptide (**Figure 2.16**).

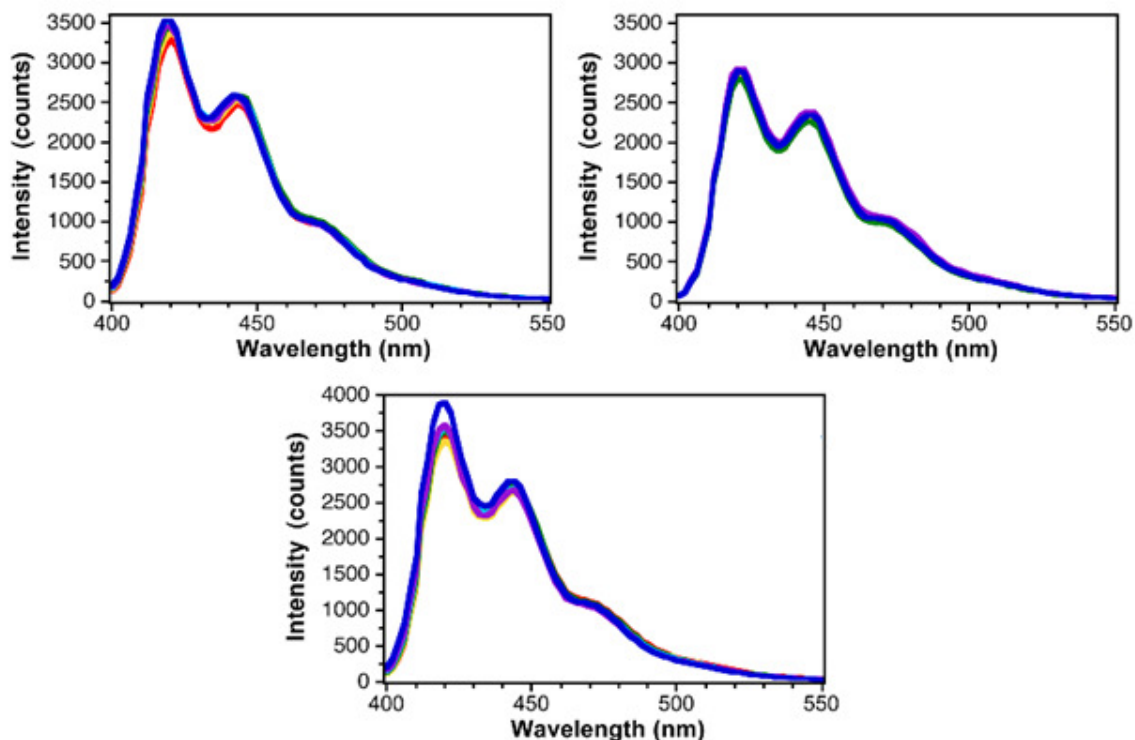


**Figure 2.16:** Fluorescence Spectra of CaM Mutants with Bound Peptides. Top Left: CaM-Phe<sub>13</sub>Acid/pOCNC, Top Right: CaM-Tyr<sub>100</sub>Acid/pOCNC, Bottom: CaM-Leu<sub>113</sub>Acid. All spectra recorded for solutions of 0 (red), 2.5 (orange), 5 (yellow), 7.5 (green), 10 (blue), and 15  $\mu$ M (purple) pOCNC solutions. Reprinted with permission from Speight, L. C.; Muthusamy, A. K.; Goldberg, J. M.; Warner, J. B.; Wissner, R. F.; Willi, T. S.; Woodman, B. F.; Mehl, R. A.; Petersson, E. J., Efficient Synthesis and In Vivo Incorporation of Acridon-2-ylalanine, a Fluorescent Amino Acid for Lifetime and Forster Resonance Energy Transfer/Luminescence Resonance Energy Transfer Studies. *Journal of the American Chemical Society* **2013**, *135* (50), 18806-18814. Copyright (2013) American Chemical Society.

In contrast, in its unbound form, CaM-Gly<sub>41</sub>Acid displayed a blue-shift in fluorescence relative to free Acid, and this blue shift was relieved upon the addition of pOCNC to the solution (**Figure 2.17**). Previous photophysical characterization of Acid by Szymanska *et al.* has shown that Acid emission undergoes a blue shift in non-polar environments. Since polycyclic aromatic compounds have been shown to bind in the helical cleft of CaM, we

believe that the change in Acd emission occurs because the binding of pOCNC forces the Acd residue to move from a hydrophobic pocket into bulk aqueous solvent<sup>110</sup>. While solvatochromic effects at position 41 could be used to monitor peptide binding to CaM, they complicate the interpretation of FRET data, so we focused our attention on the other positions.

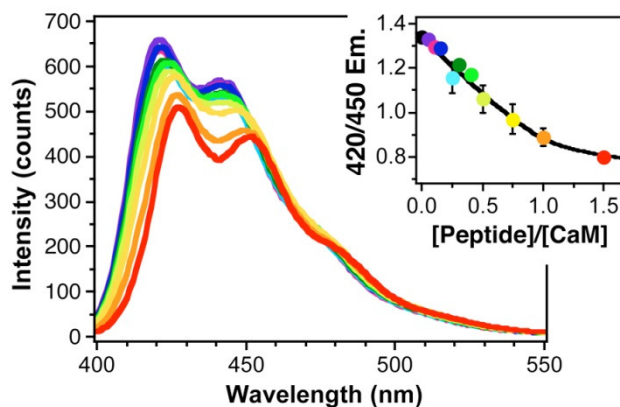


**Figure 2.17:** Monitoring CaM Binding By Changes in Acd Environment. Fluorescence spectra of 10  $\mu$ M CaM-Gly<sub>41</sub>Acd in the presence of 0, 0.1, 0.15, 0.2, 0.25, 0.3, 0.4, 0.5, 0.75, 1.0, or 1.5 equivalents of pOCNC, colored black, purple, magenta, blue, aqua, green, lime, chartreuse, yellow, orange, and red, respectively. Inset: Peptide binding monitored by changes in the ratio of emission at 420 nm and 450 nm. Reprinted with permission from Speight, L. C.; Muthusamy, A. K.; Goldberg, J. M.; Warner, J. B.; Wissner, R. F.; Willi, T. S.; Woodman, B. F.; Mehl, R. A.; Petersson, E. J., Efficient Synthesis and In Vivo Incorporation of Acridon-2-ylalanine, a Fluorescent Amino Acid for Lifetime and Forster Resonance Energy Transfer/Luminescence Resonance Energy Transfer Studies. *Journal of the American Chemical Society* **2013**, *135* (50), 18806-18814. Copyright (2013) American Chemical Society.

## ACD AS A FRET PROBE

To demonstrate the use of Acd as a FRET acceptor for Trp and Mcm, we synthesized variants of pOCNC labeled at the N-terminus with these fluorophores. The CaM Acd mutants were each titrated with Trp-pOCNC or Mcm-pOCNC, and fluorescence emission was recorded from 350 to 550 nm while exciting at 295 nm (Trp) or 325 nm (Mcm). In the case of the Mcm-pOCNC titrations, we observed a decrease in Mcm emission and an increase in Acd emission due to FRET (**Figure 2.18**). Of note, one particular mutant, Leu<sub>113</sub>Acd was calculated to have a near perfect quenching efficiency ( $E_Q$ ) of 0.97. Gratifyingly, we observed nearly the same value, 0.98. Moreover, the relationships between the observed and calculated  $E_Q$  for all Acd positions with the McM titrations were similarly well matched (**Table 2.4**). Several features of these experiments are important to highlight. First, we see that the binding reaches saturation in the 1:1 complex, as determined by examining the difference spectrum in which the emission from 0.5 equivalents of Mcm-pOCNC was subtracted from the spectra of the 1.5:1 Mcm-pOCNC/CaM-Acd. Second, Mcm and Acd are a robust FRET pair, with minimal direct excitation at 325 nm and strong emission due to FRET (emission in the 1:1 complexes is about half of the emission resulting from direct excitation of the CaM-Acd mutants studied at 385 nm). These observations, particularly the excellent quantitative agreement of the expected and observed  $E_Q$ , gave us great confidence in using the Mcm/Acd FRET pair to study protein folding.

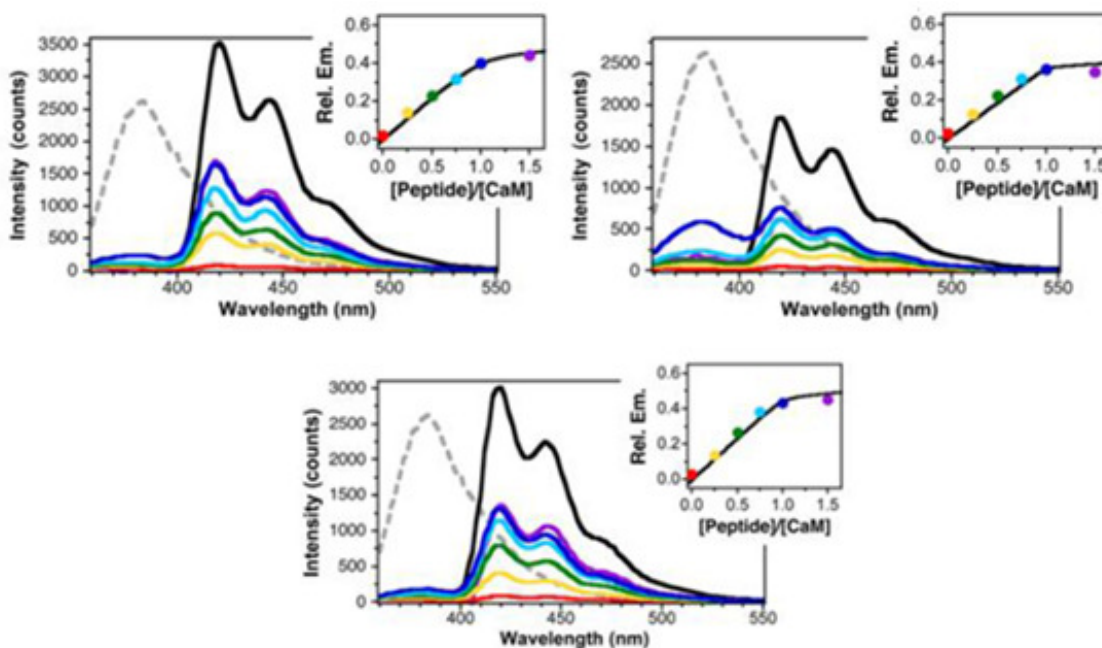


**Figure 2.18:** Fluorescence Spectra of CaM Mutants with Bound Peptides. Fluorescence Spectra of 10  $\mu\text{M}$  CaM-Phe<sub>13</sub>Acid (Top Left), CaM-Tyr<sub>100</sub>Acid (Top Right), or CaM-Tyr<sub>100</sub>Acid in the presence of 0, 0.25, 0.5, 0.75, 1.0, or 1.5 equivalents Mcm-pOCNC, colored red, orange, green, aqua, blue, and purple respectively. The fluorescence spectra of 10  $\mu\text{M}$  Mcm-pOCNC alone is shown in dashed grey. All of these spectra were recorded with excitation at 325 nm. The spectra with 1.5 equivalents Mcm-pOCNC are difference spectra in which the emission from 5  $\mu\text{M}$  Mcm-pOCNC was subtracted from the spectra of the 15  $\mu\text{M}$  Mcm-pOCNC/CaM Acid mutant mixture. The fluorescence spectra of 10  $\mu\text{M}$  CaM mutants alone with excitation at 385 nm is shown in black. Insets: Peptide binding monitored by changes in the emission at 450 nm due to excitation at 325 nm, normalized to the emission at 450 nm due to excitation at 385 nm. Reprinted with permission from Speight, L. C.; Muthusamy, A. K.; Goldberg, J. M.; Warner, J. B.; Wissner, R. F.; Willi, T. S.; Woodman, B. F.; Mehl, R. A.; Petersson, E. J., Efficient Synthesis and In Vivo Incorporation of Acridon-2-ylalanine, a Fluorescent Amino Acid for Lifetime and Forster Resonance Energy Transfer/Luminescence Resonance Energy Transfer Studies. *Journal of the American Chemical Society* **2013**, *135* (50), 18806-18814. Copyright (2013) American Chemical Society.

**Table 2.4:** FRET in CaM/Mcm-pOCNC Complexes.

<b>pOCNC/CaM Acid Mutants</b>	<b><math>E_Q</math> observed</b>	<b><math>R</math> (Å)</b>	<b><math>E_Q</math> calculated</b>
Mcm <sub>1</sub> /Phe <sub>13</sub> Acid	0.92	16	0.91
Mcm <sub>1</sub> /Tyr <sub>100</sub> Acid	0.81	18	0.81
Mcm <sub>1</sub> /Leu <sub>113</sub> Acid	0.98	13	0.97

$E_Q$  determined from quenching in 1:1 CaM/Mcm-pOCNC complex.  $R$  is an average value calculated from the twenty lowest energy structures in PDB ID 1SYD using the positions of the corresponding amino acids<sup>108</sup>.  $\Phi_D$  of 0.098 determined for Mcm-pOCNC in 1:1 complex with CaM by measurement of the fluorescence of equimolar concentrations of free Mcm-pOCNC, and 1:1 CaM/Mcm-pOCNC. Mcm-pOCNC  $\Phi_D$  assumed to be 0.18, the value for free Mcm<sup>111</sup>.  $R_0$  for Mcm/Acd calculated using  $\Phi_D$  of 0.098 is 23 Å.

Binding of Trp-pOCNC to any of the three CaM-Acid mutants was also shown to be able to be monitored by FRET. In these cases, no background subtractions were necessary for superstoichiometric complexes since Trp has no fluorescence emission above 400 nm (**Figure 2.19**). However, there is substantial direct excitation of Acid upon irradiation at 295 nm (27 % of the emission due to excitation at 385 nm). Since there is also a possibility of Trp quenching of Acid emission through PET, we cannot interpret the  $E_Q$  data in terms of distances with the same certainty that we were afforded with Mcm. In addition, if this probe pair was to be used in another system containing more than one Trp, FRET data would need to be fit to complex models with more than one donor fluorophore. Regardless, Trp FRET can still be easily used to quantify protein-protein binding energies by fitting concentration-dependent data. One of the protein partners could be WT, provided that it contained at least one Trp residue. As noted above, both

Trp and Mcm each have benefits and drawbacks as FRET donors. In summary, since Trp can both transfer energy to Acd *via* FRET as well as accept it *via* PET, we view Mcm as a more optimal FRET donor. However, as it is possible to genetically incorporate both Trp and Acd into the same protein, this may be appealing for some applications.

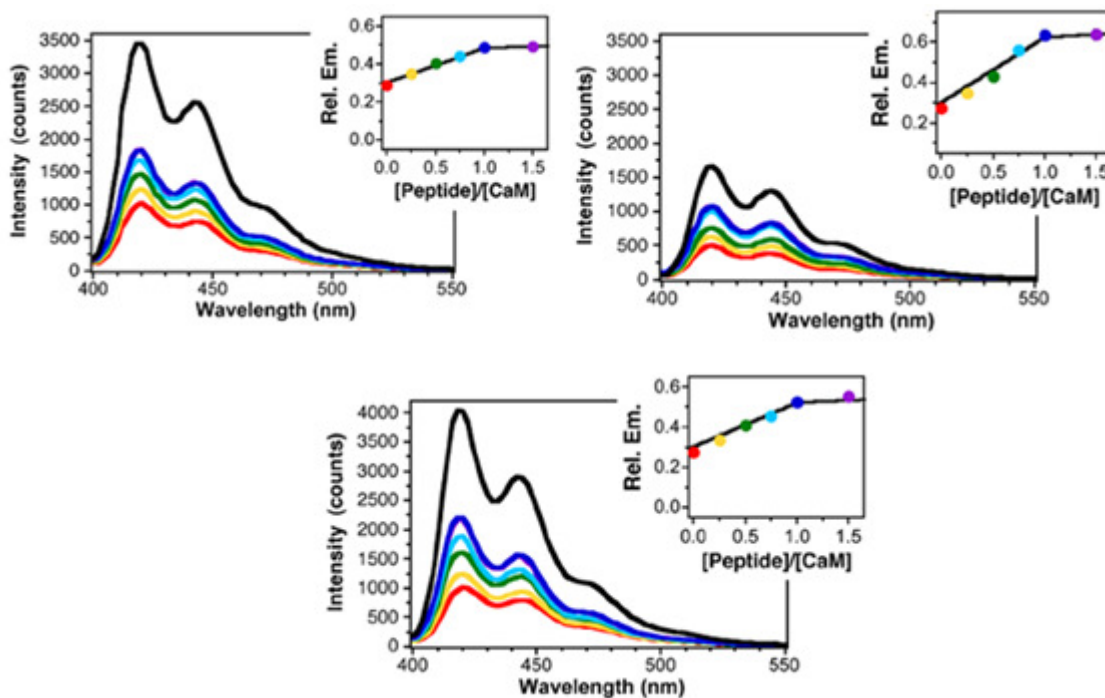


**Figure 2.19:** Fluorescence Spectra of CaM Mutants with Bound Peptides. Fluorescence spectra of 10  $\mu\text{M}$  CaM-Phe<sub>13</sub>Acd (Top Left), CaM-Tyr<sub>100</sub>Acd (Top Right), or CaM-Leu<sub>113</sub>Acd in the presence of 0, 0.25, 0.5, 0.75, 1.0, or 1.5 equivalents Trp-pOCNC, colored red, orange, green, aqua, blue, and purple, respectively. The fluorescence spectra of 10  $\mu\text{M}$  CaM Acid mutant alone or in the 1:1 Trp-pOCNC mixture with excitation at 385 nm is shown in black and grey, respectively. Inset: Peptide binding monitored by changes in the emission at 450 nm due to excitation at 295 nm, normalized to the emission at 450 nm due to excitation at 385 nm. Reprinted with permission from Speight, L. C.; Muthusamy, A. K.; Goldberg, J. M.; Warner, J. B.; Wissner, R. F.; Willi, T. S.; Woodman, B. F.; Mehl, R. A.; Petersson, E. J., Efficient Synthesis and In Vivo Incorporation of Acridon-2-ylalanine, a Fluorescent Amino Acid for Lifetime and

Forster Resonance Energy Transfer/Luminescence Resonance Energy Transfer Studies. *Journal of the American Chemical Society* **2013**, *135* (50), 18806-18814. Copyright (2013) American Chemical Society.

## **ACD AS A LANTHANIDE LUMINESCENCE SENSITIZER**

In addition to singlet energy transfer interactions with organic chromophores like Trp or Mcm, Acd can undergo intersystem crossing to donate energy to lanthanide ions such as  $\text{Eu}^{3+}$ <sup>112</sup>. While this has previously been demonstrated in short synthetic peptides, the ability to genetically encode Acd allows us to implement the same  $\text{Eu}^{3+}$  luminescence resonance energy transfer (LRET) probes in proteins expressed in *E. coli*. To demonstrate Acd-sensitized  $\text{Eu}^{3+}$  emission, we relied on the precedent for CaM binding a variety of cations, including the lanthanides  $\text{Tb}^{3+}$  and  $\text{Eu}^{3+}$ <sup>113</sup>. Since efficient LRET typically requires close contact between the donor chromophore and the lanthanide ion, we chose CaM-Tyr<sub>100</sub>Acd as a construct for LRET studies because Tyr<sub>100</sub> is within site III and proximal to site IV, two of the four cation binding sites of CaM. Following removal of both  $\text{Ca}^{2+}$  and chelators from purified CaM-Tyr<sub>100</sub>Acd by dialysis and ion-exchange chromatography respectively, titration of  $\text{Eu}(\text{NO}_3)_3$  revealed a dose-dependent increase in  $\text{Eu}^{3+}$  emission at 592 and 615 nm (**Figure 2.20**).

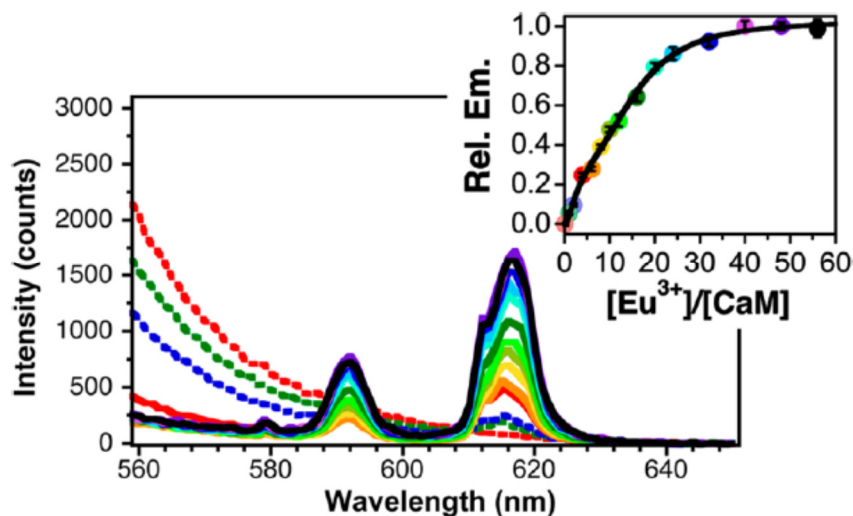


**Figure 2.20:** Monitoring  $\text{Eu}^{3+}$  Binding to CaM by LRET. Luminescence emission spectra of  $10 \mu\text{M}$  CaM-Tyr<sub>100</sub>Acid in the presence of 0, 1, 2, 5, 6, 8, 10, 12, 16, 20, 24, 32, 40, 48, 56 equivalents of  $\text{Eu}(\text{NO}_3)_3$ , colored dashed red, dashed green, dashed blue, red, orange, yellow, chartreuse, light green, dark green, aqua, light blue, dark blue, light purple, dark purple, and black, respectively. Spectra were recorded with excitation at 385 nm. Inset:  $\text{Eu}^{3+}$  binding monitored by changes in the emission at 615 nm. Data fit to two cooperative binding transitions. Reprinted with permission from Speight, L. C.; Muthusamy, A. K.; Goldberg, J. M.; Warner, J. B.; Wissner, R. F.; Willi, T. S.; Woodman, B. F.; Mehl, R. A.; Petersson, E. J., Efficient Synthesis and In Vivo Incorporation of Acridon-2-ylalanine, a Fluorescent Amino Acid for Lifetime and Forster Resonance Energy Transfer/Luminescence Resonance Energy Transfer Studies. *Journal of the American Chemical Society* **2013**, *135* (50), 18806-18814. Copyright (2013) American Chemical Society.

The 615 nm emission data could be fit to a two site binding model with  $K_d$ 's of  $28 \mu\text{M}$  and  $154 \mu\text{M}$  and Hill coefficients of 1.1 and 2.6, respectively. The 615 nm signal primarily derives from the lower-affinity binding event(s), which presumably correspond(s) to binding at the C-terminus, particularly at site III, defined by residues Asp<sub>94</sub>, Asp<sub>96</sub>, Asn<sub>98</sub>, Tyr<sub>100</sub>, Ser<sub>102</sub>, and Glu<sub>105</sub>. Previous experiments have found higher

affinity ( $K_d = 1 \mu\text{M}$ ) binding of lanthanides to this site; the lower affinity observed here may be due to disruption by the Acd residue as studies have found that minor mutations at site III can dramatically decrease  $\text{Ca}^{2+}$  affinity<sup>114, 115</sup>. For higher specificity LRET labeling, one may use lanthanide-binding sequences of the type described by Imperiali and coworkers<sup>116</sup>.

### **ACD AS A PET PROBE**

In many proteins, specific quenching interactions with nearby Trp or Tyr may occur, as indicated by our Stern-Volmer experiments. These could be engineered into either peptide or protein binding partners, and Acd quenching could be used to monitor bimolecular interactions. Indeed, we have shown that this is the case for Acd mutants of TIM. TIM forms a homodimer as seen in **Figure 2.21**. We selected Phe<sub>74</sub> and Tyr<sub>101</sub> as positions for Acd incorporation since they approach each other at the dimer interface and they are relatively far ( $\geq 13 \text{ \AA}$ ) from the other Trp and Tyr residues in TIM.

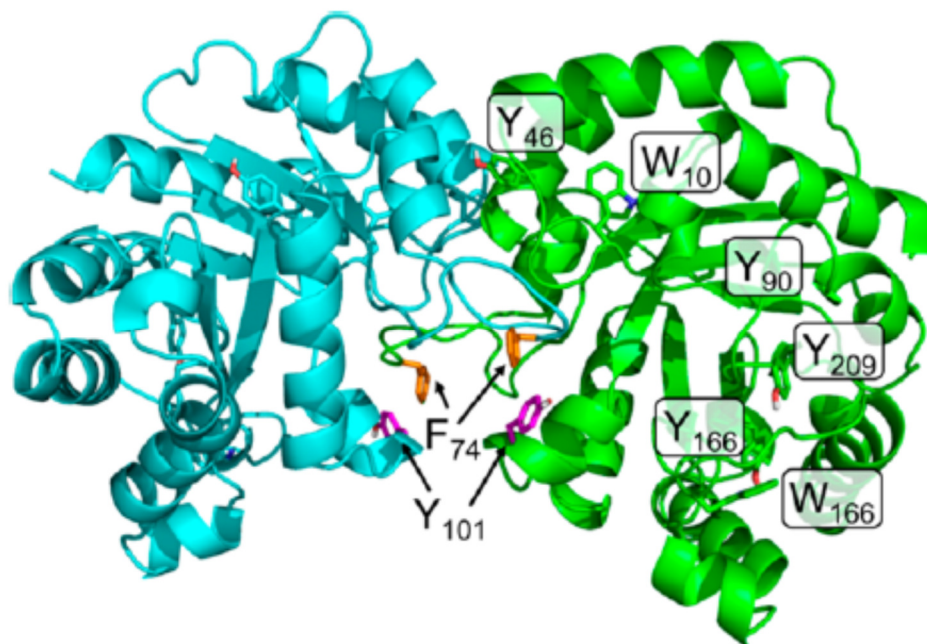


**Figure 2.21:** TIM Annotated Crystal Structure. An image showing a TIM homodimer (protomers colored cyan and green) with Phe<sub>74</sub> (orange) and Tyr<sub>101</sub> (pink) highlighted in both protomers. Other Trp and Tyr residues in both protomers are shown in stick representation and are labeled in the green protomer. Image adapted from PDB 1TRE using PyMol (Schrödinger, LLC; New York, NY)<sup>117</sup>. Reprinted with permission from Speight, L. C.; Muthusamy, A. K.; Goldberg, J. M.; Warner, J. B.; Wissner, R. F.; Willi, T. S.; Woodman, B. F.; Mehl, R. A.; Petersson, E. J., Efficient Synthesis and In Vivo Incorporation of Acridon-2-ylalanine, a Fluorescent Amino Acid for Lifetime and Forster Resonance Energy Transfer/Luminescence Resonance Energy Transfer Studies. *Journal of the American Chemical Society* **2013**, *135* (50), 18806-18814. Copyright (2013) American Chemical Society.

The single mutants TIM-Phe<sub>74</sub>Acid and TIM-Tyr<sub>101</sub>Acid were expressed in *E. coli* and purified using Ni-NTA affinity chromatography. We hypothesized that when Acid was incorporated at position 74, it would be proximal to Tyr<sub>101</sub> and thus be quenched, while when Acid was incorporated at position 101, there would be no quenching because there would not be a proximal Tyr residue. Furthermore, as the orientation of these residues is

a result of TIM's overall fold, we could disrupt the quenching interaction by chemically denaturing the protein with urea while monitoring the changes in fluorescence emission and lifetime. In the absence of urea, both mutants are quenched relative to the fluorescence of equimolar concentrations of Acd (urea had no effect on the fluorescence of Acd). In line with our predictions, TIM-Phe<sub>74</sub>Acd was quenched to a greater degree, presumably due to its proximity to Tyr<sub>101</sub>. On the other hand, TIM-Tyr<sub>101</sub>Acd places no Trp or Tyr in close proximity to the Acd residue. Thus, some non-specific quenching due to the local environment must occur. The two mutants recover comparable levels of fluorescence upon titration with urea, since quenching by Tyr<sub>101</sub> is relieved as TIM unfolds and dimer dissociation occurs (**Figure 2.22**).

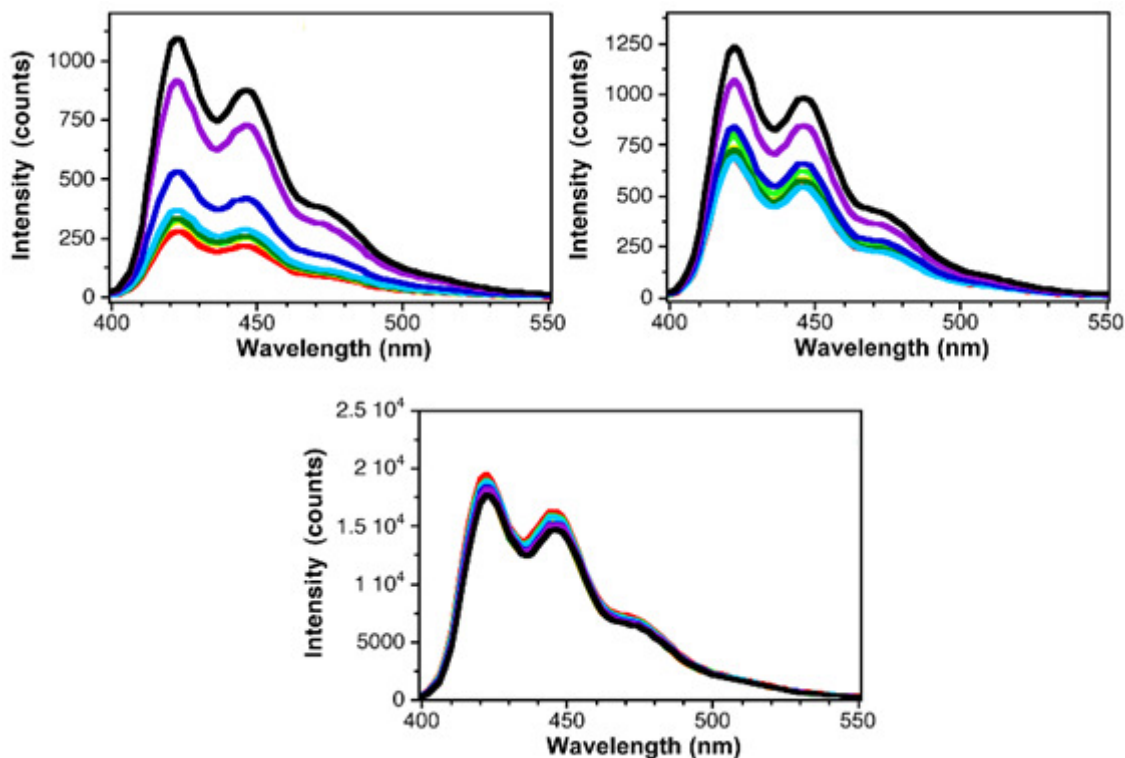


**Figure 2.22:** Fluorescence Spectra of TIM Denaturation in Urea. Top Left: TIM-Phe<sub>74</sub>Acid, Top Right: TIM-Tyr<sub>101</sub>Acid, Bottom: free Acid. All spectra recorded for solutions of TIM or Acid in 0 (red), 0.05 (pink), 0.1 (orange), 0.25 (yellow), 0.5 (light green), 0.75 (dark green), 1.0 (light blue), 2.0 (dark blue), 3.0 (purple), and 4.0 M (black) urea solutions. Reprinted with permission from Speight, L. C.; Muthusamy, A. K.; Goldberg, J. M.; Warner, J. B.; Wissner, R. F.; Willi, T. S.; Woodman, B. F.; Mehl, R. A.; Petersson, E. J., Efficient Synthesis and In Vivo Incorporation of Acridon-2-ylalanine, a Fluorescent Amino Acid for Lifetime and Forster Resonance Energy Transfer/Luminescence Resonance Energy Transfer Studies. *Journal of the American Chemical Society* **2013**, *135* (50), 18806-18814. Copyright (2013) American Chemical Society.

In addition to monitoring unfolding by changes in steady-state fluorescence, we also found it useful to measure quenching by changes in the fluorescence lifetime of Acid. Lifetime-based measurements of quenching made by time-correlated single photon counting (TCSPC) are very valuable because they are not sensitive to concentration

matching like steady-state measurements. Consistent with our steady-state data, we observed a decrease in the Acd lifetimes in both TIM-Phe<sub>74</sub>Acd and TIM-Tyr<sub>101</sub>Acd relative to free Acd:  $\tau_{\text{avg}}(\text{free}) = 15.8 \text{ ns}$ ,  $\tau_{\text{avg}}(\text{TIM-Phe}_{74}\text{Acd}) = 6.8 \text{ ns}$ , and  $\tau_{\text{avg}}(\text{TIM-Tyr}_{101}\text{Acd}) = 12.7 \text{ ns}$ . Lifetime measurements in 0, 2, 3, and 4 M urea demonstrate that the more dramatic Tyr-specific quenching in TIM-Phe<sub>74</sub>Acd is relieved by 3 M urea, and that global unfolding gives comparable lifetimes for both mutants in 4 M urea (**Figure 2.23**). These experiments show how changes in Acd lifetime, due either to general quenching phenomena and/or specific placement near a quenching residue, may be used to monitor unfolding.

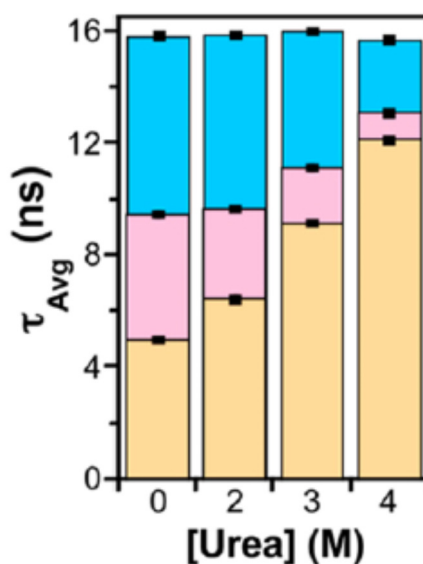


**Figure 2.23:** Monitoring TIM Unfolding By Changes in Average Fluorescence Lifetimes. Average lifetimes for 2  $\mu\text{M}$  solutions of TIM-Phe<sub>74</sub>Acd (orange), TIM-Tyr<sub>101</sub>Acd (magenta), or free Acd (blue) in 15 mM HEPES 140 mM potassium chloride (KCl) buffer with varying concentrations of urea. Acd lifetime derived from biexponential fits to the primary data. Reprinted with permission from Speight, L. C.; Muthusamy, A. K.; Goldberg, J. M.; Warner, J. B.; Wissner, R. F.; Willi, T. S.; Woodman, B. F.; Mehl, R. A.; Petersson, E. J., Efficient Synthesis and In Vivo Incorporation of Acridon-2-ylalanine, a Fluorescent

Amino Acid for Lifetime and Forster Resonance Energy Transfer/Luminescence Resonance Energy Transfer Studies. *Journal of the American Chemical Society* **2013**, *135* (50), 18806-18814. Copyright (2013) American Chemical Society.

## CONCLUSIONS AND FUTURE WORK

The fIUAA Acd had previously been shown to be a useful probe of protein conformational change, but its use had been limited to synthetic peptides and *in vitro* translation. Our work has expanded upon this, and provided a more efficient and affordable synthesis of Acd, as well as the identification of an Acd-specific o-aaRS/tRNA pair. These developments allow one to easily produce milligram quantities of Acd-labeled proteins for biophysical studies. Additionally, we have more thoroughly characterized the photophysical properties of Acd, including quenching interactions with select endogenous amino acids and FRET interactions with common fluorophores such as Trp and Mcm. We have also demonstrated the incorporation of Acd into several proteins, including CaM, and used changes in Acd fluorescence to monitor peptide binding through solvatochromic effects, FRET, LRET, and PET.

One of the advantages of our new Acd synthesis relative to previously published reports is its versatility. Some aspects of Acd photochemistry are non-ideal, such as its low extinction coefficient and blue wavelength emission. In some experiments, its sensitivity to solvent may also be problematic. To solve these problems, we have tested the compatibility of our route towards analogs of **9** and anthranilate coupling partners to generate Acd analogs with altered photophysical properties. Both 3-fluoro OTf derivatives and naphthyl anthranilate analogues have been shown to be compatible with

our methods in initial test reactions. Further expansion of this methodology will include **9** and anthranilate analogues bearing both electron-withdrawing and electron-donating groups to generate Acd derivatives containing these moieties. This strategy for the generation of fluorophores with higher extinction coefficients and more red-shifted emissions has been used previously for other chromophores<sup>118</sup>.

Finally, since the Acd o-aaRS/tRNA pair identified in these studies can also accept Brb as a substrate, we are working with the Mehl group to crystallize these complexes to determine the structural basis for substrate binding. Our preliminary analysis indicates that Glu<sub>65</sub> is likely important for Acd recognition. As noted within, it is not surprising for an aaRS that is permissive of several large amino acids to have a few key residues responsible for substrate binding. We are additionally exploring the permissivity of the Acd o-aaRS/tRNA system towards other tricyclic scaffolds such as xanthenes, acridines, and the aforementioned Acd derivatives. We expect that many such flUAAs may be incorporatable using our methods.

## **EXPERIMENTAL METHODS**

### **General Information**

L-Tyrosine, thionyl chloride, di-tert-butyl dicarbonate (Boc anhydride), methyl 2-aminobenzoate, *N,N*-diisopropylethylamine (DIPEA), (*S*)-(+)-4-Nitrophenylalanine methyl ester hydrochloride, iodobenzoic acid, and phenyl-sepharose CL-4B resin were purchased from Sigma-Aldrich (St. Louis, MO, USA). Boc-L-thionophenylalanine-1-(6-nitro)benzotriazolide and Fmoc- $\beta$ -(7-methoxycoumarin-4-yl)-alanine (Mcm) were

purchased from Bachem (Torrance, CA, USA). Rink amide resin, Fmoc-Ala-OH, Fmoc-Glu(OtBu)-OH, Fmoc-Leu-OH, Fmoc-Arg(Pbf)-OH, Fmoc-Gly-OH, Fmoc-Val-OH, Fmoc-Phe-OH, Fmoc-Ile-OH, and Fmoc-Trp(Boc)-OH purchased from Novabiochem (currently EMD Millipore; **Billerica, MA, USA**). Piperidine and 2-(1*H*-benzotriazol-1-yl)-1,1,3,3-tetramethyluronium hexafluorophosphate (HBTU) were purchased from American Bioanalytical (Natick, MA, USA). *N*-Phenyl-bis(trifluoromethanesulfonimide) was purchased from Oakwood Chemical (West Columbia, SC, USA). *E. coli* BL21(DE3) cells were purchased from Stratagene (La Jolla, CA, USA). *E. coli* ElectroMAX DH10B cells were purchased from Invitrogen (Grand Island, NY, USA). Ni-NTA resin was purchased from Qiagen (Hilden, Germany); BD Talon™ resin was purchased from Clontech (Mountain View, CA, USA). Milli-Q filtered (18 MΩ) water was used for all solutions (Millipore; Billerica, MA, USA). All other reagents and solvents were purchased from Fisher Scientific (Pittsburg, PA, USA). All peptide synthesis reaction vessels (RVs) were treated with Sigmacote prior to use.

DNA sequencing was performed at the University of Pennsylvania DNA sequencing facility. Matrix-assisted laser desorption ionization (MALDI) mass spectra were collected with a Bruker Ultraflex III MALDI-TOF-TOF mass spectrometer (Billerica, MA). UV/Vis absorbance spectra were obtained with a Hewlett-Packard 8452A diode array spectrophotometer (currently Agilent Technologies; Santa Clara, CA). NMR spectra, <sup>1</sup>H and <sup>13</sup>C, were collected with a Bruker DRX 500 MHz instrument. CDCl<sub>3</sub> was calibrated at  $\delta$  7.27 for <sup>1</sup>H and  $\delta$  77.2 for <sup>13</sup>C. CD<sub>3</sub>OD was calibrated at  $\delta$  3.31 for <sup>1</sup>H and  $\delta$  49.15 for <sup>13</sup>C. DEPT-135 Carbon NMR notation as follows: no signal is designated by (np), a positive signal is designated by (+), and a negative signal is designated by (-).

High-resolution mass spectra (HRMS) were obtained on a Waters LC-TOF mass spectrometer (model LCT-XE Premier) using electrospray ionization in positive mode. . UV absorbance spectra were obtained with a Hewlett-Packard 8452A diode array spectrophotometer (currently Agilent Technologies; Santa Clara, CA, USA). Fluorescence spectra were collected with a Varian Cary Eclipse fluorescence spectrophotometer (currently Agilent Technologies) fitted with a Peltier multicell holder, a Photon Technologies International (PTI) QuantaMaster™ fluorometer (Birmingham, NJ, USA), a Tecan M1000 plate reader (Mannedorf, Switzerland), or a BioTek Synergy2 plate reader (Winooski, VT, USA) with a UV transparent 96 well plate. Steady-state Stern-Volmer experiments were conducted on a PerkinElmer Envision Xcite multilabel reader (PerkinElmer Health Sciences Inc.; Shelton, CT, USA) with a black bottomed 96 well plate. Circular dichroism experiments were conducted with an Aviv 410 CD spectrometer (Aviv Biomedical; Lakewood, NJ, USA). Automated peptide synthesis was performed on a Liberty 1 system (CEM Corp.; Matthews, NC, USA) in the UPenn Biological Chemistry Resource Center. Protein purification was conducted on an ÄKTA fast protein liquid chromatography (FPLC) system (GE Healthcare Life Sciences; Piscataway Township, NJ, USA). Peptides were purified with a Varian ProStar High-Performance Liquid Chromatography (HPLC) instrument outfitted with a diode array detector (currently Agilent Technologies) using aqueous (**A**) ( $\text{H}_2\text{O} + 0.1\% \text{CF}_3\text{CO}_2\text{H}$ ) and (**B**) organic ( $\text{CH}_3\text{CN} + 0.1\% \text{CF}_3\text{CO}_2\text{H}$ ) phases. Small molecule analyses were performed on an Agilent 1100 HPLC instrument outfitted with a diode array detector using the same aqueous and organic phases.

## Synthesis of Acid (1) via p-NO<sub>2</sub>F Route

### Methyl (S)-2-((tert-butoxycarbonyl)amino)-3-(4-nitrophenyl)propanoate (3)

2.82 g (10.88 mmol) **2** was dissolved in 16 mL of 3:1 THF:H<sub>2</sub>O in a round bottom flask (RBF) and cooled to 0 °C in an ice water bath. 1.32 g (12.46 mmol) Na<sub>2</sub>CO<sub>3</sub> was added and the mixture was allowed to stir for 15 min. 3.20 g (14.66 mmol) Boc<sub>2</sub>O was then added and the solution was allowed to stir and warm to room temperature (RT) overnight. The solution was then acidified with 3 M HCl to pH 2, 9 mL of H<sub>2</sub>O was added, and the organics were extracted with ethyl acetate (EtOAc), dried with MgSO<sub>4</sub>, and concentrated *in vacuo*. The crude yellow oil was purified with 1:1 EtOAc:Hexanes (R<sub>f</sub> = 0.5) to yield 3.42 g **3** (97.1 %). Characterization matched that which was previously described<sup>90</sup>.

### Methyl (S)-3-(4-aminophenyl)-2-((tert-butoxycarbonyl)amino)propanoate (4)

84 mg Pd/C was added to a dry RBF with 5 mL EtOAc, sparged 3 times with alternating vacuum evacuation / argon fill, and then sparged 3 times with alternating vacuum evacuation / H<sub>2</sub> fill. 1.05 g (3.24 mmol) **3** was added in 11 mL EtOAc and then the solution was again sparged 3 times with alternating vacuum evacuation / H<sub>2</sub> fill. After 3 hr 15 min, the reaction was complete by TLC (R<sub>f</sub> = 0.3 in 1:1 EtOAc:Hexanes). The solution was then filtered through celite using EtOAc as the eluent and the organic filtrate was concentrated *in vacuo*. The crude yellow oil was then purified with 1:1 EtOAc:Hexanes to yield 0.95 g (99.1 %). Characterization matched that which was previously described<sup>90</sup>.

**(S)-2-((4-(2-((tert-butoxycarbonyl)amino)-3-methoxy-3-oxopropyl)phenyl)amino)benzoic acid (5)**

Compound **5** was synthesized essentially as described. Characterization matched previous reports<sup>90</sup>.

**(S)-2-amino-3-(9-oxo-9,10-dihydroacridin-2-yl) propanoic acid (Acd, 1).**

PPA (3 mL) was added to a flask containing **5** (0.188 g, 0.454 mmol) and the mixture was heated to 135 °C and stirred magnetically for 2 hr. The reaction was removed from heat and allowed to cool to 50 °C. Water (50 mL) was added and the flask was allowed to stand at 4 °C overnight. The resulting yellow precipitate was filtered and washed with cold water. The compound was dried under reduced pressure, then added to 3 mL of 1:1 1,4 dioxane:water and the pH adjusted to 9 by dropwise addition of 10 M NaOH. After stirring for 2 hr, the mixture was acidified with 6 M HCl to pH 2 and cooled on ice to precipitate product. The resulting solid was collected by vacuum filtration and dried to yield **1** as a yellow powder (0.081 g; 63 %). <sup>1</sup>H NMR (500 MHz, CD<sub>3</sub>OD): δ 8.33 (dd *J* = 1.8, 1.1 Hz, 1H), 8.25 (d, *J* = 1.8 Hz, 1H), 7.75 (m, 1H), 7.68 (dd, *J* = 8.6, 2.1 Hz, 1H), 7.53 (dd, *J* = 8.5, 3.8 Hz, 2H), 7.3 (m, 1 H), 4.28 (dd, *J* = 7.7, 5.4 Hz, 1H), 3.54 (m, 2H); <sup>13</sup>C NMR (125 MHz, CD<sub>3</sub>OD): δ 180.1 (np), 171.5 (np), 142.7 (np), 142.2 (np), 136.1 (+), 135.3 (+), 129.0 (np), 128.3 (+), 127.5 (+), 123.0 (+), 119.6 (+), 119.3 (np), 118.6 (+), 117.0 (np), 55.3 (+), 37.2 (-); HRMS (ESI) *m/z* calculated for C<sub>16</sub>H<sub>15</sub>N<sub>2</sub>O<sub>3</sub><sup>+</sup> [M+H]<sup>+</sup> 283.1083, found 283.1093.

## Synthesis of Acid (1) via L-Tyrosine Route

### Methyl (S)-2-((tert-butoxycarbonyl)amino)-3-(4-

### (((trifluoromethyl)sulfonyl)oxy)phenyl)propanoate (9)

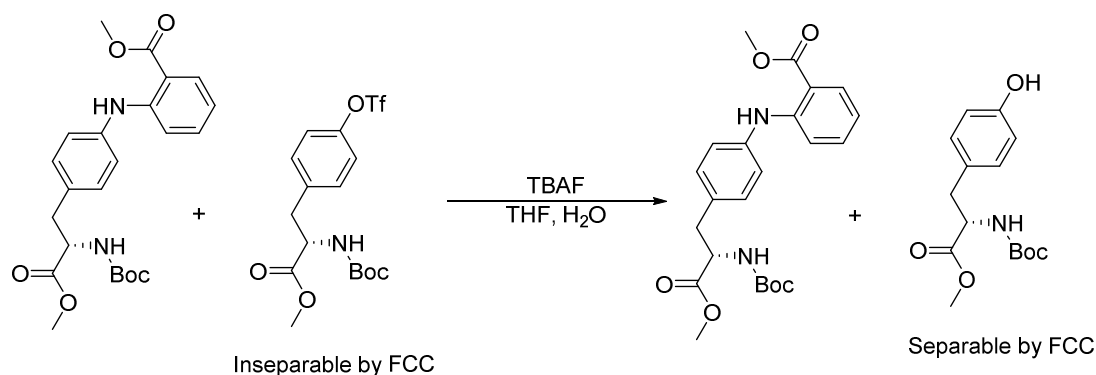
Compound **9** was synthesized essentially as described. Characterization matched previous reports<sup>99</sup>.

### (S)-methyl 2-((4-(2-((tert-butoxycarbonyl)amino)-3-methoxy-3-oxopropyl)phenyl)amino)benzoate (10)

75 mL of toluene was degassed with argon for 15 min in a 250 mL flame dried round bottom flask. Tyr derivative **9** (3.00 g, 7.02 mmol) was added to the flask followed by methyl 2-aminobenzoate (1.20 mL, 9.27 mmol). This solution was degassed with argon for 5 min. Then palladium(II) acetate (0.08 g, 0.37 mmol), and racemic 2,2'-bis(diphenyl-phosphino)-1,1'-binaphthyl (0.05 g, 0.09 mmol) were added to the flask. Cesium carbonate (6.88 g, 21.1 mmol) was ground and added to the flask. The flask was then fitted with a reflux condenser and heated to 135 °C for 23 h. After allowing the solution to cool to ambient temperature, the contents were filtered through a short plug of silica gel using CH<sub>2</sub>Cl<sub>2</sub> to transfer the material to the silica (250 mL) and then ethyl acetate (500 mL) was used to elute the product. The clarified solution was then concentrated under reduced pressure. Silica gel flash column chromatography (10% ethyl acetate in hexanes) afforded 2.759 g (6.44 mmol, 91.7%) of a pale yellow oil. *R*<sub>f</sub> = 0.2 in 15% ethyl acetate in hexanes; <sup>1</sup>H NMR (500 MHz, CDCl<sub>3</sub>) δ 9.44 (s, 1H), 7.96 (d, *J* = 8.0 Hz, 1H), 7.31 (t, *J* = 7.9 Hz, 1H), 7.23 (d, *J* = 8.5 Hz 1H), 7.18 (d, *J* = 8.2 Hz,

2H), 7.10 (d,  $J = 8.1$  Hz, 1 H), 6.73 (t,  $J = 7.5$  Hz, 1 H), 5.05 (d,  $J = 7.9$  Hz, 1 H), 4.61 – 4.57 (m, 1 H), 3.90 (s, 3H), 3.74 (s, 3H), 3.07 (dd,  $J = 26.5, 5.7$  Hz, 2 H), 1.43 (s, 9H);  $^{13}\text{C}$  NMR (125 MHz,  $\text{CDCl}_3$ ):  $\delta$  172.5 (np), 169.0 (np), 155.3 (np), 148.0 (np), 139.8 (np), 134.2 (+), 131.8 (+), 131.3 (np), 130.4 (+), 122.6 (+), 117.3 (+), 114.2 (+), 112.1 (np), 80.0 (np), 54.6 (+), 52.4 (+), 51.9 (+), 38.0 (-), 28.5 (+); HRMS (ESI)  $m/z$  calcd for  $\text{C}_{23}\text{H}_{28}\text{N}_2\text{O}_6$   $[\text{M}+\text{H}]^+$  429.2000, found 429.2026.

### Hydrolysis of **9** in the Presence of **10**



The crude product mixture (0.94 g mixture of **9** and **10**) was dissolved in 1 mL of THF in a glass vial with a stir bar. 0.7 mL of 1 M TBAF in THF with trace water was added to the vial. The vial was kept in an argon atmosphere as the reaction proceeded at room temperature for 16 hours. 2 mL of methanol was added and the reaction was then stirred for an additional 5 min. The solution was then transferred to a separatory funnel and 2 mL of saturated ammonium chloride (aq) was added. The products were extracted against four 5 mL portions of dichloromethane. The organic phase was dried over magnesium sulfate and concentrated under vacuum. The desired product was isolated using a 7:3

Hexanes:Ethyl acetate flash silica column. The desired product was isolated in 85.1% yield (0.80 g).

**(S)-2-amino-3-(9-oxo-9,10-dihydroacridin-2-yl) propanoic acid (Acid, 1)**

12 mL 13.5 M sulfuric acid was added to a flask containing **6** (1.02 g, 2.38 mmol). The flask was then fitted with a reflux condenser and heated to 115 °C for 16 h in an oil bath. 80 mL water was then added slowly to the flask and allowed to stir for 15 min. The reaction was then removed from the hot oil bath and allowed to cool with stirring. Upon reaching ambient temperature, the solution was then cooled to 4 °C, and let stand for 2 h. During the 2 h cooling period, 100 g of Dowex ion exchange resin was made into a slurry with 1.8 M aqueous sulfuric acid and applied to a flash chromatography column. The resin was washed with 350 mL 1.8 M aqueous sulfuric acid, 2 L water, 1 L 1.5 M aqueous ammonium hydroxide, and 4 L water. Following these washes, the resin was dried by passing air through the column. The cooled Acid solution was then vacuum filtered on a Büchner funnel to remove precipitated material and the clarified solution was applied to the washed and dried ion exchange resin. The resulting resin slurry was shaken in the chromatography column for 5 min before the solution was drained. This solution is then reapplied to the dried resin and shaken for an additional 5 min. The twice-passed solution was then set aside. The loaded resin was washed by 4 L water before the compound of interest was eluted with 1.45 L 1.5 M ammonium hydroxide. The solution was concentrated to 50 mL by rotary evaporation and then lyophilized to dryness, yielding a crop of Acid as a yellow powder (0.64 g 2.26 mmol 94.9 %). The ion exchange resin was recycled by washing with 4 L water and dried until further use. To

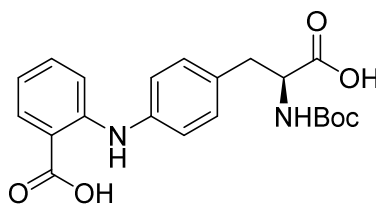
maximize yield, the twice-passed solution was reapplied to washed and dried ion exchange resin and the process repeated to yield a second crop of Acd (0.02 g 0.08 mmol 3.4 %). Total yield for the two columns was 98.3 % and purity was > 98 % by analytical HPLC. Further characterization matched that which was previously described<sup>91</sup>.

**Table 2.5.** Acd HPLC Analysis Gradient.

Time (min)	% Solvent A
0:00	99
6:00	98
12:00	95
18:00	90
30:00	50
35:00	1
40:00	1
50:00	99

### Synthesis of Acd (1) *via* LiOH saponification and PPA deprotection/cyclization

#### (S)-2-((4-(2-((tert-butoxycarbonyl)amino)-2-carboxyethyl)phenyl)amino)benzoic acid (13)



**13**

Diester **10** (2.16 g, 5.04 mmol) was added to a 250 mL round bottom flask with a stir bar and 50 mL of tetrahydrofuran (THF). This solution was then cooled to 4 °C. Lithium hydroxide (3.31 g, 138.15 mmol) was dissolved in a separate flask with 150 mL water and vigorous stirring. The LiOH solution was then slowly added to the solution

containing **10**. The flask was fitted with a rubber septum and a balloon filled with argon and stirred magnetically at 4 °C. After 24 h, the solution was warmed to ambient temperature and the pH was adjusted to 3 with 42 mL of 3 M HCl. Crude product was extracted with CH<sub>2</sub>Cl<sub>2</sub> (3 x 100 mL, 1 x 50 mL), dried with magnesium sulfate, and concentrated under reduced pressure. The resulting crude oil was re-dissolved in 20 mL DCM and cooled at 4 °C for 16 h. A first crop of recrystallized product (a fine white powder) was collected by vacuum and washed with 100 mL of cold CH<sub>2</sub>Cl<sub>2</sub> (1.63 g, 4.08 mmol, 80.8 %). The filtrate was then concentrated under reduced pressure, and a second crop was collected by repeating the recrystallization procedure with 10 mL CH<sub>2</sub>Cl<sub>2</sub> (0.04 g, 0.09 mmol, 1.8 %). The total yield for the two crops of fine white powder was 82.6 %.

<sup>1</sup>H NMR (500 MHz, CD<sub>3</sub>OD) δ 7.96 (dd, *J* = 8.0, 1.4, 1H), 7.32 – 7.27 (m, 1H), 7.24 – 7.11 (m, 5H), 6.71 (t, *J* = 7.5 Hz, 1H), 4.36 (dd, *J* = 8.8, 5.0 Hz, 1H), 3.14 (dd, *J* = 8.9, 5 Hz, 1 H), 2.90 (dd, *J* = 9.0, 4.7 Hz, 1 H), 1.4 (s, 9 H); <sup>13</sup>C NMR (125 MHz, CD<sub>3</sub>OD): δ 175.5 (np), 171.9 (np), 157.9 (np), 149.5 (np), 140.9 (np), 135.2 (+), 133.7 (np), 133.4 (+), 131.5 (+), 123.3 (+), 118.1 (+), 114.9 (+), 113.4 (np), 80.7 (np), 56.4 (+), 38.3 (-), 28.8 (+); HRMS (ESI) *m/z* calcd for C<sub>21</sub>H<sub>25</sub>N<sub>2</sub>O<sub>6</sub> [M+Na]<sup>+</sup> 423.1532, found 423.1525.

**(S)-2-amino-3-(9-oxo-9,10-dihydroacridin-2-yl) propanoic acid (Acd, 1).**

51.71 g polyphosphoric acid (PPA) was weighed into a 250 mL flask. A stir bar was added and the material was heated to 135 °C for 15 min in an oil bath. **11** (1.00 g, 2.5 mmol) was added directly to the flask of PPA and allowed to react for 2 h. 50 mL water was slowly added (2 mL portions over 10 min) and the reaction was allowed to cool to 60 °C. After stirring for 1 h at 60 °C, the flask was removed from the oil bath, the solution

decanted into a 500 mL beaker, and cooled to ambient temperature. Insoluble impurities were removed by vacuum filtration and the clarified solution was returned to a 500 mL beaker with a stir bar. The pH of the solution was adjusted to 5.5 by addition of 100 mL of 10 M NaOH (aq) and then the solution was cooled to 4 °C for 16 h. Next, crude product was collected by vacuum. After drying on the filter cake, the crude material was suspended in 50 mL water and brought into solution by drop-wise addition of 5 M NaOH (bringing the pH to 9.0). Insoluble impurities were removed by vacuum filtration. The pH of the clarified solution was then adjusted to 5.5 with 3 M HCl, cooled to 4 °C, and let stand for 4 hours. Bright yellow precipitate was collected by vacuum filtration and dried overnight by vacuum yielding 0.53 g (1.86 mmol, 74.4 %). The purity was > 99% by analytical HPLC. Further characterization matched that which was previously described<sup>91</sup>.

### **Screening of Cross-Coupling Conditions**

The experimental procedures in this work were similar to those previously reported<sup>119</sup>. The experimental design was accomplished using Accelrys Library Studio (San Diego, CA, USA). Screening reactions were carried out in 1 mL flat bottom glass vials (30 mm x 8 mm) in a 96-well plate aluminum reactor block from Analytical Sales and Services (Pompton Plains, NJ, USA).

Liquid chemicals were dosed using multi-channel or single-channel pipettors. Solid chemicals were dosed as solutions or slurries in appropriate solvents. Undesired addition solvent was removed using a JKem blow-down system (St. Louis, MO, USA) located inside the glovebox. The reactions were heated and stirred on a heating block with a

tumble-stirrer (V&P Scientific; San Diego, CA, USA) or IKA magnetic stirrer hot plate (Wilmington, NC, USA) using 1.32 mm diameter x 1.57 mm length parylene stir bars. The reactions were sealed in the 96-well plate during reaction. Below each reactor vial in the aluminum 96-well plate was a 0.062 mm thick silicon-rubber gasket. Directly above the glass vial reactor top was a Teflon perfluoroalkoxy copolymer resin sealing gasket and above that, two more 0.062 mm thick silicon-rubber gaskets. The entire assembly was compressed between an aluminum top and the reactor base with nine screws. The conditions for the coupling of **9** and methyl anthranilate included variations of the following:

Bases	Solvents	Pd loading (mol %)
Cesium carbonate	<i>n</i> -Butanol	5.2
Potassium Carbonate	<i>N</i> -Methylpyrrolidine	2.5
Sodium Carbonate	Cyclopentylmethylether	1
Lithium Carbonate	<i>N,N</i> -Dimethylacetamide	0.1
	Toluene	
	1,4-Dioxane	

The following procedure is representative of the high-throughput experimentation reaction described in this publication. Palladium diacetate (10, 25 and 50  $\mu\text{L}$  of a 0.01 M solution in THF and 101  $\mu\text{L}$  of a 0.001 M solution in THF) was used in all cases. A racemic BINAP (10, 25 and 50  $\mu\text{L}$  of a 0.014 M solution in THF and 101  $\mu\text{L}$  of a 0.0014 M solution in THF) was added to the reaction vials and this was evacuated to dryness on a JKem-blow-down block. Base (30  $\mu\text{mol}$ , stock solutions gave an approximate 25

mg/mL slurry in THF) was then added to the ligand/catalyst mixture, and this was evacuated to dryness on a JKem-blow-down block. A parylene stir-bar was added to each reaction vial. The aryl triflate **9** (10  $\mu$ mol/reaction) and methyl-2-aminobenzoate (10  $\mu$ mol/reaction) were then dosed together in the reaction solvents (100  $\mu$ L of a 0.1 M solution). The vials were then sealed and heated at 120  $^{\circ}$ C for 4 h. After cooling to ambient temperature, the reaction mixtures were diluted with a solution of internal standard in CH<sub>3</sub>CN (2  $\mu$ mol biphenyl, 500  $\mu$ L of solution), and the contents were stirred. Into a separate 96-well plate LC block was added 700  $\mu$ L of CH<sub>3</sub>CN and then 25  $\mu$ L of the diluted reaction mixtures. The 96-well plate LC block was then sealed with a polypropylene 1 mL cap mat. The reactions were analyzed using an Agilent Technologies 1200 series HPLC with a 96-well plate auto-sampler.

### **Peptide Synthesis and Purification.**

The CaM binding peptide pOCNC has the sequence FRRIARLVGVLRFAFR; two derivatives in which the N-terminal phenylalanine has been replaced with either Mcm or Trp are named Mcm-pOCNC and Trp-pOCNC respectively. The general sequence of these peptides is derived from the bOCNCp peptide fragment described by Contessa *et al.* (sequence: GGFRIARLVGVLRWAYR)<sup>108</sup>. The pOCNC and pOCNC-F'<sub>1</sub> peptides (where F' indicates thiophenylalanine) were constructed using a combination of automated and manual synthesis. Residues R<sub>17</sub>-R<sub>2</sub> were added to 100  $\mu$ mol of Rink amide resin (100 – 200 mesh; 0.6 mmol substitution/g; 100  $\mu$ mol) using a Liberty 1 peptide synthesizer as follows.

The peptide RRIARLVGVLEWAYR was synthesized (100 micromole scale) by solid phase peptide synthesis, using Fmoc chemistry, on a Liberty1 Automated Microwave Peptide Synthesizer. Piperidine (20 %) in DMF was used as the deprotection agent, 0.5 M HBTU in DMF was used as the activator, and 2 M DIPEA in NMP was used as the activator base. Five molar equivalents of the amino acid were used for each coupling on Rink Amide MBHA resin (0.59 mmol/g substitution, Novabiochem). Residues Arg<sub>1</sub>, Arg<sub>2</sub>, Arg<sub>5</sub>, Arg<sub>11</sub>, and Arg<sub>16</sub> were coupled using Method 1. Residues Ile<sub>3</sub>, Leu<sub>6</sub>, Val<sub>7</sub>, Gly<sub>8</sub>, Val<sub>9</sub>, and Phe<sub>15</sub> were coupled using Method 2. Residues Ala<sub>4</sub>, Leu<sub>10</sub>, Glu<sub>12</sub>, Phe<sub>13</sub>, Ala<sub>14</sub> were coupled using Method 3. Method 1: Initial 30 s microwave deprotection (40 W, 75 °C), followed by 3 min microwave deprotection (40 W, 75 °C). Two consecutive coupling cycles were used. The first coupling was at room temperature for 25 min followed by an additional 5 min under microwave power (25 W, 75 °C). The second coupling was performed under microwave power for 5 min (25 W, 75 °C). Method 2: Initial 30 s microwave deprotection (40 W, 75 °C), followed by 3 min microwave deprotection (40 W, 75 °C). A single microwave coupling was performed for 5 min (25 W, 75 °C). Method 3: Initial 30 s microwave deprotection (40 W, 75 °C), followed by 3 min microwave deprotection (40 W, 75 °C). Two consecutive microwave couplings were performed for 5 min (25 W, 75 °C).

Before removal of the Fmoc-group from R<sub>2</sub>, the resin beads were divided into two equal portions and transferred to clean RVs for manual coupling of either Fmoc-L-Phe-OH or Boc-L-thionophenylalanine-1-(6-nitro)benzotriazolide. The coupling of Fmoc-L-Phe-OH to R<sub>2</sub>-R<sub>17</sub> to form pOCNC was performed for 45 min with 5 equiv HBTU and 10 equiv DIPEA. The addition of Boc-L-thionophenylalanine-1-(6-nitro)benzotriazolide to form

pOCNC-F<sub>1</sub> was performed for 45 min with 10 equiv DIPEA. After removal of the *N*-terminal Fmoc-group from pOCNC with 20% piperidine, the resin beads were washed with CH<sub>2</sub>Cl<sub>2</sub>, dried under vacuum, and incubated on a rotisserie for 120 min with 10 mL TFA/TIPSH (95:5 v/v). The thioamide-containing pOCNC-F<sub>1</sub> was cleaved from the resin (without piperidine treatment) and deprotected by washing the resin with CH<sub>2</sub>Cl<sub>2</sub>, drying under vacuum, and incubating for 90 min with 10 mL TFA/TIPSH (95:5 v/v). After each incubation period, the cleavage cocktail for the peptide was expelled from the RV with nitrogen and dried by rotary evaporation. Crude peptide was redissolved in 10 mL CH<sub>3</sub>CN/H<sub>2</sub>O (3:2 v/v) and purified by reverse phase HPLC with gradients 1 and 2 (**Table 2.7**). Using this method, the peptide eluted at approximately 19.5 min. Peptide identity was confirmed by MALDI-MS (**Table 2.6**).

Similarly, the peptides M<sub>cm</sub>-pOCNC and Trp-pOCNC were made on the 50 μmol scale by manual solid phase peptide synthesis. Rink amide resin (100 – 200 mesh; 0.6 mmol substitution/g; 50 μmol) was added to a dry clean RV. Two successive 90 min incubations of 10 mL dimethylformamide (DMF) and magnetic stirring were used to swell the resin. Following swelling, DMF was removed by vacuum. 20% piperidine in DMF (5 mL) was used to deprotect the resin in two successive 15 min incubations with magnetic stirring. Then the resin was washed extensively with DMF. The first amino acid (5 equiv) and HBTU (5 equiv) were dissolved in DMF (5 mL) and added to the RV along with DIPEA (10 equiv; 44 μL). The mixture was allowed to react for 45 min with magnetic stirring. Spent solution was removed with vacuum suction and the resin beads were washed thoroughly with DMF. The coupling was repeated with an additional 5 equiv of amino acid and HBTU and 10 equiv of DIPEA (in 5 mL DMF). The second

spent solution was removed with vacuum suction and the resin beads were again washed thoroughly with DMF. The *N*-terminal Fmoc protecting group was removed by two successive 15 min treatments of 20% piperidine in DMF (5 mL). Subsequent amino acid couplings and deprotections were conducted as described above until R<sub>2</sub>. Prior to the the *N*-terminal Fmoc deprotection of R<sub>2</sub>, the beads were split into two 25 μM portions in separate vessels. In one vessel, the beads were treated twice with 5 equiv of Fmoc-Mcm-OH, 5 equiv HBTU, and 10 equiv DIPEA for 45 min while the beads in the other vessel were given the same treatment with the replacement of 5 equiv Fmoc-Trp(Boc)-OH for Fmoc-Mcm-OH. The peptides were then cleaved from the resin separately by incubating the beads with 10 mL TFA/TIPSH (95:5 v/v) for 120 min on a rotisserie. After this treatment, the resulting solutions were expelled from the RV with nitrogen and concentrated by rotary evaporation. The resulting residues were resuspended in 2 mL acetonitrile and split into two 1 mL portions. Then 14 mL diethyl ether was added to each portion to precipitate the peptide after 10 min of incubation at - 20 °C. The precipitates were collected by centrifuging for 5 min at 3000 rpm and decanting the supernatant. This precipitate was air dried and resuspended in 10 mL H<sub>2</sub>O/CH<sub>3</sub>CN/TFA (10:10:1) for HPLC purification. The crude peptide was purified by reverse phase HPLC with gradient 3 (**Table 2.7**). Using this method, the peptides eluted at approximately 17 min. Peptide identities were confirmed by MALDI MS (**Table 2.6**).

**Table 2.6:** Calculated and Observed Peptide and Protein Masses.

Peptide	Calculated m/z	Observed m/z	Calculated m/z	Observed m/z
	[M+H] <sup>+</sup>	[M+H] <sup>+</sup>	[M+Na] <sup>+</sup>	[M+Na] <sup>+</sup>
pOCNC	2106.3	2106.3	2128.6	2128.8
pOCNC-F <sub>1</sub>	2122.3	2122.6	2144.2	2144.7
Mcm-pOCNC	2204.6	2204.3	2226.6	2226.2
Trp-pOCNC	2145.6	2145.2	2167.6	2167.2
GFP-WT	27828	27828		
GFP-N <sub>150</sub> δ	27978	27978		
αS-WT	14461	14461		
αS-Y <sub>39</sub> δ	14562	14563		
αS-F <sub>94</sub> δ	14578	14578		
CaM-WT	16707	16707		
CaM-F <sub>13</sub> δ	16824	16825		
CaM-G <sub>41</sub> δ	16915	16914		
CaM-Y <sub>100</sub> δ	16808	16808		
CaM-L <sub>113</sub> δ	16858	16859		
TIM-WT	31112	31113		
TIM-F <sub>74</sub> δ	31229	31230		
TIM-Y <sub>101</sub> δ	31213	31214		
TIM-F <sub>74</sub> Y <sub>101</sub> δ	31330	31331		

**Table 2.7:** Solvent Gradients Used for Peptide Purification and Analysis.

Gradient	Time (min)	Buffer A (%)	Gradient	Time (min)	Buffer A (%)
1	0:00	98	2	0:00	98
	5:00	98		5:00	98
	8:00	71		8:00	71
	29:00	59		19:00	64
	33:00	0		23:00	0
	38:00	0		28:00	0
	43:00	98		33:00	98
3	0:00	98			
	5:00	98			
	12:00	50			
	22:00	38			
	25:00	0			
	30:00	0			
	34:00	98			

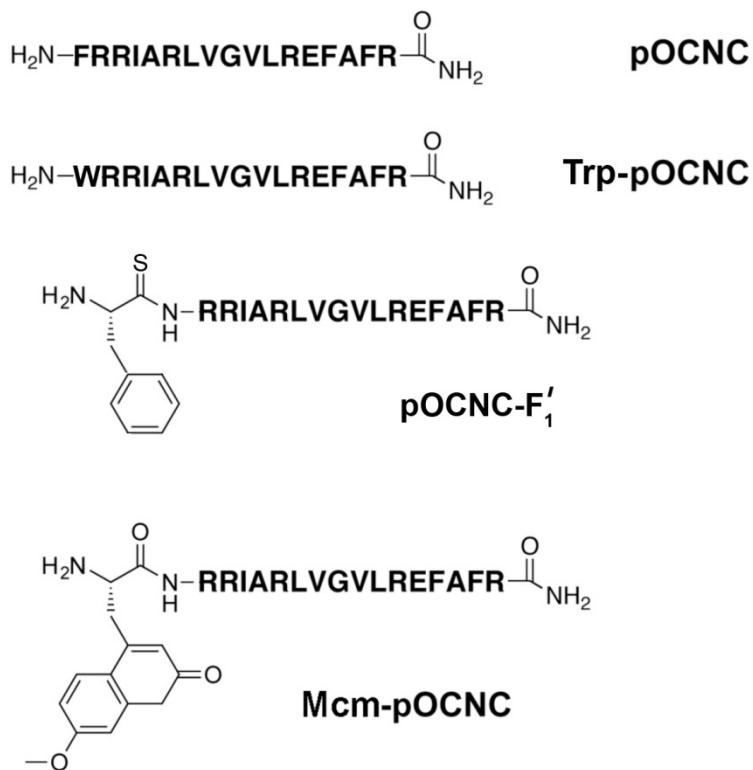


**Figure 2.24:** Representative Structures of p-OCNC Peptides Used in This Work. Reprinted with permission from Speight, L. C.; Muthusamy, A. K.; Goldberg, J. M.; Warner, J. B.; Wissner, R. F.; Willi, T. S.; Woodman, B. F.; Mehl, R. A.; Petersson, E. J., Efficient Synthesis and In Vivo Incorporation of Acridon-2-ylalanine, a Fluorescent Amino Acid for Lifetime and Forster Resonance Energy Transfer/Luminescence Resonance Energy Transfer Studies. *Journal of the American Chemical Society* **2013**, *135* (50), 18806-18814. Copyright (2013) American Chemical Society.

### Absorption and Fluorescence Spectroscopy of Fluorophore Pairs

UV/Vis absorbance and fluorescence spectra were acquired for Trp, 7-methoxycoumarin-4-yl alanine (Mcm), and Acd peptides, and BODIPY Fl, 5-carboxyfluorescein (Fam), rhodamine 6G (R6G), and 2-((7-nitrobenzo[1,2,5]oxadiazol-4-yl)amino)ethanol (NBD). Absorption spectra were collected using quartz cells with 1 cm path lengths.

Fluorescence spectra were collected as the average of three scans at 25 °C of three

samples of each solution using quartz cells with 1 cm path lengths. Excitation and emission slit widths were 5 nm, scan rate 120 nm/min, averaging time 0.5 s, and data interval 1.0 nm.

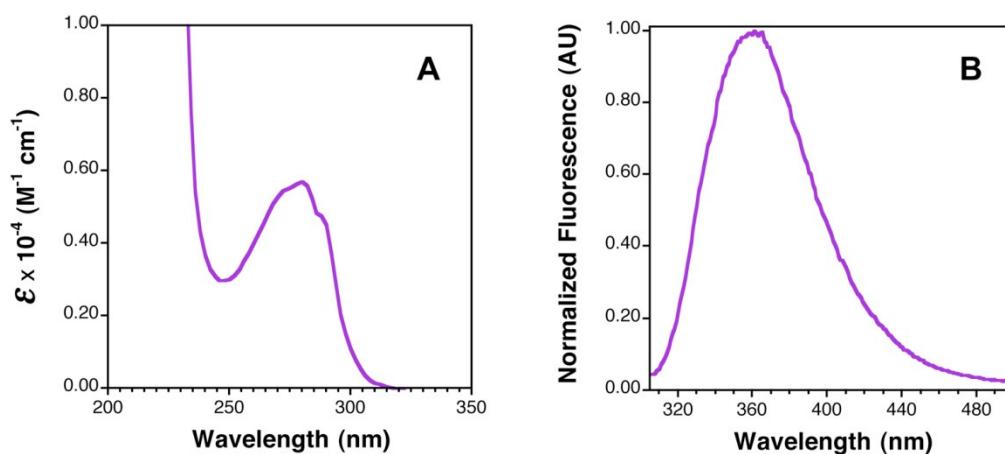


**Figure 2.25:** Absorption and Fluorescence Spectra of Trp. Absorbance (A) and fluorescence (B) spectra of 7.5  $\mu\text{M}$  LeuProProTrp in pH 7.0 phosphate buffered saline (PBS; 10 mM  $\text{Na}_2\text{HPO}_4$ , 150 mM NaCl, pH adjusted with HCl). Concentration determined using published extinction coefficient of Trp ( $\lambda_{278} = 5,700 \text{ M}^{-1} \cdot \text{cm}^{-1}$ )<sup>120</sup>. Peptide synthesized as described<sup>92</sup>. Reprinted with permission from Speight, L. C.; Muthusamy, A. K.; Goldberg, J. M.; Warner, J. B.; Wissner, R. F.; Willi, T. S.; Woodman, B. F.; Mehl, R. A.; Petersson, E. J., Efficient Synthesis and In Vivo Incorporation of Acridon-2-ylalanine, a Fluorescent Amino Acid for Lifetime and Forster Resonance Energy Transfer/Luminescence Resonance Energy Transfer Studies. *Journal of the American Chemical Society* **2013**, *135* (50), 18806-18814. Copyright (2013) American Chemical Society.

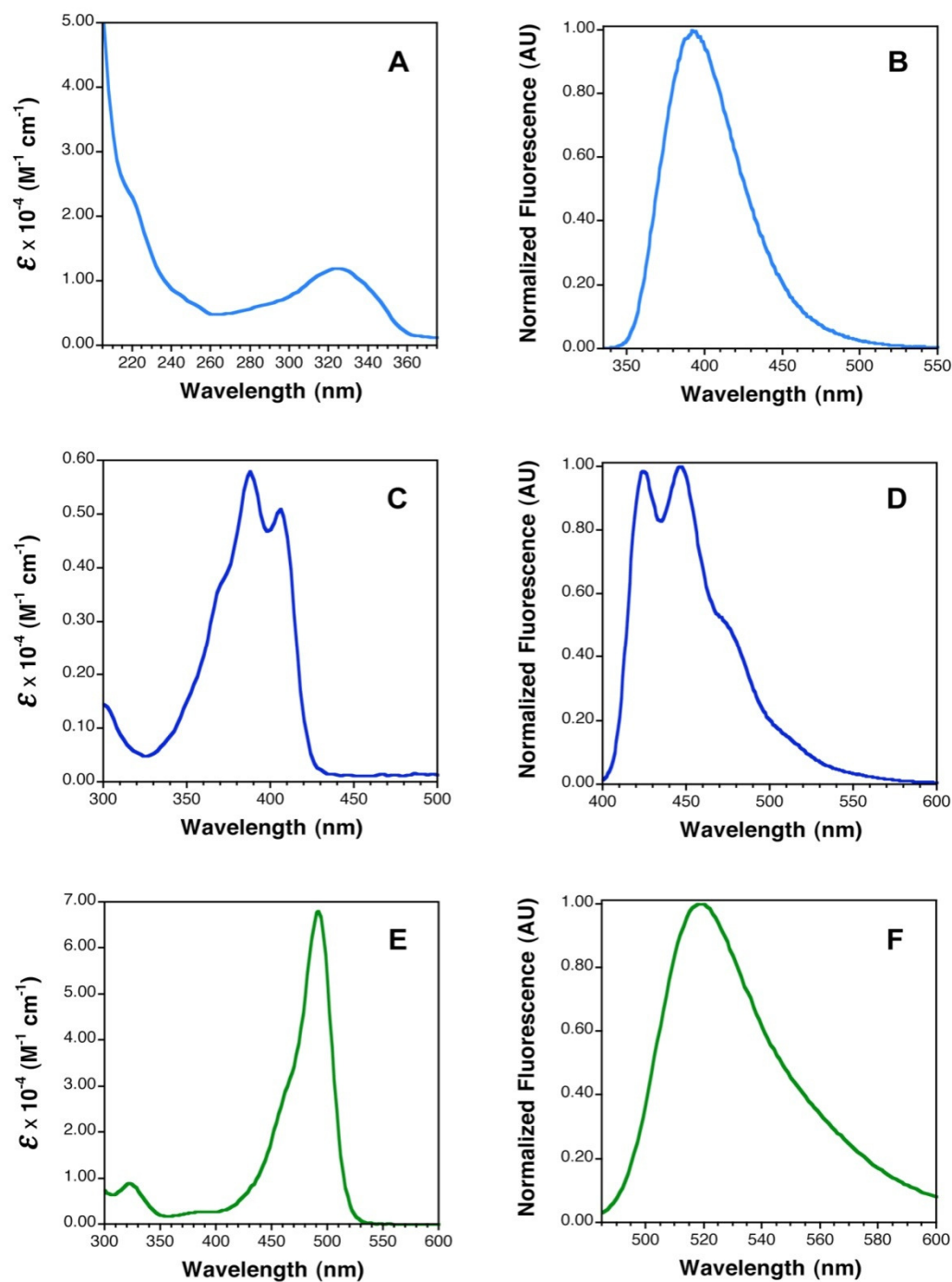


**Figure 2.26:** Absorption and Fluorescence Spectra of Mcm, Acd, and Fam. Absorbance (A) and fluorescence (B) spectra of 8.8  $\mu\text{M}$  LeuProProMcm in pH 7.0 PBS . Peptide synthesized as described<sup>92</sup>. Absorbance (C) and fluorescence (D) spectra of 0.26 mM Acd and 2  $\mu\text{M}$  Acd, respectively, in PBS, pH 7.0. Absorbance (E) and fluorescence (F) spectra of 9.5  $\mu\text{M}$  Fam and 1.5  $\mu\text{M}$  Fam, respectively, in 100 mM

phosphate buffer, pH 7.0. Concentrations determined using published extinction coefficients of Mcm ( $\lambda_{325} = 12,000 \text{ M}^{-1}\cdot\text{cm}^{-1}$ ), Acd ( $\lambda_{386} = 5,700 \text{ M}^{-1}\cdot\text{cm}^{-1}$ ), and Fam ( $\lambda_{492} = 68,000 \text{ M}^{-1}\cdot\text{cm}^{-1}$ ).<sup>111, 121</sup> Reprinted with permission from Speight, L. C.; Muthusamy, A. K.; Goldberg, J. M.; Warner, J. B.; Wissner, R. F.; Willi, T. S.; Woodman, B. F.; Mehl, R. A.; Petersson, E. J., Efficient Synthesis and In Vivo Incorporation of Acridon-2-ylalanine, a Fluorescent Amino Acid for Lifetime and Forster Resonance Energy Transfer/Luminescence Resonance Energy Transfer Studies. *Journal of the American Chemical Society* **2013**, *135* (50), 18806-18814. Copyright (2013) American Chemical Society.

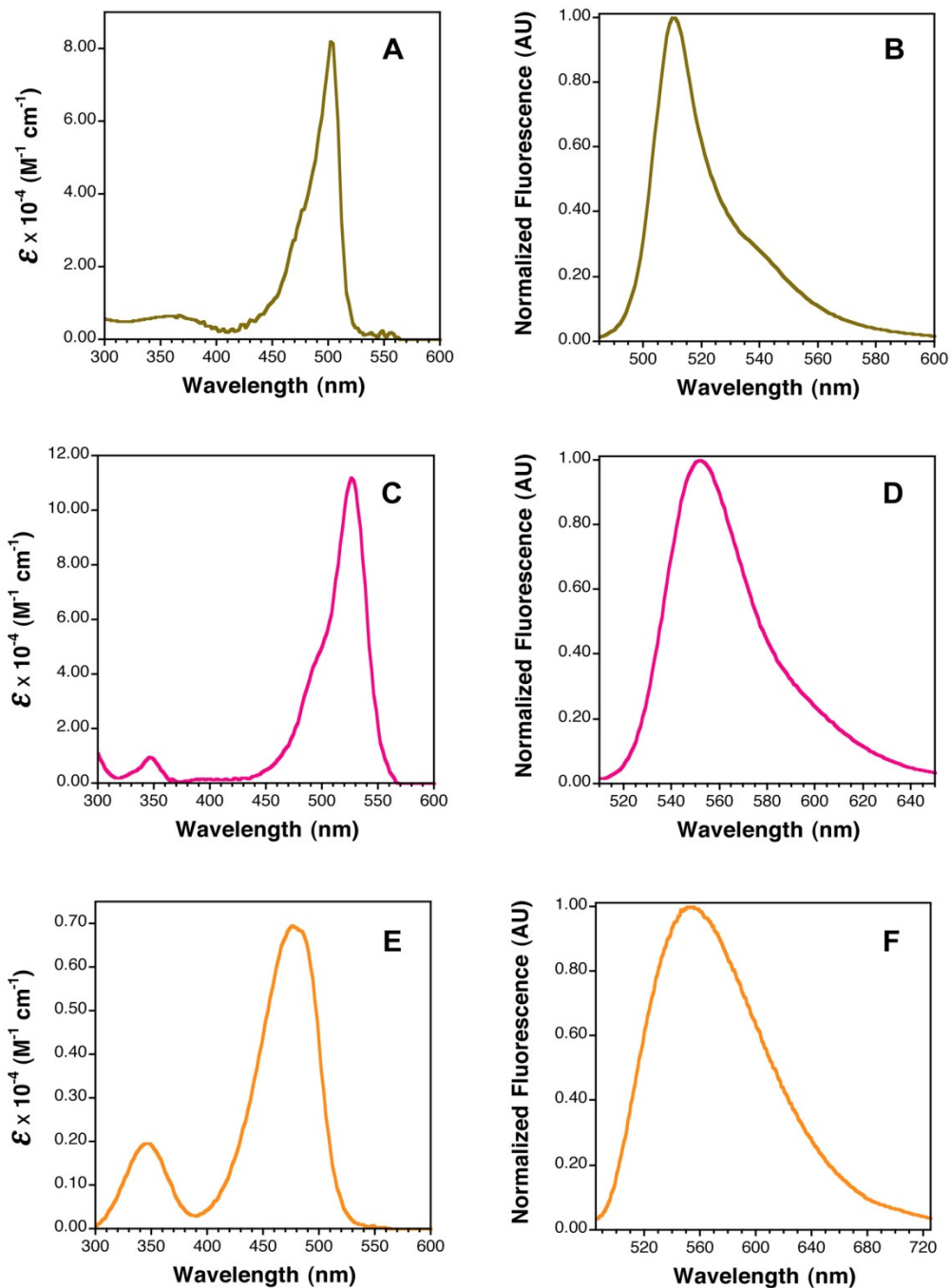


**Figure 2.27:** Absorption and Fluorescence Spectra of BODIPY FI, R6G, and NBD in 100 mM phosphate buffer, pH 7.0. Absorbance (A) and fluorescence (B) spectra of 4.3 and 1.2  $\mu\text{M}$  BODIPY FI, respectively. Absorbance (C) and fluorescence (D) spectra of 4.5 and 0.25  $\mu\text{M}$  R6G, respectively. Absorbance (E) and fluorescence (F) spectra of 86 and 15  $\mu\text{M}$  NBD, respectively. Concentrations determined using published

extinction coefficients of BODIPY Fl ( $\lambda_{502} = 82,000 \text{ M}^{-1}\cdot\text{cm}^{-1}$ ), R6G ( $\lambda_{530} = 116,000 \text{ M}^{-1}\cdot\text{cm}^{-1}$ ), and NBD ( $\lambda_{484} = 6835 \text{ M}^{-1}\cdot\text{cm}^{-1}$ ).<sup>122, 123</sup> Reprinted with permission from Speight, L. C.; Muthusamy, A. K.; Goldberg, J. M.; Warner, J. B.; Wissner, R. F.; Willi, T. S.; Woodman, B. F.; Mehl, R. A.; Petersson, E. J., Efficient Synthesis and In Vivo Incorporation of Acridon-2-ylalanine, a Fluorescent Amino Acid for Lifetime and Forster Resonance Energy Transfer/Luminescence Resonance Energy Transfer Studies. *Journal of the American Chemical Society* **2013**, *135* (50), 18806-18814. Copyright (2013) American Chemical Society.

### Acid Steady-State Stern-Volmer Experiments

Stocks of 50  $\mu\text{M}$  Acid and 100 mM tyrosine methyl ester (Tyr-OMe), cysteine, histidine, glycine, and tryptophan (83.6 mM stock solution) in 100 mM sodium phosphate buffer, pH 7.00, were used to prepare samples that were uniform in Acid concentration (5  $\mu\text{M}$ ) and variable in amino acid concentration (0, 2.5, 5, 15, 25, 35, 50, and 65 mM). The fluorescence of each sample was measured by exciting the solution at 385 nm and recording the emission at 450 nm. Measurements were made in Corning 3650 black flat-bottom microplates on a Perkin Elmer Envision Xcite instrument at 25 and 40  $^{\circ}\text{C}$ .

Excitation and emission bandwidths were 8 nm and the gain was calculated automatically from a plate containing 5  $\mu\text{M}$  Acid in four wells. The samples were allowed to equilibrate for several min at each temperature before scans were taken. The fluorescence intensity at 450 nm was averaged from three separate trials to obtain values for Stern-Volmer calculations. The data for a given temperature were fit to Equation **1a** or **1b** with KaleidaGraph (Synergy Software; Reading, PA, USA).

$$\frac{F_0}{F} = 1 + K_{\text{St}} [Q] \quad (1a)$$

$$\frac{F_0}{F} = (1 + K_{St} [Q]) (1 + K_{Dy} [Q]) \quad (\mathbf{1b})$$

$F_0$  is the average fluorescence intensity at 450 nm in the absence of quencher;  $F$  is the fluorescence intensity at 450 nm at each amino acid concentration step;  $K_{St}$  is the static Stern-Volmer constant in  $M^{-1}$ ;  $K_{Dy}$  the dynamic Stern-Volmer constant in  $M^{-1}$ , and  $[Q]$  is the quencher concentration in M. Only Trp and Tyr data were fit to equation S1b since all other quenching was negligible.  $K_{St}$  for Trp is  $21.25 \pm 0.28 M^{-1}$  at 25 °C.  $K_{St}$  for Tyr-OMe is  $8.81 \pm 0.24 M^{-1}$  at 25 °C.  $K_{Dy}$  was fixed at the value obtained from lifetime experiments (see below) for both Trp and Tyr-OMe.

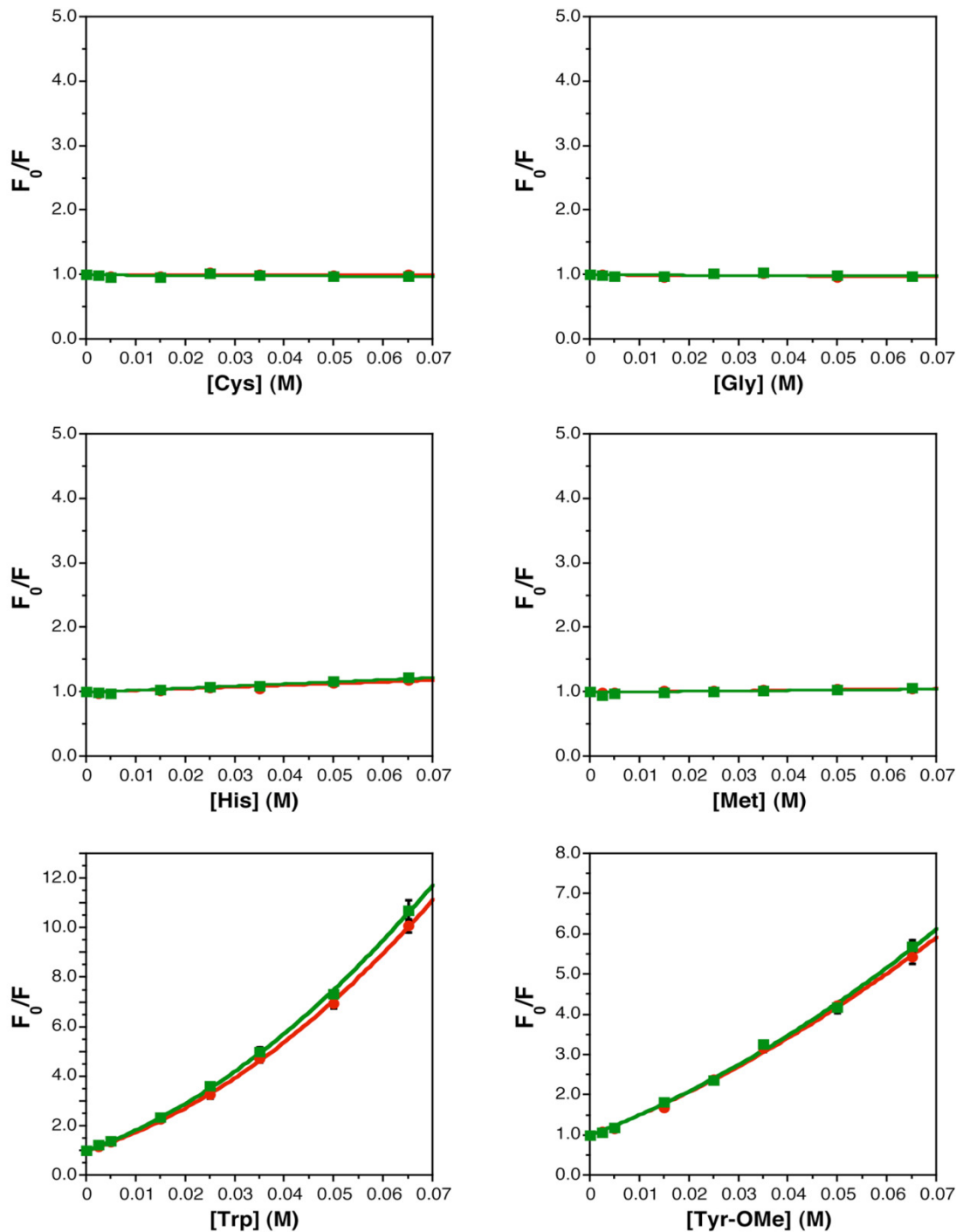


**Figure 2.28:** Steady-State Stern-Volmer Titrations of Acd with Amino Acids. Acd fluorescence ( $\lambda_{\text{ex}} = 385$  nm,  $\lambda_{\text{em}} = 450$  nm) recorded with varying concentrations of Cys, Gly, His, Met, Trp, or Tyr-OMe in 100 mM sodium phosphate buffer, pH 7.00 at 25 °C (red) or 40 °C (green). Average of three trials, error bars

are calculated from standard error. Fits to equation S1a shown for Cys, Gly, His, and Met. Fits to equation S1b shown for Trp ( $R^2 = 0.99961$  at 25 °C) and Tyr-OMe ( $R^2 = 0.99814$  at 25 °C). Reprinted with permission from Speight, L. C.; Muthusamy, A. K.; Goldberg, J. M.; Warner, J. B.; Wissner, R. F.; Willi, T. S.; Woodman, B. F.; Mehl, R. A.; Petersson, E. J., Efficient Synthesis and In Vivo Incorporation of Acridon-2-ylalanine, a Fluorescent Amino Acid for Lifetime and Forster Resonance Energy Transfer/Luminescence Resonance Energy Transfer Studies. *Journal of the American Chemical Society* **2013**, *135* (50), 18806-18814. Copyright (2013) American Chemical Society.

### Acid Fluorescence Lifetime Stern-Volmer Experiments

Fresh solutions of each sample were prepared at identical concentrations for Stern-Volmer lifetime experiments. Time-resolved fluorescence measurements were performed using the Time-Correlated Single Photon Counting (TCSPC) method. The TCSPC system consisted of a blue diode laser (PicoQuant GmbH; Berlin, Germany) generating 10 MHz output pulses at 405 nm, a subtractive double monochromator with an MCP-PMT (Hamamatsu Photonics R2809U; Bridgewater, NJ, USA), and a TCSPC computer board (Becker and Hickl SPC-630; Berlin, Germany). Emission at 450 nm was monitored. All samples were thermostatted at 25 °C. Data analysis was performed with FluoFit software (PicoQuant) using a single-exponential decay model (**Equation 2**).

$$I(t) = \sum_{i=1}^n A_i e^{-\frac{t}{\tau_i}} \quad (2)$$

Here,  $n = 1$ , for a single-exponential fit, and the parameters  $A_i$  and  $\tau_i$  are the amplitude and lifetime of the  $i^{\text{th}}$  component, respectively. Reduced  $\chi^2$  values were calculated for each fit according to **Equation 3**.

$$\chi^2 = \frac{1}{N-p} \sum_{j=1}^N W(j)^2 [\text{decay}(j) - \text{fit}(j)]^2 \quad W(j) = \frac{1}{\sqrt{\text{decay}(j)}} \quad (3)$$

In this equation,  $N$  is the number of fitted data points  $j$  (i.e. measured photon counts at a given delay time, a bin);  $p$  is the number of adjustable, fitted parameters;  $W(j)$  is a Poisson weighting factor;  $\text{decay}(j)$  is the experimentally determined decay curve; and  $\text{fit}(j)$  is the fitted model. The residuals were calculated according to **Equation 4** using these values.

$$R = W(j)[\text{decay}(j) - \text{fit}(j)] \quad (4)$$

Fluorescence lifetime data were used to construct a Stern-Volmer plot according to

**Equation 5.**

$$\frac{\tau_0}{\tau} = 1 + K_{\text{Dy}} [Q] \quad (5)$$

where  $\tau_0$  is the fluorescence lifetime in the absence of quencher ( $15.73 \pm 0.05$  ns);  $\tau$  is the lifetime at each quencher concentration;  $K_{\text{Dy}}$  is the Stern-Volmer constant in units of  $\text{M}^{-1}$ ; and  $[Q]$  is the concentration of the quencher (Tyr-OMe or Trp) in M (Fig. S6). Using this equation, we found  $K_{\text{Dy}} = 38.20 \pm 0.28 \text{ M}^{-1}$  for Tyr-OMe and  $K_{\text{Dy}} = 48.98 \pm 0.22 \text{ M}^{-1}$  for Trp.

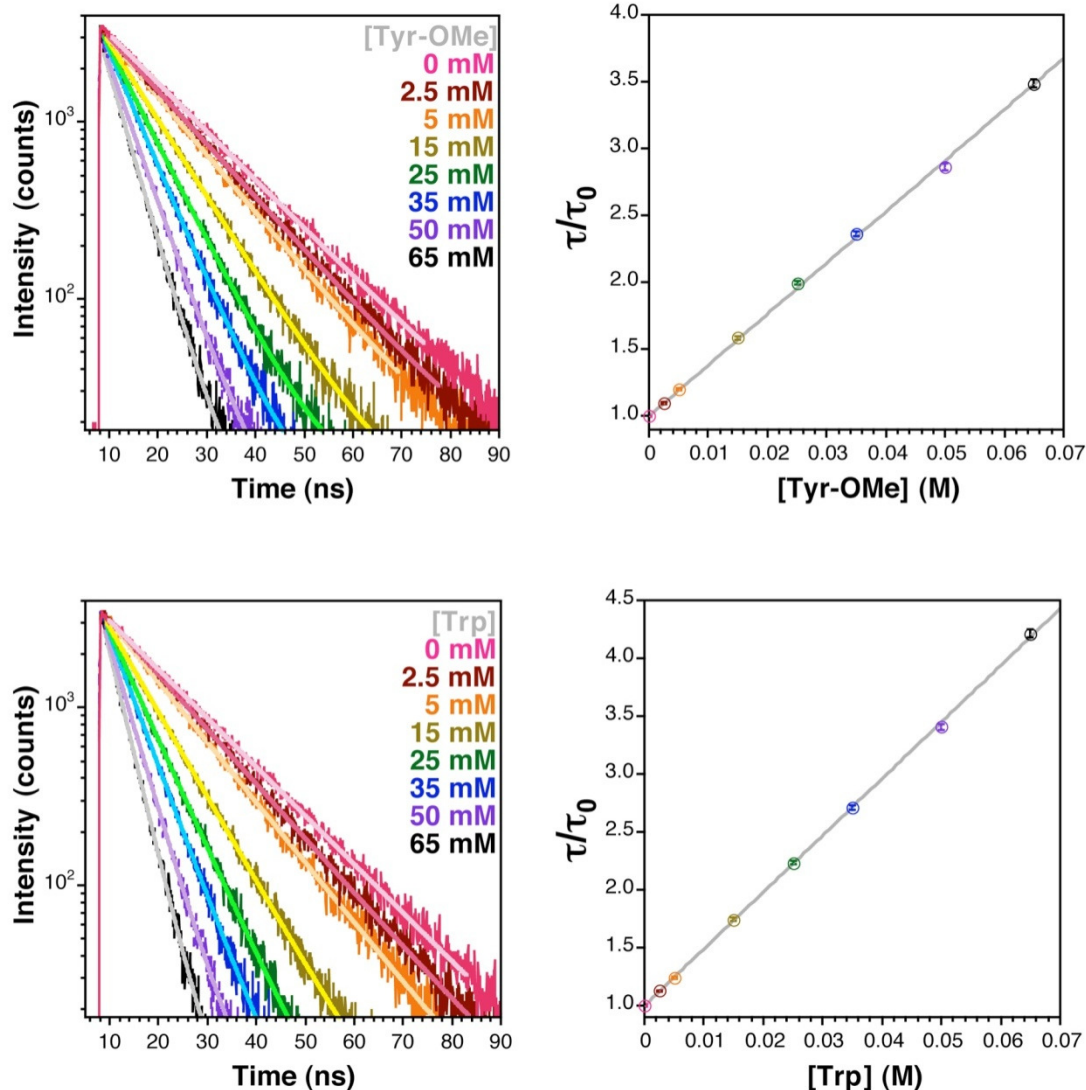


**Figure 2.29:** Lifetime Stern-Volmer experiments. Left: Fits to normalized Acrid fluorescence lifetime data with varying concentrations of tyrosine methyl ester (Tyr-OME) or tryptophan in 100 mM sodium phosphate buffer, pH 7.00 ( $\lambda_{\text{ex}} = 405 \text{ nm}$ ;  $\lambda_{\text{em}} = 450 \text{ nm}$ ). Right: Stern-Volmer plots of lifetime data at 25 °C. Error bars are calculated from fits of the raw data;  $R^2 = 0.99997$  for Tyr-OME,  $R^2 = 0.99997$  for Trp. Reprinted with permission from Speight, L. C.; Muthusamy, A. K.; Goldberg, J. M.; Warner, J. B.; Wissner, R. F.; Willi, T. S.; Woodman, B. F.; Mehl, R. A.; Petersson, E. J., Efficient Synthesis and In Vivo Incorporation of Acridon-2-ylalanine, a Fluorescent Amino Acid for Lifetime and Forster Resonance Energy Transfer/Luminescence Resonance Energy Transfer Studies. *Journal of the American Chemical Society* **2013**, *135* (50), 18806-18814. Copyright (2013) American Chemical Society.

## Förster Distance Calculations

The Förster distance,  $R_0$ , is given in Å by equation (6)

$$R_0^6 = \frac{9000(\ln 10)\kappa^2\Phi_D J}{128\pi^5 n^4 N_A} \quad (6)$$

where  $\kappa^2$  is a geometrical factor that relates the orientation of the donor and acceptor transition moments,  $\Phi_D$  is the quantum yield of the donor,  $n$  is the index of refraction of the solvent,  $N_A$  is Avogadro's number, and  $J$  is the spectral overlap integral defined in units of  $M^{-1}\cdot\text{cm}^{-1}\cdot\text{nm}^4$ . Combining constants and rearranging gives  $R_0$  as

$$R_0 = 0.211\{\Phi_D\kappa^2 n^{-4} J\}^{1/6} \quad (7)$$

$J$  is formally defined as

$$J = \int_0^{\infty} f_D(\lambda)\epsilon_A(\lambda)\lambda^4 d\lambda \quad (8)$$

where  $\epsilon_A(\lambda)$  is the molar extinction coefficient of the acceptor at each wavelength  $\lambda$  and  $f_D(\lambda)$  is the normalized donor emission spectrum given by

$$f_D(\lambda) = \frac{F_{D\lambda}(\lambda)}{\int_0^{\infty} F_{D\lambda}(\lambda) d\lambda} \quad (9)$$

where  $F_{D\lambda}(\lambda)$  is the fluorescence of the donor at each wavelength  $\lambda$ . Fluorescence spectra of Trp (LeuProProTrp), Mcm (LeuProProMcm), and Acd (LeuProProAcd) were integrated with KaleidaGraph from 305 to 500 nm for Trp, 336 to 600 nm for Mcm, and 400 to 600 nm for Acd to calculate  $f_D(\lambda)$ . UV/Vis spectra of Acd, BODIPY Fl, Fam, R6G, and NBD in water were used to determine  $\epsilon_A(\lambda)$ .  $J$  values were obtained using Equation (S8) for various donor/acceptor pairs are given in **Table 2.8**. Substituting these

results into Equation (S7), as well as the donor quantum yields in **Table 2.8**, 1.33 for the index of refraction of water, and 2/3 for  $\kappa^2$  gives the Förster distances listed in Table S3. These  $R_0$  values were used to generate plots of FRET efficiency as a function of distance using **Equation 10**.

$$E_{\text{FRET}} = \frac{1}{1 + \left(\frac{R}{R_0}\right)^6} \quad (10)$$

Here,  $E_{\text{FRET}}$  is the FRET efficiency and  $R$  is the separation between the chromophores.

Plots of FRET efficiency for each chromophores are shown in **Figure 2.30**.

**Table 2.8:** Photophysical Characteristics of Acd FRET Pairs.

FRET Pair (Donor, Acceptor)	$\Phi_D$	$J$ ( $M^{-1}\cdot\text{cm}^{-1}\cdot\text{nm}^4$ )	$R_0$ ( $\text{\AA}$ )	$\epsilon_A$ ( $M^{-1}\cdot\text{cm}^{-1}$ ) @ $\lambda_{\text{max}}$ (nm)
Trp, Acd	0.13 <sup>124</sup>	$5.47 \times 10^{13}$	22.6	5,700 @ 386
Mcm, Acd	0.18 <sup>111</sup>	$7.96 \times 10^{13}$	25.4	5,700 @ 386
Acd, Fam	0.95	$9.64 \times 10^{14}$	50.8	68,000 @ 492
Acd, BODIPY	0.95	$8.18 \times 10^{14}$	49.4	82,000 @ 504
Acd, R6G	0.95	$7.86 \times 10^{14}$	49.1	116,000 @ 530
Acd, NBD	0.95	$5.47 \times 10^{14}$	37.0	6,835 @ 484

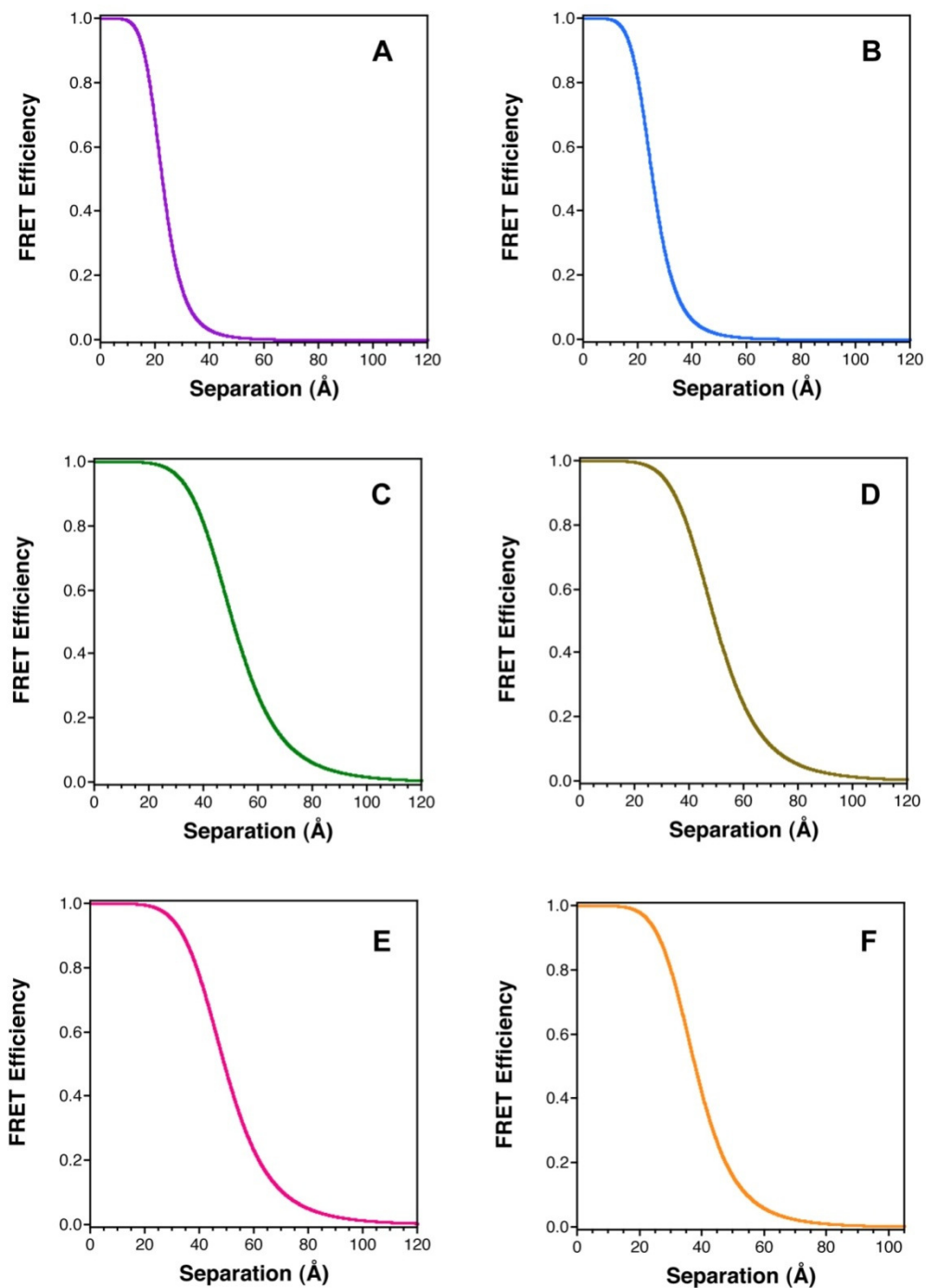


**Figure 2.30:** Distance Dependence of Acd FRET Interactions. FRET efficiencies of donor/acceptor pairs Trp/Acd (A), Mcm/Acd (B), Acd/Fam (C), Acd/BODIPY (D), Acd/R6G (E) and Acd/NBD (F) calculated according to Equations (S7), (S8), and (S10) using the values in **Table 2.8**. Reprinted with permission from Speight, L. C.; Muthusamy, A. K.; Goldberg, J. M.; Warner, J. B.; Wissner, R. F.; Willi, T. S.; Woodman,

B. F.; Mehl, R. A.; Petersson, E. J., Efficient Synthesis and In Vivo Incorporation of Acridon-2-ylalanine, a Fluorescent Amino Acid for Lifetime and Forster Resonance Energy Transfer/Luminescence Resonance Energy Transfer Studies. *Journal of the American Chemical Society* **2013**, *135* (50), 18806-18814.  
Copyright (2013) American Chemical Society.

## Synthetase Sequences

### *M. jannaschii* TyrRS

```
1 120 60  
MDEFEMIKRNTSEIISEEELREVLKKDEKSAYIGFEPGKIHLGHYLQIKKMIDLQONAGF  
61 120  
DIIIILLLADLHAYLNQKGELDEIRKIGDYNKKVFEAMGLKAKYVYGSEFQLDKDYTLNVYR  
121 180  
LALKTTLKRARRSMELIAREDENPKVAEVIYPIMQVNDIHYLGVDVAAVGGMEQRKIHMLA  
181 240  
RELLPKKVVCIHNPVLTGLDGEGKMSSSKGNFIAVDDSPPEIRAKIKKAYCPAGVVEGNP  
241 300  
IMEIAKYFLEYPLTIKRPEKFGDLTVNSYEELESLFKNKELHPMDLKNVAEELIKILE  
301  
PIRKRL
```

## Synthetase Mutants

	31	32	65	107	108	109	158	159	161	162	164	167
<b>TyrRS</b>	Ala	Tyr	Leu	Glu	Phe	Gln	Asp	Ile	Tyr	Leu	Val	Ala
<b>BrbRS1</b>		Gly	Glu				Gly	Cys				
<b>BrbRS2</b>		Gly	Val		Trp	Met	Gly	Pro				
<b>BrbRS3</b>		Gly	Glu		Trp	Met	Ser					
<b>BzfRS1</b>		Gly		Pro			Thr	Ser	Arg			
<b>BzfRS2</b>		Gly		Pro			Thr	Ser	Arg	Ala		
<b>BzfRS3</b>		Gly		Pro			Ser	Ser	Arg			
<b>BzfRS4</b>	Val	Gly		Pro			Ser	Ser	Arg			
<b>BzfRS4</b>		Gly		Pro			Ser	Ser	Arg		Ala	
<b>NapRS1</b>		Ala		Pro			Pro	Ala				Val

**Figure 2.31:** Sequences of Candidate Synthetases. Top: Amino acid sequence of parent *M. jannaschii* TyrRS. Residues where mutations were examined are highlighted in red. Bottom: Sequences of mutant synthetases screened for selective Acd incorporation using GFP assay. Amino acids listed by position number. Blank cells indicate no mutation. BrbRS1 = AcdRS. Reprinted with permission from Speight, L. C.; Muthusamy, A. K.; Goldberg, J. M.; Warner, J. B.; Wissner, R. F.; Willi, T. S.; Woodman, B. F.; Mehl, R. A.; Petersson, E. J., Efficient Synthesis and In Vivo Incorporation of Acridon-2-ylalanine, a Fluorescent Amino Acid for Lifetime and Forster Resonance Energy Transfer/Luminescence Resonance Energy Transfer Studies. *Journal of the American Chemical Society* **2013**, *135* (50), 18806-18814. Copyright (2013) American Chemical Society.

## Cloning of Calmodulin Expression Constructs

pCaM, A plasmid containing the wild-type chicken calmodulin (CaM) gene was provided by Joshua Wand from the Perelman School of Medicine at the University of Pennsylvania. An insert containing the CaM gene (458 base pairs from start to stop codon) was cloned into a pET15b vector (Novagen; Gibbstown, NJ, USA) between the NcoI and XhoI cut sites. Quikchange® site-directed mutagenesis was used to generate CaM mutants by inserting a TAG codon at the site of interest: F<sub>13</sub>δ, G<sub>41</sub>δ, Y<sub>100</sub>δ, and L<sub>113</sub>δ. The mutant plasmids were verified by DNA sequencing analysis with a T7 promoter primer.

### A. CaM Gene

```
5'-atggctgatcaactgacagaagagcagattgcagaattcaaagaagcttttcactatt
gacaaggatggtgatggtactataactacaaaggagttggggactgtgatgagatcacttgg
cagaacccacagaagcagaattacaggacatgatcaatgaagtagacgctgatggcaatggc
acaattgactcccagagtttctgacaatgatggcaagaaaaatgaaagatacagatagcgaa
gaagaaattagagaagcgttccgtgtgtttgacaaggatggtaatggttacattagtgtgca
gaacttcgcatgtgatgacaaatctggggagaagctaacagatgaagaagttgatgaaatg
attaggaagcagacattgatggtgatggtcaagtaaactatgaagagttgtacagatgatg
acagcgaagtga-3'
```

### B. Chicken CaM Amino Acid Sequence

```
MADQLTEEQIAEFKEAFSLFDKDGDGTITTKELGTVMRSLGQNPTEAELQDMINE
VDADGNGTIDFPEFLTMMARKMKDTDSEEEIREAFRVFDKDGNGYISAAELRHV
MTNLGEKLTDEEVDEMIREADIDGDGQVNYEEFVQMMTAK
```

### C. DNA Oligomers used for Quikchange® Mutagenesis

<b>F13δ_For</b>	5'-ACTGACAGAAGAGCAGATTGCAGAATAGAAAAGAAGCTTTTTCACTATTTGAC-3'
<b>F13δ_Rev</b>	5'-GTCAAATAGTGAAAAAGCTTCTTTCTATTCTGCAATCTGCTCTTCTGTCAAGT-3'
<b>G41δ_For</b>	5'-TTCTGTGGGGTTCTGCTAAAGTGATCTCATCACAGTCCCCAACTCC-3'
<b>G41δ_Rev</b>	5'-GGAGTTGGGGACTGTGATGAGATCACTTTAGCAGAACCCACAGAA-3'
<b>Y100δ_For</b>	5'-GACAAGGATGGTAATGGTTAGATTAGTGCTGCAGAACTTCG-3'
<b>Y100δ_Rev</b>	5'-CGAAGTTCTGCAGCACTAATCTAACCATTACCATCCTTGTC-3'
<b>L113δ_For</b>	5'-CTGCAGAACTTCGTCATGTGATGACAAATTAGGGGGAGAAGCTAACA-3'
<b>L113δ_Rev</b>	5'-TGTTAGCTTCTCCCCCTAATTTGTCATCACATGACGAAGTTCTGCAG-3'

**Figure 2.32:** CaM Mutagenesis. A) DNA sequence of chicken CaM gene from start to stop codon. B) Amino acid sequence of chicken CaM. F<sub>13</sub>, G<sub>41</sub>, Y<sub>100</sub>, L<sub>113</sub> highlighted in bold red. C) Forward and reverse DNA oligomers used for site-directed mutagenesis. Reprinted with permission from Speight, L. C.; Muthusamy, A. K.; Goldberg, J. M.; Warner, J. B.; Wissner, R. F.; Willi, T. S.; Woodman, B. F.; Mehl, R. A.; Petersson, E. J., Efficient Synthesis and In Vivo Incorporation of Acridon-2-ylalanine, a Fluorescent Amino Acid for Lifetime and Forster Resonance Energy Transfer/Luminescence Resonance Energy Transfer Studies. *Journal of the American Chemical Society* **2013**, *135* (50), 18806-18814. Copyright (2013) American Chemical Society.

### Wild-Type Calmodulin Protein Expression

The plasmid containing the chicken CaM gene, pCaM, was used to transform *E. coli* BL21(DE3) cells. Transformed cells were selected on the basis of ampicillin resistance. Single colonies were used to inoculate 5 mL of LB media supplemented with ampicillin (100 µg/mL). To an autoclaved solution containing 42 mM Na<sub>2</sub>HPO<sub>4</sub>, 22 mM KH<sub>2</sub>PO<sub>4</sub>, 19 mM NH<sub>4</sub>Cl, and 86 mM NaCl (M9 salts), the following autoclaved solutions were added per liter of M9 salts: 1 mL of 2 M MgSO<sub>4</sub>, 1 mL of 15 mg/mL FeCl<sub>2</sub> (in 1.0 M

HCl), 1 mL of 15 mg/mL ZnCl<sub>2</sub> (in acidified H<sub>2</sub>O), 6.25 mL of 40% glucose, 100 μL of 1M CaCl<sub>2</sub> and 2 mL of 10% Bacto™ Yeast Extract. The primary 5 mL culture was incubated at 37 °C with shaking at 250 rpm for 4 h. Upon the primary culture reaching saturation, it was added to 1 L of M9 minimal media supplemented with ampicillin (see concentrations). The 1 L culture was incubated at 37 °C with shaking at 250 rpm until the OD<sub>600</sub> reached 0.7 AU. Protein expression was induced with isopropyl D-galactoside (IPTG), and the culture was incubated at 37 °C with shaking at 250 rpm for an additional 16 h. The cells were again harvested by centrifuging at 5000 x g for 15 min and the resulting pellet was suspended in 15 mL of MOPS resuspension buffer (50 mM 3-(*N*-morpholino) propanesulfonic acid (MOPS), 100 mM KCl, 1 mM ethylenediamine tetraacetic acid (EDTA), pH 7.5). Following sonication, the cell lysate was allowed to cool on ice for 5 min. CaCl<sub>2</sub> was added to the sonicated lysate to a final concentration of 5 mM prior to centrifugation for 20 min at 30,000 x g, 4 °C.

### **Acid Mutant Calmodulin Protein Expression**

The pCaM-F<sub>13</sub>Δ, -G<sub>41</sub>Δ, -Y<sub>100</sub>Δ, or -L<sub>113</sub>Δ plasmid (with Amp resistance) was used to transform *E. coli* BL21(DE3) cells. These cells were previously transformed with the pDule2-Acd plasmid and made competent following the Hanahan method.<sup>122</sup> The pDule2-Acd plasmid encodes the AcdRS and cognate tRNA (streptomycin resistant). Transformed cells were selected on the basis of Amp and Strep resistance. Single colonies were used to inoculate 5 mL of LB media supplemented with Amp and Strep (100 μg/mL each). To an autoclaved solution containing 42 mM Na<sub>2</sub>HPO<sub>4</sub>, 22 mM

KH<sub>2</sub>PO<sub>4</sub>, 19 mM NH<sub>4</sub>Cl, and 86 mM NaCl (M9 salts), the following autoclaved solutions were added per liter of M9 salts: 1 mL of 2 M MgSO<sub>4</sub>, 1 mL of 15 mg/mL FeCl<sub>2</sub> (in 1.0 M HCl), 1 mL of 15 mg/mL ZnCl<sub>2</sub> (in acidified H<sub>2</sub>O), 6.25 mL of 40% glucose, 100 μL of 1M CaCl<sub>2</sub> and 2 mL of 10% Bacto™ Yeast Extract. The primary 5 mL culture was incubated at 37 °C with shaking at 250 rpm for 4 h. Upon reaching saturation, the primary culture was added to 1 L of M9 minimal media supplemented with Amp and Strep. The 1 L culture was incubated at 37 °C with shaking at 250 rpm until the OD<sub>600</sub> reached 0.7 AU. At this point, a solution of 282 mg Acd in 4 mL sterile water (with 4 drops 10 M NaOH to solubilize Acd) was added and protein expression was induced with IPTG. The culture was incubated at 37 °C for an additional 16 h. The cells were harvested at 5000 x g for 15 minutes and the resulting pellet was suspended in 15 mL of MOPS resuspension buffer (50 mM MOPS, 100 mM KCl, 1 mM EDTA, pH 7.5). Following sonication, the cell lysate was allowed to cool on ice for 5 min. CaCl<sub>2</sub> was added to the sonicated lysate to a final concentration of 5 mM prior to centrifugation for 20 minutes at 30,000 x g, 4 °C.

CaM was purified from the cleared cell lysate using a phenyl-sepharose (PhS) CL-4B column with EDTA as eluent. Using a total resin bed volume of 10 mL, the column was first equilibrated with 4 column volumes of PhS Buffer A (50 mM Tris base, 1 mM CaCl<sub>2</sub>, pH 7.5). After the cleared cell lysate was loaded and allowed to pass through the resin, the column was washed with 4 column volumes of PhS Buffer A, 4 column volumes of high-salt PhS Buffer B (50 mM Tris base, 0.5 M NaCl, 0.1 mM CaCl<sub>2</sub>, pH 7.5), and an additional 2 column volume washes of PhS Buffer A to restore low-salt conditions. CaM was eluted with PhS Buffer C (10 mM Tris base, 10 mM EDTA, pH

7.5) and collected in 1 mL fractions and the presence of protein was detected by SDS-PAGE. Fractions containing protein were combined and dialyzed against water for 16 h at 4 °C and dialyzed into 15 mM HEPES, 140 mM KCl, 6 mM CaCl<sub>2</sub>, pH 6.7.

For CaM-Y<sub>100</sub>Δ, additional purification was performed. Following PhS purification, fractions containing protein were directly loaded onto a HiTrap Q-Column (GE Healthcare) on an ÄKTA FPLC system. The running buffer was 50 mM Tris pH 7.5 and the eluent was 50 mM Tris, 500 mM NaCl, pH 7.5. Fractions containing CaM-Y<sub>100</sub>Δ eluted between 44 and 47 minutes (corresponding to 31 to 34 % elution buffer). These fractions were combined and dialyzed against water and then against 15 mM HEPES, 140 mM KCl, pH 6.70.

### **Cloning of TIM Expression Constructs**

The *tpiA* gene from *E. coli* genome was cloned into pBad vector (Invitrogen) between the NcoI and KpnI cut sites. Quikchange® site-directed mutagenesis was used to generate the TAG mutants F<sub>74</sub>Δ and Y<sub>101</sub>Δ. The mutant plasmids were verified by DNA sequencing analysis with a pBad primer below.

#### **A. TIM Gene**

```
5'atggggggttctcatcatcatcatcatcatggtatggctagcatgactggtggacagcaaatgggtcgg
gatctgtacgacgatgacgataaggatcgatgggatccgagctcgagcgacatccttagtgatgggta
actggaaactgaacggcagccgccacatggttcacgagctggttctaacctgcgtaaagagctggcag
gtgttgctggctgtgcggtgcaatcgaccaccgaaatgtatatcgatatggcgaagcgcgaagctga
aggcagccacatcatgctgggtgcgcaaacgtggacctgaacctgtccggcgattcaccggtgaaac
```

ctctgctgctatgctgaaagacatcggcgcacagfacatcatcatcggtcactctgaacgtcgtacttacca  
caaagaatctgacgaactgatcgcgaaaaaattcgcggtgctgaaagagcagggcctgactccggttct  
gtgcatcggtgaaaccgaagctgaaaatgaagcgggcaaaaactgaagaagtttgcgcacgtcagatcga  
cgcggtactgaaaactcagggctgctcggcattcgaaggtcgggttatcgttacgaacctgtatgggca  
atcgggtactggcaaatctgcaactccggctcaggcacaggctgttcacaaattcatccgtgaccacatcg  
taaagttgacgctaactcgtgaacaagtgatcattcagtagcggcggtctgtaaacgcgttaacgctg  
cagaactggttgctcagccgatatcgacggcgcgctggttggtggtcttctgaaagctgacgccttc  
gcagtaatcgttaaagctgcagaagcggctaaacaggcttaa-3'

### ***B. E. coli* TIM Amino Acid Sequence**

MGGSHHHHHHGMASMTGGQQMGRDLYDDDDKDRWGSELERHPLVMGNWKL  
NGSRHMHVHELVSNLKELAGVAGCAVAIAPPEMYIDMAKREAEGSHIMLGAQN  
VDLNLSGAFTGETSAAMLKDIGAQYIIIGHSERRTYHKESDELIAKKFAVLKEQG  
LTPVLCIGETEAEENEAGKTEEV CARQIDAVLKTQGAAAFEGAVIAYEPVWAIGTG  
KSATPAQAQAVHKFIRDHIAKVDANIAEQVIIQYGGSVNASNAELFAQPDIDGA  
LVGGASLKADAFVIVKAAEAAKQA

### C. DNA Oligomers used for Quikchange® Mutagenesis

<b>F74δ_For</b>	5'-CTGAACCTGTCCGGCGCATAGACCGGTGAAACCTCTGCTG-3'
<b>F74δ_Rev</b>	5'-CAGCAGAGGTTTCACCGGTCTATGCGCCGGACAGGTTTCAG-3'
<b>Y101δ_For</b>	5'-CTGAACGTCGTA CTTAGCACAAAGAATCTGAC-3'
<b>Y101δ_Rev</b>	5'-GTCAGATTCTTTGTGCTAAGTACGACGTTTCAG-3'
<b>pBad_Seq</b>	5'-ATGCCATAGCATTTTTATCC-3'

**Figure 2.33:** TIM Mutagenesis. A) DNA sequence of *E. coli* *tpiA* gene from start to stop codon. B) Amino acid sequence of *E. coli* TIM. F<sub>74</sub>, Y<sub>101</sub> highlighted in bold red. C) Forward and reverse DNA oligomers used for site-directed mutagenesis and sequencing. Reprinted with permission from Speight, L. C.; Muthusamy, A. K.; Goldberg, J. M.; Warner, J. B.; Wissner, R. F.; Willi, T. S.; Woodman, B. F.; Mehl, R. A.; Petersson, E. J., Efficient Synthesis and In Vivo Incorporation of Acridon-2-ylalanine, a Fluorescent Amino Acid for Lifetime and Forster Resonance Energy Transfer/Luminescence Resonance Energy Transfer Studies. *Journal of the American Chemical Society* **2013**, *135* (50), 18806-18814. Copyright (2013) American Chemical Society.

### Wild-Type TIM Expression

The wt-TIM plasmid containing the *E. coli* TIM gene with (with Amp resistance) was used to transform *E. coli* DH10B cells via electroporation. Single colonies were then picked and grown overnight at 37°C with 250 rpm shaking in 5 mL of LB media (with Amp antibiotic). These starter cultures were then used to inoculate 500 mL of autoinduction media (created as previously described).<sup>66</sup> The cultures were grown for 24 h under these conditions. The cells were harvested at 5000 x g for 15 min and the

resulting pellet was suspended in 15 mL 20 mM Tris Base, 300 mM KCl, and 15 mM imidazole. Following sonication, the cell lysate was allowed to cool on ice for 5 min. The cell lysate was cleared of debris by centrifugation for 20 min at 30,000 x g, 4 °C. The cleared lysate was then added to 3 mL of Ni-NTA slurry and incubated at 4 °C for 1 hour with moderate shaking to ensure thorough mixing. Following this incubation, the column flow-through was collected and the slurry was washed with the following buffers: 20 mL of 20 mM Tris Base, 300 mM KCl, and 50 mM imidazole, 20 mL of 20 mM Tris Base, 300 mM KCl, and 75 mM imidazole, and 10 mL of 20 mM Tris Base, 300 mM KCl, and 100 mM imidazole. Acd-TIM mutants were eluted from the Ni-NTA column by 4 x 1.5 mL and 1 x 5 mL portions of 20 mM Tris Base, 300 mM KCl, and 250 mM imidazole. Elution fractions containing the protein of interest were identified by SDS-PAGE analysis.

### **Acd Mutant TIM Expression**

The TIM-F<sub>74</sub>Δ or -Y<sub>101</sub>Δ plasmid (with Amp resistance) along with a pDule1 plasmid containing the AcdRS and cognate tRNA (with Tet resistance) was used to transform *E. coli* DH10B cells via electroporation. Single colonies were then picked and grown overnight at 37 °C with 250 rpm shaking in 5 mL of LB media (with Amp and Tet antibiotics). These starter cultures were then used to inoculate 500 mL of autoinduction media (created as previously described).<sup>66</sup> After 30 minutes of growth at 37 °C with 250 rpm shaking, a solution of 282 mg Acd in 4 mL sterile water (with 4 drops 10 M NaOH to solubilize Acd) was added. The cultures were grown for 24 h under these conditions. The cells were harvested at 5000 x g for 15 minutes and the resulting pellet was

suspended in 15 mL 20 mM Tris Base, 300 mM KCl, and 15 mM imidazole. Following sonication, the cell lysate was allowed to cool on ice for 5 min. The cell lysate was cleared of debris by centrifugation for 20 minutes at 30,000 x g, 4 °C. The cleared lysate was then added to 3 mL of Ni-NTA slurry and incubated at 4 °C for 1 h with moderate shaking to ensure thorough mixing. Following this incubation, the column flow-through was collected and the slurry was washed with the following buffers: 20 mL of 20 mM Tris Base, 300 mM KCl, and 50 mM imidazole, 20 mL of 20 mM Tris Base, 300 mM KCl, and 75 mM imidazole, and 10 mL of 20 mM Tris Base, 300 mM KCl, and 100 mM imidazole. Acd-TIM mutants were eluted from the Ni-NTA column by 4 x 1.5 mL and 1 x 5 mL portions of 20 mM Tris Base, 300 mM KCl, and 250 mM imidazole. Elution fractions containing the protein of interest were identified by SDS-PAGE analysis.

### **Cloning of $\alpha$ -Synuclein Expression Constructs**

A plasmid containing the human wild-type  $\alpha$ S gene cloned between NdeI and HindIII in the expression vector pRK172 was provided by Dr. Virginia Lee (Perelman School of Medicine, University of Pennsylvania). Quikchange® site-directed mutagenesis was used to generate the TAG mutants Y<sub>39</sub> $\delta$  and F<sub>94</sub> $\delta$ . Sequencing was confirmed using a T7 promoter.

## A. $\alpha$ S Gene

5'atggatgtattcatgaaaggactttcaaaggccaaggagggtgtggctgctgctgagaaaaccaa  
cagggtgtggcagaagcagcaggaagacaaaagggtgttctctatgtaggctccaaaaccaagga  
gggagtggatgcatgggtgtggcaacagtggctgagaagaccaaagagcaagtgacaaatgttgaggag  
cagtggtagcgggtgtgacagcagtagcccagaagacagtggagggagcaggagcattgcagcagc  
cactggctttgtcaaaaaggaccagttgggcaagaatgaagaaggagccccacaggaaggaattctgga  
agatatgcctgtggatcctgacaatgaggcttatgaaatgccttctgaggaagggtatcaagactacgaac  
ctgaagcctaa-3'

## B. Human $\alpha$ S Amino Acid Sequence

MDVFMKGLSKAKEGVVAAAEKTKQGVAAEAGKTKEGVLYVGSKTKEGVVHG  
VATVAEKTKEQVTNVGGAVVTGVTAVAQKTVEGAGSIAAATGFVKKDQLGKN  
EEGAPQEGILEDMPVDPDNEAYEMPSEEGYQDYEP EA

## C. DNA Oligomers used for Quikchange® Mutagenesis

<b>Y39<sub>δ</sub>_For</b>	5'-AAAAGAGGGTGTCTCTAGGTAGGCTCCAAAACCAAG-3'
<b>Y39<sub>δ</sub>_Rev</b>	5'-CTTGGTTTTGGAGCCTACCTAGAGAACACCCTCTTTT-3'
<b>F94<sub>δ</sub>_For</b>	5'-GCATTGCAGCAGCCACTGGCTAGGTCAAAAAGGACCAGTTGGG-3'
<b>F94<sub>δ</sub>_Rev</b>	5'-CCCAACTGGTCCTTTTTGACCTAGCCAGTGGCTGCTGCAATGC-3'

**Figure 2.34:**  $\alpha$ -Synuclein Mutagenesis. A) DNA sequence of human  $\alpha$ S gene from start to stop codon. B) Amino acid sequence of human  $\alpha$ S. Y<sub>39</sub> and F<sub>94</sub> are highlighted in bold red. C) Forward and reverse DNA oligomers used for site-directed mutagenesis. Reprinted with permission from Speight, L. C.; Muthusamy, A. K.; Goldberg, J. M.; Warner, J. B.; Wissner, R. F.; Willi, T. S.; Woodman, B. F.; Mehl, R. A.; Petersson,

E. J., Efficient Synthesis and In Vivo Incorporation of Acridon-2-ylalanine, a Fluorescent Amino Acid for Lifetime and Forster Resonance Energy Transfer/Luminescence Resonance Energy Transfer Studies. *Journal of the American Chemical Society* **2013**, *135* (50), 18806-18814. Copyright (2013) American Chemical Society.

### **Wild-Type $\alpha$ -Synuclein Expression**

The plasmid containing the  $\alpha$ S gene was transformed into *E. coli* BL21(DE3) cells. Single colonies were used to inoculate 4 mL of LB media supplemented with ampicillin (100  $\mu$ g/mL). The primary culture was grown at 37 °C with shaking at 250 rpm for 4 h. A 500 mL secondary culture was inoculated using 1 mL of the primary culture and grown at 37 °C with shaking at 250 rpm for 20 h. The cells were harvested at 5000 x g for 15 min and the resulting pellet was resuspended in 20 mM Tris, pH 8.0 with 1 mM PMSF and sonicated. Following sonication, the cell lysate was boiled for 30 min prior to centrifugation for 20 min at 30,000 x g, 4 °C. The cleared lysate was dialyzed overnight against 20 mM Tris pH 8.0 at 4 °C prior to loading on a Superdex 200 column (25 cm) connected to a BioCad Sprint (FPLC) system. FPLC fractions were dialyzed against 20 mM Tris pH 8.0 at 4 °C and further purified using a HiTrap Q HP column (GE Healthcare) on the BioCad FPLC. Fractions were dialyzed against Milli-Q water at stored at 4 °C. Protein was concentrated using 3KDa Amicon Ultra-0.5 mL centrifugal filters (EMD Millipore) and adjusted to 500  $\mu$ M by BCA assay and stored at -80 °C until further use. SDS-PAGE analysis was performed to analyze the purity of  $\alpha$ S.

### **Acid Mutant $\alpha$ -Synuclein Expression**

*E. coli* BL21-Gold (DE3) cells were transformed with the  $\alpha$ S-Y<sub>39</sub> $\delta$  or -F<sub>94</sub> $\delta$  plasmid and a pDule2 plasmid containing the AcdRS and tRNA<sub>CUA</sub> pair. Cells were selected for resistance to both ampicillin (100  $\mu$ g/mL) and streptomycin (100  $\mu$ g/mL). Single colonies were used to inoculate 4 mL of LB media. The primary culture was grown at 37 °C with shaking at 250 rpm for 4 h. A 500 mL secondary culture was inoculated using 1 mL of the primary culture and grown at 37 °C with shaking at 250 rpm until OD<sub>600</sub> = 0.8. Protein expression was induced with 1 mM Acd (282 mg in 4 mL sterile water solubilized with 4 drops 10 M NaOH) and 1 mM IPTG, then cells were grown at 37 °C for 18 h. The cells were harvested at 5000 x g for 15 min and the resulting pellet was resuspended in 20 mM Tris, pH 8.0 with 1 mM PMSF and sonicated. Following sonication, the cell lysate was boiled for 30 min prior to centrifugation for 20 min at 30,000 x g, 4 °C. The cleared lysate was dialyzed overnight against 20 mM Tris, pH 8.0 at 4 °C prior to loading on a Superdex 200 column (25 cm). FPLC fractions were dialyzed against 20 mM Tris, pH 8.0 at 4 °C and further purified using a HiTrap Q HP column (GE Healthcare). Fractions were dialyzed against Milli-Q water and stored at 4 °C. Protein was concentrated using 3 KDa Amicon Ultra-0.5 mL centrifugal filters (EMD Millipore) and adjusted to 500  $\mu$ M by BCA assay. Protein was then stored at -80 °C until further use. SDS-PAGE analysis was performed to analyze the purity of  $\alpha$ S.

### **Trypsin Digest Analysis of Acid Mutants**

Protein (CaM-L<sub>113</sub> $\delta$ ,  $\alpha$ S-Y<sub>39</sub> $\delta$ , or  $\alpha$ S-F<sub>94</sub> $\delta$ ) was precipitated using 1:4 8.75 M trichloroacetic acid/protein sample and incubated at 4 °C for 15 minutes. The precipitate

was centrifuged for 15 min at 13,200 rpm to pellet protein. The protein pellet was then washed three times with cold acetone to remove trace trichloroacetic acid. Trace acetone was removed by incubating protein pellets in a 95 °C water bath for 5 min open to the atmosphere. Protein pellets were then re-suspended in 6 M guanidinium hydrochloride with 50 mM Tris pH 8.0, and denatured by boiling at 95 °C for 10 minutes. Protein samples were then diluted to 0.75 M guanidinium hydrochloride with 50 mM Tris pH 7.6 and 1 mM calcium chloride. Sequencing grade modified trypsin (0.6 µg, Promega) was used to digest samples for 24 hours at 37 °C. Trypsin digest aliquots (1 µL) were combined with  $\alpha$ -cyano-4-hydroxycinnamic acid (1 µL of a saturated solution in 1:1 H<sub>2</sub>O/CH<sub>3</sub>CN with 1 % TFA) and analyzed by MALDI MS.

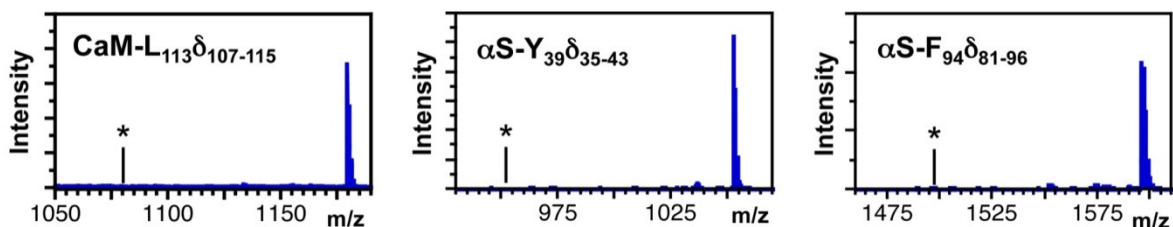


**Figure 2.35:** MALDI MS of Trypsinized Proteins. Asterisks indicate the absence of peaks corresponding to Tyr incorporation at the site of interest. CaM-L<sub>113</sub>δ<sub>107-115</sub>: Calcd m/z (M+H)<sup>+</sup> 1179.3, found 1179.5; αS-Y<sub>39</sub>δ<sub>35-43</sub>: Calcd m/z (M+H)<sup>+</sup> 1052.5, found 1052.5; αS-Y<sub>94</sub>δ<sub>81-96</sub>: Calcd m/z (M+H)<sup>+</sup> 1595.8, found 1595.8. No evidence of Npf incorporation is observed. Reprinted with permission from Speight, L. C.; Muthusamy, A. K.; Goldberg, J. M.; Warner, J. B.; Wissner, R. F.; Willi, T. S.; Woodman, B. F.; Mehl, R. A.; Petersson, E. J., Efficient Synthesis and In Vivo Incorporation of Acridon-2-ylalanine, a Fluorescent Amino Acid for Lifetime and Forster Resonance Energy Transfer/Luminescence Resonance Energy Transfer Studies. *Journal of the American Chemical Society* **2013**, *135* (50), 18806-18814. Copyright (2013) American Chemical Society.

## Calmodulin Circular Dichroism Measurements

Mutant stability was evaluated using temperature-dependent circular dichroism (CD) spectroscopy. Since calcium-bound CaM (holo-CaM) is thermostable ( $T_m > 90\text{ }^\circ\text{C}$ ), we specifically examined the thermal unfolding of the apo-enzyme. To compare the apo- and holo-forms, purified protein was dialyzed against 2 mM EDTA in 50 mM 4-(2-hydroxyethyl)piperazine-1-ethanesulfonic acid (HEPES) pH 6.70, or 10 mM  $\text{CaCl}_2$  in 50 mM HEPES pH 6.70. CD data were obtained from 20  $\mu\text{M}$  protein samples diluted in the appropriate buffer monitoring at 222 nm, between 5 and 95  $^\circ\text{C}$ , using the variable temperature module provided with the Aviv 410 CD spectrometer. Protein concentrations were determined by using the BCA assay. Data were collected with a 1  $^\circ\text{C}/\text{min}$  temperature slope, 30 s averaging time, 2 min temperature equilibration time, 5 s response time, and 1 nm band width. The resulting raw ellipticity ( $\theta_D$ ) measurements were transformed to molar residue ellipticity values ( $\theta$ ) using

$$\theta = \theta_D / (c \ell n_R) \quad (11)$$

where  $c$  is concentration (M),  $\ell$  is the path length (cm), and  $n_R$  is the number of residues.

To determine fraction folded ( $f_f$ ) for the apo-enzyme, linear baselines were fit to the low temperature ( $\theta_F = m_F T + b_F$ ) or high temperature ( $\theta_U = m_U T + b_U$ ) data. The full data range was then fit to equation (12) where  $K = e^{-(\Delta H - T\Delta S)/RT}$ ,  $\Delta H$  and  $\Delta S$  are adjustable parameters and  $R = 8.3145\text{ J}\cdot\text{mol}^{-1}\cdot\text{K}^{-1}$ . Plots are shown for each mutant in **Figure 2.12**

$$\theta = \theta_F(T)(1 - f_f(T)) + \theta_U(T)f_f(T) \quad f_f = K/(1 + K) \quad (12)$$

Since the holo-enzyme did not melt, only the molar residue ellipticity as a function of temperature is shown for each mutant (**Figure 2.12**).

## Calmodulin Peptide Binding Measurements from Steady-State Fluorescence

All peptide binding experiments shown on the following pages were conducted in 15 mM HEPES buffer, 140 mM KCl, and 6 mM CaCl<sub>2</sub>, pH 6.70. Dry peptides were brought up in a minimal amount of buffer to make fresh concentrated stock solutions for each experiment. Protein concentrations were determined by use of Thermo Scientific's Pierce BCA protein assay kit using known concentrations of bovine serum albumin as the standard. Peptide concentrations were determined on the following basis: for pOCNC, Phe absorbance was used ( $\epsilon_{257} = 600 \text{ M}^{-1}\cdot\text{cm}^{-1}$ ); for Trp-pOCNC, Trp absorbance was used ( $\epsilon_{270} = 5237 \text{ M}^{-1}\cdot\text{cm}^{-1}$ ), and for Mcm-pOCNC, methyl coumarin absorbance was used ( $\epsilon_{325} = 12,000 \text{ M}^{-1}\cdot\text{cm}^{-1}$ ).<sup>111, 124</sup> For each mutant, solutions were prepared that contained approximately 10  $\mu\text{M}$  protein and a variable amount of peptide, ranging from 0 to 15  $\mu\text{M}$  and representing at least seven distinct concentrations. Each sample was prepared in triplicate.

Corrected fluorescence measurements of each sample were taken on a Cary Eclipse fluorometer at 25 °C using quartz fluorometer cells with 1 cm path lengths for experiments with pOCNC binding to CaM-G<sub>41</sub> $\delta$ . Fluorescence spectra were obtained using a Tecan M1000 plate reader and a UV transparent 96 well plate for experiments with CaM-F<sub>13</sub> $\delta$ , CaM-Y<sub>100</sub> $\delta$ , CaM-L<sub>113</sub> $\delta$ , Trp-pOCNC, and Mcm-pOCNC. The excitation wavelength was 385 nm and emission spectra were collected from 400 to 550 nm for pOCNC and Trp-pOCNC or from 350 nm to 550 nm for Mcm-pOCNC binding. For pOCNC binding to CaM-G<sub>41</sub> $\delta$  experiments on the Cary instrument, the excitation and emission slit widths were 5 nm, the scan rate was 120 nm/min, the averaging time 0.5 s, and the data interval 1.0 nm. For the Tecan M1000 plate reader: excitation and emission

bandwidths were 5 nm, 50 flashes at 400 Hz, 20 ms integration time, a manual gain setting of 75, and a 20 mm Z-position. For CaM/peptide pairs for which no significant change in fluorescence was observed in the presence of 15  $\mu$ M peptide, representative spectra are shown in Figure S17.

### Calmodulin Binding Data Fitting

All peptide binding affinities were calculated using **Equation 13** as previously described.<sup>125</sup>

$$y = 1 - R \frac{\left( \frac{1}{K_a} + [P]_0 + [P]_0[L]_0 \right) - \sqrt{\left( \frac{1}{K_a} + [P]_0 + [P]_0[L]_0 \right)^2 - 4[P]_0^2[L]_0}}{2[P]_0} \quad (13)$$

$[L]_0$  and  $[P]_0$  are the total concentration of peptide and protein, respectively.  $K_a$  is the equilibrium constant for peptide binding to the protein to form a 1:1 complex and  $R$  is an instrumental response parameter.  $K_a$  and  $R$  are adjustable parameters in the fit.

$\text{Eu}^{3+}$  titrations with CaM-Y<sub>100</sub> $\delta$  were fit to a two-site cooperative binding model according to Equation S14, where  $F_x$ ,  $K_x$ , and  $n_x$  are the relative emissions, dissociation constants, and Hill parameters, respectively, of the two sites.<sup>115</sup>

$$F = F_1 \left\{ \frac{[\text{Eu}^{3+}]^{n_1}}{K_1^{n_1} + [\text{Eu}^{3+}]^{n_1}} \right\} + F_2 \left\{ \frac{[\text{Eu}^{3+}]^{n_2}}{K_2^{n_2} + [\text{Eu}^{3+}]^{n_2}} \right\} \quad (14)$$

### **TIM Unfolding Measurements from Steady-State Fluorescence**

Fluorescence spectra were obtained using a Tecan M1000 plate reader and a UV transparent 96 well plate with settings as described above. Acd was excited at 386 nm and emission monitored between 400 -550 nm. The fluorescence intensity at 450 nm was used to monitor the dynamics of Acd fluorescence relative to the addition of urea.

### **TIM Unfolding from Fluorescence Lifetimes**

Fluorescence lifetimes for TIM or Acd solutions in urea were recorded and fit to **Equations 2 – 4** as described for the Stern-Volmer experiments. Amplitude-weighted exponential fit data are shown in **Figures 2.36 – 2.38** and **Table 2.9**.

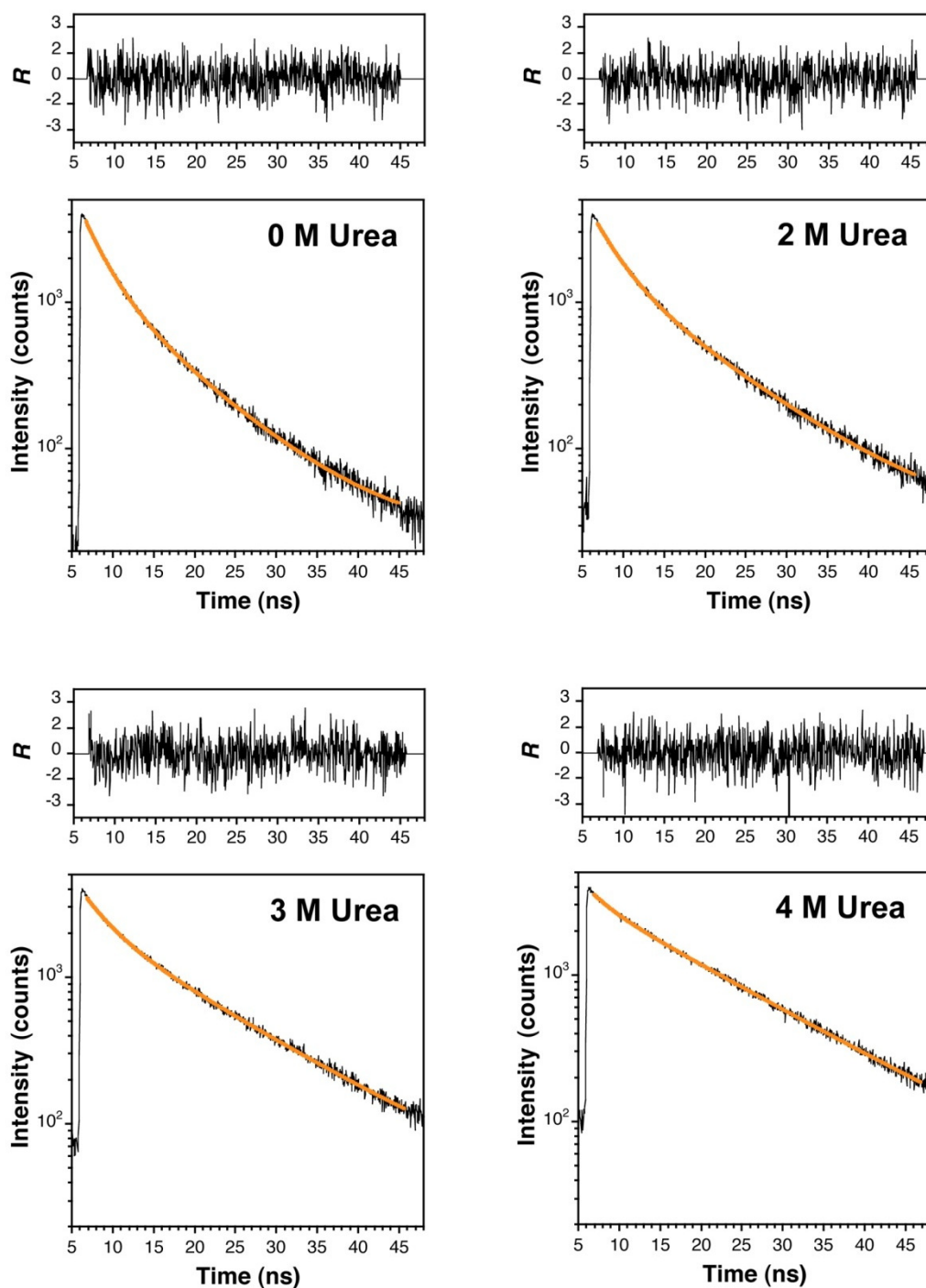


**Figure 2.36.** Lifetime TIM-F<sub>74</sub>δ Urea Denaturation Experiments. Fits to TIM-F<sub>74</sub>δ fluorescence lifetime data with varying concentrations of urea in 100 mM sodium phosphate buffer, pH 7.00 ( $\lambda_{\text{ex}} = 405 \text{ nm}$ ;  $\lambda_{\text{em}} = 450 \text{ nm}$ ) at 25 °C. Biexponential fit parameters are given in **Table 2.9**. Reprinted with permission from Speight,

L. C.; Muthusamy, A. K.; Goldberg, J. M.; Warner, J. B.; Wissner, R. F.; Willi, T. S.; Woodman, B. F.; Mehl, R. A.; Petersson, E. J., Efficient Synthesis and In Vivo Incorporation of Acridon-2-ylalanine, a Fluorescent Amino Acid for Lifetime and Forster Resonance Energy Transfer/Luminescence Resonance Energy Transfer Studies. *Journal of the American Chemical Society* **2013**, *135* (50), 18806-18814. Copyright (2013) American Chemical Society.

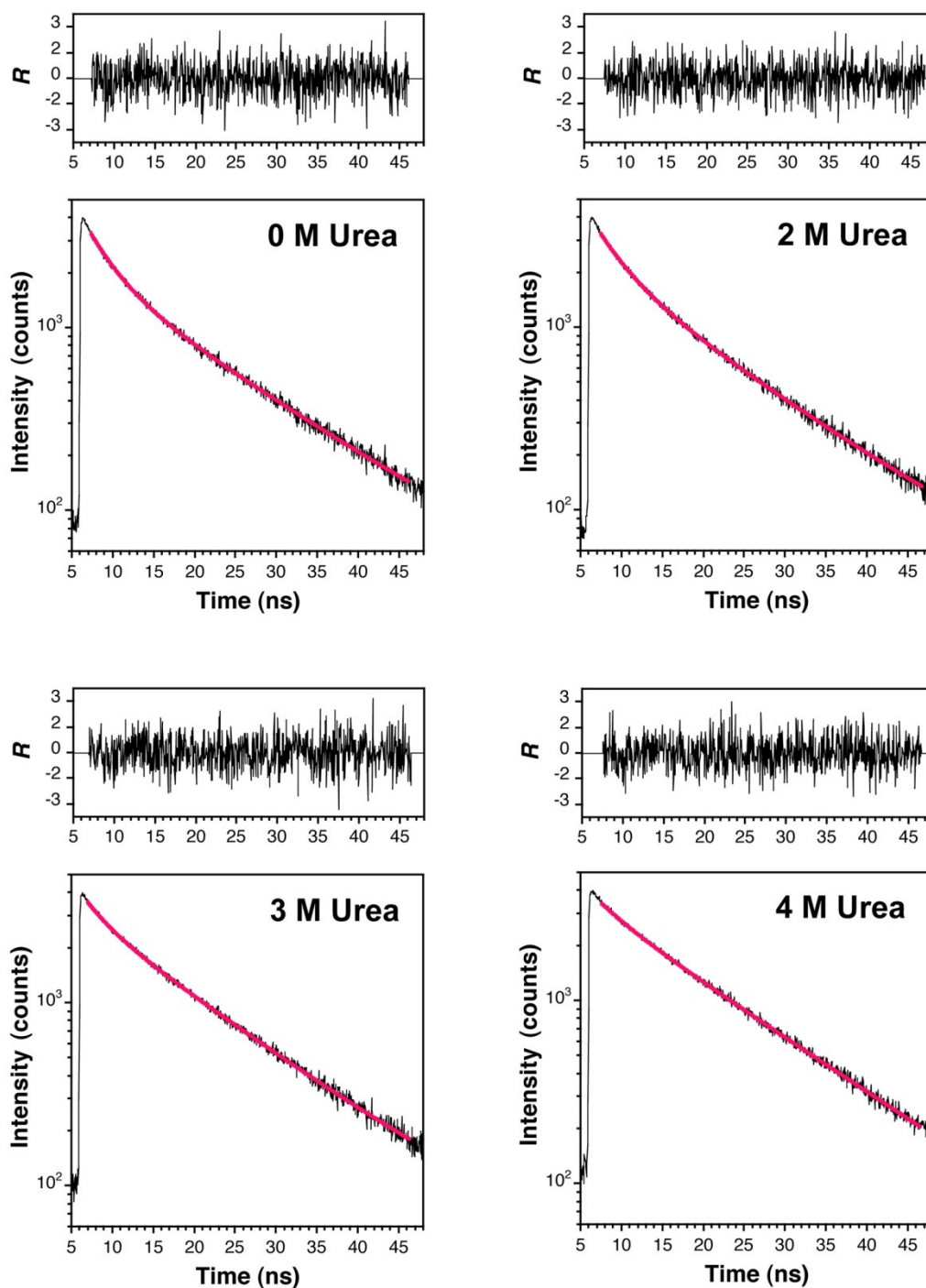


**Figure 2.37.** Lifetime TIM-Y<sub>101</sub>δ Urea Denaturation Experiments. Fits to TIM-Y<sub>101</sub>δ fluorescence lifetime data with varying concentrations of urea in 100 mM sodium phosphate buffer, pH 7.00 ( $\lambda_{\text{ex}} = 405 \text{ nm}$ ;  $\lambda_{\text{em}} = 450 \text{ nm}$ ) at 25 °C. Biexponential fit parameters are given in **Table 2.9**. Reprinted with permission from

Speight, L. C.; Muthusamy, A. K.; Goldberg, J. M.; Warner, J. B.; Wissner, R. F.; Willi, T. S.; Woodman, B. F.; Mehl, R. A.; Petersson, E. J., Efficient Synthesis and In Vivo Incorporation of Acridon-2-ylalanine, a Fluorescent Amino Acid for Lifetime and Forster Resonance Energy Transfer/Luminescence Resonance Energy Transfer Studies. *Journal of the American Chemical Society* **2013**, *135* (50), 18806-18814. Copyright (2013) American Chemical Society.

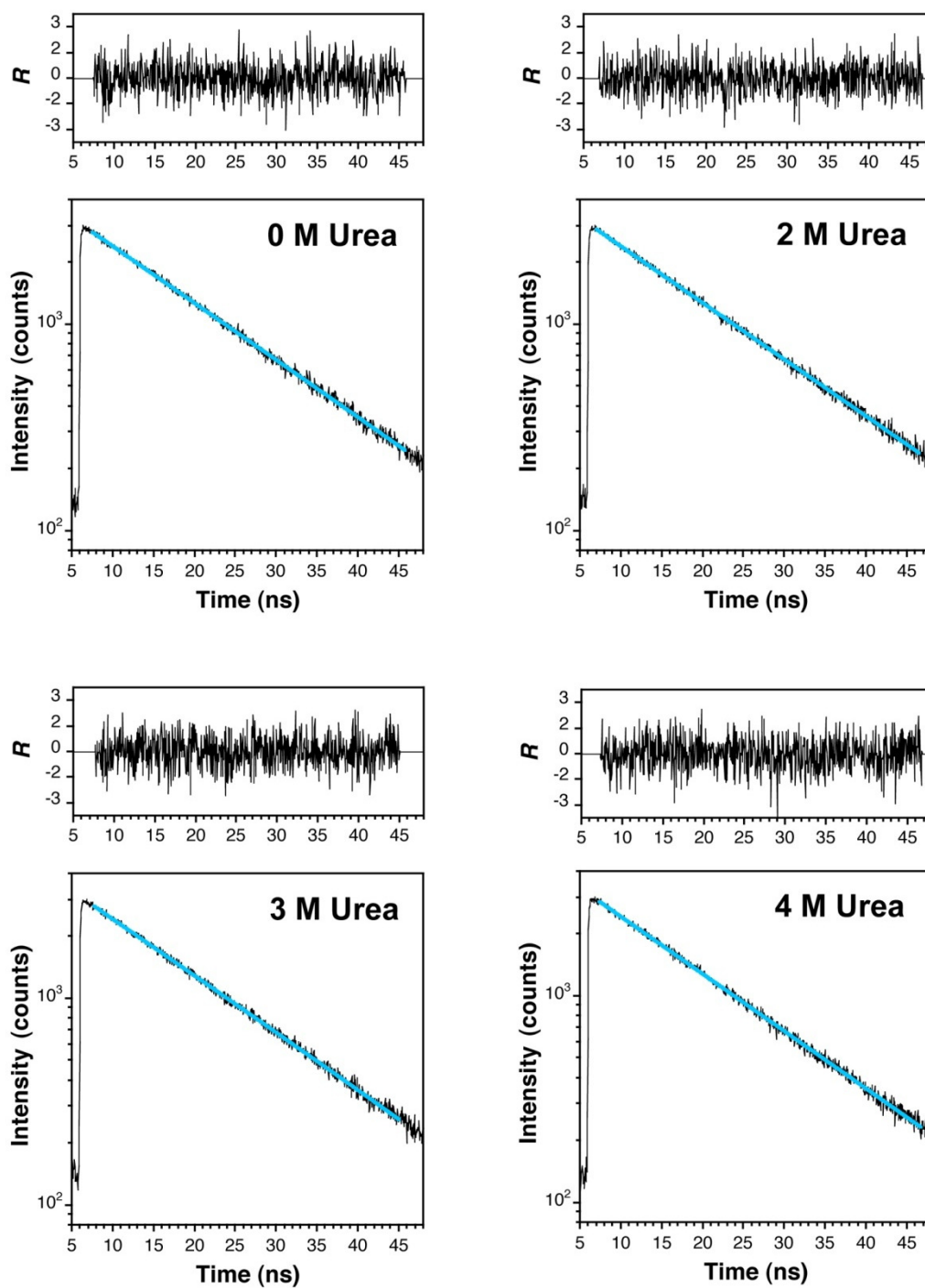


**Figure 2.38:** Lifetime Acridine Urea Experiments. Fits to Acridine fluorescence lifetime data with varying concentrations of urea in 100 mM sodium phosphate buffer, pH 7.00 ( $\lambda_{\text{ex}} = 405 \text{ nm}$ ;  $\lambda_{\text{em}} = 450 \text{ nm}$ ) at 25 °C. Exponential fit parameters are given in **Table 2.9**. Reprinted with permission from Speight, L. C.;

Muthusamy, A. K.; Goldberg, J. M.; Warner, J. B.; Wissner, R. F.; Willi, T. S.; Woodman, B. F.; Mehl, R. A.; Petersson, E. J., Efficient Synthesis and In Vivo Incorporation of Acridon-2-ylalanine, a Fluorescent Amino Acid for Lifetime and Forster Resonance Energy Transfer/Luminescence Resonance Energy Transfer Studies. *Journal of the American Chemical Society* **2013**, *135* (50), 18806-18814. Copyright (2013) American Chemical Society.

**Table 2.9:** Exponential Fits to Lifetime TIM Urea Denaturation Data.

Sample	[Urea] (M)	$\tau_1$ (ns)	% $\tau_1$	$\tau_2$ (ns)	% $\tau_2$	$\tau_{\text{avg}}$ (ns)
TIM-F <sub>74</sub> $\delta$	0	8.85 $\pm$ 0.07	37.6 $\pm$ 0.7	2.68 $\pm$ 0.05	62.4 $\pm$ 1.5	5.0 $\pm$ 0.1
	2	10.51 $\pm$ 0.07	45.5 $\pm$ 0.8	3.04 $\pm$ 0.07	54.5 $\pm$ 1.4	6.4 $\pm$ 0.1
	3	12.92 $\pm$ 0.07	61.0 $\pm$ 1.0	3.22 $\pm$ 0.11	39.0 $\pm$ 1.2	9.2 $\pm$ 0.2
	4	13.99 $\pm$ 0.07	83.6 $\pm$ 1.6	2.65 $\pm$ 0.28	16.4 $\pm$ 1.4	12.1 $\pm$ 0.3
TIM-Y <sub>101</sub> $\delta$	0	14.32 $\pm$ 0.09	56.4 $\pm$ 1.0	3.23 $\pm$ 0.10	43.6 $\pm$ 1.4	9.5 $\pm$ 0.2
	2	13.54 $\pm$ 0.08	61.6 $\pm$ 1.0	3.44 $\pm$ 0.12	38.4 $\pm$ 1.3	9.7 $\pm$ 0.2
	3	13.37 $\pm$ 0.07	78.8 $\pm$ 1.4	2.83 $\pm$ 0.21	21.2 $\pm$ 1.3	11.1 $\pm$ 0.3
	4	14.61 $\pm$ 0.07	85.7 $\pm$ 1.4	3.89 $\pm$ 0.36	14.3 $\pm$ 1.1	13.1 $\pm$ 0.3

Sample	[Urea] (M)	$\tau_1$ (ns)	% $\tau_1$	$\tau_2$ (ns)	% $\tau_2$	$\tau_{\text{avg}}$ (ns)
Acd	0	15.82 $\pm$ 0.08				
	2	15.87 $\pm$ 0.08				
	3	15.99 $\pm$ 0.08				
	4	15.70 $\pm$ 0.08				

## **CHAPTER 3: NASCENT PEPTIDES AND THE RIBOSOMAL EXIT TUNNEL**

## BACKGROUND AND PRIOR STUDIES

Many aspects of ribosomal translation have been rigorously studied,<sup>126</sup> including examinations of native aaRS permissivity<sup>127</sup>, EF-Tu binding<sup>49</sup>, and accommodation of ternary complexes into the A-site of the ribosome<sup>128</sup>. However, another structural facet of the ribosome, the nascent peptide exit tunnel, is a potential steric gate that could govern the kinetics or permissivity of incorporation of amino acids bearing large side-chains or side-chain modifications. As noted by T. Steitz, who shared in the 2009 Nobel Prize in Chemistry for his work studying the ribosome, the intricacies of the nascent peptide exit tunnel are poorly understood, despite the overall structural elucidation of the ribosome<sup>129</sup>. First confirmed to exist along with early cryo-electron microscopy images of the ribosome in 1995 (and hypothesized to exist in the mid-1980s<sup>130</sup>), the exit tunnel and its role in peptide synthesis have perplexed biophysical researchers<sup>131</sup>. Aside from facilitating the exit of polypeptides from the macromolecular machine, it has been shown that this region of the ribosome plays an important part in attenuation of the rate of ribosomal peptide synthesis; there are specific sequences that can interact with the walls of the tunnel and stall peptide synthesis<sup>132, 133</sup>, macrolide and ketolide antibiotics bind to the tunnel<sup>134</sup>, also stopping peptide synthesis, and antibiotic resistance to macrolides is achieved by translation of peptide sequences that are capable of removing the bound macrolide<sup>135, 136</sup>. However an understanding of the exact physiology of the tunnel and how its dynamics may influence the final conformation of polypeptides that emerge from the tunnel remains elusive<sup>137</sup>.

The 80 - 100 Å long peptide exit tunnel-measuring from the peptidyl transfer center (PTC) to bulk solvent at the end of the tunnel-of the ribosome was initially thought to be

a static fixture of the ribosome's overall architecture, which although varying in diameter throughout its length, is too small and rigid to allow nascent peptide chains to fold beyond an entropic adoption of  $\alpha$ -helical conformations<sup>129</sup>. In 2006 P. Moore, T. Steitz, and coworkers published a molecular dynamics study of the exit tunnel that aimed at mapping the geometry of the tunnel. While mainly examining the ability of the tunnel to accommodate water and ions, the study did note the work of others in which it was found that 30 – 40 residues of nascent peptides are protected from protease cleavage<sup>138</sup>. Consequently, the average distance allocated to each residue is 2 – 2.7 Å, a significant compaction from the 3.5 Å each residue would require if the nascent polypeptide chain was in a completely elongated conformation and a significant elongation from the 1.5 Å per residue distance typical of  $\alpha$ -helices<sup>139</sup>. These previous observations, in conjunction with P. Moore and colleagues' finding that the accessible volume of the tunnel decreased dramatically when they used probes with radii of greater than 3.0 Å, led the group to postulate that there is no regular ordered folding of nascent polypeptide chains as they traverse the tunnel. Despite these findings, the role of the exit tunnel and its impact on the folding of nascent peptides is still controversial and alternative hypotheses exist<sup>140-144</sup>.

## **ARREST PEPTIDES AS REGULATORY MECHANISMS**

The findings of this molecular dynamics study notwithstanding, the translation of specific peptides and sequences involved in cellular regulation and antibiotic resistance does imply that the ribosomal exit tunnel is capable of responding to stimuli. For example, certain peptide sequences have been shown to stall the ribosome during their translation

in the absence of certain protein or small molecule cofactors. Common examples of this phenomenon include SecM, part of the protein secretion pathways in *E. coli*, and TnaC, the leader peptide of the operon coding for tryptophanase (Tna), responsible for Trp degradation in *E. coli*. The mechanisms by which these peptides interact with the ribosomal exit tunnel and consequently arrest translation differ significantly. SecM bears a C-terminal sequence that induces pronounced ribosomal stalling in the absence of other Sec proteins at the exit of the tunnel. This binding was shown to be a property of the peptide sequence (FXXXXWIXXXGIRAGP, where X is any amino acid) as mutation of Pro to azetidine, a Pro UAA analog consisting of a 4-membered ring, greatly reduces the arresting properties of the sequence<sup>133</sup>. These observations have been corroborated by others leading to a hypothesis in which the bound nascent peptide skews the orientation of the PTC in such a manner that only Pro, the most conformationally inflexible amino acid, cannot proceed into the tunnel<sup>145</sup>. SecM translation can continue through one of two postulated mechanisms: either binding of the N-terminal domain of SecM (that, at the time of translation of the arresting C-terminal sequence has completely traversed the tunnel) by other elements of the Sec protein machinery ‘pulls’ the stalled peptide from the tunnel or binding of the Sec machinery to the ribosome induces a conformational change that allows translation to continue. The lab of K. Ito believes that experimental evidence supports the ‘pulling’ hypothesis as the translation of as many as 50 residues upstream from the stalling sequence is necessary for effective arrest cancellation<sup>133</sup>. This shows that the binding of the signal sequence to the walls of the tunnel is too tight to be released with a moderate conformational change but instead requires physical force to dislodge it from the tunnel. This is proposed to be accomplished by the high affinity

binding of an out-of-tunnel element to the N-terminal portion of SecM which pulls on the nascent peptide in addition to the translation of numerous residues which do not interact with the tunnel walls following the arresting sequence. Further supporting the ‘pulling’ hypothesis, the laboratory of G. von Heijne has shown using force microscopy that co-translational insertion of SecM into the translocon does in fact produce a pulling force that may be responsible in part for the cancellation of SecM mediated translation arrest<sup>146</sup>.

On the other hand, proponents of the induced conformational change theory in the laboratory of A. Yonath found that L22, a ribosomal protein, extends a  $\beta$ -hairpin motif into the exit tunnel<sup>147</sup>. From their study of the large ribosomal subunit from the organism *Deinococcus radiodurans* (D50S), they hypothesized that L22 acts as a gate capable of moving about two hinges. However this hypothesis has not been corroborated in the literature and computational work by K. Schulten and coworkers concerning the mechanism of TnaC mediated ribosomal stalling supports the pulling hypothesis proposed by Ito and von Heijne<sup>132</sup>.

Translational regulation of TnaC is coupled to cellular Trp concentrations. When cellular Trp concentrations are low, the ribosome translates the TnaC gene without any atypical behavior. Yet when cellular Trp concentrations are high, translation is markedly attenuated. High Trp concentrations lead to binding of the amino acid by the TnaC nascent polypeptide/ribosomal complex, most likely proximal to the PTC. This Trp binding effectively stalls the ribosome at the TnaC stop codon (just after translating the Pro in the TnaC arrest sequence), which inhibits Rho factor binding, its interaction with

the RNA polymerase complex, and subsequent transcription termination which is necessary for ribosomal read-through of the stop codon. Physiologically, the structural shifts necessary to facilitate binding of Trp to the TnaC nascent polypeptide/ribosomal complex still remain unclear; however interactions between the TnaC nascent polypeptide and the exit tunnel have been proposed. Combining methods of computational analysis and cryo-electron microscopy images of the *E. coli* 70S/TnaC complex, K. Schulten's group revealed that Arg92 of L22 makes a cation- $\pi$  interaction with Trp12 of the nascent TnaC peptide<sup>132</sup>. This residue is critical for TnaC regulation and thus it is well conserved among TnaC variants. Furthermore, Asp16, another conserved residue in the TnaC stalling sequence, makes salt bridges with ribosomal proteins. Neither of these interactions involve gate-like movements of the L22  $\beta$ -hairpin or any associated residues in the tunnel as postulated by others. However these interactions modeled by Schulten still require the tunnel to actively respond to and interact with unique residues on a nascent polypeptide chain.

### **'RESCUE' PEPTIDES PROVIDING ANTIBIOTIC RESISTANCE TO MACROLIDE AND KETOLIDE ANTIBIOTICS**

As previously alluded to, the most striking example of the exit tunnel harboring nascent peptide structural dynamics lies in the observation that the translation of specific short peptide sequences grants resistance to the macrolide and/or ketolide antibiotics. Several groups have shown that resistance to these antibiotics arises from the translation of proteins bearing unique N-terminal sequences that either evict the bound antibiotic or

facilitate the threading of a polypeptide around the exogenous compound<sup>135, 136, 148, 149</sup>. Macrolide and ketolide antibiotics are thought to inhibit ribosomal peptide synthesis by blocking nascent peptides from traversing the exit tunnel (the ‘plug-in-the-bottle’ model). Evidence for this lies primarily in the fact that in cell-free protein translation experiments conducted in the presence of macrolides, no full length protein is made, rather only 6 – 10 amino acid long peptidyl tRNAs are observed. Thus it is thought that peptide synthesis in the presence of these compounds continues until the nascent N-terminus contacts the antibiotic, sterically clashes, and propagates the clash to the PTC where the peptidyl tRNA moves into a conformation in which peptidyl transfer cannot occur (**Figure 3.1**)<sup>150, 151</sup>. The relative location of binding does differ from the macrolides to the ketolides as the use of the former yields 6 – 10 amino acid long peptidyl tRNAs while the use of the latter allows the synthesis of longer 9 – 10 residue species. In line with these observations, it has been shown that ketolides bind upstream in the tunnel while macrolides bind downstream near the PTC, adjacent to ribosomal proteins L4 and L22 and one specific nucleobase: A2062<sup>135, 149</sup>.

A. Mankin and colleagues have closely studied the mechanisms by which ‘resistance’ peptides are able to render ribosomes resistant to macrolide or ketolide antibiotics. Mankin’s initial hypothesis, called the ‘bottle brush’ model, invokes the concept that the translation of a specific peptide (the ‘brush’) interacts either directly with the bound antibiotic and forces it out of the tunnel or with the walls of the tunnel, inducing conformational changes in the rRNA and/or ribosomal proteins that lead to a dramatic decrease in affinity for the antibiotic<sup>135</sup>. It is important to note that these pathways are not mutually exclusive; ‘resistance’ peptide induced conformational changes could facilitate

a direct interaction with the antibiotic. However, both the models of inhibition and resistance rely on the assumption that the ribosomal exit tunnel cannot accommodate both the antibiotic and a nascent peptide chain. Recent findings by the Mankin group indicate that the tunnel actually is much more plastic than previously thought. In line with other groups' observations, they found that the N-terminal sequence of a nascent peptide dictates whether or not translation can proceed past a few residues in the presence of macrolide antibiotics. However, their novel discovery was that they saw translation of polypeptides without extrusion of the bound macrolide antibiotic<sup>136</sup>. As this finding was surprising, they appended the N-terminal sequence responsible for macrolide bypass onto well-studied proteins whose translation has been shown to not be resistant to ketolide antibiotics: elongation factor G (EF-G) and luciferase. In both cases, complete translation inhibition was not observed, but rather translation stalling in the middle of the protein sequences occurred after translating a significant portion of the rest of the proteins: yielding either a 40 kDa or 20 kDa truncated protein respectively. These results led the group to postulate that antibiotic-induced ribosomal stalling depends strictly on the amino acid sequence of the nascent peptide. Initially, translation in the luciferase experiments terminated at Pro189 to yield the aforementioned 20 kDa truncated protein. When this residue was mutated to a less conformationally-constrained amino acid, translation stalling occurred at the next Pro residue, 199. Crystallographic analyses of ribosome-macrolide complexes help to justify these results; many show that the exit tunnel is not completely blocked<sup>134</sup>. In fact, the narrowest portion of the tunnel with an antibiotic bound has an opening controlled by a highly flexible nucleobase: adenosine (A) 2062. As this nucleobase juts out into the tunnel and is held in place by a single carbon-nitrogen

bond, it can adopt several conformations without significantly altering the overall structure of the ribosome. It is possible that the N-terminal 'resistance' peptides force A2062 into a conformation conducive to a flexible nascent peptide snaking past, yet upon the appearance of bulky or structurally inflexible residues (i.e., Pro), A2062 restricts passage. Thus, translation arrest following successful antibiotic bypass occurs when there are structurally demanding residues or sequences. This suggests that the ribosomal-nascent peptide complex harbors residues or nucleobases capable of discriminating the structural landscape of polypeptides that traverse it. Furthermore, the binding of an antibiotic to this tunnel hypersensitizes it to the structural facets of nascent chains by constraining the movements of discriminating moieties such as A2062. The importance of A2062 as a discriminating moiety in the tunnel is highlighted further by other findings of the Mankin group in which resistance to the macrolide erythromycin is achieved by methylation of A2062, presumably precluding efficient antibiotic binding<sup>151</sup>.

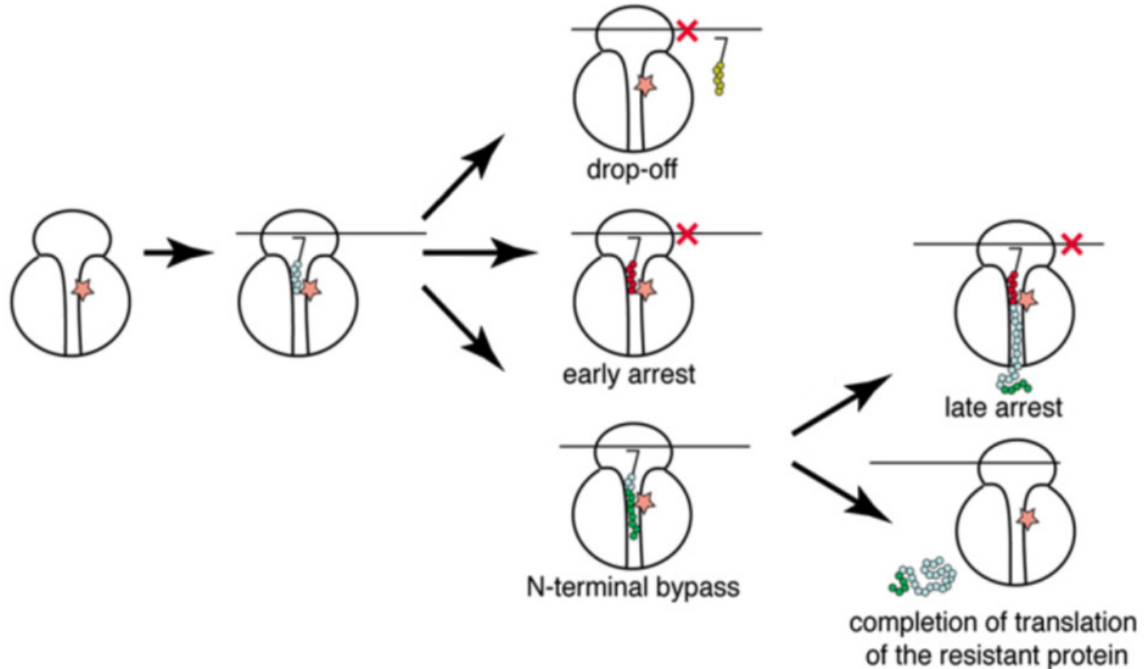


**Figure 3.1:** Models of Modes of Action for Macrolide Antibiotics Three major scenarios are possible if the macrolide does not leave the tunnel. Top: The macrolide can obscure the tunnel and block all protein synthesis. Middle: The nascent chain can traverse a portion of the drug blocked tunnel but then become arrested early in its translation. Bottom: N-terminal bypass can occur in which the nascent chain bypasses the antibiotic. Two scenarios are possible in this case. First (top far right), the N-terminal bypass can result in late state arrest leading to abortion of complete translation. Second (bottom far right), the entire protein can snake past the macrolide resulting in complete translation. Adapted from Kannan *et al.*<sup>136</sup> with permission from Elsevier.

## TOWARDS AN UNDERSTANDING OF THE PHYSIOLOGY AND FUNCTION OF THE RIBOSOMAL EXIT TUNNEL

Many questions arise from these findings: what are the structural features of the nascent peptide exit tunnel that discriminate peptides traversing it? For what purpose does the

tunnel scan the topology of newly synthesized peptides? Do interactions of the tunnel and nascent peptides affect the rate of translation? In light of these questions, several groups have postulated that the ribosomal exit tunnel is a conduit in which nascent polypeptides begin to fold<sup>140, 142, 143</sup>. The laboratory of C. Deutsch has carefully studied this hypothesis by examining the exit tunnel and its functional response to the chemical and physical properties of nascent polypeptides.

The most basic type of protein fold is the formation of secondary structures such as  $\alpha$ -helices. As such, a systematic study of the propensity of nascent polypeptide chains in the exit tunnel to form defined structures should start with an examination of helix formation. To this end, the Deutsch lab created a molecular ruler in which they could probe the relative compaction of peptide chains<sup>143</sup>. Using a Kv1.3 T1 domain sequence, modified to remove two small  $\alpha$ -helical segments, the group created a peptide platform that, according to prior studies has been shown to be completely extended. Additionally, a *BstEII*-digestion site was placed after Arg101 so that the peptide would effectively be stalled on the ribosome after translation of this residue. By placing single Cys residues at various locations in this peptide sequence (at various distances from the PTC) and post-translationally probing the accessibility of these residues with the mass-tagging reagent PEG-MAL (a polyethyleneglycol polymer functionalized with a maleimide that is 5 kDa in size), the group was able to ascertain the accessibility of each residue relative to the free peptide in solution. Accessibility was found to be a monotonic function of distance from the PTC in the last 20 Å of the tunnel next to the exit port. After these proof-of-principle experiments, the group then engineered helical segments at various locations in the nascent polypeptide. Ala has the highest helical propensity of all the amino acid

residues, and  $\alpha$ -helices are more compact than completely extended peptides. Thus, insertion of Ala repeats was expected to induce overall compaction of the previously extended peptide<sup>139</sup>. Using the same Cys / PEG-MAL tagging methodology, they probed the accessibility of three Cys residues engineered within this Ala-substituted ruler. Their results are consistent with the hypothesis that insertion of a helical domain into the molecular ruler would compact and axially retract the ruler into the ribosomal exit tunnel.

These molecular ruler experiments allowed the group to verify three previously postulated parameters inferred from other functional studies and imaging data for the ribosomal exit tunnel, including cryo-EM images of  $\alpha$ -helical nascent polypeptides in the exit tunnel<sup>152</sup>. First, testing with this method verified that compact structures can exist within the nascent polypeptide exit tunnel as shown by their comparison of reactivity with PEG-MAL from the all-extended to the compacted molecular ruler. To verify that a difference in accessibility was a function of steric hindrance of the large PEG-MAL probe entering the tunnel and not a measure of the relative chemical reactivity of the Cys residues, they also used the small molecule probe N-ethylmaleimide (NEM). Reaction of NEM with the single Cys molecular rulers, followed by ribosomal release, and then attempted reaction with PEG-MAL did not produce a significant population of PEGylated peptides, suggesting that the Cys residues, regardless of location, were reactive and their relative reactivities with PEG-MAL were a function of the accessibility of the residue while the construct was still in the tunnel. Second, the tunnel is largely exposed to bulk aqueous solvent. As the reaction between the Cys residues and PEG-MAL requires ionization of the sulfhydryl moiety and a relatively high dielectric environment, it is fair to attribute this to an aqueous environment. Finally, comparison of

the length of the molecular ruler and the sites of Cys accessibility match well with a tunnel length on the order of  $\sim 100$  Å, in line with estimates from structural determinations. These data provided the group with a verified means to test the formation of secondary structure within the ribosomal exit tunnel. However, the questions as to how secondary structure formation is facilitated by the tunnel, as well as whether or not the tunnel actively responds to diverse structural landscapes of various nascent peptides, remained ambiguous.

To address the question of how secondary structure formation could be facilitated by the ribosomal nascent peptide exit tunnel, the Deutsch lab extended their molecular ruler methodology by the creation of several molecular rulers with Ala repeats located at various locations in the nascent peptide sequence. Using Ala repeats of either 5, 10, or 15 residues and locating these sequences at various distances from the PTC, they determined whether if there are preferred locations for helix formation<sup>141</sup>. While these experiments did show locations in the tunnel that are particularly conducive to helix formation, they did not identify the exact mechanism or moieties responsible for this phenomena. Is the exit tunnel actively responding to the sequence-specific structure of the nascent polypeptide or is it merely providing an entropic trap in which helices can form?

Eager to answer these questions, the Deutsch lab began a new series of experiments to probe the response of the ribosomal exit tunnel to probes with varying steric bulk. To do this, steric probes constructed from tetraalkylammonium-decorated maleimides of increasing volume (from trimethyl, triethyl, tripropyl, to tributyl functionalized probes) were used to modify a single Cys engineered at different locations along the molecular

ruler spanning the length of the tunnel<sup>142</sup>. The kinetics of modification at each location was used to obtain modification rate constants. This study demonstrated that the tunnel is capable of discriminating between exogenous probes of volumes from 220 Å<sup>3</sup> (TMA) to 388 Å<sup>3</sup> (TBA). However the most interesting findings of these experiments arose when they examined the ability of the tunnel to discriminate between differently sized residues on the nascent peptide itself. By placing either an Ala or a Trp residue C-terminally adjacent to the Cys site of labeling and comparing the solvent accessible, the Deutsch group showed that at locations 22, 20, and 18 residues away from the PTC, solvent accessibility is sensitive to the identity of an adjacent residue; that is, accessibility increases with increasing the van der Waals' volume of an adjacent side-chain, suggesting that when a nascent polypeptide chain has a bulky residue at these locations either the tunnel changes conformation to accommodate it, or the nascent peptide itself rearranges to account for the larger moiety. This scenario was not detected at the vestibule, nor at the constriction site within the tunnel<sup>153</sup>.

All of the discussed experiments by the Deutsch lab carry one important caveat: they are probing the contours of the ribosomal nascent peptide exit tunnel by examining the ability of various reagents to enter *via* the exit tunnel and react with a Cys residue on a stalled peptide, after translation has ceased. To examine movement of a nascent peptide and its impact on the tunnels' contours (or conversely, the impact of the tunnel's contours on the transit of a nascent peptide), one would need a steric probe to be incorporated into a nascent chain at the PTC and traverse the length of the tunnel.

## AMINOACYLATION AND *IN VITRO* SENSE REPROGRAMING STRATEGIES

One strategy to study the contours of the ribosome nascent peptide exit tunnel is to create a nascent chain containing UAAs of systematically increasing size. Based on the studies of modified Cys residues in the tunnel (above), the Deutsch laboratory chose to incorporate Cys modified UAAs to accomplish this task. The first step in beginning such experiments was to implement an efficient method to derivatize Cys and attach the resulting amino acid derivative to a tRNA bearing an anticodon that would allow for site-specific incorporation of the resulting probe. Derivatization of Cys residues with maleimide probes occurs *via* a three step mechanism in which the thiol is deprotonated to reveal the nucleophilic sulfhydryl which then attacks one of the alkene carbons in the maleimide ring. This results in a keto-enol tautomerism that reverses upon protonation of the carbon adjacent to the newly formed thioether and yields the final succinimide product. Commonly, this transformation is referred to as a thia-Michael reaction.

However, a variety of reaction conditions aimed at mimicking these conditions on a protected Cys to form a NEM-Cys adduct failed to produce the desired product. Instead, it was observed that the resulting succinimide ring is prone to hydrolysis during the reaction, work-up, and/or purification. Atypical conditions, such as the use of boric acid as a catalyst<sup>154</sup>, were also employed, however we were unable to replicate the reported results under conditions in our laboratory (**Figure 3.2**). We were concerned with this hydrolysis as the ring-open form of the derivative has many more degrees of freedom and as such would be less likely to be sampling the same steric space of the tunnel in each experiment as opposed to a more rigid ring structure. The lability of the succinimide rings made it clear that mild thia-Michael reaction conditions were necessary and, ideally,

should be done late in the synthesis of the amino acid derivative to minimize hydrolysis.

As such, a new synthetic plan was needed.

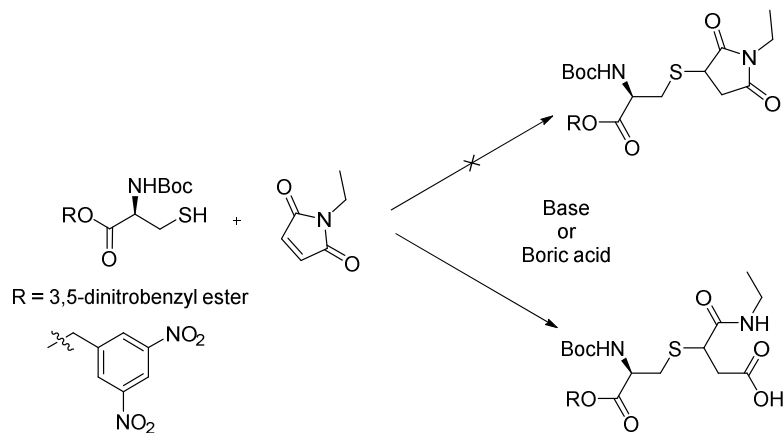


**Figure 3.2:** Conditions Tested for the Thia-Michael Reaction Between NEM and a Protected Cys.

As previously discussed in this document there are two main strategies that have been used to create aminoacyl tRNAs bearing UAAs: semi-synthetic tRNAs and the use of an o-aaRS/tRNA pair. Each of these methods has its benefits and complications: semi-synthetic tRNA requires the production of both a truncated tRNA and an aminoacylated dinucleotide while an o-aaRS/tRNA pair requires either evolution or robust screening. Intrinsic to both methods is the use of significantly modified tRNA species. Semi-synthetic tRNA methods yield an aminoacyl tRNA with a deoxycytidine at the 75 position of the tRNA while the use of an o-aaRS/tRNA pair necessitates the use of a tRNA that cannot be charged by any endogenous aaRSs. It is not uncommon for the tRNAs used in o-aaRS/tRNA pairs to have significantly perturbed binding to the host ribosome, a disadvantage the Schultz group often notes and has published efforts to alleviate<sup>63</sup>. As all of the Deutsch laboratory experiments are *in vitro* translations in a rabbit reticulocyte extract kit, it would be ideal to use a Cys tRNA carrying a modified

Cys UAA to more closely imitate the natural process of ribosomal translation.

Fortunately, H. Suga has devised a general method for the acylation of any tRNA species with virtually any amino acid using an evolved RNA catalyst<sup>155</sup>.

Noting that other groups have discovered RNA molecules capable of aminoacylating tRNA like structures (RNA sequences bearing the 3' CCA aminoacyl- acceptor structural hallmark of a tRNA) and that such RNAzymes are a crucial facet of the RNA world hypothesis, H. Suga was inspired to explore the *in vitro* evolution of such a RNA catalyst<sup>156</sup>. Using the 5' leader sequence of pre-tRNAs that is cleaved *in vivo* by RNase P, H. Suga used random mutagenesis and *in vitro* selection to identify a RNA sequence capable of charging *in cis* the 3' acceptor stem of a pre-tRNA<sup>157</sup>. By activating the carboxylate of Phe with a cyanomethyl ester (CME) and 15 rigorous rounds of *in vitro* selection, the group was able to evolve the 5'-leader sequence to recognize the aromatic ring of Phe and aminoacylate the activated amino acid onto the 3' end of the tRNA. Further refinement of this RNA aminoacylation catalyst allowed the group to cleave the 5'-leader sequence and aminoacylate tRNAs *in trans* as well as show that the catalyst selectively aminoacylates the 3' hydroxyl of tRNAs, a specificity feature common to one class of aaRSs<sup>158</sup>. Suga and coworkers named this RNAzyme flexizyme (Fx) for its ability to aminoacylate any tRNA.

Optimization of the original Fx that recognizes Phe led to the publication of eFx, a Fx variant with enhanced aminoacylation properties, but it only recognizes the aromatic amino acids (Phe, Trp, and Tyr) activated with a CME. Of most interest to chemical biologists however was the development of a Fx in which the specificity for the aromatic

side-chain of Phe was transferred to the activating ester moiety. Other Fx catalysts have been developed by the Suga group to recognize distinct aromatic moieties positioned off the carboxylate as either esters or thioesters. Interestingly, eFx has been shown to work with all tested amino acids functionalized with a *p*-chlorobenzyl thioester, showing that the RNAzyme truly is flexible not only with regards to its tRNA substrate scope, but also to its method of recognizing an activated amino acid. However the use of the thioester activating group appeared problematic to us as we desired to use Cys derivatives and the possibility of transthioesterification with the Cys thiol posed an unwanted complication. However, the Suga group did identify a Fx they called dFx due to its ability to utilize any amino acid functionalized with a 3,5-dinitrobenzyl ester (DBE)<sup>159</sup>. The broad substrate scope of this Fx appealed to us and was thus chosen as our tRNA aminoacylation catalyst.

Thus, we sought to develop synthetic routes to the DBE-activated amino acids. Since the test reactions with NEM and Cys revealed the necessity of attaching the maleimide probes at the latest stage possible in the synthetic scheme, a new retrosynthetic analysis was conducted (**Figure 3.3**). It was envisioned that the route could start with cystine. The use of this homodisulfide was chosen as a late-stage reduction to the free thiol would yield 2 equivalents of reactive Cys-DBE for each molecule of starting homodisulfide. This procedure increases the efficiency of the process because a protecting group is necessary to prevent undesired reactions with the nucleophilic thiol and the use of any other protecting groups would result in those moieties being discarded as waste or reacting with the maleimide probes.

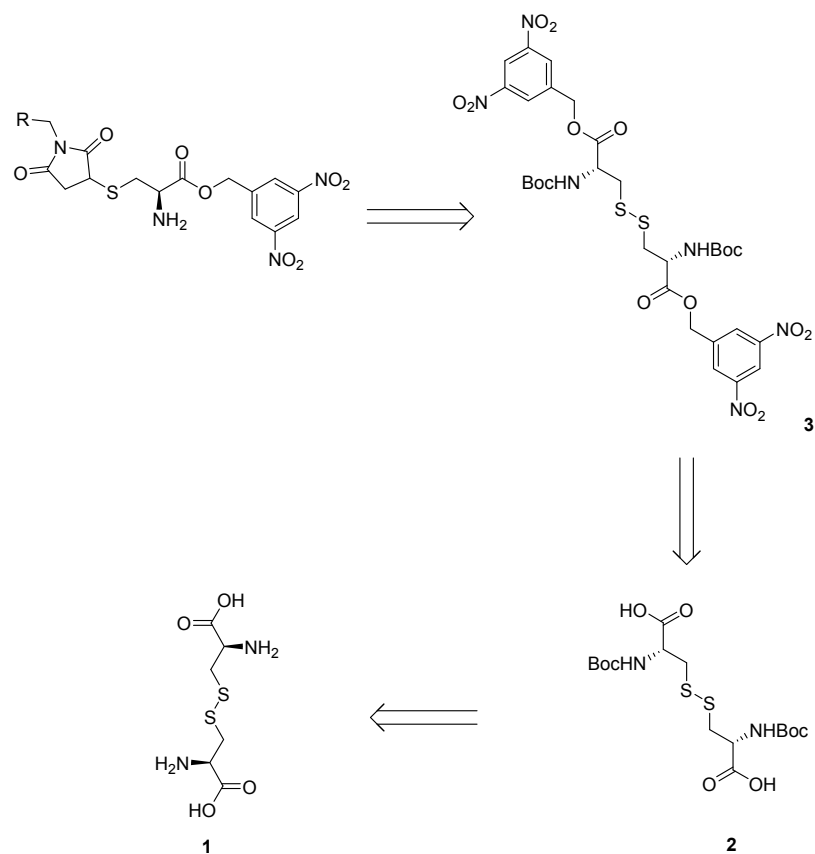
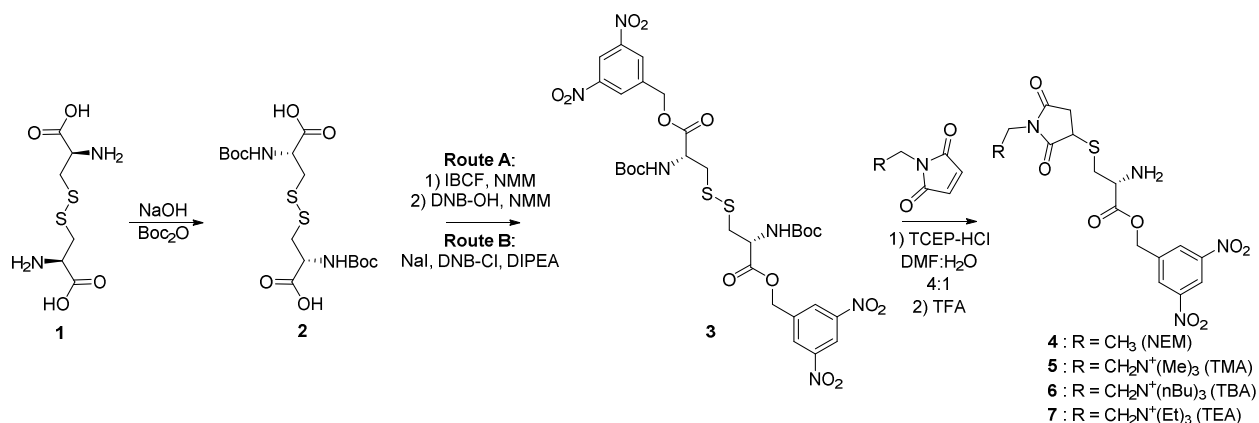


**Figure 3.3:** Retrosynthetic Analysis of Succinimide Functionalized Cys-DBEs.

In practice, the route began with protection of the two amines of cystine with *t*-butyl carbamates (Boc) to yield *N,N'*-diboc-cystine (**2**). Attachment of the dinitrobenzyl moiety was markedly more difficult than in any of Suga's reports, presumably because in this case we are forming a bis-DBE. Cross-reaction of one carboxylic acid with a formed DBE on the other half of the molecule could result in a cyclic anhydride, which would then decompose into the starting bis-acid. Two routes were explored to optimize this step and both nucleophilic and electrophilic dinitrobenzyl reagents were tested to provide the most efficient transformation of *N,N'*-diBoc-cystine into *N,N'*-diBoc-cystine-bis-DBE (**3**). Since the use of DNB-Cl afforded the desired product in 62.4 % yield and the use of

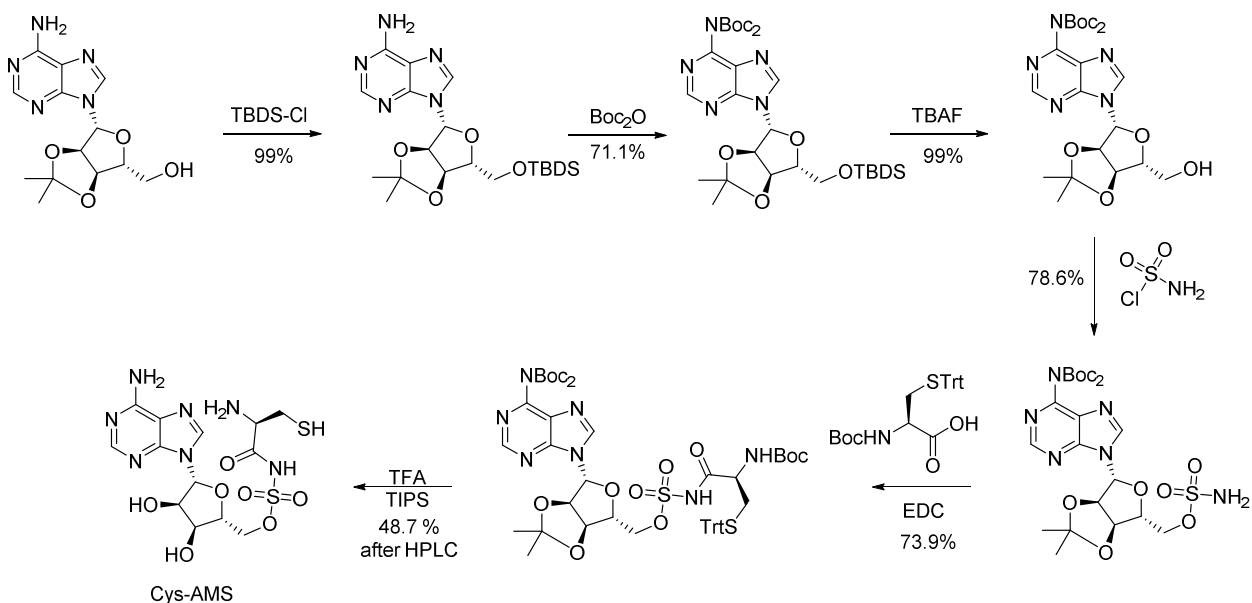
DNB-OH yielded considerably less (18.8 %), all future reactions were conducted using DNB-Cl and the appropriate reaction conditions. Efficient synthesis in hand, compound **3** was then used as the scaffold to create all of the succinimide derivatized Cys-DBE compounds.

As previous experiments highlighted the tendency of the succinimide ring to hydrolyze under basic conditions, it was envisioned that the use of the hydrochloric salt of (TCEP-HCl) would allow generation of the free thiol from the homodisulfide **3** under acidic conditions. Additionally, it was envisioned that these conditions could still facilitate the thia-Michael reaction between the newly revealed thiols and maleimides of interest, despite the low pH. Fortunately, this strategy worked and provided the desired attachment of the steric probes to the Cys-DBE. Removal of the Boc group from the  $\alpha$ -amine was accomplished with a 30 min treatment with trifluoroacetic acid on ice. Test reactions with NEM were conducted in neat DMF, however the use of the tetraalkylammonium derivatized maleimides required a water/DMF mixture to completely solvate all reactants. Since these compounds were then going to be used in an *in vitro* flexizyme charging reaction, purity was of the utmost concern. As previous test reactions showed that the succinimide ring was labile to hydrolysis during an aqueous work-up or on silica columns, they were purified to homogeneity by reverse-phase (RP) HPLC under acidic conditions (0.1% trifluoroacetic acid (TFA)) (**Scheme 3.1**). Preliminary results with collaborators at Thomas Jefferson University show that compounds **4** and **5** are substrates for flexizyme aminoacylation reactions.



**Scheme 3.1:** Synthetic Route to Succinimide Derivatized Cys DBEs.

To use the tRNA<sup>Cys</sup> harboring our modified Cys UAAs in the rabbit reticulocyte *in vitro* translation system we needed to develop a strategy to inhibit endogenous Cys aaRS activity. This is important because the Fx reaction does not go to completion, leaving some unacylated tRNA<sup>Cys</sup> that co-precipitates with our desired UAA-tRNA<sup>Cys</sup>. To avoid aminoacylation of this material, we needed to inhibit the endogenous Cys aaRS. The group of D. Tan has published the synthesis and use of nonhydrolyzable aminosulfonamides (AMS) as inhibitors of aaRSs and other adenylating enzymes and we sought to replicate their results. Following literature procedures<sup>160, 161</sup>, we were able to synthesize Cys-AMS in 6 steps and 25 % total yield following HPLC purification of the final product (**Scheme 3.2**). Gratifyingly, this compound shows significant inhibition (75 – 85 %) of Cys incorporation in the rabbit reticulocyte *in vitro* translation system and thus provides a means for us to site-specifically incorporate our Cys derivatives. Furthermore, preliminary results show that incorporation of compounds **4** and **5** is possible in the presence of Cys-AMS.



**Scheme 3.2:** Synthesis of the Cys aaRS Inhibitor: Cys-AMS.

Using these steric probe amino acids and Cys aaRS inhibitors, the process of probing the transit rates of probe-containing nascent peptides through the ribosomal exit tunnel has begun. These experiments will use a slightly modified version of the Kv1.3 protein sequence in which a single Cys codon has been engineered immediately N-terminal to a polyArg sequence. This polyArg sequence is predicted to pause the nascent peptide in the tunnel<sup>162</sup>. Synthesis of the remaining residues of the nascent chain after the Cys and polyArg sequences allows the Cys derivatives to move along the distal 60 – 80 Å of the tunnel. Thus the kinetics of translation of the Cys derivatives can be compared to ascertain the difference in transit time between the different steric probes without worrying about the probes different interactions with species such as EF-Tu.

## EXPERIMENTAL METHODS

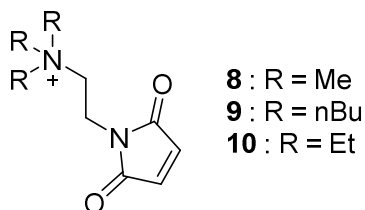
### General Information

2',3'-isopropylidene adenosine, *tert*-butyldimethylchlorosilane (TBDS-Cl), tetrahydrofuran (THF), *N,N*-dimethylformamide, imidazole, tetrabutylammonium fluoride (TBAF) (1 M in THF), chlorosulfonyl isocyanate, *N*-(*tert*-butoxycarbonyl)-*S*-trityl-L-cysteine (Boc-Cys(Trt)-OH), trifluoroacetic acid (TFA), L-cystine, 3,5-dinitrobenzyl alcohol (DNB-OH), 3,5-dinitrobenzyl chloride (DNB-Cl), triethylamine, tributylamine, *N*-(2-bromoethyl)phthalimide, *N*-methoxycarbonylmaleimide, (2-aminoethyl)trimethylammonium chloride hydrochloride, *N,N*-diisopropylethylamine (DIPEA), 4-methylmorpholine (NMM), sodium iodide (NaI), isobutyl chloroformate (IBCF), *N*-ethylmaleimide, di-*tert*-butyl dicarbamate (Boc<sub>2</sub>O), and sodium hydroxide (NaOH) were purchased from Sigma-Aldrich (St. Louis, MO, USA). Triisopropyl silane was purchased from Santa Cruz Biotechnology (Santa Cruz, CA, USA). 1-ethyl-3-(3-dimethylaminopropyl)carbodiimide hydrochloride (EDC-HCl) was purchased from AnaSpec, Inc. (Fremont, CA, USA). (Tris(2-carboxyethyl)phosphine) hydrochloride (TCEP-HCl) was purchased from CalBioChem, a subsidiary of EMD Chemicals, Inc. (San Diego, CA, USA). All other reagents and solvents were purchased from Fisher Scientific (Pittsburg, PA, USA).

Matrix-assisted laser desorption ionization (MALDI) mass spectra were collected with a Bruker Ultraflex III MALDI-TOF-TOF mass spectrometer (Billerica, MA, USA). NMR spectra, <sup>1</sup>H and <sup>13</sup>C, were collected with a Bruker DRX 500 MHz instrument. CDCl<sub>3</sub> was calibrated at  $\delta$  7.27 for <sup>1</sup>H and  $\delta$  77.2 for <sup>13</sup>C. DEPT-135 Carbon NMR notation as follows:

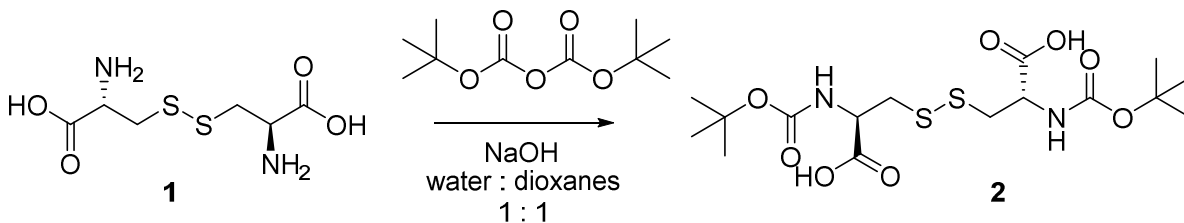
no signal is designated by (np), a positive signal is designated by (+), and a negative signal is designated by (-). High-resolution mass spectra (HRMS) were obtained on a Waters LC-TOF mass spectrometer (model LCT-XE Premier) using electrospray ionization in positive mode (Milford, MA, USA).

### Synthesis of Tetraalkylammonium Maleimides



Synthesis of these compounds was conducted according to procedures previously reported by the Deutsch laboratory. Characterization by low resolution liquid chromatography/mass spectrometry (LR-LCMS) and reverse phase (RP) HPLC matched those in the cited reports<sup>142, 163</sup>.

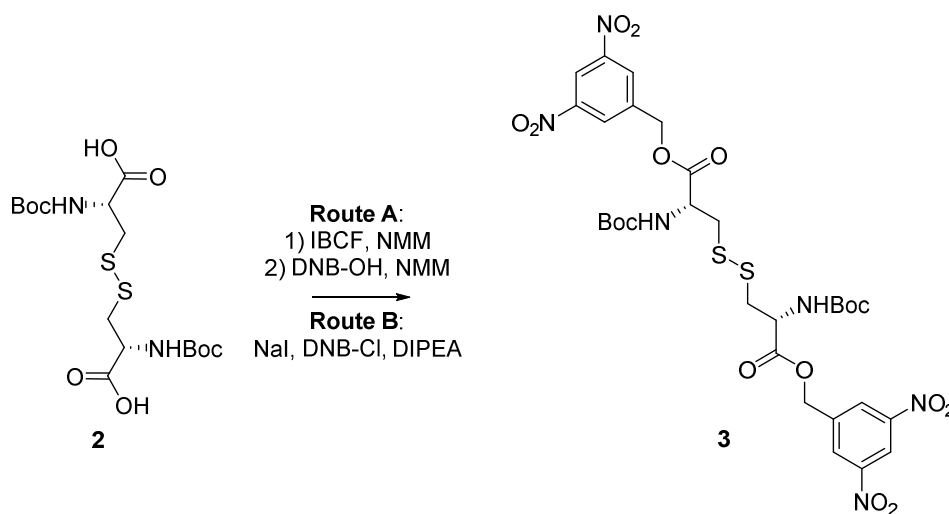
### Synthesis of (2R,2'R)-3,3'-disulfaneylbis(2-((tert-butoxycarbonyl)amino)propanoic acid) (2)



50 mL of 1:1 water : dioxanes was added to a round bottom flask (RBF) and cooled to 0° C under an Ar atmosphere. 1.33 g (33.29 mmol) NaOH was added to the flask and

allowed to stir 5 min. 2.0 g (8.32 mmol) L-cystine and 4.54 g (20.81 mmoles) di-*tert*-butyl dicarbamate were then added to the flask. After 4 hours, the mixture was acidified to pH 3 by dropwise addition of 3 M hydrochloric acid (HCl). The product was then extracted from the aqueous solution with ethyl acetate (EtOAc) (3 x 100 mL), dried with magnesium sulfate (MgSO<sub>4</sub>), and concentrated *in vacuo*. The compound was then used without further purification. 3.25 g (88.8 % yield) of pure product were retrieved using this method. <sup>1</sup>H NMR and LR-LCMS matched that of a previous report<sup>164</sup>.

**Synthesis of bis(3,5-dinitrobenzyl 3,3'-disulfanediyl(2*R*,2'*R*)-bis(2-((*tert*-butoxycarbonyl)amino)propanoate) (3)**



**Route A:**

1.0 g (2.27 mmol) of (*2R,2'R*)-3,3'-disulfanediylbis(2-((*tert*-butoxycarbonyl)amino)propanoic acid) (**2**) was added to 5 mL of dry THF in an oven dried RBF and cooled to 0° C under an Ar atmosphere. 0.46 g (500 μL; 4.54 mmol) NMM was added dropwise *via* syringe. 1.24 g (1180 μL; 9.08 mmol) IBCF was then

added dropwise *via* syringe and the resulting solution was allowed to stir at 0° C for 30 min. 1.01 g (4.54 mmol) DNB-OH was then dissolved in 7 mL dry THF and added to the solution dropwise *via* syringe. After 1 hour at 0° C the reaction was allowed to warm to room temperature (RT) and 0.46 g (500  $\mu$ L; 4.54 mmol) additional NMM was slowly added to the RBF *via* syringe. After 16 hr, the reaction was washed with 50 mL saturated ammonium chloride (NH<sub>4</sub>Cl), extracted with EtOAc (3 x 100 mL), dried with MgSO<sub>4</sub>, and concentrated *in vacuo*.

#### **Route B:**

1.0 g (2.27 mmol) of **2**, 1.97 g (13.17 mmol) NaI, and 1.62 mL (9.31 mmol) DIPEA were added to 2.5 mL dry DMF in a RBF under an Ar atmosphere and the mixture was allowed to stir for 10 min. 1.97 g (9.08 mmol) DNB-Cl was then added to the flask and the reaction was allowed to stir overnight at RT. After 16 hr, the mixture was diluted with 50 mL methylene chloride (DCM), washed with 50 mL water twice (which was back-extracted with 20 mL DCM each time), dried with MgSO<sub>4</sub>, and concentrated *in vacuo*.

#### **Purification and characterization for both routes:**

The resulting crude yellow-orange oil was then subjected to flash column chromatography (FCC) for purification.  $R_f$  = 0.26 in (7:3 Hexanes/EtOAc). Route A yielded 0.34 g (18.8 %) while route B yielded 1.13 g (62.4 %) and was thus this route was used for all subsequent syntheses of this compound. <sup>1</sup>H NMR (500 MHz, CDCl<sub>3</sub>)  $\delta$  9.02 (s, 2 H), 8.60 (s, 4 H), 5.4 (br. s, 6 H), 4.71 – 4.65 (m, 2 H), 3.24 – 3.14 (br. s, 4 H), 1.42 (s, 9 H); <sup>13</sup>C NMR (125 MHz, CDCl<sub>3</sub>):  $\delta$  170.6 (np), 155.2 (np), 148.9 (np), 139.3

(np), 128.3 (+), 119.0 (+), 81.0 (np), 65.2 (-), 53.2 (+), 40.8 (-), 28.4 (+); HRMS (ESI)  $m/z$  calcd for  $C_{30}H_{36}N_6O_{16}S_2Na$   $[M+Na]^+$  823.1527, found 823.1520.

### General Method for the Syntheses of Succinimide Functionalized Cys-DBEs (4 – 7)

Homodisulfide **3** (0.053 mmol) was combined with 0.117 mmol NEM, compounds **8**, **9**, or **10** and 0.265 mmol of TCEP-HCl in 1 mL of 80 % DMF / 20 % water. The mixture was allowed to react at rt for 2.5 hrs then 20 mL of water with 0.1 % TFA was added and the resulting solution was lyophilized to dryness. The solution was redissolved in 2 mL TFA and allowed to react on ice for 30 minutes before being concentrated *in vacuo*. Each compound synthesized utilizing these methods was purified by RP-HPLC as described below using a  $C_{18}$  HPLC column.

### HPLC Tables for Purification of 4 – 7

**Table 3.1:** Purification of **4**.. (Buffer A is 100 %  $H_2O$ , 0.1 %  $CF_3CO_2H$ . Buffer B is 90 % Acetonitrile, 10 %  $H_2O$ , 0.1 %  $CF_3CO_2H$ )

Time (min)	% Buffer B
0.01	1
5	30
30	50
35	100
40	100
45	5

$R_f = 18.23$  min

**Table 3.2:** Purification of **5.** (Buffer A is 100 % H<sub>2</sub>O, 0.1 % CF<sub>3</sub>CO<sub>2</sub>H. Buffer B is 90 % Acetonitrile, 10 % H<sub>2</sub>O, 0.1 % CF<sub>3</sub>CO<sub>2</sub>H)

Time (min)	% Buffer B
0.01	1
30.00	50
35.00	100
40.00	100
45.00	20

$$R_f = 19.14 \text{ min}$$

**Table 3.3:** Purification of **6.** (Buffer A is 100 % H<sub>2</sub>O, 0.1 % CF<sub>3</sub>CO<sub>2</sub>H. Buffer B is 100 % Acetonitrile, 0.1 % CF<sub>3</sub>CO<sub>2</sub>H)

Time (min)	% Buffer B
0.01	1
7.00	25
15.00	35
28.00	45
32.00	55
34.00	100
38.00	100
40.00	2

$$R_f = 11.25 \text{ min}$$

**Table 3.4:** Purification of **7.** (Buffer A is 100 % H<sub>2</sub>O, 0.1 % CF<sub>3</sub>CO<sub>2</sub>H. Buffer B is 90 % Acetonitrile, 10 % H<sub>2</sub>O, 0.1 % CF<sub>3</sub>CO<sub>2</sub>H)

Time (min)	% Buffer B
0.01	1
50.00	65
55.00	100
60.00	100
65.00	5

$$R_f = 18.85 \text{ min}$$

## MS Table for the Characterization of 4 – 7

**Table 3.5:** MS Analyses of Cys-Succinimide-DBEs.

Compound	Calculated Ion Mass	Observed Ion Mass
<b>4</b>	427.09	427.24
<b>5</b>	484.15	484.12
<b>6</b>	610.29	610.22
<b>7</b>	526.20	526.18

### Synthesis of Cys-AMS

The synthesis of this compound was conducted as described in a report by the laboratory of D. Tan<sup>160</sup>. Of note, sulfamoyl chloride, a necessary reagent for this synthesis, was also made in-house according to another literature procedure<sup>161</sup>. All characterizations matched those of prior reports<sup>160, 161</sup>.

## REFERENCES

1. Anfinsen, C. B., Principles that Govern Folding of Protein Chains. *Science* **1973**, *181* (4096), 223-230.
2. Kresge, N.; Simoni, R. D.; Hill, R. L., The Thermodynamic Hypothesis of Protein Folding: The Work of Christian Anfinsen. *Journal of Biological Chemistry* **2006**, *281* (14), 3.
3. RCSB Protein Data Bank. <http://www.rcsb.org/pdb/home/home.do> (accessed March 3).
4. Garman, E. F., Developments in X-ray Crystallographic Structure Determination of Biological Macromolecules. *Science* **2014**, *343* (6175), 1102-1108; Rule, G. S. a. H., T. Kevin, *Fundamentals of Protein NMR Spectroscopy*. Springer: Dordrecht, The Netherlands, 2006; Vol. 5, p 530.
5. Selenko, P.; Wagner, G., NMR mapping of protein interactions in living cells. *Nature Methods* **2006**, *3* (2), 80-81; Koopmann, R.; Cupelli, K.; Redecke, L.; Nass, K.; DePonte, D. P.; White, T. A.; Stellato, F.; Rehders, D.; Liang, M. N.; Andreasson, J.; Aquila, A.; Bajt, S.; Barthelmess, M.; Barty, A.; Bogan, M. J.; Bostedt, C.; Boutet, S.; Bozek, J. D.; Caleman, C.; Coppola, N.; Davidsson, J.; Doak, R. B.; Ekeberg, T.; Epp, S. W.; Erk, B.; Fleckenstein, H.; Foucar, L.; Graafsma, H.; Gumprecht, L.; Hajdu, J.; Hampton, C. Y.; Hartmann, A.; Hartmann, R.; Hauser, G.; Hirsemann, H.; Holl, P.; Hunter, M. S.; Kassemeyer, S.; Kirian, R. A.; Lomb, L.; Maia, F.; Kimmel, N.; Martin, A. V.; Messerschmidt, M.; Reich, C.; Rolles, D.; Rudek, B.; Rudenko, A.; Schlichting, I.; Schulz, J.; Seibert, M. M.; Shoeman, R. L.; Sierra, R. G.; Soltau, H.; Stern, S.; Struder, L.; Timneanu, N.; Ullrich, J.; Wang, X. Y.; Weidenspointner, G.; Weierstall, U.; Williams, G. J.; Wunderer, C. B.; Fromme, P.; Spence, J. C. H.; Stehle, T.; Chapman, H. N.; Betzel, C.; Duszynko, M., *In Vivo Protein Crystallization Opens New Routes in Structural Biology*. *Nature Methods* **2012**, *9* (3), 259.
6. Bryant, R. G., The NMR Time Scale. *Journal of Chemical Education* **1983**, *60* (11), 933-935.
7. Miller, R. J. D., Femtosecond Crystallography with Ultrabright Electrons and X-rays: Capturing Chemistry in Action. *Science* **2014**, *343* (6175), 1108-1116; Otten, R.; Villali, J.; Kern, D.; Mulder, F. A. A., Probing Microsecond Time Scale Dynamics in Proteins by Methyl H-1 Carr-Purcell-Meiboom-Gill Relaxation Dispersion NMR Measurements. Application to Activation of the Signaling Protein NtrC(r). *Journal of the American Chemical Society* **2010**, *132* (47), 17004-17014; Krushelnitsky, A.; Zinkevich, T.; Reichert, D.; Chevelkov, V.; Reif, B., Microsecond Time Scale Mobility in a Solid Protein As Studied by the N-15 R-1 rho Site-Specific NMR Relaxation Rates. *Journal of the American Chemical Society* **2010**, *132* (34), 11850-11853; Zhang, J. P.; Zhang, Y. L., Molecular Dynamics Studies on the NMR and X-ray Structures of Rabbit Prion Proteins. *Journal of Theoretical Biology* **2014**, *342*, 70-82; Vieville, J. M. P.; Charbonnier, S.; Eberling, P.; Starck, J. P.; Delsuc, M. A., A New NMR Technique to Probe Protein-Ligand Interaction. *Journal of Pharmaceutical and Biomedical Analysis* **2014**, *89*, 18-23; Cala, O.; Guilliere, F.; Krimm, I., NMR-based Analysis of Protein-Ligand Interactions. *Analytical and Bioanalytical Chemistry* **2014**, *406* (4), 943-956.
8. Bastiaens, P. I. H.; Pepperkok, R., Observing Proteins in Their Natural Habitat: The Living Cell. *Trends in Biochemical Sciences* **2000**, *25* (12), 631-637; Kenworthy, A. K., Imaging Protein-Protein Interactions Using Fluorescence Resonance Energy Transfer Microscopy. *Methods* **2001**, *24* (3), 289-296; Eftink, M. R.; Ghiron, C. A.,

- Fluorescence Quenching Studies with Proteins. *Analytical Biochemistry* **1981**, *114* (2), 199-227; Matyus, L.; Szollosi, J.; Jenei, A., Steady-State Fluorescence Quenching Applications for Studying Protein Structure and Dynamics. *Journal of Photochemistry and Photobiology B-Biology* **2006**, *83* (3), 223-236; Coffman, V. C.; Wu, J. Q., Counting Protein Molecules Using Quantitative Fluorescence Microscopy. *Trends in Biochemical Sciences* **2012**, *37* (11), 499-506; Wang, Z. P.; Ding, X. Z.; Li, S. J.; Shi, J.; Li, Y. M., Engineered Fluorescence Tags for *In Vivo* Protein Labelling. *Rsc Advances* **2014**, *4* (14), 7235-7245; Fernandez-Duenas, V.; Llorente, J.; Gandia, J.; Borroto-Escuela, D. O.; Agnati, L. F.; Tasca, C. I.; Fuxe, K.; Ciruela, F., Fluorescence Resonance Energy Transfer-Based Technologies in the Study of Protein-Protein Interactions at the Cell Surface. *Methods* **2012**, *57* (4), 467-472; Sun, Y. S.; Hays, N. M.; Periasamy, A.; Davidson, M. W.; Day, R. N., Monitoring Protein Interactions in Living Cells with Fluorescence Lifetime Imaging Microscopy. *Imaging and Spectroscopic Analysis of Living Cells: Optical and Spectroscopic Techniques* **2012**, *504*, 371-391.
9. Yang, F.; Moss, L. G.; Phillips, G. N., The Molecular Structure of Green Fluorescent Protein. *Nature Biotechnology* **1996**, *14* (10), 1246-1251.
  10. Taskent-Sezgin, H.; Marek, P.; Thomas, R.; Goldberg, D.; Chung, J.; Carrico, I.; Raleigh, D. P., Modulation of p-Cyanophenylalanine Fluorescence by Amino Acid Side Chains and Rational Design of Fluorescence Probes of alpha-Helix Formation. *Biochemistry* **2010**, *49* (29), 6290-6295.
  11. Lakowicz, J. R.; Weber, G., Quenching of Protein Fluorescence by Oxygen - Detection of Structural Fluctuations in Proteins on Nanosecond Time Scale. *Biochemistry* **1973**, *12* (21), 4171-4179; Lakowicz, J. R., Fluorescence Spectroscopic Investigations of the Dynamic Properties of Proteins, Membranes, and Nucleic Acids. *Journal of Biochemical and Biophysical Methods* **1980**, *2* (1-2), 91-119; Richards, F. M., Interpretation of Protein Structures - Total Volume, Group Volume Distributions and Packing Density. *Journal of Molecular Biology* **1974**, *82* (1), 1-14.
  12. Liu, C. C.; Schultz, P. G., Adding New Chemistries to the Genetic Code. *Annual Review of Biochemistry*, Vol 79 **2010**, *79*, 413-444; Kim, C. H.; Axup, J. Y.; Schultz, P. G., Protein Conjugation with Genetically Encoded Unnatural Amino Acids. *Current Opinion in Chemical Biology* **2013**, *17* (3), 412-419.
  13. Shimomura, O.; Johnson, F. H.; Saiga, Y., Extraction, Purification and Properties of Aequorin, a Bioluminescent Protein from Luminous Hydromedusan, Aequorea. *Journal of Cellular and Comparative Physiology* **1962**, *59* (3), 223.
  14. Tsien, R. Y., The Green Fluorescent Protein. *Annual Review of Biochemistry* **1998**, *67*, 509-544.
  15. Carlson, H. J.; Campbell, R. E., Genetically Encoded FRET-based Biosensors for Multiparameter Fluorescence Imaging. *Current Opinion in Biotechnology* **2009**, *20* (1), 19-27.
  16. Van Dongen, E.; Dekkers, L. M.; Spijker, K.; Meijer, E. W.; Klomp, L. W. J.; Merkx, M., Ratiometric Fluorescent Sensor Proteins with Subnanomolar Affinity for Zn(II) Based on Copper Chaperone Domains. *Journal of the American Chemical Society* **2006**, *128* (33), 10754-10762.
  17. van Dongen, E.; Evers, T. H.; Dekkers, L. M.; Meijer, E. W.; Klomp, L. W. J.; Merkx, M., Variation of Linker Length in Ratiometric Fluorescent Sensor Proteins Allows Rational Tuning of Zn(II) Affinity in the Picomolar to Femtomolar Range. *Journal of the American Chemical Society* **2007**, *129* (12), 3494.
  18. Vinkenborg, J. L.; Nicolson, T. J.; Bellomo, E. A.; Koay, M. S.; Rutter, G. A.; Merkx, M., Genetically Encoded FRET Sensors to Monitor Intracellular Zn<sup>2+</sup> Homeostasis. *Nature Methods* **2009**, *6* (10), 737.
  19. Los, G. V.; Encell, L. P.; McDougall, M. G.; Hartzell, D. D.; Karassina, N.; Zimprich, C.; Wood, M. G.; Learish, R.; Ohane, R. F.; Urh, M.; Simpson, D.; Mendez, J.; Zimmerman, K.; Otto,

- P.; Vidugiris, G.; Zhu, J.; Darzins, A.; Klaubert, D. H.; Bulleit, R. F.; Wood, K. V., HatoTag: A Novel Protein Labeling Technology for Cell Imaging and Protein Analysis. *Acs Chemical Biology* **2008**, *3* (6), 373-382.
20. Keppler, A.; Kindermann, M.; Gendreizig, S.; Pick, H.; Vogel, H.; Johnsson, K., Labeling of Fusion Proteins of O-6-alkylguanine-DNA Alkyltransferase with Small Molecules *In Vivo* and *In Vitro*. *Methods* **2004**, *32* (4), 437-444.
21. Gautier, A.; Juillerat, A.; Heinis, C.; Correa, I. R.; Kindermann, M.; Beaufils, F.; Johnsson, K., An Engineered Protein Tag for Multiprotein Labeling in Living Cells. *Chemistry & Biology* **2008**, *15* (2), 128-136.
22. Gallagher, S. S.; Sable, J. E.; Sheetz, M. P.; Cornish, V. W., An *In Vivo* Covalent TMP-Tag Based on Proximity-Induced Reactivity. *Acs Chemical Biology* **2009**, *4* (7), 547-556; Miller, L. W.; Cai, Y. F.; Sheetz, M. P.; Cornish, V. W., *In Vivo* Protein Labeling with Trimethoprim Conjugates: A Flexible Chemical Tag. *Nature Methods* **2005**, *2* (4), 255-257.
23. Jing, C.; Cornish, V. W., A Fluorogenic TMP-Tag for High Signal-to-Background Intracellular Live Cell Imaging. *Acs Chemical Biology* **2013**, *8* (8), 1704-1712.
24. Griffin, B. A.; Adams, S. R.; Tsien, R. Y., Specific Covalent Labeling of Recombinant Protein Molecules Inside Live Cells. *Science* **1998**, *281* (5374), 269-272.
25. Andresen, M.; Schmitz-Salue, R.; Jakobs, S., Short Tetracysteine Tags to beta-Tubulin Demonstrate the Significance of Small Labels for Live Cell Imaging. *Molecular Biology of the Cell* **2004**, *15* (12), 5616-5622; Dyachok, O.; Isakov, Y.; Sagetorp, J.; Tengholm, A., Oscillations of Cyclic AMP in Hormone-Stimulated Insulin-Secreting beta-Cells. *Nature* **2006**, *439* (7074), 349-352; Enninga, J.; Mounier, J.; Sansonetti, P.; Van Nhieu, G. T., Secretion of Type III Effectors into Host Cells in Real Time. *Nature Methods* **2005**, *2* (12), 959-965; Hoffmann, C.; Gaietta, G.; Bunemann, M.; Adams, S. R.; Oberdorff-Maass, S.; Behr, B.; Vilardaga, J. P.; Tsien, R. Y.; Eisman, M. H.; Lohse, M. J., A FIAsh-based FRET Approach to Determine G Protein - Coupled Receptor Activation in Living Cells. *Nature Methods* **2005**, *2* (3), 171-176; Nakanishi, J.; Takarada, T.; Yunoki, S.; Kikuchi, Y.; Maeda, M., FRET-based Monitoring of Conformational Change of the beta(2) Adrenergic Receptor in Living Cells. *Biochemical and Biophysical Research Communications* **2006**, *343* (4), 1191-1196.
26. Adams, S. R.; Campbell, R. E.; Gross, L. A.; Martin, B. R.; Walkup, G. K.; Yao, Y.; Llopis, J.; Tsien, R. Y., New Biarsenical Ligands and Tetracysteine Motifs for Protein Labeling *In Vitro* and *In Vivo*: Synthesis and Biological Applications. *Journal of the American Chemical Society* **2002**, *124* (21), 6063-6076.
27. Luedtke, N. W.; Dexter, R. J.; Fried, D. B.; Schepartz, A., Surveying Polypeptide and Protein Domain Conformation and Association with FIAsh and ReAsH. *Nature Chemical Biology* **2007**, *3* (12), 779-784.
28. Lee, J.; Culyba, E. K.; Powers, E. T.; Kelly, J. W., Amyloid-beta Forms Fibrils by Nucleated Conformational Conversion of Oligomers. *Nature Chemical Biology* **2011**, *7* (9), 602-609.
29. Martin, B. R.; Giepmans, B. N. G.; Adams, S. R.; Tsien, R. Y., Mammalian Cell-Based Optimization of the Biarsenical-Binding Tetracysteine Motif for Improved Fluorescence and Affinity. *Nature Biotechnology* **2005**, *23* (10), 1308-1314; Stroffekova, K.; Proenza, C.; Beam, K., The Protein-Labeling Reagent FIAsh-EDT<sub>2</sub> Binds Not Only to CCXXCC Motifs but Also Non-Specifically to Endogenous Cysteine-Rich Proteins. *Pflügers Archiv* **2001**, *442* (6), 859-866.
30. Chen, I.; Howarth, M.; Lin, W. Y.; Ting, A. Y., Site-Specific Labeling of Cell Surface Proteins with Biophysical Probes Using Biotin Ligase. *Nature Methods* **2005**, *2* (2), 99-104; Slavoff, S. A.; Chen, I.; Choi, Y. A.; Ting, A. A. Y., Expanding the Substrate Tolerance of Biotin

- Ligase Through Exploration of Enzymes from Diverse Species. *Journal of the American Chemical Society* **2008**, *130* (4), 1160.
31. Beckett, D.; Kovaleva, E.; Schatz, P. J., A Minimal Peptide Substrate in Biotin Holoenzyme Synthetase-Catalyzed Biotinylation. *Protein Science* **1999**, *8* (4), 921-929; de Boer, E.; Rodriguez, P.; Bonte, E.; Krijgsveld, J.; Katsantoni, E.; Heck, A.; Grosveld, F.; Strouboulis, J., Efficient Biotinylation and Single-Step Purification of Tagged Transcription Factors in Mammalian Cells and Transgenic Mice. *Proceedings of the National Academy of Sciences of the United States of America* **2003**, *100* (13), 7480-7485.
  32. Lin, C. W.; Ting, A. Y., Transglutaminase-Catalyzed Site-Specific Conjugation of Small-Molecule Probes to Proteins *In Vitro* and on the Surface of Living Cells. *Journal of the American Chemical Society* **2006**, *128* (14), 4542-4543.
  33. Uttamapinant, C.; White, K. A.; Baruah, H.; Thompson, S.; Fernandez-Suarez, M.; Puthenveetil, S.; Ting, A. Y., A Fluorophore Ligase for Site-Specific Protein Labeling Inside Living Cells. *Proceedings of the National Academy of Sciences of the United States of America* **2010**, *107* (24), 10914-10919.
  34. Puthenveetil, S.; Liu, D. S.; White, K. A.; Thompson, S.; Ting, A. Y., Yeast Display Evolution of a Kinetically Efficient 13-Amino Acid Substrate for Lipoic Acid Ligase. *Journal of the American Chemical Society* **2009**, *131* (45), 16430-16438.
  35. Fernandez-Suarez, M.; Chen, T. S.; Ting, A. Y., Protein-Protein Interaction Detection *In Vitro* and in Cells by Proximity Biotinylation. *Journal of the American Chemical Society* **2008**, *130* (29), 9251; Slavoff, S. A.; Liu, D. S.; Cohen, J. D.; Ting, A. Y., Imaging Protein-Protein Interactions inside Living Cells via Interaction-Dependent Fluorophore Ligation. *Journal of the American Chemical Society* **2011**, *133* (49), 19769-19776.
  36. Brown, M. P.; Royer, C., Fluorescence Spectroscopy as a Tool to Investigate Protein Interactions. *Current Opinion in Biotechnology* **1997**, *8* (1), 45-49; Millar, D. P., Time-Resolved Fluorescence Spectroscopy. *Current Opinion in Structural Biology* **1996**, *6* (5), 637-642.
  37. Pardee, A. B.; Shore, V. G.; Prestidge, L. S., Incorporation of Azatryptophan into Proteins of Bacteria and Bacteriophage. *Biochimica Et Biophysica Acta* **1956**, *21* (2), 406-407.
  38. Budisa, N.; Pal, P. P., Designing Novel Spectral Classes of Proteins with a Tryptophan-Expanded Genetic Code. *Biological Chemistry* **2004**, *385* (10), 893-904.
  39. Lepthien, S.; Wiltschi, B.; Bolic, B.; Budisa, N., *In Vivo* Engineering of Proteins with Nitrogen-Containing Tryptophan Analogs. *Applied Microbiology and Biotechnology* **2006**, *73* (4), 740-754.
  40. Lepthien, S.; Hoesl, M. G.; Merkel, L.; Budisa, N., Azatryptophans Endow Proteins with Intrinsic Blue Fluorescence. *Proceedings of the National Academy of Sciences of the United States of America* **2008**, *105* (42), 16095-16100.
  41. Merkel, L.; Hoesl, M. G.; Albrecht, M.; Schmidt, A.; Budisa, N., Blue Fluorescent Amino Acids as *In Vivo* Building Blocks for Proteins. *Chembiochem* **2010**, *11* (3), 305-314.
  42. Twine, S. M.; Szabo, A. G., Fluorescent Amino Acid Analogs. *Biophotonics, Pt A* **2003**, *360*, 104-127.
  43. Hogue, C. W. V.; Rasquinha, I.; Szabo, A. G.; Macmanus, J. P., A New Intrinsic Fluorescent-Probe for Proteins - Biosynthetic Incorporation of 5-Hydroxytryptophan into Oncomodulin. *Febs Letters* **1992**, *310* (3), 269-272; Ross, J. B. A.; Senear, D. F.; Waxman, E.; Kombo, B. B.; Rusinova, E.; Huang, Y. T.; Laws, W. R.; Hasselbacher, C. A., Spectral Enhancement of Proteins - Biological Incorporation and Fluorescence Characterization of 5-Hydroxytryptophan in Bacteriophage-Lambda Ci Repressor. *Proceedings of the National Academy of Sciences of the United States of America* **1992**, *89* (24), 12023-12027.

44. Li, Q.; Du, H. N.; Hu, H. Y., Study of Protein-Protein Interactions by Fluorescence of Tryptophan Analogs: Application to Immunoglobulin G Binding Domain of Streptococcal Protein G. *Biopolymers* **2003**, *72* (2), 116-122.
45. Petrovic, D. M.; Leenhouts, K.; van Roosmalen, M. L.; KleinJan, F.; Broos, J., Monitoring Lysin Motif-Ligand Interactions via Tryptophan Analog Fluorescence Spectroscopy. *Analytical Biochemistry* **2012**, *428* (2), 111-118.
46. Twine, S. M.; Murphy, L.; Phillips, R. S.; Callis, P.; Cash, M. T.; Szabo, A. G., The Photophysical Properties of 6-Azaindole. *Journal of Physical Chemistry B* **2003**, *107* (2), 637-645.
47. Hohsaka, T.; Sato, K.; Sisido, M.; Takai, K.; Yokoyama, S., Adaptability of Nonnatural Aromatic-Amino-Acids to the Active-Center of the Escherichia-Coli Ribosomal A-Site. *Febs Letters* **1993**, *335* (1), 47-50.
48. Doi, Y.; Ohtsuki, T.; Shimizu, Y.; Ueda, T.; Sisido, M., Elongation factor Tu Mutants Expand Amino Acid Tolerance of Protein Biosynthesis System. *Journal of the American Chemical Society* **2007**, *129* (46), 14458-14462; Ohtsuki, T.; Yamamoto, H.; Doi, Y.; Sisido, M., Use of EF-Tu Mutants for Determining and Improving Aminoacylation Efficiency and for Purifying Aminoacyl tRNAs with Non-Natural Amino Acids. *Journal of Biochemistry* **2010**, *148* (2), 239-246; Dale, T.; Fahlman, R. P.; Olejniczak, M.; Uhlenbeck, O. C., Specificity of the Ribosomal A Site for Aminoacyl-tRNAs. *Nucleic Acids Research* **2009**, *37* (4), 1202-1210.
49. Nakata, H.; Ohtsuki, T.; Abe, R.; Hohsaka, T.; Sisido, M., Binding Efficiency of Elongation Factor Tu to tRNAs Charged with Nonnatural Fluorescent Amino Acids. *Analytical Biochemistry* **2006**, *348* (2), 321-323.
50. Chapeville, F.; Ehrenstein, G. V.; Benzer, S.; Weisblum, B.; Ray, W. J.; Lipmann, F., On Role of Soluble Ribonucleic Acid in Coding for Amino Acids. *Proceedings of the National Academy of Sciences of the United States of America* **1962**, *48* (6), 1086.
51. Hecht, S. M.; Alford, B. L.; Kuroda, Y.; Kitano, S., Chemical Aminoacylation of Transfer-RNAs. *Journal of Biological Chemistry* **1978**, *253* (13), 4517-4520.
52. Noren, C. J.; Anthonycahill, S. J.; Griffith, M. C.; Schultz, P. G., A General Method for Site-Specific Incorporation of Unnatural Amino-Acids into Proteins. *Science* **1989**, *244* (4901), 182-188.
53. Robertson, S. A.; Noren, C. J.; Anthonycahill, S. J.; Griffith, M. C.; Schultz, P. G., The Use of 5'-Phospho-2 Deoxyribocytidylriboadenosine as a Facile Route to Chemical Aminoacylation of Transfer-RNA. *Nucleic Acids Research* **1989**, *17* (23), 9649-9660.
54. Hohsaka, T.; Kajihara, D.; Ashizuka, Y.; Murakami, H.; Sisido, M., Efficient Incorporation of Nonnatural Amino Acids with Large Aromatic Groups into Streptavidin in *In Vitro* Protein Synthesizing Systems. *Journal of the American Chemical Society* **1999**, *121* (1), 34-40.
55. Murakami, H.; Hohsaka, T.; Ashizuka, Y.; Hashimoto, K.; Sisido, M., Site-Directed Incorporation of Fluorescent Nonnatural Amino Acids into Streptavidin for Highly Sensitive Detection of Biotin. *Biomacromolecules* **2000**, *1* (1), 118-125.
56. Kajihara, D.; Abe, R.; Iijima, I.; Komiyama, C.; Sisido, M.; Hohsaka, T., FRET Analysis of Protein Conformational Change Through Position-Specific Incorporation of Fluorescent Amino Acids. *Nature Methods* **2006**, *3* (11), 923-929.
57. Hamada, H.; Kameshima, N.; Szymanska, A.; Wegner, K.; Lankiewicz, L.; Shinohara, H.; Taki, M.; Sisido, M., Position-Specific Incorporation of a Highly Photodurable and Blue-Laser Excitable Fluorescent Amino Acid into Proteins for Fluorescence Sensing. *Bioorganic & Medicinal Chemistry* **2005**, *13* (10), 3379-3384.
58. Furter, R., Expansion of the Genetic Code: Site-Directed p-fluoro-phenylalanine Incorporation in Escherichia Coli. *Protein Science* **1998**, *7* (2), 419-426.

59. Wang, L.; Brock, A.; Herberich, B.; Schultz, P. G., Expanding the Genetic Code of Escherichia Coli. *Science* **2001**, *292* (5516), 498-500.
60. Wang, L.; Magliery, T. J.; Liu, D. R.; Schultz, P. G., A New Functional Suppressor tRNA/aminoacyl-tRNA Synthetase Pair for the *In Vivo* Incorporation of Unnatural Amino Acids into Proteins. *Journal of the American Chemical Society* **2000**, *122* (20), 5010-5011.
61. Kobayashi, T.; Nureki, O.; Ishitani, R.; Yaremchuk, A.; Tukalo, M.; Cusack, S.; Sakamoto, K.; Yokoyama, S., Structural Basis for Orthogonal tRNA Specificities of Tyrosyl-tRNA Synthetases for Genetic Code Expansion. *Nature Structural Biology* **2003**, *10* (6), 425-432.
62. Xie, J. M.; Schultz, P. G., Innovation: A Chemical Toolkit for Proteins - An Expanded Genetic Code. *Nature Reviews Molecular Cell Biology* **2006**, *7* (10), 775-782.
63. Guo, J. T.; Melancon, C. E.; Lee, H. S.; Groff, D.; Schultz, P. G., Evolution of Amber Suppressor tRNAs for Efficient Bacterial Production of Proteins Containing Nonnatural Amino Acids. *Angewandte Chemie-International Edition* **2009**, *48* (48), 9148-9151.
64. Stokes, A. L.; Miyake-Stoner, S. J.; Peeler, J. C.; Nguyen, D. P.; Hammer, R. P.; Mehl, R. A., Enhancing the Utility of Unnatural Amino Acid Synthetases by Manipulating Broad Substrate Specificity. *Molecular Biosystems* **2009**, *5* (9), 1032-1038; Miyake-Stoner, S. J.; Refakis, C. A.; Hammill, J. T.; Lusic, H.; Hazen, J. L.; Deiters, A.; Mehl, R. A., Generating Permissive Site-Specific Unnatural Aminoacyl-tRNA Synthetases. *Biochemistry* **2010**, *49* (8), 1667-1677.
65. Schultz, K. C.; Supekova, L.; Ryu, Y. H.; Xie, J. M.; Perera, R.; Schultz, P. G., A Genetically Encoded Infrared Probe. *Journal of the American Chemical Society* **2006**, *128* (43), 13984-13985.
66. Miyake-Stoner, S. J.; Miller, A. M.; Hammill, J. T.; Peeler, J. C.; Hess, K. R.; Mehl, R. A.; Brewer, S. H., Probing Protein Folding Using Site-Specifically Encoded Unnatural Amino Acids as FRET Donors with Tryptophan. *Biochemistry* **2009**, *48* (25), 5953-5962.
67. Taskent-Sezgin, H.; Chung, J.; Patsalo, V.; Miyake-Stoner, S. J.; Miller, A. M.; Brewer, S. H.; Mehl, R. A.; Green, D. F.; Raleigh, D. P.; Carrico, I., Interpretation of p-Cyanophenylalanine Fluorescence in Proteins in Terms of Solvent Exposure and Contribution of Side-Chain Quenchers: A Combined Fluorescence, IR and Molecular Dynamics Study. *Biochemistry* **2009**, *48* (38), 9040-9046.
68. Wissner, R. F.; Batjargal, S.; Fadzen, C. M.; Petersson, E. J., Labeling Proteins with Fluorophore/Thioamide Forster Resonant Energy Transfer Pairs by Combining Unnatural Amino Acid Mutagenesis and Native Chemical Ligation. *Journal of the American Chemical Society* **2013**, *135* (17), 6529-6540.
69. Wang, J. Y.; Xie, J. M.; Schultz, P. G., A Genetically Encoded Fluorescent Amino Acid. *Journal of the American Chemical Society* **2006**, *128* (27), 8738-8739.
70. Mills, J. H.; Lee, H. S.; Liu, C. C.; Wang, J. Y.; Schultz, P. G., A Genetically Encoded Direct Sensor of Antibody-Antigen Interactions. *ChemBiochem* **2009**, *10* (13), 2162-2164.
71. Lacey, V. K.; Parrish, A. R.; Han, S. L.; Shen, Z. X.; Briggs, S. P.; Ma, Y. G.; Wang, L., A Fluorescent Reporter of the Phosphorylation Status of the Substrate Protein STAT3. *Angewandte Chemie-International Edition* **2011**, *50* (37), 8692-8696.
72. Farr, G. W.; Fenton, W. A.; Chaudhuri, T. K.; Clare, D. K.; Saibil, H. R.; Horwich, A. L., Folding with and without Encapsulation by cis- and trans-only GroEL-GroES Complexes. *Embo Journal* **2003**, *22* (13), 3220-3230; Guo, F.; Tao, H. A.; Buss, J.; Coltharp, C.; Hensel, Z.; Jie, X. A., *In Vivo* Structure of the E. coli FtsZ-ring Revealed by Photoactivated Localization Microscopy (PALM). *Plos One* **2010**, *5* (9).
73. Ogino, H.; Wachi, M.; Ishii, A.; Iwai, N.; Nishida, T.; Yamada, S.; Nagai, K.; Sugai, M., FtsZ-Dependent Localization of GroEL Protein at Possible Division Sites. *Genes to Cells* **2004**, *9* (9), 765-771; Winkler, J.; Seybert, A.; Konig, L.; Pruggnaller, S.; Haselmann, U.; Sourjik, V.; Weiss, M.;

- Frangakis, A. S.; Mogk, A.; Bukau, B., Quantitative and Spatio-Temporal Features of Protein Aggregation in Escherichia Coli and Consequences on Protein Quality Control and Cellular Ageing. *Embo Journal* **2010**, *29* (5), 910-923.
74. Charbon, G.; Wang, J. Y.; Brustad, E.; Schultz, P. G.; Horwich, A. L.; Jacobs-Wagner, C.; Chapman, E., Localization of GroEL Determined by *In Vivo* Incorporation of a Fluorescent Amino Acid. *Bioorganic & Medicinal Chemistry Letters* **2011**, *21* (20), 6067-6070.
75. Charbon, G.; Brustad, E.; Scott, K. A.; Wang, J. Y.; Lobner-Olesen, A.; Schultz, P. G.; Jacobs-Wagner, C.; Chapman, E., Subcellular Protein Localization by Using a Genetically Encoded Fluorescent Amino Acid. *Chembiochem* **2011**, *12* (12), 1818-1821.
76. Saraogi, I.; Zhang, D. W.; Chandrasekaran, S.; Shan, S. O., Site-Specific Fluorescent Labeling of Nascent Proteins on the Translating Ribosome. *Journal of the American Chemical Society* **2011**, *133* (38), 14936-14939.
77. Wang, L.; Brock, A.; Schultz, P. G., Adding L-3-(2-naphthyl)alanine to the Genetic Code of E-coli. *Journal of the American Chemical Society* **2002**, *124* (9), 1836-1837.
78. Lee, H. S.; Guo, J. T.; Lemke, E. A.; Dimla, R. D.; Schultz, P. G., Genetic Incorporation of a Small, Environmentally Sensitive, Fluorescent Probe into Proteins in Saccharomyces cerevisiae. *Journal of the American Chemical Society* **2009**, *131* (36), 12921-+.
79. Chatterjee, A.; Guo, J. T.; Lee, H. S.; Schultz, P. G., A Genetically Encoded Fluorescent Probe in Mammalian Cells. *Journal of the American Chemical Society* **2013**, *135* (34), 12540-12543.
80. Kalstrup, T.; Blunck, R., Dynamics of Internal Pore Opening in K-V Channels Probed by a Fluorescent Unnatural Amino Acid. *Proceedings of the National Academy of Sciences of the United States of America* **2013**, *110* (20), 8272-8277.
81. Pantoja, R.; Rodriguez, E. A.; Dibas, M. I.; Dougherty, D. A.; Lester, H. A., Single-Molecule Imaging of a Fluorescent Unnatural Amino Acid Incorporated Into Nicotinic Receptors. *Biophysical Journal* **2009**, *96* (1), 226-237.
82. Schoppa, N. E.; Sigworth, F. J., Activation of Shaker Potassium Channels III. An Activation Gating Model for Wild-Type and V2 Mutant Channels. *Journal of General Physiology* **1998**, *111* (2), 313-342.
83. Cohen, B. E.; McAnaney, T. B.; Park, E. S.; Jan, Y. N.; Boxer, S. G.; Jan, L. Y., Probing Protein Electrostatics with a Synthetic Fluorescent Amino Acid. *Science* **2002**, *296* (5573), 1700-1703.
84. Steward, L. E.; Collins, C. S.; Gilmore, M. A.; Carlson, J. E.; Ross, J. B. A.; Chamberlin, A. R., *In Vitro* Site-Specific Incorporation of Fluorescent Probes into beta-Galactosidase. *Journal of the American Chemical Society* **1997**, *119* (1), 6-11.
85. Summerer, D.; Chen, S.; Wu, N.; Deiters, A.; Chin, J. W.; Schultz, P. G., A Genetically Encoded Fluorescent Amino Acid. *Proceedings of the National Academy of Sciences of the United States of America* **2006**, *103* (26), 9785-9789.
86. Shen, B.; Xiang, Z.; Miller, B.; Louie, G.; Wang, W. Y.; Noel, J. P.; Gage, F. H.; Wang, L., Genetically Encoding Unnatural Amino Acids in Neural Stem Cells and Optically Reporting Voltage-Sensitive Domain Changes in Differentiated Neurons. *Stem Cells* **2011**, *29* (8), 1231-1240.
87. Parrish, A. R.; She, X. Y.; Xiang, Z.; Coin, I.; Shen, Z. X.; Briggs, S. P.; Dillin, A.; Wang, L., Expanding the Genetic Code of Caenorhabditis elegans Using Bacterial Aminoacyl-tRNA Synthetase/tRNA Pairs. *Acs Chemical Biology* **2012**, *7* (7), 1292-1302.
88. Murakami, H.; Hohsaka, T.; Ashizuka, Y.; Sisido, M., Site-directed Incorporation of p-Nitrophenylalanine into Streptavidin and Site-to-Site Photoinduced Electron Transfer from a

- Pyrenyl Group to a Nitrophenyl Group on the Protein Framework. *Journal of the American Chemical Society* **1998**, *120* (30), 7520-7529; Taki, M.; Hohsaka, T.; Murakami, H.; Taira, K.; Sisido, M., Position-Specific Incorporation of a Fluorophore-Quencher Pair into a Single Streptavidin Through Orthogonal Four-Base Codon/Anticodon Pairs. *Journal of the American Chemical Society* **2002**, *124* (49), 14586-14590.
89. Tsao, M. L.; Summerer, D.; Ryu, Y. H.; Schultz, P. G., The Genetic Incorporation of a Distance Probe into Proteins in *Escherichia coli*. *Journal of the American Chemical Society* **2006**, *128* (14), 4572-4573.
90. Szymanska, A.; Wegner, K.; Lankiewicz, L., Synthesis of N- (tert-butoxy)carbonyl -3-(9,10-dihydro-9-oxoacridin-2-yl)-L-alanine, a New Fluorescent Amino Acid Derivative. *Helvetica Chimica Acta* **2003**, *86* (10), 3326-3331.
91. Goldberg, J. M.; Speight, L. C.; Fegley, M. W.; Petersson, E. J., Minimalist Probes for Studying Protein Dynamics: Thioamide Quenching of Selectively Excitable Fluorescent Amino Acids. *Journal of the American Chemical Society* **2012**, *134* (14), 6088-6091.
92. Goldberg, J. M.; Wissner, R. F.; Klein, A. M.; Petersson, E. J., Thioamide Quenching of Intrinsic Protein Fluorescence. *Chemical Communications* **2012**, *48* (10), 1550-1552.
93. Batjargal, S.; Wang, Y. J.; Goldberg, J. M.; Wissner, R. F.; Petersson, E. J., Native Chemical Ligation of Thioamide-Containing Peptides: Development and Application to the Synthesis of Labeled alpha-Synuclein for Misfolding Studies. *Journal of the American Chemical Society* **2012**, *134* (22), 9172-9182; Goldberg, J. M.; Batjargal, S.; Chen, B. S.; Petersson, E. J., Thioamide Quenching of Fluorescent Probes through Photoinduced Electron Transfer: Mechanistic Studies and Applications. *Journal of the American Chemical Society* **2013**, *135* (49), 18651-18658.
94. Speight, L. C.; Muthusamy, A. K.; Goldberg, J. M.; Warner, J. B.; Wissner, R. F.; Willi, T. S.; Woodman, B. F.; Mehl, R. A.; Petersson, E. J., Efficient Synthesis and In Vivo Incorporation of Acridon-2-ylalanine, a Fluorescent Amino Acid for Lifetime and Forster Resonance Energy Transfer/Luminescence Resonance Energy Transfer Studies. *Journal of the American Chemical Society* **2013**, *135* (50), 18806-18814.
95. Goerke, A. R.; Swartz, J. R., High-Level Cell-Free Synthesis Yields of Proteins Containing Site-Specific Non-Natural Amino Acids. *Biotechnology and Bioengineering* **2009**, *102* (2), 400-416.
96. Albayrak, C.; Swartz, J. R., Cell-free Co-production of an Orthogonal Transfer RNA Activates Efficient Site-Specific Non-Natural Amino Acid Incorporation. *Nucleic Acids Research* **2013**, *41* (11), 5949-5963.
97. Schlummer, B.; Scholz, U., Palladium-catalyzed C-N and C-O coupling - A Practical Guide from an Industrial Vantage Point. *Advanced Synthesis & Catalysis* **2004**, *346* (13-15), 1599-1626; Schlummer, B.; Scholz, U., Buchwald-Hartwig Amination - A Modern Technology for the Synthesis of Intermediates and APIs. *Chimica Oggi-Chemistry Today* **2005**, *23* (2), 18-20.
98. Ousmer, M.; Boucard, V.; Lubin-Germain, N.; Uziel, J.; Auge, J., Gram-scale Preparation of a p-(C-glucopyranosyl)-L-phenylalanine Derivative by a Negishi Cross-Coupling Reaction. *European Journal of Organic Chemistry* **2006**, (5), 1216-1221.
99. Tang, P. P.; Furuya, T.; Ritter, T., Silver-Catalyzed Late-Stage Fluorination. *Journal of the American Chemical Society* **2010**, *132* (34), 12150-12154.
100. Correa, A.; Tellitu, I.; Dominguez, E.; SanMartin, R., An Advantageous Synthesis of New Indazolone and Pyrazolone Derivatives. *Tetrahedron* **2006**, *62* (48), 11100-11105; Urganekar, S.; Xu, J. H.; Verkade, J. G., Application of a New Bicyclic Triaminophosphine Ligand in Pd-catalyzed Buchwald-Hartwig Amination Reactions of Aryl Chlorides, Bromides, and Iodides. *Journal of Organic Chemistry* **2003**, *68* (22), 8416-8423.

101. Ohgiya, T.; Nishiyama, S., A Simple Deprotection of Triflate Esters of Phenol Derivatives. *Tetrahedron Letters* **2004**, *45* (33), 6317-6320.
102. Young, D. D.; Young, T. S.; Jahnz, M.; Ahmad, I.; Spraggon, G.; Schultz, P. G., An Evolved Aminoacyl-tRNA Synthetase with Atypical Polysubstrate Specificity. *Biochemistry* **2011**, *50* (11), 1894-1900.
103. Antonczak, A. K.; Simova, Z.; Yonemoto, I. T.; Bochtler, M.; Piasecka, A.; Czapinska, H.; Brancale, A.; Tippmann, E. M., Importance of Single Molecular Determinants in the Fidelity of Expanded Genetic Codes. *Proceedings of the National Academy of Sciences of the United States of America* **2011**, *108* (4), 1320-1325; Antonczak, A. K.; Morris, J.; Tippmann, E. M., Advances in the Mechanism and Understanding of Site-Selective Noncanonical Amino Acid Incorporation. *Current Opinion in Structural Biology* **2011**, *21* (4), 481-487.
104. Cantel, S.; Desgranges, S.; Martinez, J.; Fehrentz, J. A., Saponification of Esters of Chiral alpha-Amino Acids Anchored Through Their Amine Function on Solid Support. *Journal of Peptide Science* **2004**, *10* (6), 326-328.
105. Cosnier, S.; Ionescu, R. E.; Herrmann, S.; Bouffier, L.; Demeunynck, M.; Marks, R. S., Electroenzymatic Polypyrrole-Intercalator Sensor for the Determination of West Nile Virus cDNA. *Analytical Chemistry* **2006**, *78* (19), 7054-7057; Wang, Y. N.; Gao, D.; Chen, Z.; Li, S. F.; Gao, C. M.; Cao, D. L.; Liu, F.; Liu, H. X.; Jiang, Y., Acridone Derivative 8a Induces Oxidative Stress-Mediated Apoptosis in CCRF-CEM Leukemia Cells: Application of Metabolomics in Mechanistic Studies of Antitumor Agents. *Plos One* **2013**, *8* (5).
106. Diaz, E.; Ferrandez, A.; Prieto, M. A.; Garcia, J. L., Biodegradation of Aromatic Compounds by Escherichia Coli. *Microbiology and Molecular Biology Reviews* **2001**, *65* (4), 523.
107. Zhang, H. T.; Javor, G. T., Identification of the ubiD Gene on the Escherichia Coli Chromosome. *Journal of Bacteriology* **2000**, *182* (21), 6243-6246.
108. Contessa, G. M.; Orsale, M.; Melino, S.; Torre, V.; Paci, M.; Desideri, A.; Cicero, D. O., Structure of Calmodulin Complexed with an Olfactory CNG Channel Fragment and Role of the Central Linker: Residual Dipolar Couplings to Evaluate Calmodulin Binding Modes Outside the Kinase Family. *Journal of Biomolecular NMR* **2005**, *31* (3), 185-199.
109. Liu, M. Y.; Chen, T. Y.; Ahamed, B.; Li, J.; Yau, K. W., Calcium-Calmodulin Modulation of the Olfactory Cyclic Nucleotide-Gated Cation Channel. *Science* **1994**, *266* (5189), 1348-1354.
110. Getahun, Z.; Huang, C. Y.; Wang, T.; De Leon, B.; DeGrado, W. F.; Gai, F., Using Nitrile-Derivatized Amino Acids as Infrared Probes of Local Environment. *Journal of the American Chemical Society* **2003**, *125* (2), 405-411.
111. Brun, M. P.; Bischoff, L.; Garbay, C., A Very Short Route to Enantiomerically Pure Coumarin-Bearing Fluorescent Amino Acids. *Angewandte Chemie-International Edition* **2004**, *43* (26), 3432-3436.
112. Dadabhoy, A.; Faulkner, S.; Sammes, P. G., Long Wavelength Sensitizers for Europium(III) Luminescence Based on Acridone Derivatives. *Journal of the Chemical Society-Perkin Transactions 2* **2002**, (2), 348-357.
113. Bruno, J.; Horrocks, W. D.; Zauhar, R. J., Europium(III) Luminescence and Tyrosine to Terbium(III) Energy-Transfer Studies of Invertebrates (Octopus) Calmodulin. *Biochemistry* **1992**, *31* (31), 7016-7026; Garipey, J.; Sykes, B. D.; Hodges, R. S., Lanthanide-Induced Peptide Folding - Variations in Lanthanide Affinity and Induced Peptide Conformation. *Biochemistry* **1983**, *22* (8), 1765-1772; Horrocks, W. D.; Tingey, J. M., Time-Resolved Europium(III) Luminescence Excitation Spectroscopy - Characterization of Calcium-Binding Sites of Calmodulin. *Biochemistry* **1988**, *27* (1), 413-419.

114. Ohashi, W.; Hirota, H.; Yamazaki, T., Solution Structure and Fluctuation of the Mg<sup>2+</sup>-Bound Form of Calmodulin C-terminal Domain. *Protein Science* **2011**, *20* (4), 690-701; Yang, J. J.; Gawthrop, A.; Ye, Y. Y., Obtaining Site-Specific Calcium-Binding Affinities of Calmodulin. *Protein and Peptide Letters* **2003**, *10* (4), 331-345.
115. Wu, X. C.; Reid, R. E., Structure Calcium Affinity Relationships of Site III of Calmodulin: Testing the Acid Pair Hypothesis Using Calmodulin Mutants. *Biochemistry* **1997**, *36* (28), 8649-8656.
116. Nitz, M.; Sherawat, M.; Franz, K. J.; Peisach, E.; Allen, K. N.; Imperiali, B., Structural Origin of the High Affinity of a Chemically Evolved Lanthanide-Binding Peptide. *Angewandte Chemie-International Edition* **2004**, *43* (28), 3682-3685; Reynolds, A. M.; Sculimbrene, B. R.; Imperiali, B., Lanthanide-Binding Tags with Unnatural Amino Acids: Sensitizing Tb<sup>3+</sup> and Eu<sup>3+</sup> Luminescence at Longer Wavelengths. *Bioconjugate Chemistry* **2008**, *19* (3), 588-591; Franz, K. J.; Nitz, M.; Imperiali, B., Lanthanide-Binding Tags as Versatile Protein Coexpression Probes. *Chembiochem* **2003**, *4* (4), 265-271; Franz, K. J.; Nitz, M.; Lukovic, E.; Imperiali, B., Development of Lanthanide-Binding Peptides as Natively Expressed Protein Probes. *Journal of Inorganic Biochemistry* **2003**, *96* (1), 131.
117. Noble, M. E. M.; Zeelen, J. P.; Wierenga, R. K.; Mainfroid, V.; Goraj, K.; Gohimont, A. C.; Martial, J. A., Structure of Triosephosphate Isomerase from Escherichia-Coli Determined at 2.6-Angstrom Resolution. *Acta Crystallographica Section D-Biological Crystallography* **1993**, *49*, 403-417.
118. Dong, Y. M.; Bolduc, A.; McGregor, N.; Skene, W. G., Push-Pull Aminobithiophenes - Highly Fluorescent Stable Fluorophores. *Organic Letters* **2011**, *13* (7), 1844-1847; Lord, S. J.; Conley, N. R.; Lee, H. L. D.; Samuel, R.; Liu, N.; Twieg, R. J.; Moerner, W. E., A Photoactivatable Push-Pull Fluorophore for Single-Molecule Imaging in Live Cells. *Journal of the American Chemical Society* **2008**, *130* (29), 9204; Morales, A. R.; Frazer, A.; Woodward, A. W.; Ahn-White, H. Y.; Fonari, A.; Tongwa, P.; Timofeeva, T.; Belfield, K. D., Design, Synthesis, and Structural and Spectroscopic Studies of Push-Pull Two-Photon Absorbing Chromophores with Acceptor Groups of Varying Strength. *Journal of Organic Chemistry* **2013**, *78* (3), 1014-1025.
119. Dreher, S. D.; Dormer, P. G.; Sandrock, D. L.; Molander, G. A., Efficient Cross-Coupling of Secondary Alkyltrifluoroborates with Aryl Chlorides-Reaction Discovery Using Parallel Microscale Experimentation. *Journal of the American Chemical Society* **2008**, *130* (29), 9257.
120. Edelhoch, H., Spectroscopic Determination of Tryptophan and Tyrosine in Proteins. *Biochemistry* **1967**, *6* (7), 1948.
121. van Rooijen, B. D.; van Leijenhorst-Groener, K. A.; Claessens, M.; Subramaniam, V., Tryptophan Fluorescence Reveals Structural Features of alpha-Synuclein Oligomers. *J. Mol. Biol.* **2009**, *394* (5), 826-833; Szymanska, A.; Wegner, K.; Lankiewicz, L., Synthesis of N-[(tert-butoxy)carbonyl]-3-(9,10-dihydro-9-oxoacridin-2-yl)-L-alanine, a New Fluorescent Amino Acid Derivative. *Helv. Chim. Acta* **2003**, *86* (10), 3326-3331.
122. Hanahan, D.; Jessee, J.; Bloom, F. R., Plasmid Transformation of Escherichia-Coli and Other Bacteria. *Methods Enzymol.* **1991**, *204*, 63-113.
123. Giehm, L.; Lorenzen, N.; Otzen, D. E., Assays for alpha-Synuclein Aggregation. *Methods* **2010**, *53* (3), 295-305; Fink, A. L., The Aggregation and Fibrillation of alpha-Synuclein. *Acc. Chem. Res.* **2006**, *39* (9), 628-634; Ferreon, A. C. M.; Moran, C. R.; Ferreon, J. C.; Deniz, A. A., Alteration of the alpha-Synuclein Folding Landscape by a Mutation Related to Parkinson's Disease. *Angew. Chem. Int. Ed.* **2010**, *49* (20), 3469-3472.

124. Du, H.; Fuh, R. C. A.; Li, J. Z.; Corkan, L. A.; Lindsey, J. S., PhotochemCAD: A Computer-Aided Design and Research Tool in Photochemistry. *Photochem. Photobiol.* **1998**, *68* (2), 141-142.
125. Goldberg, J. M.; Wissner, R. F.; Klein, A. M.; Petersson, E. J., Thioamide Quenching of Intrinsic Protein Fluorescence. *Chem. Commun.* **2012**, *48*, 1550-1552.
126. Blanchard, S. C.; Cooperman, B. S.; Wilson, D. N., Probing Translation with Small-Molecule Inhibitors. *Chemistry & Biology* **2010**, *17* (6), 633-645.
127. Hartman, M. C. T.; Josephson, K.; Lin, C. W.; Szostak, J. W., An Expanded Set of Amino Acid Analogs for the Ribosomal Translation of Unnatural Peptides. *Plos One* **2007**, *2* (10).
128. Whitford, P. C.; Geggier, P.; Altman, R. B.; Blanchard, S. C.; Onuchic, J. N.; Sanbonmatsu, K. Y., Accommodation of Aminoacyl-tRNA into the Ribosome Involves Reversible Excursions Along Multiple Pathways. *RNA - a Publication of the RNA Society* **2010**, *16* (6), 1196-1204.
129. Voss, N. R.; Gerstein, M.; Steitz, T. A.; Moore, P. B., The Geometry of the Ribosomal Polypeptide Exit Tunnel. *Journal of Molecular Biology* **2006**, *360* (4), 893-906.
130. Bernabeu, C.; Lake, J. A., Nascent Polypeptide-Chains Emerge from the Exit Domain of the Large Ribosomal-Subunit - Immune Mapping of the Nascent Chain. *Proceedings of the National Academy of Sciences of the United States of America-Biological Sciences* **1982**, *79* (10), 3111-3115.
131. Frank, J.; Zhu, J.; Penczek, P.; Li, Y. H.; Srivastava, S.; Verschoor, A.; Radermacher, M.; Grassucci, R.; Lata, R. K.; Agrawal, R. K., A Model of Protein-Synthesis Based on Cryoelectron Microscopy of the *E*-Coli Ribosome. *Nature* **1995**, *376* (6539), 441-444.
132. Trabuco, L. G.; Harrison, C. B.; Schreiner, E.; Schulten, K., Recognition of the Regulatory Nascent Chain TnaC by the Ribosome. *Structure* **2010**, *18* (5), 627-637.
133. Nakatogawa, H.; Murakami, A.; Ito, K., Control of CsaA and SecM Translation by Protein Secretion. *Current Opinion in Microbiology* **2004**, *7* (2), 145-150.
134. David-Eden, H.; Mankin, A. S.; Mandel-Gutfreund, Y., Structural Signatures of Antibiotic Binding Sites on the Ribosome. *Nucleic Acids Research* **2010**, *38* (18), 5982-5994.
135. Vimberg, V.; Xiong, L. Q.; Bailey, M.; Tenson, T.; Mankin, A., Peptide-Mediated Macrolide Resistance Reveals Possible Specific Interactions in the Nascent Peptide Exit Tunnel. *Molecular Microbiology* **2004**, *54* (2), 376-385.
136. Kannan, K.; Vazquez-Laslop, N.; Mankin, A. S., Selective Protein Synthesis by Ribosomes with a Drug-Obstructed Exit Tunnel. *Cell* **2012**, *151* (3), 508-520.
137. Wilson, D. N., Peptides in the Ribosomal Tunnel Talk Back. *Molecular Cell* **2011**, *41* (3), 247-248.
138. Hardesty, B.; Kramer, G., Folding of a Nascent Peptide on the Ribosome. *Progress in Nucleic Acid Research and Molecular Biology, Vol 66* **2001**, *66*, 41-66.
139. Creighton, T. E., *Proteins: Structures and Molecular Properties*. Second ed.; W. H. Freeman and Company: New York, NY, USA, 1993.
140. Fedyukina, D. V.; Cavagnero, S., Protein Folding at the Exit Tunnel. *Annual Review of Biophysics, Vol 40* **2011**, *40*, 337-359.
141. Lu, J. L.; Deutsch, C., Folding Zones Inside the Ribosomal Exit Tunnel. *Nature Structural & Molecular Biology* **2005**, *12* (12), 1123-1129.
142. Lu, J. L.; Hua, Z. M.; Kobertz, W. R.; Deutsch, C., Nascent Peptide Side Chains Induce Rearrangements in Distinct Locations of the Ribosomal Tunnel. *Journal of Molecular Biology* **2011**, *411* (2), 499-510.
143. Lu, J. L.; Deutsch, C., Secondary Structure Formation of a Transmembrane Segment in Kv Channels. *Biochemistry* **2005**, *44* (23), 8230-8243.

144. Woolhead, C. A.; McCormick, P. J.; Johnson, A. E., Nascent Membrane and Secretory Proteins Differ in FRET-Detected Folding Far Inside the Ribosome and in Their Exposure to Ribosomal Proteins. *Cell* **2004**, *116* (5), 725-736.
145. Yap, M. N.; Bernstein, H. D., The Plasticity of a Translation Arrest Motif Yields Insights into Nascent Polypeptide Recognition inside the Ribosome Tunnel. *Molecular Cell* **2009**, *34* (2), 201-211; Muto, H.; Nakatogawa, H.; Ito, K., Genetically Encoded but Nonpolypeptide Prolyl-tRNA Functions in the A Site for SecM-Mediated Ribosomal Stall. *Molecular Cell* **2006**, *22* (4), 545-552; Ha, H. J.; Yeom, J. H.; Song, W. S.; Jeon, C. O.; Hahn, Y.; Lee, K., Identification of a Hyperactive Variant of the SecM Motif Involved in Ribosomal Arrest. *Current Microbiology* **2012**, *64* (1), 17-23.
146. Ismail, N.; Hedman, R.; Schiller, N.; von Heijne, G., A Biphasic Pulling Force Acts on Transmembrane Helices During Translocon-Mediated Membrane Integration. *Nature Structural & Molecular Biology* **2012**, *19* (10), 1018.
147. Berisio, R.; Schlutzen, F.; Harms, J.; Bashan, A.; Auerbach, T.; Baram, D.; Yonath, A., Structural Insight into the Role of the Ribosomal Tunnel in Cellular Regulation. *Nature Structural Biology* **2003**, *10* (5), 366-370.
148. Starosta, A. L.; Karpenko, V. V.; Shishkina, A. V.; Mikolajka, A.; Sumbatyan, N. V.; Schlutzen, F.; Korshunova, G. A.; Bogdanov, A. A.; Wilson, D. N., Interplay between the Ribosomal Tunnel, Nascent Chain, and Macrolides Influences Drug Inhibition. *Chemistry & Biology* **2010**, *17* (5), 504-514; Lovmar, M.; Vimberg, V.; Lukk, E.; Nilsson, K.; Tenson, T.; Ehrenberg, M., Cis-Acting Resistance Peptides Reveal Dual Ribosome Inhibitory Action of the Macrolide Josamycin. *Biochimie* **2009**, *91* (8), 989-995; Verdier, L.; Gharbi-Benarous, J.; Bertho, G.; Mauvais, P.; Girault, J. P., Antibiotic Resistance Peptides: Interaction of Peptides Conferring Macrolide and Ketolide Resistance with Staphylococcus Aureus Ribosomes. Conformation of Bound Peptides as Determined by Transferred NOE Experiments. *Biochemistry* **2002**, *41* (13), 4218-4229.
149. Kannan, K.; Mankin, A. S., Macrolide Antibiotics in the Ribosome Exit Tunnel: Species-Specific Binding and Action. *Antimicrobial Therapeutics Reviews: Antibiotics That Target the Ribosome* **2011**, *1241*, 33-47.
150. Bhushan, S.; Hoffmann, T.; Seidelt, B.; Frauenfeld, J.; Mielke, T.; Berninghausen, O.; Wilson, D. N.; Beckmann, R., SecM-Stalled Ribosomes Adopt an Altered Geometry at the Peptidyl Transferase Center. *Plos Biology* **2011**, *9* (1).
151. Ramu, H.; Vazquez-Laslop, N.; Klepacki, D.; Dai, Q.; Piccirilli, J.; Micura, R.; Mankin, A. S., Nascent Peptide in the Ribosome Exit Tunnel Affects Functional Properties of the A-Site of the Peptidyl Transferase Center. *Molecular Cell* **2011**, *41* (3), 321-330.
152. Berndt, U.; Oellerer, S.; Zhang, Y.; Johnson, A. E.; Rospert, S., A Signal-Anchor Sequence Stimulates Signal Recognition Particle Binding to Ribosomes from Inside the Exit Tunnel. *Proceedings of the National Academy of Sciences of the United States of America* **2009**, *106* (5), 1398-1403; Bhushan, S.; Gartmann, M.; Halic, M.; Armache, J. P.; Jarasch, A.; Mielke, T.; Berninghausen, O.; Wilson, D. N.; Beckmann, R., alpha-Helical Nascent Polypeptide Chains Visualized Within Distinct Regions of the Ribosomal Exit Tunnel. *Nature Structural & Molecular Biology* **2010**, *17* (3), 313.
153. Nakatogawa, H.; Ito, K., The Ribosomal Exit Tunnel Functions as a Discriminating Gate. *Cell* **2002**, *108* (5), 629-636.
154. Chaudhuri, M. K.; Hussain, S., Boric Acid Catalyzed Thia-Michael Reactions in Water or Alcohols. *Journal of Molecular Catalysis a-Chemical* **2007**, *269* (1-2), 214-217.

155. Ohuchi, M.; Murakami, H.; Suga, H., The Flexizyme System: A Highly Flexible tRNA Aminoacylation Tool for the Translation Apparatus. *Current Opinion in Chemical Biology* **2007**, *11* (5), 537-542.
156. Illangasekare, M.; Sanchez, G.; Nickles, T.; Yarus, M., Aminoacyl-RNA Synthesis Catalyzed by an RNA. *Science* **1995**, *267* (5198), 643-647; Jenne, A.; Famulok, M., A Novel Ribozyme with Ester Transferase Activity. *Chemistry & Biology* **1998**, *5* (1), 23-34.
157. Saito, H.; Kourouklis, D.; Suga, H., An *In Vitro* Evolved Precursor tRNA with Aminoacylation Activity. *Embo Journal* **2001**, *20* (7), 1797-1806.
158. Saito, H.; Suga, H., A Ribozyme Exclusively Aminoacylates the 3'-Hydroxyl Group of the tRNA Terminal Adenosine. *Journal of the American Chemical Society* **2001**, *123* (29), 7178-7179.
159. Murakami, H.; Ohta, A.; Ashigai, H.; Suga, H., A Highly Flexible tRNA Acylation Method for Non-Natural Polypeptide Synthesis. *Nature Methods* **2006**, *3* (8), 655-655.
160. Cisar, J. S.; Ferreras, J. A.; Soni, R. K.; Quadri, L. E. N.; Tan, D. S., Exploiting Ligand Conformation in Selective Inhibition of Non-Ribosomal Peptide Synthetase Amino Acid Adenylation with Designed Macrocyclic Small Molecules. *Journal of the American Chemical Society* **2007**, *129* (25), 7752.
161. Brodsky, B. H.; Du Bois, J., Oxaziridine-Mediated Catalytic Hydroxylation of Unactivated 3 Degrees C-H bonds Using Hydrogen Peroxide. *Journal of the American Chemical Society* **2005**, *127* (44), 15391-15393.
162. Lu, J. L.; Deutsch, C., Electrostatics in the Ribosomal Tunnel Modulate Chain Elongation Rates. *Journal of Molecular Biology* **2008**, *384* (1), 73-86.
163. Lu, J. L.; Kobertz, W. R.; Deutsch, C., Mapping the Electrostatic Potential Within the Ribosomal Exit Tunnel. *Journal of Molecular Biology* **2007**, *371* (5), 1378-1391.
164. Das, S.; Kar, M.; Sen Gupta, S., Synthesis of End-Functionalized Phosphate and Phosphonate-Polypeptides by Ring-Opening Polymerization of Their Corresponding N-Carboxyanhydride. *Polymer Chemistry* **2013**, *4* (15), 4087-4091.